MICROWAVE-INDUCED, EFFICIENT, CONVENIENT AND RAPID SYNTHESIS OF SUBSTITUTED 2-PYRAZOLINES AS POTENTIALLY ANTIMICROBIAL AGENT

Sainath B. Zangade[a], Avinash T. Shinde,[b] Yogesh S. Nalwar[b] and Yeshwant B. Vibhute[b]

Keywords: 2-Pyrazolines; 2-methoxyethanol; 2'-hydroxychalcones; microwave irradiation; antimicrobial activity;

Microwave-induced an efficient, rapid and enviromentally begin condensation of substituted 2'-hydroxychalcones with hydrazine hydrate in 2-methoxyethanol afford 2-pyrazolines **2a-h** in high 88-95 % yields. The structure of newly synthesized compounds established on the basis of spectroscopic technique and laboratory chemical test. Further these compounds were screened for antimicrobial activity against *Bacillus subtilis, Staphylococcus aureus, Aspergillus flavus* and *Candida albicans*. The most of the compounds shows good to better inhibitory activity.

Corresponding Authors
Tel: +919822939699
E-Mail: drsbz@rediffmail.com
[a] Department of Chemistry, Madhavrao Patil College, Palam, Dist. Parbhani-431720 (M.S.) India.
[b] Laboratory of Organic Synthesis, Department of Studies in Chemistry, YeshwantMahavidylaya, Nanded-431602, India.

Introduction

The use of the hazardus reagent, solvent and high loading catalyst in synthetic organic chemistry leads to impact on environment. Due to this varied nature of the chemicals, chemist requiresvarious greener pathways in our quest towards attaining sustainability.[1] Microwave (MW) irradiation is one of them rout has been gaining increased popularity as an alternative heat source in green chemistry towards development of organic synthesis.[2] This technique has been applied to a variety of reactions resulting in reduction of reaction time, higher yield, greater selectivity, cleaner reaction products, and to reduce tadious job for isolation of product.[3] It also provides an opportunity to work with open vessels, thus avoiding the risk of high pressure and hazards of inflammable solvents.[4]

Among a wide range of biologically active heterocycles, a significant amount of research activity has been directed toward the study of pyrazolines. A number of pyrazoline derivatives have been found to exhibit physiological and pharmacological properties such as antiinnammatory,[5-6] antibacteria1,[7] antineoplastic,[8] antiallergic,[9] analgesic,[10] and hypoglycemic[11] activities. Classical route for the preparation of these compounds involesthe condensation of α,β-unsaturated carbonyl compounds with hydrazines.[12] The various modified methods have been reported for synthesis of 2-pyrazolines using different catalysts such as $KHSO_4H_2O/SiO_2$,[13] porous calcium hydroxyapatite,[14] chlorahine-T,[15] mercuric acetate,[16] $Bi(NO_3)_3{\cdot}5H_2O$,[17] Zn,[18] $H_3PW_{12}O_{40}$,[19] and Lewis acid/Lewis bases.[20] Many of these procedure invole combinations of solvents with various catalyst and long reaction time make these methods environmentally hazardous, economical expensive. Chemist require to improve these methods towards organic synthesis and reaction, increasing attention is being focused on green chemistry using environmentally benign reagents and conditions, particularly non-conventional heating. In view of these observations, it was thought worthwhile to synthesize 2-pyrazoline derivatives from α,β-unsaturated carbonyl compounds in 2-methoxyethanol by using nonconventional tool.

Methods and Materials

Instrumentation

Melting points were determined in an open capillary tube and are uncorrected. IR spectra were recorded in KBr on a Perkin-Elmer spectrometer. ^{1}H NMR spectra were recorded on a Gemini 300 MHz instrument in DMSO-d_6 as solvent and TMS as an internal standard. The mass spectra were recorded on Shimadzu GC/MS spectrometer. Elemental analyses were performed on a Perkin-Elmer 240 CHN elemental analyzer. A multimode microwave oven (2450 MHz, 300 W, Brand LG, India) were used for performing reaction. Reaction progress monitored on TLC using using hexane/ethyl acetate/petrolium ether combination as the mobile phase.

Typical procedure for synthesis of 2-pyrazolines

A mixture of 3-(3-bromo-4,5-dimethoxyphenyl)-1-(4-bromo-1-hydroxy-naphthalen-2-yl)propenone (10 mmol) and $NH_2NH_2{\cdot}H_2O$ (50 mmol) dissolved in 2-methoxyethanol (5 ml) in round bottom flask. To this reaction solution 0.001 mmol of glacial acetic acid was added. The resulting reaction mixtures were irradiated in microwave oven for 2-3 minutes with short interval of 20 seconds to avoid the excessive evaporation of solvent. Progress of reaction was monitored on TLC (mixture of hexane, ethyl acetate, petroleum ether). The separated solid was filtered and recrystallized from ethyl alcohol to give **2c**. Physical data of synthesized compounds **2a-h** are given in Table **1**.

Table 1. Synthesis of substitut ed 2-pyrazolines under microwave irradiation

Compund	R	R_1	R_2	R_3	Time, min.	Melting point,[a] ^{0}C	Yield,[b] %
2a	H	H	OMe	H	4	148-150	91
2b	H	OMe	OMe	Br	5-6	161-163	90
2c	Br	OMe	OMe	Br	2-3	177-179	92
2d	I	H	OMe	H	3	154	88
2e	H	H	F	H	4-5	130	93
2f	H	H	Cl	H	3-4	135-137	95
2g	I	OMe	OMe	Br	4	188	89
2h	H	OMe	OMe	OMe	5-6	190-192	88

[a]M.P. referred with solvent-free and other technique.[24-26] [b]Yield of isolated desired product.

2-[5-(4-Methoxyphenyl)-4,5-dihydro-1*H*-pyrazol-3-yl]naphthalen-1-ol. (2a)

UV/VIS (λ_{max}, nm): 413, 328. IR (KBr pellets): 1590 (C=N), 1474, 1542 (C=C), 1234 (C-N) cm^{-1}. ^{1}H NMR (300 MH$_Z$, DMSO-d$_6$) δ 12.45 (s, 1H, OH), 7.81-7.64 (m, 10H, Ar-H), 6.82 (s, 1H, NH), 3.26 (dd, *J* = 5.0, 17.4 H$_Z$, 1H, H$_A$), δ 3.64 (dd, *J* = 12.1, 17.5 H$_Z$, 1H, H$_B$), δ 4.82 (dd, *J* = 5.0, 12.1 H$_Z$, 1H, H$_X$), 3.77 (s, 3H, OCH$_3$). ^{13}CNMR (DMSO): 160.15 (C *of* Ar-OCH$_3$), 154.85 (C *of*Ar-OH), 152.29 (C *of* C=N), 138.28 (Ar-C), 137.92 (Ar-C), 136.26 (Ar-C), 135.88 (Ar-C), 134.74 (Ar-C), 128.64 (Ar-C), 128.49 (Ar-C), 127.75 (Ar-C), 127.70 (Ar-C), 126.93 (Ar-C), 126.80 (Ar-C), 124.19 (Ar-C), 122.38 (Ar-C), 117.26 (Ar-C), 56.74 (C *of* OCH$_3$), 52.10 (C *of* CH), 44.75 (C *of* CH$_2$). MS (EI, *m/z* (%): 318(M$^+$, 68 %). Anal.Cacld. for $C_{20}H_{18}O_2N_2$: C, 75.47; H, 5.66. found: C, 75.55; H, 5.59.

2-[5-(3-Bromo-4,5-dimethoxyphenyl)-4,5-dihydro-1*H*-pyrazol-3-yl]naphthalen-1-ol. (2b)

UV/VIS (λ_{max}, nm): 409, 326. IR (KBr pellets):1585 (C=N), 1475, 1538 (C=C), 1228 (C-N) cm^{-1}. ^{1}H NMR (300 MH$_Z$, DMSO-d$_6$) δ 12.52 (s, 1H, OH), 7.76-7.39 (m, 8H, Ar-H),6.89 (s, 1H, NH), 3.31 (dd, *J* = 5.2, 17.6 H$_Z$, 1H, H$_A$), δ 3.67 (dd, *J* = 12.1, 17.6 H$_Z$, 1H, H$_B$), δ 4.86 (dd, *J* = 5.1, 12.1 H$_Z$, 1H, H$_X$), 3.83 (s, 3H, OCH$_3$), 3.76 (s, 3H, OCH$_3$).^{13}CNMR (DMSO): 154.65 (C *of*Ar-OH), 152.56 (C *of* C=N), 152.29 (C *of* Ar-OCH$_3$), 149.47 (C *of* Ar-OCH$_3$) 138.27 (Ar-C), 137.86 (Ar-C), 128.45 (Ar-C), 127.48 (Ar-C), 127.27 (Ar-C), 125.34 (Ar-C), 124.93 (Ar-C), 121.29 (Ar-C), 118.87 (Ar-C), 116.70 (Ar-C), 115.39 (Ar-C), 113.79 (Ar-C), 109.19 (C *of*Ar-Br), 57.84 (C *of* OCH$_3$), 56.45 (C *of* OCH$_3$), 53.28 (C *of* CH), 43.96 (C *of* CH$_2$).MS (EI, *m/z* (%): 427 (M$^+$, 42 %). Anal.Cacld. for $C_{21}H_{19}O_3N_2Br$: C, 59.01; H, 4.44; X (Br), 18.73. found: C, 59.16; H, 4.53; X (Br), 18.85.

4-Bromo-2-[5-(3-bromo-4,5-dimethoxyphenyl)-4,5-dihydro-1*H*-pyrazol-3-yl]naphthalen-1-ol. (2c)

UV/VIS (λ_{max}, nm): 411, 329. IR (KBr pellets):1594 (C=N), 1472, 1543 (C=C), 1231 (C-N) cm^{-1}. ^{1}H NMR (300 MH$_Z$, DMSO-d$_6$) δ 12.61 (s, 1H, OH), 7.89-7.46 (m, 7H, Ar-H),6.83 (s, 1H, NH), 3.26 (dd, *J* = 5.1, 17.5 H$_Z$, 1H, H$_A$), δ 3.65 (dd, *J* = 12.0, 17.5 H$_Z$, 1H, H$_B$), δ 4.88 (dd, *J* = 5.1, 12.1 H$_Z$, 1H, H$_X$), 3.86 (s, 3H, OCH$_3$), 3.78 (s, 3H, OCH$_3$).^{13}CNMR (DMSO): 155.32 (C *of*Ar-OH), 152.72 (C *of* C=N), 152.37 (C *of* Ar-OCH$_3$), 149.45 (C *of* Ar-OCH$_3$) 139.29 (Ar-C), 137.13 (Ar-C), 129.46 (Ar-C), 128.88 (Ar-C), 127.47 (Ar-C), 126.30 (Ar-C), 124.97 (Ar-C), 121.73 (Ar-C), 118.28 (Ar-C), 116.71 (Ar-C), 116.39 (Ar-C), 115.39 (C *of*Ar-Br), 109.22 (C *of*Ar-Br), 57.92 (C *of* OCH$_3$), 56.45 (C *of* OCH$_3$), 53.27 (C *of* CH), 43.98 (C *of* CH$_2$). MS (EI, *m/z* (%):506 (M$^+$, 78 %). Anal.Cacld. for $C_{21}H_{18}O_3N_2Br_2$: C, 49.80; H, 3.55; X (Br), 31.62. found: C, 49.74; H, 3.58; X (Br), 31.68.

4-Iodo-2-[5-(4-methoxyphenyl)-4,5-dihydro-1H-pyrazol-3-yl]naphthalen-1-ol (2d**)**

UV/VIS (λ_{max}, nm): 413, 331. IR (KBr pellets):1590 (C=N), 1479, 1544 (C=C), 1231 (C-N) cm^{-1}. ^{1}H NMR (300 MH$_Z$, DMSO-d$_6$) δ 12.56 (s, 1H, OH), 7.80-7.36 (m, 9H, Ar-H), 6.85 (s, 1H, NH), 3.28 (dd, *J* = 5.1, 17.5 H$_Z$, 1H, H$_A$), δ 3.66 (dd, *J* = 12.1, 17.5 H$_Z$, 1H, H$_B$), δ 4.87 (dd, *J* = 5.1, 12.1 H$_Z$, 1H, H$_X$), 3.74 (s, 3H, OCH$_3$).^{13}CNMR (DMSO): 159.97 (C *of* Ar-OCH$_3$), 155.13 (C *of*Ar-OH), 152.34 (C *of* C=N), 137.87 (Ar-C), 137.94 (Ar-C), 136.48 (Ar-C), 136.85 (Ar-C), 135.67 (Ar-C), 129.40 (Ar-C), 128.45 (Ar-C), 128.79 (Ar-C), 127.18 (Ar-C), 126.92 (Ar-C), 126.77 (Ar-C), 124.28 (Ar-C), 123.63 (Ar-C), 108.15 (C *of*Ar-I), 56.73 (C *of* OCH$_3$), 52.17 (C *of* CH), 44.62 (C *of* CH$_2$).MS (EI, *m/z* (%): 444 (M$^+$, 90 %). Anal.Cacld. for $C_{20}H_{17}O_2N_2I$: C, 54.05; H, 3.82; X (I), 28.60. found: C, 54.18; H, 3.79; X (I), 28.67.

2-[5-(4-Fluorophenyl)-4,5-dihydro-1*H*-pyrazol-3-yl]-4-iodonaphthalen-1-ol. (2e)

UV/VIS (λ_{max}, nm): 410, 330. IR (KBr pellets): 1588 (C=N), 1468, 1542 (C=C), 1228 (C-N) cm^{-1}. ^{1}H NMR (300 MH$_Z$, DMSO-d$_6$) δ 12.48 (s, 1H, OH), 7.88-7.37 (m, 9H, Ar-H),6.87 (s, 1H, NH), 3.30 (dd, *J* = 5.2, 17.6 H$_Z$, 1H, H$_A$), δ 3.70 (dd, *J* = 12.1, 17.6 H$_Z$, 1H, H$_B$), δ 4.89 (dd, *J* = 5.2, 12.1 H$_Z$, 1H, H$_X$).^{13}CNMR (DMSO): 155.23 (C *of*Ar-OH), 152.48 (C *of* C=N), 137.18 (Ar-C), 137.82 (Ar-C), 136.25 (Ar-C), 136.96 (Ar-C), 135.27 (Ar-C), 129.31 (Ar-C), 129.57 (Ar-C), 128.62 (Ar-C), 127.19 (Ar-C), 127.91 (Ar-C), 126.73 (Ar-C), 125.57 (Ar-C),

 DOI: 10.17628/ecb.2014.3.310-314

124.88 (Ar-C),122.65 (Ar-C), 109.98 (C *of*Ar-I),52.26 (C *of* CH), 44.60 (C *of* CH_2).MS (EI, *m/z* (%): 432 (M^+, 38 %). Anal.Cacld. for $C_{19}H_{14}N_2OIF$: C, 52.77; H, 3.24; X (I); 29.39. found: C, 52.85; H, 3.27; X (I), 29.45.

2-[5-(4-Chloro-phenyl)-4,5-dihydro-1*H*-pyrazol-3-yl]-4-iodo-naphthalen-1-ol. (2f)

UV/VIS (λ_{max}, nm): 409, 328. IR (KBr pellets):1590 (C=N), 1475, 1552 (C=C), 1232 (C-N) cm^{-1}. ^1H NMR (300 MH_Z, DMSO-d_6) δ 12.56 (s, 1H, OH), 7.92-7.39 (m, 9H, Ar-H), 6.90 (s, 1H, NH), 3.28 (dd, *J* = 5.1, 17.6 H_Z, 1H, H_A), δ 3.69 (dd, *J* = 12.1, 17.6 H_Z, 1H, H_B), δ 4.87 (dd, *J* = 5.1, 12.1 H_Z, 1H, H_X).^{13}CNMR (DMSO): 156.14 (C *of*Ar-OH), 152.67 (C *of* C=N), 138.41(Ar-C), 138.63 (Ar-C), 136.87 (Ar-C), 135.19 (Ar-C), 135.54 (Ar-C), 133.27 (Ar-C), 131.39 (Ar-C), 128.50 (Ar-C), 127.47 (Ar-C), 127.98 (Ar-C), 126.25 (Ar-C), 125.52 (Ar-C), 124.90 (Ar-C),122.69 (Ar-C) 109.83 (C *of*Ar-I),53.16 (C *of* CH), 44.65 (C *of* CH_2).MS (EI, *m/z* (%): 448 (M^+, 40 %). Anal.Cacld. for $C_{19}H_{14}N_2OICl$: C, 50.89; H, 3.12; X (I,Cl), 36.27. found: C, 50.82; H, 3.15; X (I,Cl), 36.30.

2-[5-(3-Bromo-4,5-dimethoxyphenyl)-4,5-dihydro-1*H*-pyrazol-3-yl]-4-iodonaphthalen-1-ol. (2g)

UV/VIS (λ_{max}, nm): 410, 330. IR (KBr pellets):1592 (C=N), 1470, 1560 (C=C), 1234 (C-N) cm^{-1}.^1H NMR (300 MH_Z, DMSO-d_6) δ 12.48 (s, 1H, OH), 7.78-7.34 (m, 7H, Ar-H), 6.92 (s, 1H, NH) 3.32 (dd, *J* = 5.2, 17.5 H_Z, 1H, H_A), δ 3.70 (dd, *J* = 12.1, 17.5 H_Z, 1H, H_B), δ 4.88 (dd, *J* = 5.2, 12.1 H_Z, 1H, H_X), 3.88 (s, 3H, OCH_3), 3.73 (s, 3H, OCH_3).^{13}CNMR (DMSO): 154.88 (C *of*Ar-OH), 152.48 (C *of* C=N), 151.89 (C *of* Ar-OCH_3), 149.50 (C *of* Ar-OCH_3) 138.37 (Ar-C), 138.86 (Ar-C), 128.25 (Ar-C), 127.92 (Ar-C), 126.13 (Ar-C), 125.75 (Ar-C), 124.40 (Ar-C), 121.27 (Ar-C), 118.59 (Ar-C), 114.94 (Ar-C), 115.80 (Ar-C), 113.19 (Ar-C), 109.22 (C *of*Ar-Br), 57.66 (C *of* OCH_3), 56.40 (C *of* OCH_3), 53.29 (C *of* CH), 43.85 (C *of* CH_2).MS (EI, *m/z* (%): 553(M^+, 96 %). Anal.Cacld. for $C_{21}H_{18}O_3N_2IBr$: C, 45.56; H, 3.25; X(I, Br), 37.43. found: C, 45.64; H, 3.18; X (I,Br), 37.49.

2-[5-(3,4,5-Trimethoxyphenyl)-4,5-dihydro-1*H*-pyrazol-3-yl]-naphthalen-1-ol. (2h)

UV/VIS (λ_{max}, nm): 413, 328. IR (KBr pellets): 1589 (C=N), 1472, 1542 (C=C), 1232 (C-N) cm^{-1}. ^1H NMR (300 MH_Z, DMSO-d_6) δ 12.40 (s, 1H, OH), 7.48-8.37 (m, 8H, Ar-H), 6.87 (s, 1H, NH), 3.28 (dd, *J* = 4.9, 17.5 H_Z, 1H, H_A), δ 3.72 (dd, *J* = 11.9, 17.5 H_Z, 1H, H_B), δ 4.89 (dd, *J* = 5.0, 11.9 H_Z, 1H, H_X), δ 3.86 (s, 3H, OCH_3), 3.72 (s, 6H, OCH_3). ^{13}CNMR (DMSO): 154.05 (C *of* Ar-OH), 153.28 (C *of* C=N), 148.67 (C *of* Ar-OCH_3), 148.42 (2C *of* Ar-OCH_3) 134.13 (Ar-C), 133.19 (Ar-C), 128.23 (Ar-C), 128.36 (Ar-C), 127.41 (Ar-C), 126.30 (Ar-C), 124.97 (Ar-C), 122.71 (Ar-C), 121.28 (Ar-C), 112.65 (Ar-C), 110.86 (Ar-C), 110.32 (Ar-C), 62.39 (3C *of* OCH_3), 56.36 (C *of* CH), 42.37 (C *of* CH_2). MS m/z: 378 (M^+, 80 %), 377, 361, 347, 287, 231, 211, 210, 181, 168, 140, 128, 115, 109, 95, 77, 65, 51, 40. Anal.Cacld. for $C_{22}H_{22}O_4N_2$: C, 69.84; H, 5.82. Found: C, 70.91; H, 5.96.

Results and discussion

Synthesis

In continuation of earlier research work on organic heterocyclic synthesis[21-23] and reported methods for compounds **2a-h** using various proceduure[24-26], we try to investigate herein a convenient route for synthesis of 2-pyrazolines using microwave irradiation. The reaction of 2'-hydroxychalcones with hydrazine in 2-methoxyethanol in presence of glacial acetic acid under MW irradiation gives 2-pyrazolines, Scheme-**1**.

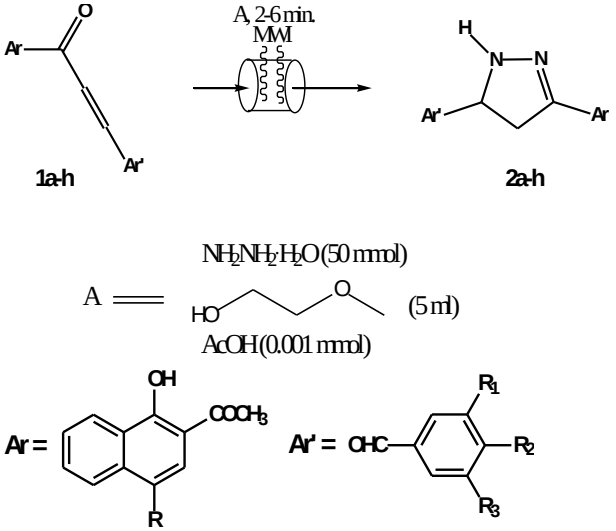

Scheme 1. Synthesis of substituted 2-pyrazolines under microwave irradiation

The combination of 2-methoxyethanol with microwave technique found to be efficient process towards synthesis heterocyclic compounds [27,28]. Initially, we attempted the condensation of 3-(3-Bromo-4,5-dimethoxy-phenyl)-1-(4-bromo-1-hydroxy-naphthalen-2-yl)-propenone (10 mmol) with $NH_2NH_2{\cdot}H_2O$ (50 mmol) using 0.001 mmol of AcOH in 2-methoxyethanol as reaction solvent. The reaction went to completion within 2-3 minutes and corresponding product **2c** was obtained in 92% yield. In order to optimize the reaction conditions, we carried out the above reaction in different reaction medium such as ethanol, dichloromethane, dioxane, acetonitrile, DMF and 2-methoxyethanol, Table **2**. We found that use of 2-methoxyethanol as an efficient reaction medium in terms of clean reaction conditions, not expensive, higher yields of product and environmentally eco-friendly. As results observed from Table **2**, we pay our attention towards various substituted 2'-hydroxy chalcones. In all cases, reaction proceeded efficiently in high yields using 2-methoxyethanol.

 DOI: 10.17628/ecb.2014.3.310-314

Table 2. Optimization of solvent effect on model reaction.[a]

Entry	Solvent	Time,min	Yield, %
1	Ethanol (10 ml)	12	78
2	Dichloromethane (10 ml)	18	63
3	Dioxane (15 ml)	15	68
4	Acetonitrile (15 ml)	20	75
5	DMF (10 ml)	16	60
6	2-Methoxyethanol (5 ml)	2-3	92

[a]Reaction of 3-(3-Bromo-4,5-dimethoxyphenyl)-1-(4-bromo-1-hydroxynaphthalen-2-yl)propenone (10 mmol) with $NH_2NH_2{\cdot}H_2O$ (50 mmol) using 0.001 mmol of AcOH under microwave irradiation.

The structure characterization of compounds **2a-h**confirmed on the basis of spectral technique, UV, IR, ^{1}H NMR, MS, ^{13}C-NMR and elemental analysis. In IR spectral data ofcondensed products, compounds **2a-h** display disappearance of band at 1625-1635 cm^{-1} due to C=O of 2'-hydroxychalcone and appearance of a band near 1588 cm^{-1}due to C=N formed. The N-H stretching band of pyrazoline nucleus appears near 3320 cm^{-1}.

The ^{1}H NMR spectra showing an ABX pattern were observed for H_A, H_B, and H_X proton which appear as pair of doublets near δ 3.28, 3.67, and 4.90 ppm with J_{AB}=17.6 Hz, J_{Ax} = 5.0 Hz, J_{AB}= 12.1 Hz. The chemical shift for aromatic protons was observed at δ 7.25-8.20 ppm and that of N-H pyrazolo at d 6.90 ppm.^{13}C NMR of five membered pyrazolo nucleous reveals the presence of peak near 44 and 53 which assign for methylene and methyne carbon. The peak near 161, 155 and 153 reveals the presence OCH_3, C-OH and C=N functionality in the basic structure of pyrazolines respectively.

Antimicrobial activity

The antibacterial activities of the synthesized compounds (**2a-h**) were determined by agar well diffusion method.[27] The compounds were evaluated for antibacterial activity against *Bacillus subtilis* [MTCC 2063] and *Staphylococcus aureus* [MTCC 2901]. The antifungal activity performed against *Aspergillus flavus* [MTCC 2501] and *Candida albicans* [MTCC 183] were procured from Institute of Microbial Technology (IMTech), Chandigarh, India. The antibiotic streptomycin (25μ/mL) and fluconazole used as reference drug for antibacterial and antifungal activity, respectively. Dimethyl sulphoxide (1 %, DMSO) used a control without compound.

The culture strains of bacteria were maintained on nutrient agar slant at 37±0.5 °C for 24 h. The antibacterial activity was evaluated using nutrient agar plate seeded with 0.1 mL of respective bacterial culture strain suspension prepared in sterile saline (0.85 %) of 105 CFU/mL dilutions. The wells of 6 mm diameter were filled with 0.1 mL of compound solution at fixed concentration 25 μ mL^{-1} separately for each bacterial strain. All plates were incubated at 37±0.5 ^{0}C for 24 h. Zone of inhibition were noted in mm, Table **3**.

Table 3. Antmicrobial data of 2-pyrazolines.

Com-pound	Zone of inhibition in mm and minimum inhibitory concentration, μg mL^{-1}			
	A	**B**	**C**	**D**
2a	23 (50)	14 (<100)	14 (100)	16 (>100)
2b	21 (50)	17(<100)	12 (<200)	10 (<200)
2c	24 (25)	28 (15.5)	25 (50)	26 (50)
2d	20 (<100)	21(100)	19 (<100)	19 (<100)
2e	23 (50)	22 (<50)	21 (<100)	24 (<50)
2f	26 (12.5)	21 (100)	10 (200)	16 (100)
2g	28 (10.5)	30 (<10)	26 (<50)	29 (10)
2h	25 (12.5)	26 (50)	24 (50)	27 (12.5)
Fluco-nazole	26 (12.5)	28 (10)	--	--
Strepto-mycin	--	--	30 (25)	28 (10.5)

A: *B. subtilis* B: *S. aureus* C: *A. flavus* D: *C. albicans*

For antifungal activity, all culture strains of fungi maintained on potato dextrose agar (PDA) slant at 27 ± 0.2 ^{0}C for 24-48 hr, until sporulation. Spore of strains were transferred into 5 mL of sterile distilled water containing 1 % Tween-80 (to suspend the spore properly). The spores were counted by haemocytometer (106 CFU/mL). Sterile PDA plate was prepared containing 2 % agar; 0.1 mL of each fungal spore suspension was spread on each plate and incubated at 27± 0.2 ^{0}C for 12 h. After incubation well prepared using sterile cork borer and each agar well was filled with 0.1 mL of compound solution at fixed concentration 25 μ mL^{-1}. The plates were kept in refrigerator for 20 min for diffusion and then incubated at 27± 0.2 ^{0}C for 7 days except *Candida albicans*. After incubation, zone of inhibition of compounds were measured in mm along with standard, Table-**3**.

The minimum inhibitory concentration values were determined by comparison to standard drugs at 10, 12.5, 25, 50, 100 and 200 μ mL^{-1}. A lower MIC's values indicate that less drug is required for inhibiting growth of the organism, therefore, drug with lower MIC scores more effective antimicrobial agent.

Conclusion

In summary we developed new methodology towards the synthesis of substituted 2'-pyrazolines from 2'-hydroxy chalcones using 2-methoxyethanol in presence of slightly acidic medium. The combination of microwave with 2-methoxyethanol found to be excellent and convenient reaction route in terms of simple reaction procedure, quick reaction time giving percent yield of product. The preliminary *in vitro* antimicrobial screening of this series revealed that compounds **2c**, **2g** and **2h** showed potent activity when compared with standard drug. Therefore, the present study is useful drug in medicinal investigation against bacterial and fungal diseases.

 DOI: 10.17628/ecb.2014.3.310-314

Acknowledgement

The authors gratefully acknowledge University Grant Commission (UGC) New Delhi for sanctioning major research grant (No. 38-267/2009). Authors are also thankful to Director Indian Institute of Chemical Technology (IICT), Hyderabad, KTHM College, Nasik for providing necessary instrumental facilities.

References

[1]Gedye, R., Smith, F., Westaway, K., Ali, H., Baldisera, L., Laberge, L., Rousell, J., *Tetrahedron Lett.*, **1986**, *27*, 279.

[2]Olofson, R. A., Kendall, R. V., *J. Org. Chem.*, **1970**, *35*, 2246.

[3]Lindstrom, P., Tierney, J., Wathey, B., Westman, J., *Tetrahedron*, **2001**, *57*, 9225.

[4]Toda, F., Tanaka, K., Hamai, K., *J. Chem. Soc. Perkin Trans.*, **1990**, *11*, 3207.

[5]Kerntzberger, A., Burgwitz, K., *Arch. Pharm.*, **1979**, *312*, 873.

[6]Singh, H., Ghosh, M. N., *J. Pharm. Pharmacol.*, **1958**, *20*, 316.

[7]Descacq, P., Nuhrich, A., Capdepuy, M., Devaux, G., *Eur. J. Med. Chem.*, **1990**, *25*, 285.

[8]Mokhtar, H. M., Faidallah, H. M., *Pharmazie.*, **1987**, *42*, 481.

[9]Roman, B., *Pharmazie.*, **1990**, *45*, 214.

[10]Kostel, A., Anderson, H., De Beer, E. J. D., *Fed. Proc.*, **1959**, *16*, 412.

[11]Wright, J. B., Dulin, W. E., Makillie, J. H., *J. Med. Chem.*, **1964**, *7*, 102.

[12]Seebacher, W., Michi, G., Belaj, F., Brun, R., Saf, R., Weis, R., *Tetrahedron*, **2003**, *59*, 2811.

[13]Kamal, K. K., Bilal, A. G., Kumar, S., Charanjeet, S. A., *Synth. Commun.*, **2006**, *36*, 2727.

[14]Atir, R., Mallouk, S., Bougrin, K., Soufiaoui, M., *Synth. Commun.*, **2006**, *36*, 111.

[15]Lokanatha, R. K. M., Hassner, A., *Synth. Commun.*, **1989**, *19*, 2799.

[16]Lokanatha, R. N., Linganna, N., *Synth. Commun.*, **1997**, *21*, 3737.

[17]Azarifar, D., Maleki, B., *Synth. Commun.*, **2005**, *35*, 2581.

[18]Alex, K., Tilack, A., Schwarz, N., Beller, M., *Org. Lett.*, **2008**, *10*, 2377.

[19]Fazaeli, R., Aliyan, H., Mallakpour, S., Rafiee, Z., Bordbar, M., *Chin. J. Catal.*, **2011**, *32*, 582.

[20]Krishna, P. R., Sekhar, E. R., Morgin, F., *Tetrahedron Lett.*, **2008**, *49*, 6768.

[21]Karamunge, K. G., Sayed, M. A., Vibhute, A. Y., Vibhute, Y. B., *J. Indian. Chem. Soc.*, **2011**, *88*, 443.

[22]Zangade, S. B., Shinde, A. T., Vibhute, A. Y., Vibhute, Y. B., *Pak. J. Chem.*, **2012**, *2*, 1-6.

[23]Chavan, S., Zangade, S., Vibhute, A., Vibhute, Y., *Eur. J. Chem.* **2013**, *4*, 98.

[24]Zangade, S. B., Mokle, S. S., Shinde, A. T., Vibhute, Y. B., *Green Chem. Lett. Rev.* **2013**, *6*, 123.

[25]Zangade, S., Shinde, A., Patil, A., Vibhute, Y., *Eur. J. Chem.* **2012**, *3*, 208.

[26]Zangade, S. B., Shinde, A. T., Chavan, S. B., Mokle, S. S., Vibhute, Y. B., *Eur. Chem. Bull.*, **2013**, *2*, 208-210.

[27]Shrinivasan, D., Sangeetha, N., Suresh, T., Lakshmanaperumasamy, P. J., *Ethnophrmacol.*, **2001**, *74*, 217.

Received: 23.02.2014.
Accepted: 12.03.2014.

COMBINED BIO- AND CHEMOSORPTION OF Mn(VII) FROM AQUEOUS SOLUTION BY *PROSOPIS CINERARIA* LEAF POWDER

Chandresh Virvadiya[a], Sharda Kumari[a], Vimla Choudhary[a] and Vikal Gupta[a]*

Keywords: Permanganate; *Prosopis cineraria* leaf powder; adsorption isotherms; biosorption; chemosorption.

The present work describes of a combined bio- and chemosorption of permanganate by *Prosopis cineraria* leaf powder using batch process. The plant is locally available in arid region and called as Khejari. The permanganate removal capacity of PCLP have been studied at various parameters like concentration of Mn (VII) ion, adsorbent dosage, *p*H, contact time, shaking speed, etc. The Langmuir and Freundlich adsorption models have been applied to describe the isotherms and isotherm constant are given.

* Corresponding Authors
E-Mail: vikal_chem@yahoo.co.in
[a] Department of chemistry, Jai Narain Vyas University, Jodhpur-342001, Rajasthan, India.

Introduction

Climate change and sustainable use of the environment have been recognized among the main threats for the future of mankind. Water is major part for environment.

Manganese is an essential trace nutrient in all known forms of life. Manganese poisoning, however, has been linked to impaired motor skills and cognitive disorders. Higher levels of exposure to manganese in water are associated with increased intellectual impairment and reduced intelligence quotients in school-age children.[1]

Removal of toxic heavy metals including manganese from industrial waste water has been practicing for several years.[2-7] The conventional physico-chemical removal methods such as electroplating, chemical precipitation, membrane separation, and evaporation or resin ion-exchange are usually expensive and sometimes not effective. Therefore, there is a need for some alternative technique which is efficient and cost effective. In recent years, several studied have been carried out on the removal of toxic metals by bio-sorption from the aqueous effluents using agricultural by-products.[8-12]

Bio sorption can be defined as the ability of biological materials to accumulate heavy metals through metabolically mediated or physico-chemical pathways of uptake.[13]

The aim of the present work is to use an abundantly available plant based renewable resource dry *Prosopis cineraria* leaf powder (PCLP) as an adsorbent for removal of toxic heavy metal ions such as permanganate. The manganese (VII) is a strong oxidant, thus its reaction around neutral *p*H leads to change the surface of original adsorbent, and the formed manganese dioxide might play role as adsorbent and autocatalyst of the oxidation reactions.[14-17] Since the oxidation and biosorption reaction cannot be separated and occurred as concurrent and stepwise reaction as well, at the equilibrium state a result of two processes – a biosorption and a chemosorption process can be found.

The adsorption capacities of this at room temperature have been estimated using equilibrium studies. Effects of various parameters like metal ion concentration, adsorbent dosage, *p*H, contact time and shaking speed have been studied.

Material and Methods

Preparation of adsorbent

Prosopis cineraria leaves were collected from Jai Narain Vyas University, New Campus of Jodhpur and washed repeatedly from double distilled water to remove impurities, dust and surface adhered particle. The washed materials were dried in a hot air oven for 48 hours at 60 ^{0}C. Dry leaves were crushed into small particles by mechanical grinder and sieve through 100 µm mesh sieve to obtain Prosopis cineraria leaf powder (PCLP). PCLP were activated with concentrate sulphuric acid and stored this activated PCLP into glass bottle for further use.

Preparation of Mn(VII) solution

A stock solution of Mn(VII) was prepared by dissolving 2.876 g of 99.3 % of $KMnO_4$ in 1 liter double distilled water to obtain 1000 mg L^{-1} stock solution. For further requirement of experiment the other solutions of strength 50-300 mg L^{-1} of Mn(VII) were prepared with the help of stock solution. The *p*H of solutions was adjusted with 0.1 N H_2SO_4 and 0.1 N NaOH solutions as per the requirement and *p*H was measured by *p*H meter.

Table 1. Experimental conditions

Experimental conditions	C_o, mgL^{-1}	M_s, gL^{-1}	*p*H	*t*, min	*S*, rpm
Effect of concentration of Mn(VII), C_o, mg L^{-1}	50-300	12	3	80	200
Effect of adsorbent dosage M_s, g L^{-1}	150	2-12	3	80	200
Effect of *p*H	150	12	2-7	80	200
Effect of contact time, *t*, min	150	12	3	20-120	200
Effect of shaking speed *S*, rpm	150	12	3	80	50-300

Adsorption experiment

Adsorption experiment were carried out by batch experiment as function of metal concentration (50, 100, 150, 200, 250 and 300) mg L^{-1}, *p*H (2-7), adsorbent dosage (2, 4, 6, 8, 10 and 12) g, contact time (20, 40, 60, 80, 100, 120) minutes and as function of shaking speed (50, 100, 150, 200, 250) rpm at room temperature.

Parameters were changed according at a time and all other were maintained constant according to table 1. After completion of every set of experiment finally metal bearing solution were allowed to settle and then the residual metal ion solutions were filtered using sintered glass G-3. The 20 mL of each sample was stored for residual Mn(VII) analysis.

After the completion of experiment, the concentration of residual Mn(VII) content was directly measured by atomic adsorption spectroscopy.

Equation (1) is used to determine the percentage adsorption of metal (Φ, in %) by adsorbent.

$$\Phi = \frac{C_o - C_e}{C_o} \times 100 \qquad (1)$$

where C_0 is initial metal ion concentration and C_e is the concentration of metal ion after adsorption.

Adsorption isotherm

According to Langmuir theory, the saturated monolayer isotherm can be represented as:

$$q_e = \frac{q_{max} b C_e}{1 + bC_e} \qquad (2)$$

The eqn. 2 can be rearranged by following linear form:

$$\frac{C_e}{q_e} = \frac{1}{bq_{max}} + \frac{1}{q_{max}} C_e \qquad (3)$$

where C_e is the equilibrium concentration, q_e is the amount of metal ion adsorbed, q_{max} is q_e for a complete monolayer (mg L^{-1}) and b is sorption equilibrium constant (L mg^{-1}). A graph of C_e versus C_e/q_e should indicate a straight line of slope $1/q_{max}$ and an intercept of $1/bq_{max}$.

Freundlich found that if the concentration of solute in solvent at equilibrium C_e (mgL^{-1}) was raised to the power of m, the amount of solute adsorbed being q_e, then C_e^m/q_e was a constant at a given temperature. This fairly satisfactory empirical isotherm can be used for non ideal sorption and is expressed by the following equation in the form of logarithm of both sides.

$$\log q_e = \log K_f + m \log C_e \qquad (4)$$

An adsorption isotherm is characterized by certain constant, the value of which express the surface properties and affinity of the sorbent and can also be used to compare bio-chemosorptive capacity of biomass for different metal ions. Out several isotherm equations, two have been applied for this study i.e. the Freundlich and Langmuir isotherms.

Result and Discussion

Effect of concentration of MnO_4^- ion

The experiments were carried out, with the change in the concentration of permanganate ion from 50-300 mg L^{-1} and maintaining constant adsorbent dosage (12 g L^{-1}) at *p*H 3 and also at constant shaking speed 200 rpm for 80 min. As increasing the concentration of metal ion, the adsorption % decreases because the numbers of active sites are fixed in the adsorbent as shown in Fig.1.

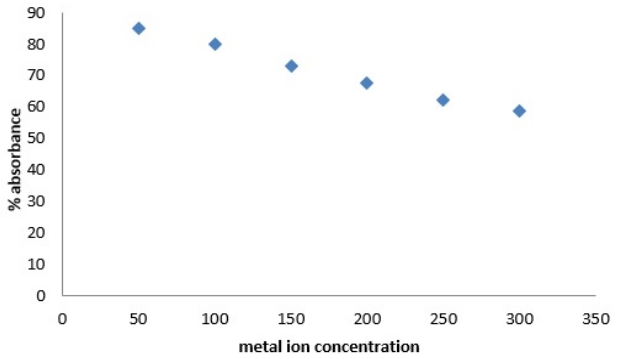

Figure 1. Effect of concentration of MnO_4^- ion on the removal efficiency

Since the rate of oxidation definitely increases with increasing the concentration of permanganate ion the oxidation leads to a changed absorbent surface (coverage with manganese dioxide and oxidative changes of surface molecules) which might cause the unavailability of adsorbent sites and changing the adsorbing abilities of the formed surface functions towards Mn(VII).

Effect of adsorbent dosage

The experiments were carried out, with the change in the adsorbent dosage from 2-12 g L^{-1} and maintaining constant the concentration of permanganate ion 150 mg L^{-1} at *p*H 3 and constant shaking speed 200 rpm for 80 min. As in Fig.2, with the increase in the dosage of adsorbent, the % of adsorption is increased because increase in adsorbent dosages. Here the number of available adsorbing sites and oxidable sites for capturing and reducing permanganates respectively are increased.

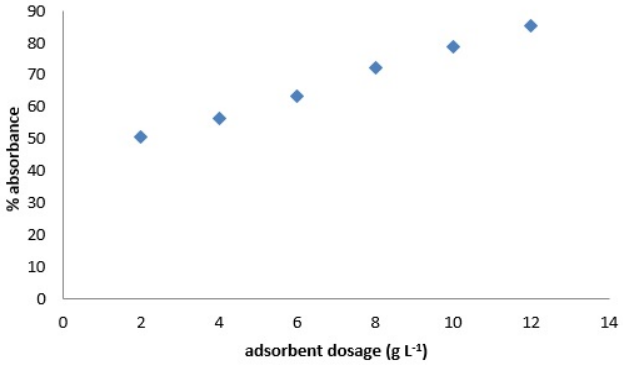

Figure 2. Effect of adsorbent dosage on the removal efficiency

Effect of *p*H

The experiments were also carried out, with the change in the *p*H from 2-7 and maintaining constant adsorbent dosage 12 g L^{-1} and the concentration of permanganate 150 mg L^{-1} and constant shaking speed 200 rpm for 80 min. The maximum removal of metal ion at pH 3 is 80.8% as shown in Fig.3. The oxidation power (chemosorption) is strongly *p*H dependent process. As we increase the *p*H, the numbers of hydrogen ions and the permanganate ion oxidation power are reduced and manganese dioxide formation takes place.

In acidic solution a five-electron oxidation process is occurred:

$$MnO_4^- + 8H^+ + 5e^- \rightarrow Mn^{2+} + 4H_2O \quad (5)$$

In neutral *p*H, the main process is a three-electron oxidation:

$$MnO_4^- + 4H^+ + 3e^- \rightarrow MnO_2 + 2H_2O \quad (6)$$

In a strongly alkaline solution, only a one-electron process takes place:

$$MnO_4^- + e^- \rightarrow MnO_4^{2-} \quad (7)$$

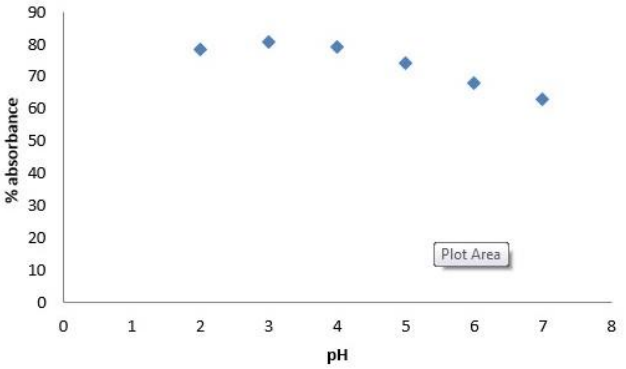

Figure 3. Effect of pH on the removal efficiency

At *p*H=3, the main process is the reaction (5), however, with consumption of hydrogen ions in the primary oxidation (chemosorption) process, the *p*H is increased and the reaction (6) will be dominant. This phenomenon and the formation of manganese dioxide can play the main role in the decreasing the chemosorption/adsorption of leaf powder with increasing the permanganate ion concentration.

Effect of contact time

The other experiments were carried out, with the change in the contact time from 20-120 minutes and maintaining constant adsorbent dosage from 12 g L^{-1}, the concentration of permanganate ion 150 mg L^{-1} at *p*H 3 and constant shaking speed 200 rpm. As in Fig.4, with increase the duration of contact time, firstly the removal efficiency increases rapidly up to 60 minutes and at 80 minutes it is increased slowly and after it becomes constant.

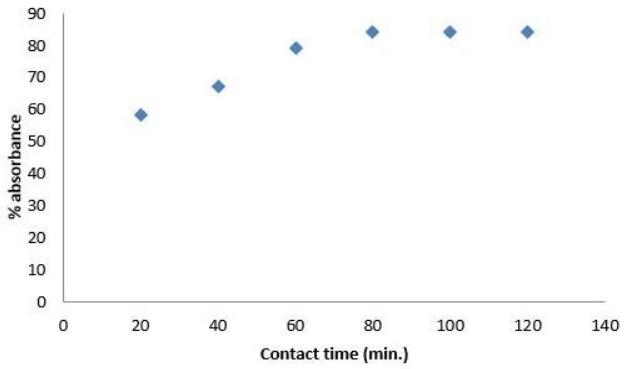

Figure 4. Effect of contact time on the removal efficiency

This behaviour can be explained by the presence of two concurrent reactions – chemosorption and adsorption, because the fast oxidation in acidic environment has large increment in the removed (reduced) permanganate amount, and with increasing the *p*H (due to consumption of hydrogen ions in the primary oxidation in the first 60 min) leads to another secondary oxidation process. This weaker oxidation ability (reaction (6)) causes slower chemosorption and covering the adsorbing sites with MnO_2 which leads to fast saturation of the residual adsorbent sites.

Effect of shaking speed

The experiments were carried out, with the change in the shaking speed from 50-300 minutes and maintaining constant adsorbent dosage from 12 g L^{-1} and the concentration of permanganate ion 150 mg L^{-1} at *p*H 3 for contact time 80 minutes as shown in Fig.5.

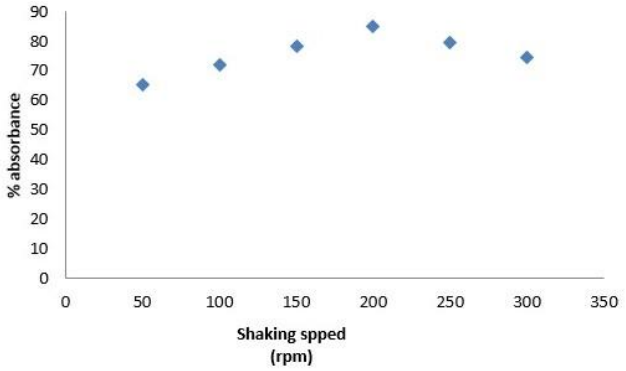

Figure 5. Effect of shaking time on the removal efficiency

The removal of permanganate ion has a maximum at 200 rpm. It means the diffusion rate of permanganate ion is lower than its consumption by the chemosorption process which will be equal around 200 rpm.

Table 2. Langmuir and Freundlich model parameters estimated from the fitting of experimental point of Mn (VII) adsorption

Langmuir isotherm			**Freundlich isotherm**		
R^2	q_{max}, mg g^{-1}	b, L mg^{-1}	R^2	K_f, mg g^{-1}	m
0.99	10.06	0.884	0.932	1.071	0.691

Conclusion

The present study concludes that the *Prosopis cineraria* leaf powder is an effective adsorbent for the removal of Mn (VII) from aqueous solution. Experimental data indicate that the adsorption efficiency is dependent on operating variable such as permanganate ion concentration, adsorbent dosage, *p*H, contact time and shaking speed.

The adsorption data fit well with Langmuir and Freundlich adsorption isotherm model. We can also suggest that main adsorption form is the chemosorption, but ion exchange and hydrogen bonding as secondary effects also plays important role in the removal of Mn(VII) species.

Acknowledgements

Chandresh Virvadiya and Sharda Kumari are thankful to the UGC, New Delhi for award of Junior Research Fellowship and Project Fellowship respectively.

References

[1]World Health Organization (WHO), *Guidelines for Drinking – Water Quality*, 3rd ed., Recommendations, Geneva, **2004**, *1*, 334.

[2]Paterson, J. W., *Wastewater Treatment Technology: Ann Arbour Science, Michigan*, **1975**, 43.

[3]Benito, Y. and Ruiz, M. L., *Desalination*, **2002**, *142*, 229.

[4]Fourest, E. and Roux, J. C., *Appl. Microbiol. Biotechnol.*, **1992**, *37*, 399.

[5]Reed, Brain, F., Arunachalam, Selvam and Thomas, B., *Environ. Progr.*, **1994**, *13(1)*, 60.

[6]Kuyucak, N. and Volesky, B., *J. Water Pollut. Res.*, **1988**, *23*,424.

[7]Yu, L. J., Shukla, S. S., Dorris, K. L., Shukla, A. and Margrave, J. L., *J. Hazard. Mater.*, **2003**, *27*, 56.

[8]Gupta, V. K. and Sharma, S., *Environ. Sci. Technol.*, **2002**, *36*, 3612.

[9]Kobya, M., Demirbas, E., Senturk, E. and Ince, M., *Bioresour. Technol.*, **2005**, *96*, 1518.

[10]Demirbas, E., Kobya, M. and Konukman, A. E. S., *J. Hazard. Mater.*, **2008**, *154*, 787.

[11]Gupta, S., Krishna, M., Prasad, R. K., Gupta, S. and Kansal, A., *Resour. Conserv. Recycl.*, **1998**, *24(2)*, 137.

[12]Robinson, T., Chandran, B., Nigam, P., *Water Res.*, **2002**, *36*, 2824.

[13]Sekhar, K.C., Chery, N. S., Kamala, C. T., Rao, J. V., Balaram, V. and Anjaneyuly, Y., *Environ. Int.*, **2003**, *29*, 601.

[14]Bhatnagar, A. and Minocha, A.K., *Indian J. Chem. Tech*., **2006**, *13*, 203.

[15]Babu, B. V. and Gupta, S., *Adsorption*, **2008**, *14*, 85.

[16]Eu, F. C., Tseng, R. L., Juang, R. S., *J. Environ. Manag.*, **2010**, *91*, 798.

[17]Sinha, R., Bhati, M., Sumit, Lal, M., and Gupta, V., *Indian J. Chem. Technol.*, **2013**, *20*, 312.

Received: 20.02.2014.
Accepted: 12.03.2014.

THERMODYNAMIC ANALYSIS OF THE Ti-O-C SYSTEM

Jondo Bagdavadze,[a] Zurab Tsiskaridze[a] and Ketevan Ukleba[a]

Keywords: thermodynamic analysis, carbothermal reduction, vacuum

Complete thermodynamic analysis of the system Ti-O-C both under pressure and vacuum resulted the following reaction: $TiO_2 + 3C = TiC + 2CO$. The basic results for all structures are presented in the form of diagrams (dependence of the contents of components on temperature range 1000-2300 K).

Corresponding Authors
Fax: +995 599 47 99 12
E-Mail: jondo_bagdavadze@hotmail.com
[a] F.Tavadze Institute of Metallurgy and materials science, Georgia, Tbilisi, Kazbegi str.#15

INTRODUCTION

Production of composite and nanostructural materials in most cases is realized through the reactions connected with reduction of oxides. Study of the processes of this type is one of the main tasks of theoretical and applied metallurgy.

Recent years are marked with intensive development of research of chemical and phase equilibrium in multicomponent and multiphase systems with the use of computer simulation technique (full thermodynamic analysis – FTA).[1,2] In particular great is the interest toward applying this approach[1] to studying the processes of producing composite and nanostructured materials.

It should be noted that the proposed method (FTA) gives an opportunity to control not only equilibrium conditions of the proceeding processes in the system, but also the mechanism of interaction of components in complicated systems and therefore, to correct structure of a final product.

FTA of interaction of titanium oxide (TiO_2) with carbon (C) was carried out at atmospheric pressure as well as in vacuum by the reaction:

$$TiO_2 + 3C = TiC + 2CO$$

Data on FTA of the considered system have not been found. Therefore results of the research of this specified system are of a great interest.

RESULTS AND DISCUSSIONS

Among the possible condensed components were considered: C, Ti, TiO, Ti_2O_3, TiO_2, Ti_3O_5, Ti_4O_7, TiC, $TiCO_{0,04}$, $TiC_{0.1}$, $TiC_{0.4}O_{0.6}$, $TiC_{0.75}O_{0.25}$; gaseous: O, O_2, O_3, C, C_2, C_3, C_4, C_5, CO, CO_2, C_2O, C_3O_2, Ti, TiO, TiO_2.

For research of balance of the specified reaction it is necessary to have a set of reliable data on thermodynamic properties of the elements and compounds, participating in the processes. However in the available reference books some data on thermodynamic properties (ΔH_{298}, T_m, C_p, C_{pl}) of those oxycarbides are absent.

With regard to the above mentioned there were estimated values of thermodynamic constants of oxycarbides and they were brought in the databank in ASTRA-4 program; estimation methods of the program were developed and described in Ref.[3] Main results of the provided FTA are presented in the form of charts.

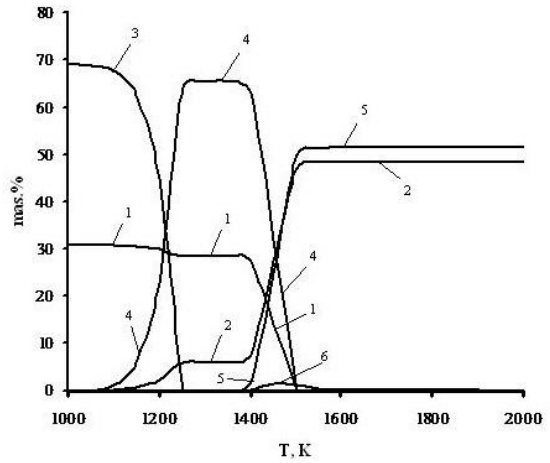

Figure 1. Temperature dependence of the comprised components at atmospheric pressure for reaction 1: 1-C; 2-CO; 3-TiO_2; 4-Ti_4O_7; 5-TiC; 6-$TiC_{0.75}O_{0.25}$

Fig. 1 presents a thermodynamic model of the carbothermal reduction process of TiO_2 (c) in the temperature range of 1000-2000 K at atmospheric pressure. Recovery of titanium starts at 1100 K with the formation of Ti_4O_7 (c) and CO in gaseous phase; content of TiO_2 (c) in the system starting from 1100 K sharply decreases and at ~ 1250 K completely disappears; in parallel, Ti_4O_7 (c) sharply increases to ~ 1250 K and further above 1350 K goes down to disappear at 1500 K. Carbothermal reduction of Ti_4O_7 (c) with the formation of TiC starts above ~ 1350 K and at 1550 K reaches maximum (~ 51.5 wt. %). Lower than 1500 K the condensed carbon disappears.

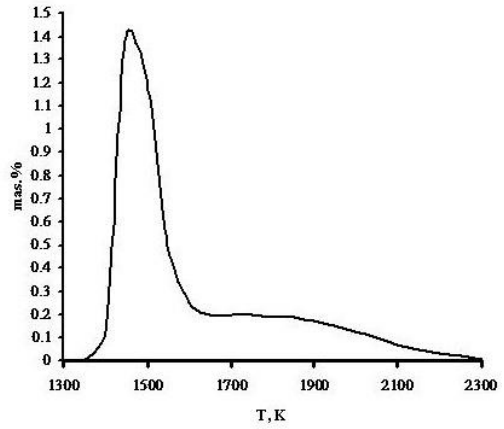

Figure 2. Temperature dependence of the content of oxycarbide ($TiC_{0.75}O_{0.25}$) at atmospheric pressure for reaction 1: 1-$TiC_{0.75}O_{0.25}$

Fig. 2 presents a separate chart of temperature dependent changes of the content of titanium oxycarbide. It is seen that starting from 1400 K oxycarbides release $TiC_{0.75}O_{0.25}$ in the system, reaching the maximum at 1450 K (~ 1.4 wt. %); above this temperature content of $TiC_{0.75}O_{0.25}$ sharply drops down to ~ 1600 K, and further smoothly decreases to ~ 2300 K (reaching 0.01 wt. %). Above 2300 K content of oxycarbide is of an order of 10^{-4} - 10^{-5} wt. %.

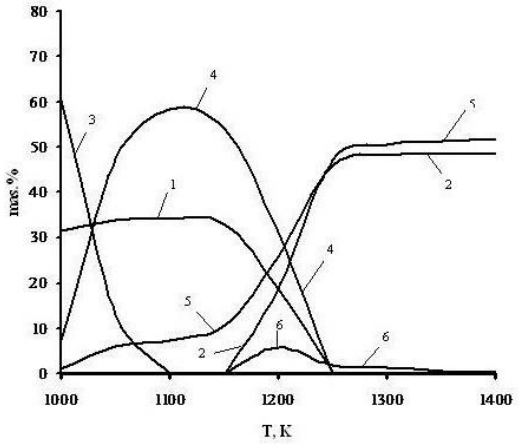

Figure 3. Temperature dependence of the content of components in vacuum (0.01atm) for reaction 1: 1-C; 2-CO; 3-TiO_2; 4-Ti_4O_7; 5-TiC; 6-$TiC_{0.75}O_{0.25}$

Fig. 3 presents a thermodynamic model of carbothermal reduction process of TiO_2 (c) in the temperature range 1000-1400 K in vacuum (0.01 atm). Recovery of the titanium starts at 1000 K with the formation of Ti_4O_7 (c) and CO in gaseous phase; content of TiO_2 (c) in the system sharply decreases and at ~ 1100 K completely disappears; in parallel, content of Ti_4O_7 (c) sharply increases to ~ 1100 K, further goes down and at 1200 K disappears. Carbothermal reduction of Ti_4O_7 (c) with the formation of TiC starts at 1200K and at 1350 K reaches maximum (~ 51.0 wt. %). Approximately above ~ 1250 K the condensed carbon disappears.

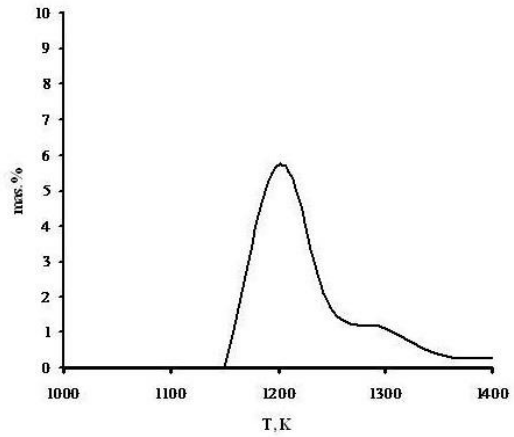

Figure 4. Temperature dependence of the content of oxycarbide ($TiC_{0.75}$ $O_{0.25}$) in vacuum (0.01atm) for reaction 1.

Fig. 4 presents a separate chart of temperature dependent changes of the content of titanium oxycarbide. It is seen that starting from 1150 K oxycarbides release $TiC_{0.75}O_{0.25}$ in the system, reaching the maximum at 1200 K (~ 5.7 wt. %); above this temperature content of $TiC_{0.75}O_{0.25}$ sharply decreases to ~ 1250 K, and further smoothly goes down to ~ 1400 K.

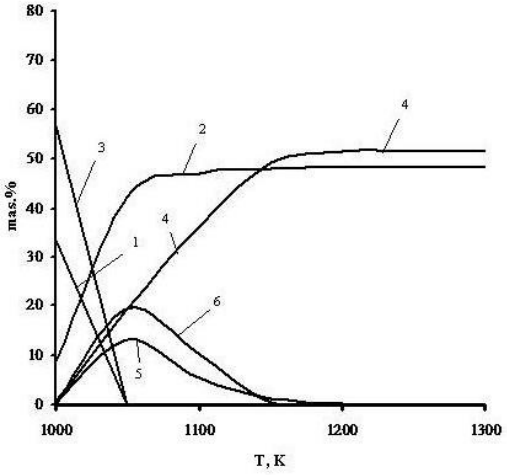

Figure 5. Temperature dependence of the content of components for reaction 1 in vacuum (0.01 atm): 1-C; 2-CO; 3-Ti_4O_7; 4-TiC; 5-$TiC_{0.75}O_{0.25}$; 6. $TiCO_{0.04}$

Fig. 5 presents a thermodynamic model of the carbothermal reduction process of TiO_2 (c) in the temperature range 1000-2300 K in vacuum (0.0001 atm).

Recovery of the titanium starts at temperature lower than 1000 K with the formation of Ti_4O_7 (c) and CO in gaseous phase; content of TiO_2 (c) in the system sharply decreases and at ~ 1050 K completely disappears; Carbothermal reduction of Ti_4O_7 (c) with the formation of TiC starts below~ 1050 K and at 1250 K reaches maximum (~ 51.5 wt. %). Below 1100 K the condensed carbon disappears.

 DOI: 10.17628/ecb.2014.3.319-321

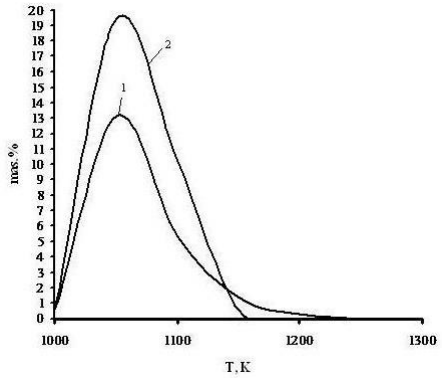

Figure 6. Temperature dependence of the content of oxycarbide in vacuum (0.0001 atm) for reaction 1: 1-$TiC_{0.75}O_{0.25}$; 2-$TiCO_{0.04}$

Fig. 6 presents a separate chart of temperature dependent changes of the content of titanium oxycarbide. It is seen that starting from 1000 K oxycarbides release $TiC_{0.75}O_{0.25}$ in the system, reaching the maximum at 1050 K (~ 13 and 19 wt. %, respectively); above this temperature the content of $TiC_{0.75}O_{0.25}$ sharply decreases to ~ 1200 K.

Issued from the thermodynamic analysis it is better to provide experiments in vacuum (< 0.0001 atm) as the process proceeds at lower temperatures.

REFERENCES

[1]Vatolin, N. A., Moiseev, G. K., Trusov, B. G., *Thermodynamic modeling in high-temperature inorganic systems*. M. Metallurgy **1994**, 352 pp.

[2]Voronin G. F. *Estimations of phase and chemical equilibrium in complex systems* //in book: Physical chemistry. Contemporary problems, M. **1984**, 112-143

[3]Gvelesiani G. G., Bagdavadze J. I., *Estimation methods for determining functions of inorganic materials and their application at full thermodynamic analysis of metallurgical processes*, Universal, **2006**, 127.

Received: 15.02.2014.
Accepted: 12.03.2014.

STUDIES ON HEAVY METAL AND HETEROCYCLIC COMPOUNDS CONTENT IN MILKFISH (CHANOS CHANOS) FRIED IN USED COOKING OIL

M. Sjahrul[a]

Keywords: fried milk fish; reused frying oil; nickel; 2-amino-1-methyl-6-phenyilimidazo[4,5-b]pyridine (PhIP).

This study is aimed to analyze the content of heterocyclic aromatic amine compounds along with heavy metals (Ni, Pb, Hg and Cd) in milkfish fried in used cooking oil. Chemical components were identified using gravity chromatography with Gel 60 as the stationary phase and purified by column Sephadex LH20, and checked by UV spectrometry, IR, and HPLC. The compound PhIP (2-amino-1-methyl-6-phenyilimidazo[4,5-b]pyridine) was found to be formed is thought to be caused by the influence of cooking oil. By atomic absorption spectrophotometer nickel (Ni) was found to have an average concentration of 1.6075 ± 0.2405 mg kg^{-1}. The role of nickel compounds in milkfish genotoxicity is suspected as a trigger effect on PhIP compound.

Corresponding Authors
E-Mail: eddievedder_jie@yahoo.com
[a] Faculty of Mathematic and Natural Sciences Hasanuddin University, Makassar, Indonesia.

INTRODUCTION

Some studies have shown that heterocyclic aromatic amines are formed during maturation process of protein containing foods such as meat and fish at high temperatures. Heterocyclic aromatic amines (HAA) were classified as endogenous compounds which are carcinogenic in animals, and capable of inducing and then developing into cancer.[1] Mortality of the Iceland population is very high due to gastric cancer in relation to consumption of smoked fish in their diet.[2] One example of HAA compounds found by Ito et al,[3] is 2- amino-1 methyl-6- phenylimidazo[4,5-b]pyridine (PhIP) as a carcinogen that induces lymphomas in mice, colon and breast tumors in female mice, and prostate tumor male rats.[3] HAA and PhIP are mutagenic even in small amounts and can be absorbed from food and are extensively activated by N-hydroxy derivatives, which are genotoxic by the enzyme cytochrome P 4501A.[4]

Carcinogenic HAA compounds are produced during the pyrolysis of creatine in muscles with amino acids from protein.[5] Heterocyclic aromatic amines are formed in a simulated mixture of free amino acids, creatine, and glucose from beef or chicken on heating at 200 ºC.[6] During cooking meat 17 different HAA compounds were identified as possible reason for risk of cancer in humans.[7]

The process of maturation of meat or fish by using direct fire can causes producing smoke containing polycyclic aromatic hydrocarbons (PAH) from fats drop onto the hot fire which can get attached to the surface of the food. These compounds are known to play a role in contributing to the inception of cancer. Baking meat produces PAHs which can also cause cancer by damaging DNA.[8]

Approximately 35 % cancer is caused from food each year.[9] In Indonesia, 182,000 women are diagnosed with breast cancer and 43,300 of them die in each year.[8]

Fish in South Sulawesi is a main menu which is generally cooked with spices, baked or fried.[10] In 2003, found that 93.9 % of respondents having breast cancer generally consumed more fried fish with using cooking oil. Used cooking oil is actually a vegetable oil that has peroxide bonding, and contains epoxides and other carcinogenic and mutagenic compounds.[11] It is, therefore, likey that the fish fried in cooking oil contains PhIP or 2-amino-1-methyl-6-phenylimidazo[4,5-b]pyridine compound.

MATERIALS AND METHODS

Milk fish from a farming area in South Sulawesi was randomly mixed, cleaned of scales and entrails and then washed. Fish was fried in used cooking oil at a temperature of 150-165 ºC until lightly browned.

Column chromatography with gravitational cross sections 2.5 and 1.25 x 50 cm x 30 cm was used. Agilent 8453 UV-Visible Spectrophotometer, Thermo Nicolet Avatar 360 FTIR infra red Spectrophotometer, HPLC (LC 10 ATP Shimadzu) and atomic absorption spectrophotometer (Varian spectra Aso and Shimadzu AA-6200) were used.

Silica gel 60 (E.Merck, 0.2-0.5 mm), Sephadex TMLH-20, NaOH (E.Merck), anhydrous Na_2SO_4, chloromethane (Univar), Methanol (Univar), Aqua and acetic acid (E.Merck).

Analysis of Heavy Metals

25 grams of milkfish collected from a pond were fried in used cooking oil and placed in a preheated oven at 375ºC till it were converted to ash. It was cooled and treated with 2-3 drops of concentrated HNO_3. The acidified ash was then

placed into the surface and heated again to white ash. The white ash was cooled and treated with 5 drops of 3 N HCl , filtered into 100 mL volumetric flask and then dipped in distilled water. Levels of Ni, Pb were determined at 235.6 nm and 217 nm, respectively using AAS.

Isolation and Identification of Chemical Components[12]

100 gram of fried milkfish was added to 300 ml of 5 % NaOH in a 2.5 liter beaker and the pH was adjusted to 12 with 30 % NaOH. The mixture was stirred continuously while adding 500 grams of silica gel till the resulting mixture became homogeneous. It was left for few minutes before introducing into the chromatography column (70 cm x 6 cm). Dichloromethane was then allowed to pass through the column with a speed of 5-10 ml min^{-1} for extracting neutral and alkaline fractions. After removing the organic phase with a rotary evaporator, it was dried by adding anhydrous Na_2SO_4. The residue was dissolved in 100 ml of HCl (0.1 N) to remove neutral components. Water solution was made up to pH 11 with 30 % NaOH, and the alkaline phase was extracted with 100 ml dichloromethane. The process was repeated 5 times. The organic phase, after being dried by addition of anhydrous Na_2SO_4, was extracted and the solvent was evaporated with a rotary evaporator. The residue was dissolved in 10 ml of methanol.

Alkaline extract was dissolved in methanol and 300-400 µL was injected into a glass column (40 cm x 9 mm) filled with Sephadex LH 20 resin. Operating conditions wwre as follows: solvent A: Water, solvent B: methanol containing 0.1 % acetic acid. The spectrum of each fraction was checked spectrophotometrically. The fractions were collected and then lyophilized on a freeze dryer, then identified UV,. IR and HPLC. The results are shown in Figure 1, Figure 2 and Figure 3.

RESULT AND DISCUSSION

Analysis of Heavy Metals by AAS

Samples were obtained from milkfish marketed by Makassar Fish Eagles, and were analysed for Pb, Ni, Hg and Cd content using atomic absorption spectrophotometry. Only metallic nickel was found to be present. The average nickel content in the samples was found to be 1.6075±0.2405 mg kg^{-1} (Table 1) and did not exceed the threshold value allowed by the Great Hall of the POM, which is 2 mg kg^{-1}.[13]

Table 1. Nickel content found in fried milkfish samples

Samples	Weight, g	Uptake, mg	Content, mg kg^{-1}	Average, mg kg^{-1}
1	25	0.0055	1.37	
2	25	0.0056	1.39	
3	25	0.0054	1.34	
4	25	0.0072	1.84	1.6075
5	25	0.0074	1.89	
6	25	0.0071	1.81	

Description: 1-6 is looping sampling

The presence of nickel in an average of 1.6075 mg kg^{-1} amount in fish could increase the intensity of gene mutations, because Ni compounds are carcinogenic that are either directly or indirectly bound to DNA. Ni levels were found are remained below the threshold value which is allowed by the Great Hall of the POM, but the long exposure can cause accumulation and ultimately an effective dose can be achieved that can cause mutations. Nickel metal analysis was conducted on the raw fish. Thus the existing contamination is thought to have come from farms which are likely to have compounds of nickel metal. Metal is thought to lead to the induction of gene mutations, adding to the effect of compound HAA[14] found that nickel compounds can increase the potential genotoxic effects.

Nickel subsulfide (Ni_3S_2) is mutagenic and nickel chloride ($NiCl_2$) can raise hydroxylation reaction of 2-deoxiguanosin (dG) of DNA which contribute to genotoxic and carcinogenic properties.[1,5] Nickel also plays an important role in the effect of oxidative stress and it has a potential as genotoxic.[16]

Analysis results of PhIP

Powdered fried milk fish was mixed with cooking oil and its chemical components were isolated following the method of Gross gives results in the form of a white powder which point is 302-304 ºC. White powder was then identified by spectrophotometry, HPLC and UV and IR. The resulting spectra is shown in Figures 1, 2 and 3.

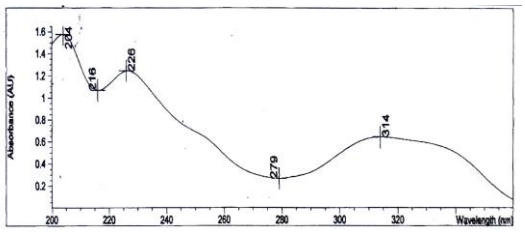

Figure 1. UV spectrum of PhIP isolated.

UV spectrum shows peaks (maximum) at λ_{max} at 204, 226, and 314nm, while the library value of PhIP is 203, 226, and 315 nm. The peak of the other heterocyclic amine compound such as AC (2-amino-3,4-dimethylimidazo[4,5-f] quinoline) peak occurs at 215, 257, and 337 nm, and that of MeIQx (2-amino-3,8-dimethylimidazo[4,5-f]quinoxalin) peaks are at 210, 264 and 336 nm. These data support the opinion that the detected compound is PhIP.

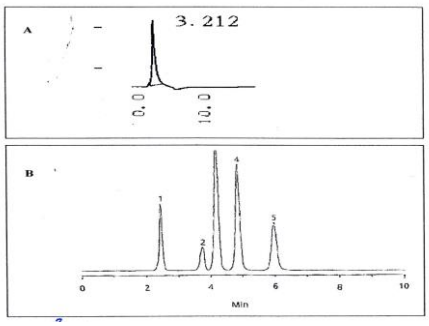

Figure 2. HPLC retention time curve PhIP compound (A) and some of the HAA compounds Instruments Data Bank (B). Note: 1 = AC, 2 = PhIP, 3 = IQ, 4 = MeIQ = 5, MeIQx

 DOI: 10.17628/ecb.2014.3.322-325

The analysis of HPLC retention times showed that the isolated compound of fried milkfish is PhIP. Other heterocyclic aromatic amines as AC (2-amino-9H-pyrido[2,3-b]indole, 2,4 min), IQ (2-amino-3-methyl-imidazo[4,5-f]quinoline, 4 min), 2-MeIQ (2-amino-3,4-di-methylimidazo[4.5]quinoline, 8 min) and finally MeIQx (2-amino-3,8-dimethylimidazo[4,5-f]quinoxaline, 6 min) retention times proved to be different.

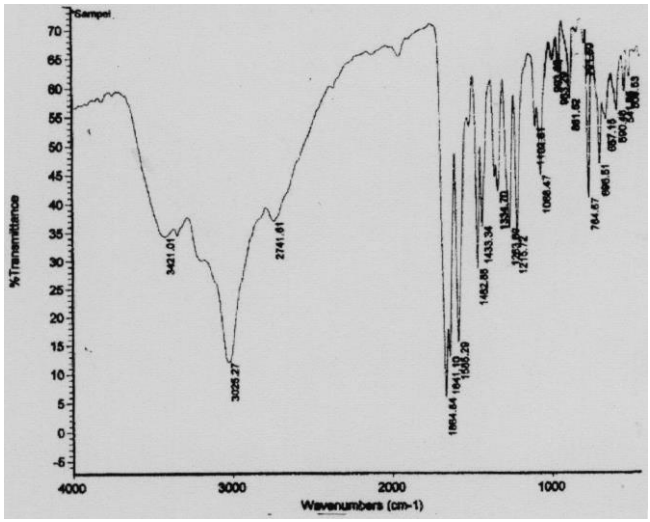

Figure 3. IR spectrum of isolated PhIP

The peaks found in the IR spectrum of isolated PhIP can be seen in Table 2.

The peak at 3421 cm^{-1} and at 1250 cm^{-1} in the IR spectrum of the isolated PhIP indicates the presence of NH_2 groups (primary amines) and the peaks at 3025.27 cm^{-1} and 1641.10 cm^{-1} show the presence of aromatic C-H. The peak at 2742 cm^{-1} belongs to N-CH_3. The peaks at 1433 and 1335 indicate the presence of-CH and -CH_3. The peak at 1585 cm^{-1} belong to an -N=N- group, while the peaks at 1665, 1433 791 and 657 cm^{-1} indicate the presence of pyridine ring.[17]

Milkfish obtained from several ponds contained nickel compounds - known carcinogens- can even strengthen the genotoxic effects of benzo[a]pyrene[14] and raise the hydroxylation reaction and deglycolization of 2-deoxiguanosin which can contribute to the genotoxic and carcinogenic effects of such metal compounds.[15]

The spectra suggested the presence of the suspected compound PhIP or 2-amino-6-phenylimidazo-1-metil-[4,5-b]pyridine. The UV spectrum showed a cluster of chromophores with spectral peaks at 204.226 and 314 nm corresponding to the known spectrum of PhIP at 203.226 and 315 nm). HPLC showed a retention time of 3.212 min (PhIP 3.60 min) and looks different from the other HAA compounds. IR spectra also showed the presence of an aromatic group, primary amine group, pyridine ring and -CH, -CH_3 and =N-CH_3 groups. The results obtained confirmed that the isolated compound is the suspected PhIP.

Table 2. Numbers of wave IR spectral peaks by intensity

Wave numbers, cm^{-1}	Intensity
1664.84	5.811
3025.27	11.998
1641.10	12.978
1585.29	15.516
1462.88	28.555
1215.72	34.180
3421.01	34.307
1263.69	35.634
1433.34	36.018
2741.61	36.911
764.57	40.715
1334.70	41.929
1068.47	44.727
696.51	46.659
1102.61	53.057
657.15	54.345
590.46	55.829
881.52	57.958
541.95	59.228
509.53	61.756
953.29	62.476
993.32	64.681
791.50	67.466

CONCLUSION

1. The analysis results showed the presence of nickel in fish which strengthens the genotoxic effects of heterocyclic aromatic amine compounds.

2. The analysis results showed the presence of carcinogenic 2-amino-1-methyl-6-phenylimidazol[4,5-b]pyridine (PhIP).

REFERENCES

[1]Baranczewski, P., Gustafsson, J. A., Moller L., *Int. Nature Chem.*, **2004**, *32*, 85-92

[2]Pitot, H. C., *Fundamentals of Oncology*, Marcel Dekker, Inc, N.Y and Basel,, **1981**, 29-80.

[3]Ito, N., *Carcinogenesis*, **1991**(12), 1503-1506.

[4]Zhu, H., Boobis, A. R., Goorderham, N .J., *Cancer Res.*, **2000**, *60*, 1283-1289.

[5]Schutt, H. A. J., Snyderwine, E. G., *Carcinogenesis*, **1999**, *20 (3)*, 353-368.

[6]Felton, J. S.,.Pais, P., Salmon, C. P., Knize, M. G., Z. *Lebensmittleuntersuch. Forsch. A*, **2004**, *207 (6)*,

[7]National Cancer Institute, *Heterocyclic Amine in Cooked Meats*, **1996**.

[8]*http://www.cancer.gov/cancertopics/factsheet/Risk/cooked-meats* 2002 .

[9]Dool, R., Peto, R., *The Cause of Cancer*, New York : Oxford University Press, **1981**, *123.*

[10]Djabrud, L., *Studi Kasus Faktor Resiko yang berhubungan dengan insiden Kanker Payudara di RSUP Dr. Wahidin Sudirohusodo tahun 2000,* Skripsi Jurusan Farmasi FMIPA UNHAS, **2005**.

[11]*Dibalik gurihnya minyak goreng jelantah. Merangsang kanker kolon.*, Info Teknologi Pangan, Dept. Food Sci. Technol., **2005**.

[12]Gross, G. A., *Carcinogenesis*, **1990**, *11* (9), 1597 – 1603.

[13]Dirjen P. O. M., *Kumpulan Peraturan Perundang-undangan Bidang Makanan. Ed 3.*, Departemen Kesehatan RI., **1998**, 272.

[14]Deng, D. Z., Fons, M. P., Rosenblatt, J., El-Zein, J. A., Abdelrahman, S. Z., Albrecht, T., Environ. Mol. Mutagen., **2005**, *3*, 150-161.

[15]Kasprzak, K. S., Hernandez, L., *Cancer Res.*,, **1989**, *49*, 5964-5968.

[16]Sabu, E.F., Sjahrul, M., Hatta, M., Ahmad, A., *Componential Analysis 7 Chemical Consinogen in Fried Milkfish (Chanos Chanos) and Its Mechanism as Risk Factor of Breast Cancer*, **2007**.

[17]Silverstein, R. M., Clayton, G. B., Terence, C. M., *Penerbit Erlangga Jakarta*, **1986**, *95-179*, 305-314.

Received: 14.01.2014.
Accepted: 12.03.2014.

DETERMINATION OF TRACE OF HEAVY METALS IN WATER SAMPLES BY ATOMIC SPECTROMETRY BY PRECONCENTRATION WITH SOFT HUSK OF PISTACHIO

Mehdi Ghodsbin[a], Hassan Zavvar Mousavi[a]* and Aisan Khaligh[a]

Keywords: Preconcentration, Heavy metals, Pistachio husk, FAAS

This study uses solid phase extraction method to measure trace amount of metal ions of Cd^{2+}, Pb^{2+}, Cu^{2+}, Ni^{2+} and Zn^{2+} in aqueous samples by using herbal absorbent called soft husk of Pistachio. To do so, aqueous solution of these metal ions was passed through a column containing adsorbent. Meanwhile, existing metal ions in solution were adsorbed, and then preconcentrated via eluting by nitric acid. Finally, they were measured by Flame Atomic Absorption Spectrometry (FAAS). Effective parameters such as pH, amount of adsorbent, volume and concentration of eluent, velocity of solution and interfering ions were examined Calibration curve related to metal ions: lead, nickel, cadmium, copper and zinc in the range of 30-800, 10-400, 5-90, 10-350 and 5-90 μg L^{-1} was linear and the limits of detection for metal ions lead, nickel, cadmium, copper and zinc were respectively: 2.581, 0.988, 0.139, 0.527 and 1.385 μg L^{-1}. The proposed method was applied to measure metal ions in real samples with acceptable accuracy.

Corresponding Authors
Tel: +98 231 3366194
Fax: +98 231 3354110
E-Mail: hzmousavi@semnan.ac.ir
[a] Department of Chemistry, College of Science, Semnan University, Semnan, Iran. Zip Code: 35131-19111

Introduction

Industrial sewerages resulting from different factories are among the main pollution sources of heavy metal.[1-4] Due to toxicity and damaging effects of heavy metals, removing their ions is a concern for many of environmental studies.[5] Lead is the most common toxic heavy element in the environment.[6] Cadmium compounds in mines, galvanizing, paint making are of its polluting sources in environment.[7] Over-absorption of cupper in human body causes intense mucus corrosion, extensive capillary, digestion system, and central neural system damages, and lead to depression.[8] Over-absorption of zinc makes skin urticarial, vomit, nausea, and anemia.[9] Nickel sources include fossil fluids burned in power plants, mines, and refineries.[10,11] Due to harming effects of heavy metals, various methods are presented to remove them including chemical sedimentation, reverse osmosis ion exchange, adsorption etc.[12-15] One of the most applicable methods is adsorption.[16] There is a need for sample preparing methods because direct measurement of heavy metal ions in complex matrices is limited due to low concentrations and matrix disruption,[17,18] which extracting method is one of the most basic methods. Specimen values are used for separating and pre-concentrate from the sample blank. Common extracting methods, such as Soxhlet, liquid-liquid extraction (LLE), are usually time consuming and require a large volume of toxic solution.[19, 20] It is emphasized on limited use of these solutions because of their destroying effects on environment.[21] According to these facts, SPE is a proper and effective technic in which extracting is easy and fast, and is capable of being automate. It consumes less time and solution than other methods such as LLE.[22] The aim of the present paper is to optimize the various experimental working conditions in the processes of preconcentration of analytical ions from water samples collected from different locations followed by AAS determinations.

Materials and methods

Preparation of adsorbent

After collecting soft husk pistachio from Damghan City, we eluted it with natural water and then triple-distillated water. Then, we dried it in oven at 100 °C, and next we pulverized it with mill. The powder is used as adsorbent after sieving the powder with mesh-16 sieve. Fig. 1 shows scanning electron microscopy (SEM) images of adsorbent before adsorption.

Chemicals and apparatus

All solutions for experiments were prepared using metal ions nitrate salts (Merck, Darmstadt, Germany) by dissolving the analytical grade sample in distilled water. The buffer solutions were prepared from formic acid for pH 2–4, from acetic acid for pH 5–6, from phosphate for pH 7, and from ammonium for pH 8–10.The pH measurements were made with a pH-meter (W3B, Italy) and analysis of Cd (II), Pb(II), Ni(II), Cu(II) and Zn(II) was performed by SHIMADZU AA-680 flame atomic absorption spectrophotometer. A Thermoelectric Auto Sampling pump model AS-21P was used for passing sample solutions through a column containing adsorbent.

A syringe tube (58 mm × 8 mm i.d.) with a fine bore packed with cotton was used as a preconcentration column. The column loaded with adsorbent was lightly compressed with the flat end of a plastic rod so that its height would be about 18 mm.

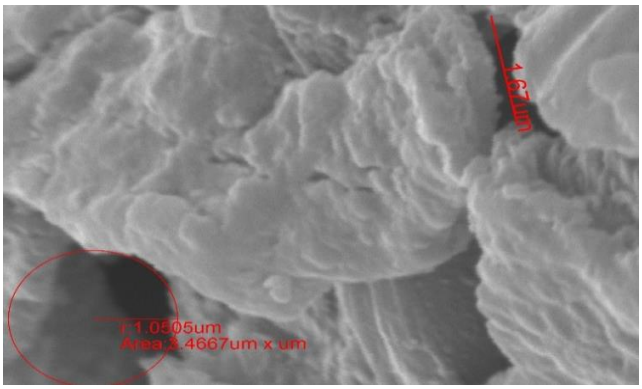

Figure 1. scanning electron microscopy (SEM) images of adsorbent before adsorption.

Recommended procedure

Initially, for column conditioning, distilled water was passed through the column. To measure negligible amounts of heavy metal ions of lead, copper, cadmium, zinc, and nickel, an aqueous solution is prepared with volume of 50 mL and concentration of 50 µg L^{-1} for each ion, containing 5 mL buffer solution to stabilize pH=6. Then, this solution is passed through a column containing 0.3 g of adsorbent, which its bottom is closed by some cotton, by a pump with flow rate of 5 mL min^{-1}. Next, the column is washed by 3 mL of nitric acid of 1.5 molar. Finally, adsorption of considered ions in recovery solution is measured by Atomic Absorption Spectrometer.

Results and Discussion

Effect of solution pH

pH is among effective factors in adsorption process.[23] Particularly, pH influences adsorption capacity. Amount of ion adsorption on adsorbent's surface is affected by adsorbent's surface charge, which is influenced by pH of solution.[24] In this study, pH of metal ions solution is adjusted by Buffer solutions, and effect of pH on adsorption of metal ions is studied in the range of pH=2 to 10. Figure 2 shows that maximum recovery is for pH=6. According to competitiveness between H^+ ion and cations, more basic pH leads to more recovery in lower ranges of pH. In other hand, in basic pH range recovery reduces, due to formation of metallic cation compounds, adsorbed not very well on the surface of adsorbent.

Effect of mass of adsorbent

In order to study the effect of this parameter, six solution samples with volume of 50 mL is prepared, containing 5mL of Buffer to stabilize pH in the optimum state (pH=6). They contain metal ions with concentration of 50 µg $^{L-1}$. These solutions pass a pump in flow rate of 3.5 mL min^{-1} through prepared columns containing different values of adsorbent (0.05 - 0.3g). After eluting it with 3 mL of nitric acid of 1.5 mol L-1 concentration, it is measured by atomic absorption spectrometer. As shown in Figure 3, adsorption and recovery increase by increasing adsorbent amount because of enhancing area of adsorbent surface and adsorption sites. Amount of 0.3g adsorbent is chosen as optimum value.

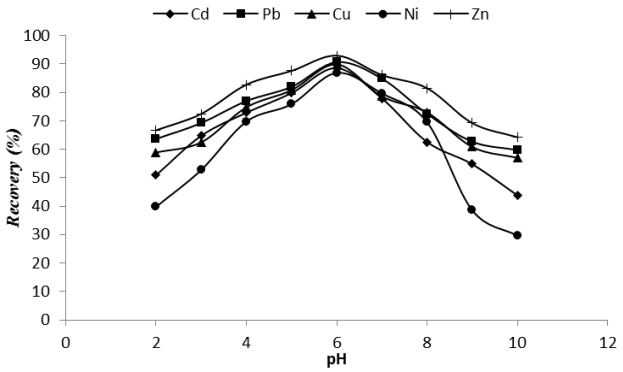

Figure 2. Effect of solution pH. *Experimental conditions*: 50 mL of sample containing 50 µg L^{-1} metal ions, sorbent, 0.2 g, eluent 3 mL of 1.5 mol L^{-1} HNO_3 and flow rate 3.5 mL min^{-1}.

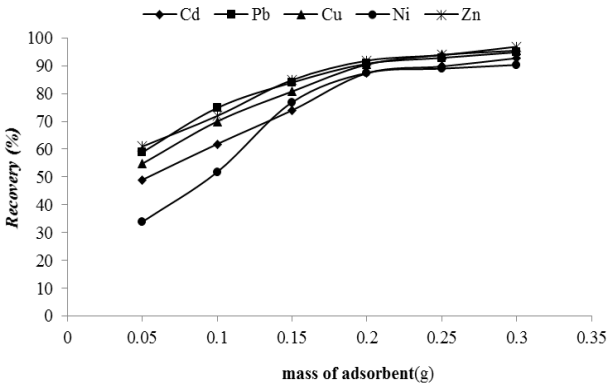

Figure 3. Effect of mass of adsorbent. *Experimental conditions*: 50 mL of sample containing 50 µg L^{-1} metal ions, eluent 3 mL of 1.5 mol L^{-1} HNO_3 and flow rate 3.5 mL min^{-1}

Elution

Selecting appropriate eluent is so important, because it should have three features: efficiency, selectivity, and compatibility. To select proper eluent for desorption of metal ions from adsorbent surface, effect of 3 mL of eluents, such as nitric acid, hydrochloric acid, and sulfuric acid with concentration of 1.5 M is examined. Using nitric acid, as an eluent, leads to formation of metal cations nitrates. Nitrate has more solubility than sulfates and chlorides of metal cations, formed because of elution with hydrochloric and nitric acids. As seen in Figure 4 and Table 1, nitric acid has the most recovery extent, and so, this solvent is chosen as proper eluent for next steps.

In one side, volume of eluent should reach an amount that is able to desorb analyte ions, in the other hand, enhancing volume of eluent reduces concentrate factor. Thus, this parameter is investigated.

Table 1. Effect of different eluent on recovery of analytes.

Eluent	Recovery, %				
	Pb	**Zn**	**Cu**	**Ni**	**Cd**
HNO_3	94.7989	96.0866	95.9643	91.0964	93.0643
HCl	89.7432	90.5434	88.7532	86.9653	87.8654
H_2SO_4	80.8542	79.7439	83.9653	85.9654	78.0755

Experimental conditions: 50 mL of sample containing 50 µg L^{-1} metal ions at pH 6, sorbent, 0.3 g, eluent 3 mL of 1.5 mol L^{-1} different eluent and flow rate 3.5 mL min^{-1}.

To optimize eluents' volume, regarding to simultaneous measuring of 5 metal ions, volumes of 3, 4, and 5 mL is studied. According to Fig.5, the maximum adsorption extent is observed for 3 mL of eluent volume. However, the recovery is same for all three volumes. Hence, volume of 3 mL is used as optimum value for next stages, in a view that enhancing volume of eluent decreases the concentrate factor.

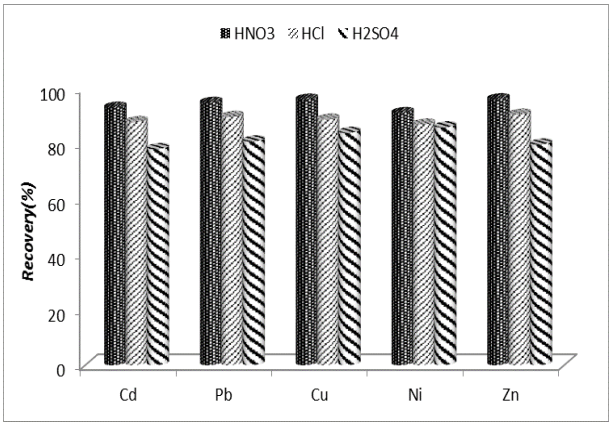

Figure 4. Effect of different eluent on recovery of analytes. *Experimental conditions*: 50 mL of sample containing 50 µg L^{-1} metal ions at pH 6, sorbent, 0.3 g, eluent 3 mL of 1.5 mol L^{-1} different eluent and flow rate 3.5 mL min^{-1}

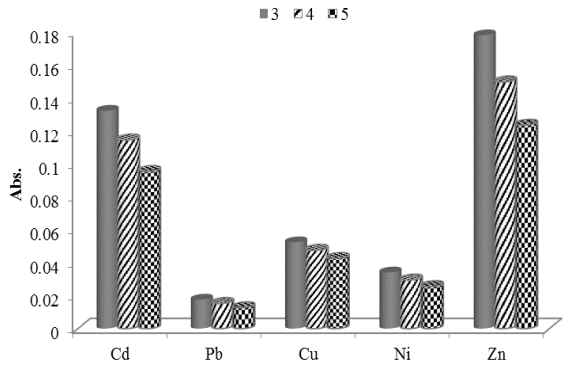

Figure 5. Effect of eluents' volume on recovery of analytes. *Experimental conditions*: 50 mL of sample containing 50 µg L^{-1} metal ions at pH 6, sorbent: 0.3 g, eluent: different volum of 1.5 mol L^{-1} HNO_3 and flow rate 3.5 mL min^{-1}

Concentration effect of nitric acid, on recovery level of metal cations, is examined. In this study, desorption is tested by 3 mL of HNO_3 with different concentrations (0.5-4 M), and concentration of 1.5 M is picked out as optimum eluent concentration considering the results (Fig. 6).

Effect of flow rate of sample

In the SPE method, rate of sample solution is one of the most important parameters affecting both return efficiency of analytes and extracting time.[25]

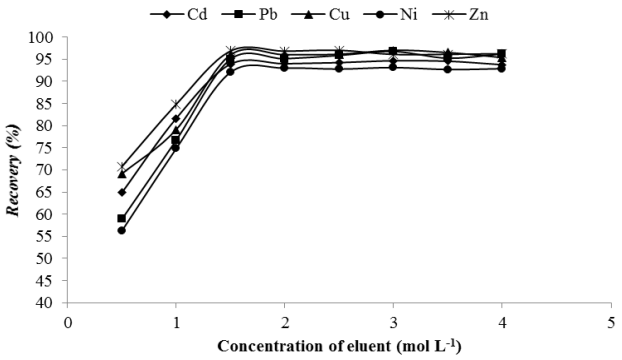

Figure 6. Effect of eluent concentration. *Experimental conditions*: 50 mL of sample containing 50 µg L^{-1} metal ions at pH 6, sorbent, 0.3 g, eluent 3 mL of different concentration HNO_3 and flow rate 3.5 mL min^{-1}

Effect of sample solution rate is examined in the range of 1-8 mL min^{-1}. To do this, solutions with size of 50 mL are passed through columns in optimum conditions with different rates. After elution and desorption of analytes by 3 mL nitric acid of 1.5 Molar, Atomic absorption spectrometer measures them.

As shown in Figure 7, rates more than 5 mL min^{-1} cause to reduce in recovery of considered cations. Therefore, we choose flow rate of 5 mL min^{-1} as optimum rate for next steps.

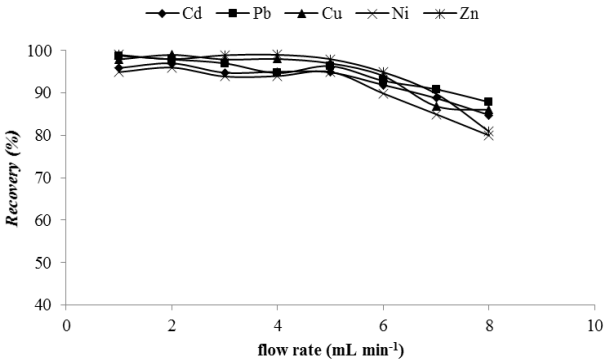

Figure 7. Effect of flow rate of sample. *Experimental conditions*: 50 mL of sample containing 50 µg L^{-1} metal ions at pH 6, sorbent, 0.3 g, eluent 3 mL of 1.5 mol L^{-1} HNO_3

Effect of interfering ions

In this section, interfering effect of other ions, as well as interfering effect of considered cations extracted simultaneously, on recovery of analyte on adsorbent is examined in optimum conditions. Allowed error for ion's concentration is determined less than ±5% for pre-concentrate and measuring analytes. Interfering ion refers to an ion that makes a change more than allowed error in recovery extent. Table 2 lists the results.

Due to results, mentioned ions have no interfering effect on recovery of analyte ions.

Table 2. Tolerance limits for coexisting ions in adsorption of 50 μg L^{-1} of Zn, Pb, Cu, Cd and Ni.

Foreign ions	Interferent /ion ratio				
	Cu^{2+}	Pb^{2+}	Ni^{2+}	Zn^{2+}	Cd^{2+}
Zn^{2+}	500	1000	500	-	500
Pb^{2+}	500	-	1000	500	1000
Cu^{2+}	-	500	500	1000	500
Ni^{2+}	1000	1000	-	1000	1000
Cd^{2+}	1000	1000	500	1000	-
Ag^{+}, Ca^{2+}, Na^{+}, Mn^{2+}, Cr^{3+}, Cl^{-}, Li^{+}, NO_3^{-}, Fe^{2+}, K^{+}, Br^{-}, CH_3COO^{-}	1000	1000	1000	1000	1000
$S_2O_3^{2-}$	500	250	1000	1000	1000
F^{-}	500	1000	1000	1000	1000
Co^{2+}	1000	1000	500	1000	1000
Mg^{2+}	1000	1000	1000	500	1000
Al^{3+}	500	1000	250	100	100
I^{-}	1000	500	1000	1000	1000

Table 3. Analytical characteristics of proposed method at the optimum conditions.

Ions	Linear range, μg L^{-1}	Regression equation	Correlation coefficient (*r*)	*LOD*, μg L^{-1} (*n* = 10)	R.S.D., % (*n*= 10)
Ni^{2+}	10-400	y=0.0016x+0.0032	0.9996	0.988	1.682
Pb^{2+}	30-800	y=0.0006x+0.0031	0.9992	2.581	2.151
Zn^{2+}	5-90	y=0.0086x+0.206	0.9996	1.385	2.276
Cu^{2+}	10-350	y=0.0024x-0.0007	0.9995	0.527	0.928
Cd^{2+}	5-90	y=0.0104x+0.0045	0.9998	0.139	1.202

Effect of sample volume

To study concentrate capability of analyte, effect of sample volume on recovery of considered ions is examined by passing various sample volumes (50-750 mL) with optimum flow rate (5 mL) through columns containing 0.3 g of adsorbent, in which each pH of solution is stabilized by adding proper amount of Buffer in optimum condition.

According to Fig. 8, adsorption is done well, with up to 400 mL of solution containing heavy metal ions. Then, adsorbed ions are eluted by 3 mL of nitric acid 1.5 molar. The resulted pre-concentrate factor is 133.

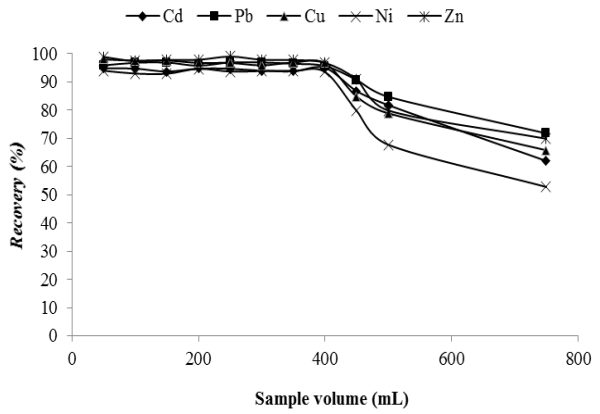

Figure 8. Effect of sample volume. *Experimental conditions*:, sorbent, 0.3 g, eluent 3 mL of 1.5 mol L^{-1} different eluent and flow rate 5 mL min^{-1}

Detection limit

Detection limit is the least concentration or amount, which is traceable by analytical method with a certain assurance. Based on IUPAC recommendation, signal of detection limit is average value of instance plus thrice of its standard deviation.

$$LOD = \frac{3S_b}{m} \quad (1)$$

where,

S is standard deviation, and

m is calibration curve slope.[26]

By this way, 10 solutions of triple-distillated water of 50 mL volume are pre-concentrated in optimum solution, and measured by atomic absorption spectrometer. Results are listed in Table 3.

Measuring metal cations in real samples

Based on obtained optimum conditions, proposed method is employed to measure considered metal cations in three real samples. To do this, columns containing 3 g of adsorbent is prepared, and 50 mL of real sample solution are passed through them with flow rate of 5 mL min^{-1}. Pre-concentrate method is used too. That is, after passing the solution, columns are eluted by 3 mL of 1.5 molar nitric acid and atomic absorption spectrometer measures concentration of metal cations.

 DOI: 10.17628/ecb.2014.3.326-332

Table 4. Comparing results of preconcentration factor and detection limit of current work with other works.

Analytical ions	Method/Instrumental	Preconcentration factor	Detection limit µg L^{-1}	References
Ir(III)	SPE on naphthalene/spectrophotomety	40	20	[27]
Ni(II)	SPE on MIP/spectrometry	72.66	0.3	[28]
Cd(II)	SPE on naphthalene/DDP	40	70	[29]
Cu(II)	SPE on mini column of sisal fiber/FAAS	75	0.01	[30]
In(III)	SPE on naphthalene/DDP	25–50	200	[31]
Co(II)	SPE on surfactant-coated alumina/AAS	100	-	[32]
Cr(III)	SPE on activated carbon/FAAS	50	0.27	[33]
Cd(II), Pb(II), Cu(II), Ni(II), Zn(II)	SPE on soft husk of Pistachio/FAAS	133	0.13-2.58	Present work

SPE: solid phase extraction, MIP: molecularly imprinted polymers, DDP: differential pulse polarography, AAS: atomic absorption spectrometry

Table 5. Analytical result for determination of metal ions in tap water from Tehran city

Ions	Added, µg L^{-1}	Found, µg L^{-1}	RSD, %	Recovery, %
	-	n.d.	-	-
Cd^{2+}	50	52.14	2.141	104.28
	100	101	1.429	101.0
	-	8.98	3.978	-
Pb^{2+}	50	58.85	3.890	99.74
	100	109.0	2.561	100.02
	-	18.79	3.988	-
Cu^{2+}	30	48.1	3.521	97.70
	60	78.51	1.926	99.53
	-	n.d.	-	-
Ni^{2+}	75	75.42	3.951	100.56
	150	149.38	3.891	99.58
	-	16.05	1.091	-
Zn^{2+}	25	43.15	0.633	108.4
	50	66.12	0.581	100.14

Table 6. Analytical result for determination of metal ions in mineral water

Ions	Added, µg L^{-1}	Found, µg L^{-1}	RSD, %	Recovery, %
	-	-	-	-
Cd^{2+}	75	76.50	1.952	102.0
	150	155.21	1.614	103.47
	-	-	-	-
Pb^{2+}	75	76.10	3.921	101.46
	150	150.0	3.031	100.0
	-	7.512	4.012	-
Cu^{2+}	50	57.42	3.029	99.82
	100	107.55	3.321	100.04
	-	-	-	-
Ni^{2+}	75	75.03	4.258	100.04
	150	150.12	4.012	100.08
	-	23.20	1.234	-
Zn^{2+}	50	73.08	0.439	99.76
	100	124.5	0.331	101.3

Table 7. Analytical result for determination of metal ions in well water from Semnan city

Ions	Added (µg L^{-1})	Found (µg L^{-1})	RSD(%)	Recovery(%)
	-	0.654	3.152	-
Cd^{2+}	75	76.0	1.823	100.46
	150	150.98	1.021	100.22
	-	n.d.	-	-
Pb^{2+}	75	76.5	4.080	102.0
	150	149.4	3.120	99.60
	-	6.814	4.112	-
Cu^{2+}	50	56.94	3.021	100.26
	100	108.01	2.890	101.20
	-	n.d.	-	-
Ni^{2+}	75	74.10	4.150	98.80
	150	150.0	3.980	100.0
	-	14.701	2.354	-
Zn^{2+}	50	62.94	0.951	96.48
	100	115.01	0.873	100.31

Here, to verify results, we apply standard addition method. Hence, we add a certain amount of standard metal cations solution to sample solution, and pass it through column again. Tables 5 to 7 list the results. As results show, the observed value is almost equal to initial value of metal cation plus the added amount that demonstrates accuracy of method.

Conclusion

In this study, the wastage of soft husk of pistachio was used as an absorbent. Preparation of absorbent out of this wastage is easy and considering of the fact that the wastage of soft husk of pistachio has no function except being animals' food, its consumption is economical. Effective parameters were optimized and a high retrieval for metal ions from water solution was gained. The speed of optimal flow equaled 5 ml min; therefore we need a short time to analyze the samples. Concentration factor (133) was suitable and the result of examination of efficiency number and measurement of heavy metals in real samples approved the validity and accuracy of this method.

References

[1]Goksungur, Y., Uren, S., Guvence, U., *Bioresour. Technol*. **2005**, *96*, 103-109.

[2]Khraisheh, M. A. M., Al-degs Y. S, Meminn, W. A. M., *J. Chem. Eng*. **2004**, *99*, 177–184.

[3]Sekhar, K. C., Kamala, C. T., Chary, N. S., Sastry, A. R. K., *J. Hazard. Mater.* **2004**, *108*, 111-117.

[4]Mohammadi, T., Moheb, A., Sadrzadeh, M., Razmi, A., *Sep. Purif. Technol*. **2005**, *41*, 73–82.

[5]Mulligan, C. N., Yong, R. N., Gibbs, B. F., *Eng. Geol*. **2001**, *60*, 193–207.

[6]Naseem, R., Tahir, S. S., *Water Res*. **2001**, *35*, 3982-3986.

[7]Ahluwalia, S. S., Goyal, D., *Bioresour. Technol*. **2007**, *98*, 2243-2257.

[8]Habib, A., Wahiduzzaman, M., Rashid, H. O., *J. Anal. Environ. Chem*. **2008**, *9*, 6-10.

[9]Nriagu, J. O., Pacyna, J. M., *Nature* **1988**, *333*, 134-139.

[10]Kersten, M., Vlasova, N., *Appl. Geochem*. **2009**, *24*, 32-43.

[11]Yu, Q., Kaewsam, P., *Sep. Sci. Technol*. **2000**, *35*, 689–701.

[12]Mellah, A., Chegrouche, S., Barkat, M., *J. Colloids Interf Sci*. **2006**, *296*, 434–441.

[13]Prasad, M., Saxena, S., *Ind. Eng. Chem. Res*. **2004**, *43*, 1512–1522.

[14]Liu, C. C., Wang, M. K., Li, Y. S., *Ind. Eng. Chem. Res*. **2005**, *44*, 1438-1445.

[15]Özcan, A., Özcan, A. S., Tunali, S., *J. Hazard. Mater*. **2005**, *124*, 200-208.

[16]Kobya, M., *Adsorpt. Sci Technol*. **2004**, *22*, 51–64.

[17]Pyrzynska, K., *Crit. Rev. Anal. Chem*. **1999**, *29*, 313–321.

[18]Cai, Y., Q., Jiang, G., B., Liu, J. F., Zhou, Q. X., *Anal. Chem*. **2003**, *75*, 2517–2521.

[19]Smith, R. M., *J. Chromatogr. A* 2003, *1000*, 3-27.

[20]Majors, R. E., *LC-GC Int*. **1991**, *4*, 10-14.

[21]Pawliszyan, J., *Anal. Chem*. **2003**, *75*, 2543-2558.

[22]Mahmoud, M. E., Kenawy, I. M. M., Hafez, M. M. A. H., Lashein, R. R. *Desalination* **2010**, *250*, 62-70.

[23]Nie, R., Chang, X., He, Q., Hu, Z., Li, Z., *J. Hazard. Mater*. **2009**, *169*, 203-209.

[24]Pourreza, N., Parham, H., Kiasat, A. R., Ghanemi, K., *Talanta* **2009**, *78*, 1293-1297.

[25]Unuabonah, E. I., Adebowale, K. O., Olu-Owolabi, B. I., Yang, L. Z., Kong, L. X., *Hydrometallurgy* **2008**, *93*, 1-9.

[26]Langmuir, I., *J. Am. Chem. Soc*. **1918**, *40*, 136–403.

[27]Taher, M. A., Puri, S., Bansal, R. K., Puri, B. K., *Talanta* **1997**, *45*, 411–416.

[28]Ersöz, A., Say, R., Denizli, A., *Anal. Chim. Acta* **2004**, *502*, 91–97.

[29]Taher, M. A., *Turk. J. Chem*. **2003**, *27*, 529–537.

[30]Dias, F. D. S., Bonsucesso, J. S., Oliveira, L. C., Santos, W. N. L. D., *Talanta* **2012**, *89*, 276– 279.

[31]Taher, M. A., *Talanta* **2000**, *52*, 301–309.

[32]Manzoori, J. L., Sorouradin, M. H., Shabani, A. M. H., *Microchem. J*. **1999**, *63*, 295–301.

[33]Duran, C., Ozdes, D., Gundogdu, A., Imamoglu, M., Senturk, H. B., *Anal. Chim. Acta* **2011**, *688*, 75–83.

Received: 24.02.2014.
Accepted: 13.03.2014.

SYNTHESIS OF SOME SUBSTITUTED PYRAZOLO[4,3-c]PYRIDINE-3-OLS AS A NOVEL FUSED HETEROBICYCLES

P. Karthikeyan[a], V. Vijayakumar*,[a] and S. Sarveswari[a]

Keywords: 4-oxo-N,2,6-triphenylpiperidine-3-carboxamides, 4,5,6,7-tetrahydro-4,6-diphenyl-2*H*-pyrazolo[4,3-c]pyridine-3-ols, 4,5,6,7-tetrahydro-2,4,6-triphenyl-2*H*-pyrazolo[4,3-c]pyridine-3-ols.

The 4-oxo-N,2,6-triphenylpiperidine-3-carboxamides (**1a-f**) were synthesized using arylaldehydes, ammonium formate and acetoacetanilide, which in turn converted into 4,5,6,7-tetrahydro-4,6-diphenyl-2*H*-pyrazolo[4,3-c]pyridine-3-ols (**2a-f**) and 4,5,6,7-tetrahydro-2,4,6-triphenyl-2*H*-pyrazolo[4,3-c]pyridine-3-ols (**3a-f**), by condensing with hydrazine hydrate or phenylhydrazine, respectively. .

* Corresponding Authors
Fax: +91 416 220 3091
E-Mail: kvpsvijayakumar@gmail.com
[a] Centre for Organic and Medicinal Chemistry, VIT University, Vellore-632014, Tamilnadu, India.

Introduction

Heterocyclic systems with piperdin-4-one nucleus was an interesting subject area of research in the past and recent years due to their various biological properties such as antiviral, anti-inflammatory, local anesthetic, anticancer, antimicrobial activity.[1-5] One of the piperidine derivative, piperidones were also biologically important and act as neurokinin receptor antagonists, analgesic and anti-hypertensive agents.[6-12] The importance of piperdin-4-one as intermediates in the synthesis of a diversity of compounds with potent physiological activity has been reviewed by Prostakov and Gaivoronskaya.[13] The studies undertaken on 4-piperidones have direct relation to the synthesis of drug molecules. The effect of substituent at second, third and sixth position particularly, aryl substituent at second and/or sixth positions with regard to its biological activity have been well documented. Therefore, the institution of general methods for the synthesis of piperidone has been the topic of considerable synthetic effort.[14-19] N-Benzyl-β-chloro propionamide was a well-proven anticonvulsant agent and marketed under the trade name Hibicon and Hydrae.

The aryl piperidine scaffold was a key factor involved in binding to a diverse receptors and therefore can be named as a privileged vast array of piperidine containing compounds, both natural and synthetic, for their biological and medicinal interest and this had led to the development of many synthetic approaches to these scaffolds.[20] However, the biological properties of piperidines are highly dependent on the type and locations of substituent on the heterocyclic ring continue to drive the search for new methodologies. Therefore, keen care has been compensated to the construction of functionalized piperidines and its synthetic methodologies. It is noteworthy that 4-arylpiperidine was an important structural motif in many biologically active compounds, including paroxetine, femoxetine, Roche-haloperidol, and meperidine.[21] Similarly imidazole, oxazole and pyrazole were also exhibiting several activities and the fused bicycles of 4-piperidones with imidazole, pyrazole, and oxazole are not available in the literature and hence this prompted us to carry out the synthesis of fused heterocycles with 4-piperidone moiety with other heterocycles.

Experimental

General Procedure for the synthesis of (1a-f)

Dry ammonium formate (0.01 mol, 0.63 g) was dissolved in ethanol and this solution was mixed with arylaldehyde (0.02 mol, 2.02 g) and acetoacetanilide (0.01 mol, 1.77 g). The mixture was just heated to boil and allowed to stand at room temperature overnight. Then Conc. HCl (5 ml) was added and the precipitated hydrochloride was collected, washed with ethanol-ether mixture (1:5). A suspension of the hydrochloride in acetone was treated with strong liquid ammonia and the free base was obtained by pouring water. The product was twice recrystallized from ethanol. The purity of these compounds was checked by TLC and the melting point recorded by open capillary method.

General Procedure for the synthesis of 4,5,6,7-tetrahydro-4,6-diaryl-2*H*-pyrazolo[4,3-c]pyridin-3-ol (2a-f)

About 0.003246 mol of **1a** and 0.003246 mol of hydrazine hydrate in ethanol was taken in the R. B. flask. The contents were allowed to reflux on a water bath for 4 h. The reaction mixture was concentrated and cooled to room temperature; the obtained solid product was washed with ethanol-ether (1:5) solution, and then recrystallized using ethanol. The reproducibility was checked with **1b-f** to get **(2b-f)**.

General procedure for the synthesis 4,5,6,7-tetrahydro-2,4,6-triaryl-2*H*-pyrrolo[3,2-c]pyridin-3-ol (3a-f)

About 0.003246 mol of **1a** was taken in the R.B. flask in ethanol and about 0.003246 mol. of phenyl hydrazine (0.4g) was added. The contents were allowed to reflux on a water bath for 6 hr. The reaction mixture was cooled to room temperature; the solid product was washed with ethanol-ether (1:5) solution and recrystallized using ethanol. The purity of product was checked through TLC and the melting point was observed.

Spectral data of newly prepared compounds

1a: Yield (85 %), m.p =110°C. FT-IR data in cm^{-1}: 1655 (Ring C=O str), 1722 (NH C=O str), 3458 (NH str), 3353 (Aromatic str). ^{1}H-NMR (400MHz, $CDCl_3$): δ 1.89 (s, 1H), 2.68-2.90 (t, 2H), 3.87 (d, 1H), 4.06 (t, 1H), 4.40 (d, 1H), 7.19-7.29 (m, 7H), 7.40-7.43 (m, 6H), 7.61 (d, 2H). $C_{24}H_{22}N_2O_2$ (Calculated) C = 77.81, H = 5.99, N = 7.56; (Found) C = 77.54, H = 6.09, N = 7.76

1b: Yield (79 %), m.p =108°C. IR data (cm^{-1}): 1634 (Ring C=O str), 1727 (NH C=O str), 3425 (NH str), 3285, 3218 (Aromatic str).^{1}H-NMR (400MHz, $CDCl_3$): δ 1.91 (s, 1H), 2.70-2.73 (t, 2H), 3.84 (s, 6H), 3.93 (d, 1H), 4.10 (t, 1H), 4.37 (d, 1H),6.94 (d, 4H), 7.15-7.23 (m, 6H), 7.43 (t, 2H), 7.60 (d, 2H). $C_{26}H_{26}N_2O_4$ (Calculated) C = 72.54, H = 6.09, N = 6.51. Found; C = 72.58, H = 5.99, N = 6.54.

1c: Yield (93 %), m.p =110°C. IR data in cm^{-1}: 1609 (Ring C=O str), 1738 (NH C=O str), 3429 (NH str), 3382 (Aromatic str). ^{1}H-NMR (400MHz, $CDCl_3$): δ 1.89 (s, 1H), 2.68-2.74 (t, 2H), 3.87 (d, 1H), 4.21 (t, 1H), 4.50 (d, 1H), 6.43-6.46 (m, 4H), 7.19-7.20 (m, 2H), 7.40 (t, 2H), 7.60-7.64 (m, 4H). $C_{20}H_{18}N_2O_4$ (Calculated): C = 68.56; H= 5.18; N = 8.00 Found: C = 68.44; H = 4.08; N = 8.10.

1d: Yield (75 %), m.p =105°C. IR data in cm^{-1}: 1646 (Ring C=O str), 1749 (NH C=O str), 3417 (NH str), 3172, 3139 (Aromatic str). ^{1}H-NMR (400MHz, $CDCl_3$): δ 1.88 (s, 1H), 2.74-2.78 (t, 2H), 3.83 (s, 6H), 3.89 (d, 1H), 4.13 (t,3H), 4.30 (d, 1H), 6.75-6.80 (m, 4H), 7.07 (s, 2H), 7.19-25 (m, 4H), 7.46 (t, 2H), 7.61 (t, 2H). $C_{26}H_{26}N_2O_4$ (Calculated) C = 72.54, H = 6.09, N = 6.51; Found: C = 72.54, H = 5.13, N= 6.12.

1e: Yield (91 %), m.p =109°C. IR data in cm^{-1}: 1634 (ring C=O str), 1727 (NH C=O str), 3425 (NH str), 3285, 3218 (Aromatic str). ^{1}H-NMR (400MHz, $CDCl_3$): δ 1.90 (s, 1H), 2.70-2.74 (t, 2H), 3.83 (s, 6H), 3.91 (d,1H), 4.10 (t, 1H), 4.40 (d, 1H), 6.80 (t, 2H),6.90-94 (m,4H), 7.16-7.20 (m, 4H), 7.43 (t, 2H), 7.61 (d, 2H). $C_{26}H_{26}N_2O_4$ (Calculated), C = 72.54, H = 6.09; N = 6.51; Found: C = 72.34, H = 4.99; N = 6.43.

1f: Yield (79 %), m.p =107°C. IR data in cm^{-1}: 1645 (Ring C=O str), 1716 (NH C=O str), 3434 (NH str), 3300, 3201(Aromatic str). GC-Mass Base Peak = 298, ^{1}H-NMR (400MHz, $CDCl_3$): ä 1.92 (s, 1H), 2.70-2.72 (m, 2H), 3.90 (d, 1H), 4.15 (t, 1H), 4.30 (d, 1H), 7.19-7.20 (m, 2H), 7.45-7.48 (m, 10H), 7.61 (d, 2H). $C_{24}H_{20}N_2Cl_2O_2$,(Calculated): C = 65.61; H = 4.59; Cl = 16.14; N = 6.38**;** Found: C = 65.51; H = 5.53; N = 6.33.

2a: Yield (81 %), m.p =175°C. FT-IR data in cm^{-1}: 3318 (NH str), 3198 (Aromatic str), 3076 (Aromatic str), 3435 (OH str). ^{1}H-NMR (400MHz, $CDCl_3$): δ 1.90 (s, 1H), 1.5-1.60 (t, 2H), 2.0 (s, 1H), 2.1 (d, 1H), 3.9 (t,1H), 5.19 (s,1H), 7.26-7.30 (m,10H). GC-Mass Base Peak = 272. $C_{18}H_{17}N_3O$ (Calculated) C = 74.20; H = 5.88; N = 14.42; O = 5.49; Found: C = 73.80; H = 4.98; N = 14.56.

2b: Yield (78 %), m.p =197 °C. IR data in cm^{-1}: 3436 (NH str), 3267, 3096 (Aromatic str), 3436 (Aromatic OH str), 1690 (C-O-C str). ^{1}H-NMR (400MHz, $CDCl_3$): δ 1.85 (s, 1H), 1.56-1.60 (t, 2H), 2.04 (s, 1H), 2.02 (d, 1H), 3.83 (s,6H), 3.89 (t, 2H), 6.90 (d, 4H), 7.20 (d, 4H). $C_{20}H_{21}N_3O_3$ (Calculated): C = 68.36; H = 6.02; N = 11.96; Found: C = 68.52; H = 6.58; N = 12.03.

2c: Yield (73 %), m. p =207 °C. IR data in cm^{-1}: 3454 (NH str), 3271, 3102 (Aromatic str), 3445 (Aromatic OH str), 1592 (C-O-C furyl str). ^{1}H-NMR (400MHz, $CDCl_3$): δ 1.88 (s, 2H), 1.64-1.70 (t, 2H), 2.12 (d, 1H), 4.1 (t, 2H), 6.43-6.46 (m, 4H), 7.70 (d, 2H). $C_{14}H_{13}N_3O_3$ (Calculated) C = 61.99; H = 4.83; N = 15.49; Found: C = 62.77; H = 3.71; N = 14.42.

2d: Yield (78 %), m.p =199 °C. IR data in cm^{-1}: 3435 (NH str), 3267, 3097 (Aromatic str), 3436 (Aromatic OH str), 1690 (C-O-C str). ^{1}H-NMR (400MHz, $CDCl_3$): δ 1.90 (s, 2H), 1.60-1.64 (t, 2H), 2.09 (d, 1H), 3.83 (s, 6H), 3.85 (t, 2H), 6.86 (t, 2H), 6.94-6.98 (m, 4H), 7.15 (d, 2H). $C_{20}H_{21}N_3O_3$ (Calculated): C = 68.36; H = 6.02; N = 11.96; Found: C = 68.52; H = 6.52; N = 12.03.

2e: Yield (80 %), m.p =197 °C. IR data in cm^{-1}: 3436 (NH str), 3267, 3096 (Aromatic str), 3434 (Aromatic OH str), 1693 (C-O-C str). ^{1}H-NMR (400MHz, $CDCl_3$): δ 1.92 (s, 2H), 1.61-1.63 (t, 2H), 2.10 (d, 1H), 3.83 (s,6H), 3.90 (t, 2H), 6.85 (t, 2H), 6.94-6.98 (m, 4H), 7.15 (d, 2H). $C_{20}H_{21}N_3O_3$ (Calculated): C = 68.36; H = 6.02; N = 11.96; Found: C = 69.02; H = 6.48; N = 11.83.

2f: Yield (85 %), m.p =217 °C. IR data in cm^{-1}: 3359 (NH str), 3187, 3087 (Aromatic str), 3432 (OH str), 684 C-Cl str. ^{1}H-NMR (400MHz, $CDCl_3$): δ 1.85 (s, 1H), 1.55-1.60 (t, 2H), 2.10 (s, 1H), 3.95 (t, 2H), 7.50-7.60 (m, 8H). $C_{18}H_{15}N_3Cl_2O$ (Calculated): C = 60.01; H = 4.20; Cl = 19.68; N = 11.66; Found; C = 59.77; H = 3.23; N = 11.23.

3a: Yield (74 %), m.p =170 °C. IR data in cm^{-1}: 3251 (NH str), 3182, 3058 (Aromatic str), 3409 (Aromatic OH str). ^{1}H-NMR (400MHz, $CDCl_3$): δ 1.90 (s, 1H), 2.70-2.90 (t, 2H), 4.27 (t, 1H), 5.20 (s, 1H, 7.29-7.45 (m, 11H), 7.62-7.70 (m, 4H), 10.90 (s, 1H). GC-Mass Base Peak = 208. ES-Ms: 367; $C_{24}H_{21}N_3O$ (calculated): C = 78.45; H = 5.76; N = 11.44; Found: C = 78.85; H = 5.47; N = 11.24.

3b: Yield (85 %), m.p =263 °C. IR data in cm^{-1}: 3249 (NH str), 3194, 3078 (Aromatic str), 3421 (Aromatic OH str), 1625 (C-O-C str). ^{1}H-NMR (400MHz, $CDCl_3$): δ 1.93 (s, 1H), 2.75-2.87 (t, 2H), 3.80 (s, 6H), 4.30 (t, 1H), 5.20 (s, 1H, 6.87-6.98 (m, 4H), 7.15-7.20 (m, 4H), 7.45 (t, 1H), 7.60-7.65 (m, 4H), 11.02 (s, 1H). ES-Ms: 427. $C_{26}H_{25}N_3O_3$ (Calculated): C = 73.05; H = 5.89; N = 9.83; Found: C = 73.23; H = 4.78; N = 8.93.

3c: Yield (70 %), m.p =212 °C. IR in cm^{-1}: 3287 (NH str), 3136 (Aromatic str), 3470 (Aromatic OH str), 3060 (C-C str furan). ^{1}H-NMR (400MHz, $CDCl_3$): δ 1.93 (s, 1H), 2.80-2.85 (t, 2H), 4.60 (t, 1H), 5.51 (s, 1H), 6.30 (d, 1H), 6.58-6.70 (m, 4H), 7.52 (d, 1H), 7.64-7.67 (m, 5H), 11.0 (s, 1H). EI-MS= 347[M+]; $C_{20}H_{17}N_3O_3$ (Calculated): C = 69.15; H = 4.93; N = 12.10; Found: C = 68.95; H = 3.98; N = 12.02.

3d :Yield (78 %), m.p =204 °C. IR in cm^{-1}: 3245 (NH str), 3198, 3082 (Aromatic str), 3421 (Aromatic OH str), 1626 (C-O-C str). ^{1}H-NMR (400MHz, $CDCl_3$): δ 1.93 (s, 1H),

2.75-2.87 (t, 2H), 3.80 (s, 6H), 4.30 (t, 1H), 5.20 (s, 1H), 6.87-6.98 (m, 4H), 7.15-7.20 (m, 4H), 7.45 (t, 1H), 7.60-7.65 (m, 4H), 11.02 (s, 1H). ES-Ms: 427; $C_{26}H_{25}N_3O_3$ (Calculated): C = 76.03; H = 6.14; N = 6.57; Found: C = 73.10; H = 5.89; N = 6.87.

3e:Yield (78 %), m.p =198 °C. IR in cm^{-1}: 3249 (NH str), 3194, 3078 (Aromatic str), 3421 (Aromatic OH str), 1625 (C-O-C str). ^{1}H-NMR (400MHz, $CDCl_3$): δ 1.93 (s, 1H), 2.75-2.87 (t, 2H), 3.80 (s, 6H), 4.30 (t, 1H), 5.20 (s, 1H, 6.87-6.98 (m, 4H), 7.15-7.20 (m, 4H), 7.45 (t, 1H), 7.60-7.65 (m, 4H), 11.02 (s, 1H). ES-Ms: 427; $C_{26}H_{25}N_3O_3$ (Calculated): C = 76.03; H = 6.14; N = 6.57; Found: C = 73.08; H = 5.79; N = 6.86.

3f:Yield (83 %), m.p =206 °C. IR data in cm^{-1}: 3276 (NH str), 3176, 3082 (Aromatic str), 3423 (Aromatic OH str), 691 C-Cl str. ^{1}H-NMR (400MHz, $CDCl_3$): δ 1.90 (s, 1H), 2.80-3.0 (t, 2H), 4.28 (t, 1H), 5.20 (s, 1H), 7.20 (d, 2H), 7.45-7.60 (m, 11H), 11.02 (s, 1H). ES-MS: 435 [M+]; $C_{24}H_{19}N_3Cl_2O$ (Calculated): C = 66.06; H = 4.39; Cl = 16.25; N = 9.63; Found: C = 65.97; H = 3.43; N = 9.73.

Results and Discussion

The 4-oxo-N,2,6-triphenylpiperidine-3-carboxamides (**1a-f**) were synthesized by adopting the procedure available in literature[1]. In this method about 0.01 mol of dry ammonium formate (0.63 g) was dissolved in ethanol and the solution was mixed with 0.02 mol of arylaldehyde (2.02 g) and 0.01 mol of acetoacteanilide (1.77 g). The mixture was just heated to boil and kept at room temperature over night. Then Conc. HCl (5 ml) was added and the precipitated hydrochloride was collected, washed with ethanol-ether mixture (1:5). A suspension of the hydrochloride in acetone was treated with liquid ammonia and the free base was obtained by pouring on to water. Product was purified by repeated recrystallization from ethanol.

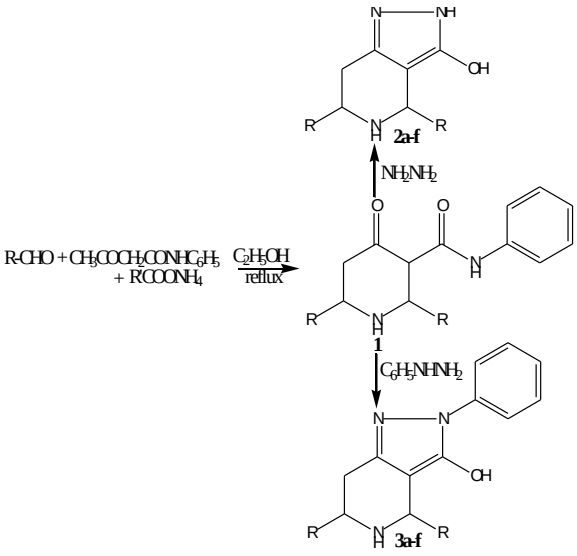

Scheme 1. Synthesis of substituted pyrazolo[4,3-c]pyridine-3-ols

Table 1. Physical data of the compounds (**1a-f**), (**2a-f**) and (**3a-f**)

S. No	R	M.P. °C	Yield, %
1a	Phenyl	110-12	90
1b	4-Methoxyphenyl	108-10	78
1c	Furfural	110-12	98
1d	3-Methoxyphenyl	105-08	75
1e	2-Methoxyphenyl	107-09	91
1f	4-Chlorophenyl	109-13	70
2a	Phenyl	175-78	81
2b	4-Methoxyphenyl	197-201	78
2c	Furfural	207-08	73
2d	3-Methoxyphenyl	195-99	80
2e	2-Methoxyphenyl	198-202	79
2f	4-Chlorophenyl	217-19	85
3a	Phenyl	170-74	74
3b	4-Methoxyphenyl	194-96	78
3c	Furfural	212-15	70
3d	3-Methoxyphenyl	195-98	76
3e	2-Methoxyphenyl	198-203	78
3f	4-Chlorophenyl	263-64	85

The compounds were characterized by IR and ^{1}H-NMR. The formation of piperidones confirmed by the appearance of two signals for the carbonyl function in IR spectra around 1610cm^{-1} and 1710-1750 cm^{-1}. ^{1}H-NMR for the compound **1f** shows the following peaks. A doublet appeared at 4.51 ppm due to the methylene proton at C5. The other aliphatic signals may be merged with aromatic protons due to the anisotropic effect of amide group. δ7.24 (d, *J* = 7.88 Hz, 2H), δ 7.48-7.50 multiplet (12H), δ 7.68 (d *J*=8.44Hz, 2H), δ 8.40 (s 2H). The physical parameters synthesized 4-piperidones **1a-f** were given in Table 1.

The 4,5,6,7-tetrahydro-4,6-diphenyl-2*H*-pyrazolo[4,3-c] pyridine-3-ols (**2a-f**) were synthesized by dissolving a mixture of about of 4-piperidone (0.003246 mol, 1.20 g) (**1a-f**) and 0.003246 mol of hydrazine hydrate in ethanol. The contents were refluxed on a water bath for 4 h. The reaction mixture was cooled to room temperature; the obtained solid was washed with ethanol-ether (1:5) and recrystallized using ethanol. The purity of the product was checked through TLC and the melting point. The formation of the product was confirmed by the absence of carbonyl peaks which appeared in the piperidones. The yield and physical parameters of **2a-f** are given in the Table 1.

Similarly the 4,5,6,7-tetrahydro-2,4,6-triphenyl-2*H*-pyrazolo[4,3-c]pyridine-3-ols (**3a-f**) was synthesized by refluxing the mixture of dissolving about 0.003246 mol of 4-piperidones (**1a-f**) in ethanol and 0.003246 mol of phenyl hydrazine for about 6 hrs. Then reaction mixture was cooled to room temperature; the solid obtained was washed with ethanol-ether (1:5) and recrystallized using ethanol. The purity of the product was checked through TLC and the melting point was recorded. The formation of the product was confirmed by the absence of carbonyl stretching frequency in IR spectrum which was present in piperidones.

The yield and other physical parameters of **3a-f** are given in the Table 1.

 DOI: 10.17628/ecb.2014.3.333-336

Conclusion

In conclusion, synthesis of some fused heterocycles with 4-piperidone moiety and 4,5,6,7-tetrahydro-4,6-diaryl-2*H*-pyrazolo[4,3-c]pyridin-3-ols, 4,5,6,7-tetrahydro-4,6-diaryl-2*H*-pyrazolo[4,3-c]pyridin-3-ols, were attempted successfully, the compounds with fused pyrazole were proved as biologically important molecules. In the present work molecules with pyrazole moiety were obtained using a simple reaction protocol with moderate yield. The synthesized compounds were characterized by IR, Mass, ^{1}H NMR data along with elemental analysis.

Acknowledgements

Authors gratefully acknowledge the management of VIT University for providing required basic facilities and SAIF (IIT-M) for providing the spectral data to carry out the present work.

References

[1]Vijayakumar, V., Sundaravadivelu, M., Perumal, S., *Mag. Reson. Chem.*, **2001**, *39*, 101.

[2]Vijayakumar, V., Rajesh, K., Suresh, J., Narasimhamurthy, T., Lakshman, P. L. N., *Acta Cryst.*, **2010**, *E66***,** o170.

[3]Aridoss, G., Balasubramanian, S., Parthiban, P., Kabilan, S., *Eur. J. Med. Chem.*, **2007**, *42*, 851.

[4]Priya, S., Sinha, S.S., Vijayakumar, V., Narasimhamurthy, T., Vijay, T., Rathore, R.S., *Acta Cryst.*, **2006**, E62, 5367.

[5]Schon, U., Messinger, J., Buckendahl, M., Prabhu, M. S., Konda, A., *Tetrahedron Lett.* **2007**, *48*, 2519.

[6]Ramalingam, C., Balasubramanian, S., Kabilan, S., *Eur. J. Med. Chem.*, **2004,** *39*, 527.

[7]Thenmozhiyal, J. C., Venkatraj, M., Ponnuswanmy, S., Jeyaraman, R., *Indian. J. Chem.*, **2007,** *46B*, 1526.

[8]Ramalingam, C., Balasubramanian, S., Kabilan, S., *Indian. J. Chem.*, **2002,** *41B*, 2402.

[9]Aridass, G. Balasubramanian, S. Parthian, P. Kablian, S., *Eur. J. Med. Chem.*, **2006,** *41*, 268.

[10]Chow, Y. L Colon, C. J., Tam, J. N. S., *Can. J. Chem.*, **1968**, *46*, 282.

[11]Sander, P., Bottger, E. C., *Chemotherapy*, **1999,** *45*, 95

[12]Arthur, M., Courvalin, P., *Antimicrob. Agents Chemother.*, **1993**, *37*, 1563.

[13]Kuznetsov, V. V., Prostakov, N. S., *Chem. Heterocyclic Compd.* **1994(**1), 3.

[14]Sayre, L. M., Engelhart, D. A., Nadkarni, D. V., Babu, M. K. M., Klein, M. E., McCoy, G., *Xenobiotica,* **1995**, *25*, 769.

[15]Brunner, H., Kagan, H. B., Kreutzer, G., *Tetrahedron: Asymmetry*, **2003**, *14*, 2177.

[16]Compain, P., Gore, J., Vatele, J. M., *Tetrahedron*, **1996**, *52*, 6647.

[17]Ooi, T., Saito, A., Maruoka, K., *J. Am. Chem. Soc.*, **2003**, *125*, 3220.

[18]Hagishita, S., Shirahase, M. K., Okada, T., Murakami, Y., *Med Chem.*, **1996,** *39*, 3636.

[19]Lounasma, M., Karvinen, E., Koskinen, A., Jokela, R., *Tetrahedron*, **1987,** *43*, 2135.

[20]Goes, A. D., Ferroud, C., Santamaria, J., *Tetrahedron Lett.* **1995**, *36*, 2235.

[21]De Risi, C., Fanton, G., Pollini, G. P., Trapella, C., Valente, F., Zanirato, V., *Tetrahedron: Asymmetry*, **2008**, *19*, 131.

Received: 05.03.2014.
Accepted: 14.03.2014.

SYNTHESIS AND X-RAY STRUCTURE OF 2-HYDRAZINYL-1,3-BENZOTHIAZOLE

Ratika Sharma,[a] Prakash S. Nayak,[b] B. Narayana,[b] Vivek K. Gupta[a] and Rajni Kant[a]*

Keywords: 2-hydrazinyl-1,3-benzothiazole; single crystal XRD; inter-molecular interactions; hydrogen bonding;

The title compound, $C_7H_7N_3S$, (2-hydrazinyl-1,3-benzothiophene) was prepared from the reaction of 2-amino-benzothiazole treated with hydrazine hydrate. It crystallizes in the monoclinic space group $P2_1/n$ with unit cell parameters a = 10.839(5), b = 5.752(5), c = 12.961(5) Å, β = 110.005(5)º, Z = 4. The crystal structure is stabilized by N-H…N [N2-H5...N3, N1-H12...N1] intermolecular interactions, N2-H5...N3 interaction is responsible for the formation of dimers corresponding to $R_2^2(8)$ graph-set motif and the dimers are further connected by N1-H12…N1 hydrogen bonding forming dimeric chains. Besides this, there is N1-H11… π interaction which is responsible for the stabilization of the crystal structure. The packing diagram of the title compound represents the dimeric chains extending along the b-axis.

Corresponding Authors*
Fax: +91 191 243 2051
E-Mail: rkvk.paper11@gmail.com
[a] Department of Physics& Electronics, Jammu University , Jammu Tawi -180 006, India.
[b] Department of Studies in Chemistry, Mangalore University, Mangalagangotri-574 199, Karnataka, India.

Introduction

Benzothiazoles are very important bicyclic ring compounds which are of great interest because of their biological activities. The substituted benzothiazole derivatives have emerged as significant components in various diversified therapeutic applications. The literature review reveals that benzothiazoles and their derivatives show considerable activity, including potent inhibition of human immunodeficiency virus type 1 (HIV-1) replication by HIV-1 protease inhibition, antitumor,[1] anthelmintic,[2] analgesic and anti-inflammatory,[3] antimalarial,[4] anticandidous activities [5] and various CNS activities.[6]

Experimental

Materials and methods

All chemicals were purchased commercially and used without prior purification. Melting point was taken in open capillary tube and was uncorrected. The purity of the compound was confirmed by thin layer chromatography using Merck silica gel 60 F_{254} coated aluminium plates.

Synthetic procedure of 2-hydrazinyl-1,3-benzothiazole (I)

2-Amino-1,3-benzothiazole (0.03 mol) and hydrazine hydrate (85 %) (0.12 mol) in 50 ml of ethylene glycol were refluxed by stirring for 4 h at 333 K. A white solid was precipitated at the end of the reflux period. The mixture was cooled and the product was filtered and then washed with water several times. Then the product was air-dried and recrystallized by using ethanol. The single crystals were grown by slow evaporation from solvent ethanol and dichloromethane (1:1, v/v). Yield obtained 62 %.

X-ray Crystallography

X-ray intensity data of a crystal (0.30 X 0.20 X 0.10 mm) having well-defined crystal morphology were collected at 293(2)K on *X'calibur* CCD area-detector diffractometer equipped with graphite monochromated Mo$K\alpha$ radiation (λ=0.71073 Å). The intensities were measured by employing ω scan mode for the diffraction angle ranging from 3.92 to 25.00º. A total number of 2657 reflections were measured of which 1335 were found to be unique. The criterion ($I > 2\sigma(I)$) was employed to the unique data set and hence 1080 reflections were treated as observed. Data were corrected for Lorentz and Polarization factors. The structure was solved by direct methods using SHELXS97.[7] All non-hydrogen atoms of the molecule were located in the best E-map. Full-matrix least-squares refinement was carried out using SHELXL97.[7] The final refinement cycles converged to R = 0.0372 and $wR(F^2)$ = 0.0825 for 1080 observed reflections. Residual electron densities ranged from -0.227 to 0.157 eÅ^{-3}. Atomic scattering factors were taken from International Tables for X-ray Crystallography (1992, Vol. C, Tables 4.2.6.8 and 6.1.1.4).The crystallographic data are summarized in Table 1. Selected bond lengths and bond angles are given in Table 2. An ORTEP[8] view of the title compound with atomic labeling is shown in Fig. 1. The geometry of the molecule was calculated using the PLATON[9]and PARST[10] software.

Results and discussion

The title compound was prepared from 2-amino-1,3-benzothiazole and hydrazine hydrate in ethylene glycol under 4 h reflux with 62 % yield.

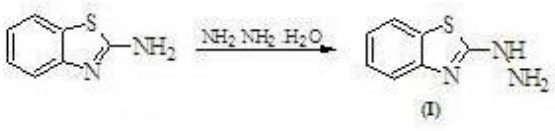

(I)

The white solid was recrystallized from ethanol and single crystals were grown from EtOH:CH2Cl2 (1:1, v/v) mixture.

 DOI: 10.17628/ecb.2014.3.337-339

Table 1. Crystal data and other experimental details

CCDC Number	983692
Crystal description	Block
Crystal size	0.30 x 0.20 x 0.10 mm
Empirical formula	$C_7H_7N_3S$
Formula weight	165.22
Radiation, Wavelength	Mo *Kα,* 0.71073 Å
Unit cell dimensions	*a* = 10.839(5), *b* = 5.7552(5), *c* = 12.961(20) Å, *β* = 110.005(5)º
Crystal system, Space group	Monoclinic, $P2_1/n$
Unit cell volume	759.3(8)Å^3
No. of molecules per unit cell, Z	4
F(000)	344
θ range for entire data collection	3.92< θ < 25.00
Reflections collected / unique	2657/1335
Reflections observed(I > 2σ(I))	1080
Range of indices	*h*= -12 to 10, *k*= -4 to 6, *l*= -9 to 15
No. of parameters refined	112
Final *R*-factor	0.0372
wR(F^2)	0.0825
Goodness-of-fit	1.073
(Δ/σ)max	0.000
Final residual electron density	-0.227< Δρ >0.157 eÅ^{-3}

The N1-N2 (=1.413 Å) bond length is comparable to the pure single bond length.[11] The nitrogen-carbon distance [N3-C5=1.389(3)Å] is shorter than the distance characteristics of single C-N bond length (1.45 Å) but is comparable with the values reported in the analogous structures.[12,13] The benzothiazole moiety is planar and the hydrazinyl group is slightly deviated with respect to the plane of benzothiazole moiety [deviation being -0.01717 Å].

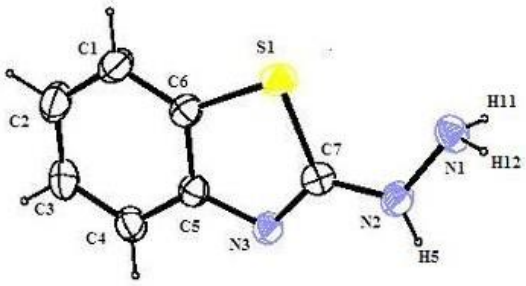

Figure 1. Ortep view of the molecules with displacement ellipsoids at the 40 % probability level. H atoms shown as small spheres of arbitrary radii.

Table 2. Selected bond lengths (Å) and bond angles (º) for non-hydrogen atoms (e.s.d.'s are given in parentheses)

Bond lengths, Å		**Bond angles, °**	
N2-N2	1.413(3)	C6-S1-C7	88.2(1)
N3-C7	1.305(3)	C7-N2-N1	117.7(2)
N2-C7	1.341(3)	N3-C7-N2	123.1(2)
N3-C5	1.389(3)	N3-C7-S1	120.5(2)
S1-C7	1.759(3)	C7-N3-C5	110.2(2)
S1-C6	1.748(2)		

In the crystal structure, molecules are inter-linked *via* intermolecular N2-H5…N3 and N1–H12…N1 interactions. N2-H5…N3 hydrogen bond is responsible for the formation of dimers (Fig. 2) corresponding to $R_2^2(8)$ graph-set motif[14] and the dimers are further connected by N1-H12…N1 hydrogen bonding forming dimeric chains along the *b*- axis (Fig. 3).

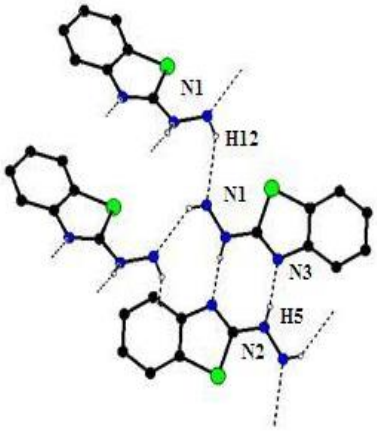

Figure 2. Intermolecular N2-H5….N3 hydrogen bond giving rise to dimer

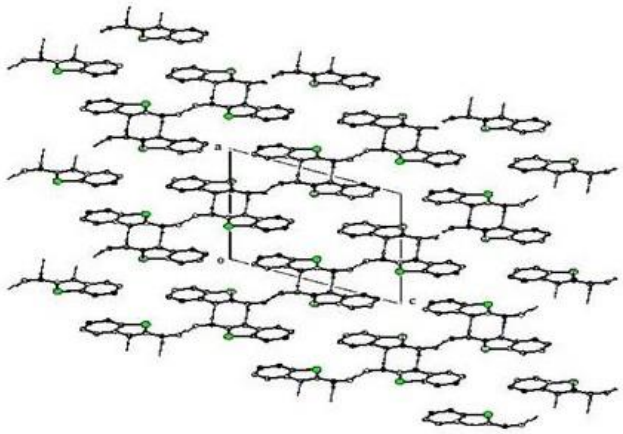

Figure 3. Unit cell molecular packing viewed down the b-axis

The crystal packing also features N1-H11…π interaction, where atom N1 acts as hydrogen- bond donor to the six membered ring (C1/C2/C3/C4/C5/C6), helps in the stabilization of the crystal structure. Hydrogen bond parameters are presented in Table 3.

Acknowledgement

One of the authors (Rajni Kant) acknowledges the Department of Science & Technology for single crystal X-ray diffractometer as a National Facility under Project No. SR/S2/CMP-47/2003. RS acknowledges University Grant Commission (UGC) for the award of NET-JRF scholarship under ref. No. 23/12/2012 (ii) EU-V dated 01.07.2013. BN thanks UGC for financial assistance through BSR grant. PSN thanks PURSE-DST project for financial assistance.

Table 3. Geometry of N-H…H and N-H…π hydrogen bonding geometry

D-H…A	D-H, Å	H…A, Å	D…A, Å	θ[D-H…A,º]
N2- H5…N3[i]	0.90(3)	2.04(3)	2.936(4)	174
N1- H12…N1[ii]	0.82(3)	2.54(2)	3.232(4)	144
N1- H11…Cg1[iii]	2.442	2.45(3)	3.345(4)	167

Symmetry Codes: (i) –x+1, -y+1, -z+2 (ii) –x+1/2+1, y+1/2, -z+1/2+2 (iii) –x,1-y,1-z

References

[1]Kini, S., Swain, S. P., Gandhi, A. M., *Indian J. Pharm. Sci.*, **2007**, *9*, 46–50.

[2]Munirajasekhar, D., Himaja, M., Sunil, V. M., *Int. Res. J. Pharm.*, **2011,** *2*, 114–117.

[3]Gurupadayya, B. M., Gopal, M., Padmashali, B., Manohara, Y. N., *Indian J. Pharm. Sci.*, **2008,** *70*, 572–577.

[4]Bowyer, P. W., Gunaratne, R. S., Grainge, M., Withers-Martinez, C., Wickramsinghe, S. R., Tate, E. W., Leatherbarrow, R. J., Brown, K. A., Holder, A. A., Smith, D. F., *Biochem. J.*, **2007,** *408*, 173–180.

[5]Pozas, R., Carballo, J., Castro, Rubio J., *Bioorg. Med. Chem. Lett.*, **2005,** *15*, 1417–1421.

[6]Rana, A., Siddiqui, N., Khan, S., *Eur. J. Med. Chem.*, **2008,** *43*, 1114–1122.

[7]Sheldrick, G. M., *Acta Cryst.*, **2008,** *A64*, 112.

[8]Farrugia, L. J., *J. Appl. Cryst.*, **2012,** *45*, 849-854.

[9]Spek, A. L., *Acta Cryst.*, **2009,** *D65*, 148-155.

[10]Nardelli, M. J., *Appl. Cryst.*, **1995,** *28*, 659.

[11]Burke-Laing, M., Laing, M., *Acta Cryst.*, **1976,** *B32*, 3216-3224.

[12]Hoong-Kun, F., Ching Kheng Q., Sarojini, B. K., Mohanb, B. J., Narayanac B., Acta Cryst., **2012,** *E68*, o2682.

[13]Md. Abu, A., Philip G. J., Md. Abdus S., Siti Nadiah B. A. H., Edward, R. T. T., *Acta Cryst.*, **2013,** *E69*, o1273.

[14]Bernstein, J., Davis, R. E., Shimoni, L., Chang, N.L., *Angew. Chem. Int. Ed. Engl.*, **1995**, *34*, 1555–1573.

Received: 12.03.2014.
Accepted: 14.03.2014.

PHYSICO-CHEMICAL STUDIES OF A NOVEL CADMIUM(II) COORDINATION COMPOUND [(3-Ampy)$_2$CdCl$_4$].0.305H$_2$O (3-Ampy=3-AMINOMETHYLPYRIDINE)

M. Ben Nasr,[a] M. Zeller,[b] F. Lefebvre,[c] and C. Ben Nasr[a]*

Keywords: cadmium(II) coordination compound ; MAS-NMR spectroscopy ; infrared spectroscopy; intermolecular N-H..Cl hydrogen bond

The crystal structure of the title organic-inorganic hybrid material, [(3-Ampy)$_2$CdCl$_4$].0.305H$_2$O (3-Ampy=3-aminomethylpyridine), contains two crystallographically independent but chemically equivalent cadmium complexes with essentially the same geometry (rms deviation of all atoms: 0.152 Å). The metal centers have a 6-coordinated octahedral geometry and both Cd atoms exhibit exact crystallographic inversion symmetry. Crystal packing is stabilized by intermolecular N-H...Cl hydrogen bonds that connect individual zwitter-ionic complexes into a three dimensional lattice, which is further stabilized through π–π stacking interactions between aromatic rings of neighboring complexes, with centroid to centroid distances of 3.4406(14) and 3.7022(13) Å and interplanar separations of 3.299(1) and 3.302(1) Å. Interstitial space is partially filled with water molecules which are connected to the network through O-H...Cl and C-H...O hydrogen bonds. The ^{13}C and ^{15}N CP-MAS NMR spectra are in agreement with the X-ray structure. Four resonance peaks for the C3 carbon atom are observed due to the different environments of the aromatic rings caused by the presence of 0.305 water molecule per unit cell. DFT calculations allow the attribution of the carbon and nitrogen peaks to the different atoms.

* Corresponding Authors
E-Mail: cherif_bennasr@yahoo.fr
[a] Laboratoire de Chimie des Matériaux, Faculté des Sciences de Bizerte, 7021 Zarzouna, Tunisie.
[b] Youngstown State University, Department of Chemistry, One University Plaza, Youngstown, Ohio 44555-3663, USA.
[c] Laboratoire de Chimie Organométallique de Surface (LCOMS), Ecole Supérieure de Chimie Physique Electronique, 69622 Villeurbanne Cedex, France.

Introduction

Polynuclear d^{10}-metal complexes can exhibit important structural and photoluminiscent properties.[1] Among the d^{10} metals, cadmium gives rise to structural flexibility with coordination numbers varying between 4 and 8 with often severely distorted coordination geometries.[2-5] A disadvantage of the use of Cd^{2+} in functional materials is its toxic effects, which are well established and documented.[6]

The ions have been found to induce various pathological conditions, such as e.g. cardiovascular diseases,[7] hypertension, and cancer.[8] It is also known, however, that most of cadmium ions in biological systems is not in the form of free Cd^{2+} ions, but is coordinated by the abundance of biological ligands therein.[9-11] Therefore, the coordination chemistry of Cd^{2+} ions with such ligands is of interest.

As a contribution to the investigation of the above materials, we report here the crystal structure of one such compound, [(C$_6$H$_9$N$_2$)$_2$CdCl$_4$]0.305H$_2$O, formed through the reaction of 3-aminomethylpyridine with cadmium chloride and hydrochloric acid in an aqueous medium.

Experimental

Chemical preparation

324 mg (3 mmol) of 3-aminomethylpyridine and 549 mg (3 mmol) of $CdCl_2$ were dissolved in 20 ml of HCl (2 M) aqueous solution. The obtained solution was slowly evaporated at room temperature over six days leading to formation of transparent prismatic crystals with suitable dimensions for single crystal structural analysis (*m*=932 mg, *n*=1.95 mmol, yield 65 %). The crystals are stable for months under normal conditions of temperature and humidity.

Investigation techniques

The characterization of this coordination compound was carried out using X-ray diffraction, solid state NMR, DFT calculations and IR spectroscopy.

X-ray single crystal structural analysis

Diffraction data were collected on a Bruker AXS SMART APEX CCD diffractometer at 100 K using monochromatic Mo Kα radiation with the omega scan technique. Data were collected, the unit cell determined, and the data integrated and corrected for absorption and other systematic errors using the Apex2 suite of programs.[12] The structures were solved by direct methods using Shelxs and refined by full matrix least squares against F^2 with all reflections using Shelxl[13] and Shelxle.[14] Carbon and nitrogen bound hydrogen atoms were placed in calculated positions guided by difference electron density Fourier maps. C---H distances

were set to 0.95 and 0.99 Å for aromatic and methylene H atoms, respectively, with U_{iso} values 1.2 times that of the U_{eq} of the respective carrier atom. Ammonium H atoms were placed at a distance of 0.91 Å and were allowed to rotate, but not to tip, to best fit the experimental electron density. U_{iso}(H) were set to 1.5 times U_{eq}(N) of the carrier atom. A water solvate molecule is only partially occupied with a refined occupancy rate of 0.305(6). Positions of the water H atoms were refined with a distance restraint of 0.84(2) Å, and U_{iso}(H) were set to 1.5 times U_{eq}(O). The drawings were made with Diamond[15] and Mercury.[16] Crystal data and experimental parameters used for the intensity data collection are summarized in Table 1.

Physical measurements

The NMR spectra were recorded on a solid-state high-resolution Bruker DSX-300 spectrometer operating at 75.49 MHz for ^{13}C and 30.30 MHz for ^{15}N with a classical 4 mm probehead allowing spinning rates up to 10 kHz. ^{13}C and ^{15}N NMR chemical shifts are given relative to tetramethylsilane and liquid ammonia, respectively (precision 0.5 ppm). The spectra were recorded by use of cross-polarization (CP) from protons (contact time 5 ms) and MAS. Before recording the spectrum it was checked that there was a sufficient delay between the scans allowing a full relaxation of the protons. The IR spectrum was recorded in the range 4000-400 cm^{-1} with a "Perkin-Elmer FTIR" spectrophotometer 1000 using a sample dispersed in spectroscopically pure KBr pressed into a pellet.

Results and discussion

X-ray diffraction study

A depiction of the structure of [(C$_6$H$_9$N$_2$)$_2$CdCl$_4$]0.305H$_2$O is shown in Figure 1. In the structure, there are two crystallographically independent complexes. Both complexes exhibit crystallographic inversion symmetry with the cadmium atoms located on centers of inversion at either on the face of the a-c face of the unit cell, or at 1/2 of the b-axis.

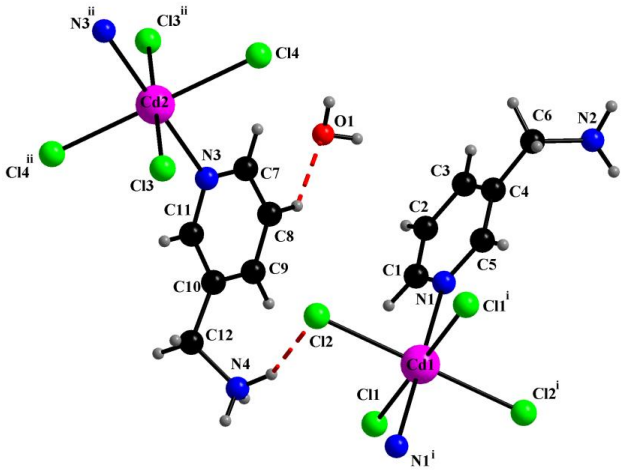

Fig.1. Asymmetric unit of [(3-Ampy)$_2$CdCl$_4$]0.305H$_2$O with the atom numbering scheme and thermal ellipsoids at 50 % probability. Symmetry code : (i) 1-x, y, 0.5-z.

Table 1. Experimental details of [(3-Ampy)$_2$CdCl$_4$].0.305H$_2$O.

CCDC Number	961746
Crystal description	Plate
Crystal size	0.39 × 0.25 × 0.12 mm
Formula	[(C$_6$H$_9$N$_2$)$_2$CdCl$_4$]0.305H$_2$O
Formula weight	478.01
Radiation	MoK_α
Wavelength	0.71073 Å
Temperature	100 K
Unit cell dimensions	a = 8.5313 (13) Å b = 8.6849 (13) Å c = 13.682 (2) Å α = 74.049 (2)° β = 75.276 (3)° γ = 66.681 (2)°
Crystal system, Space group	Triclinic, P1
Unit cell volume	882.9 (2) Å^3
No. of molecules per unit cell, Z	2
μ	1.84 mm^{-1}
Data collection	
	Bruker AXS SMART APEX CCD diffractometer Absorption correction: multi-scan Apex2 v2011.2-0 (Bruker, 2011) T_{min} = 0.604, T_{max} = 0.746 10570 measured reflections 5486 independentreflections 5065 reflections with $I > 2\sigma(I)$ R_{int} = 0.014
Refinement	
	$R[F^2 > 2\sigma(F^2)]$ = 0.026 $wR(F^2)$ = 0.064 S = 1.07 5486 reflections 211 parameters 2 restraints H atoms treated by a mixture of independent and constrained refinement $\Delta\rho_{max}$ = 1.08 e Å^{-3} $\Delta\rho_{min}$ = −0.77 e Å^{-3}

The overall geometry of the two complexes is very similar, with an rms deviation of 0.152 Å. The geometry around the metal centers is virtually identical, which can be seen at the Cd-N and Cd-Cl distances: Cd-N bond lengths are 2.3878(16) and 2.3168(17) Å for Cd1 and Cd2, respectively, and Cd-Cl distances are 2.6313(6) and 2.6508(5) Å for Cd1, and 2.6365(6) and 2.6651(6) Å for Cd2 (Table 2).

These geometrical parameters agree with those of similar cadmium complexes.[17] Slight differences between the two complexes are observed for the methylene ammonium fragments, which are oriented marginally different in the two molecules (Fig. 3).

 DOI: 10.17628/ecb.2014.3.340-345

Table 2. Selected bond lengths (Å) and angles (º) of CdN_2Cl_4 octahedra in the title compound.

Cd1—N1	2.3878 (16)	N1i—Cd1—N1	179.998 (2)
Cd2—N3	2.3168 (17)	N1i—Cd1—Cl2	90.81 (4)
Cd1—N1^{i}	2.3878 (16)	N1—Cd1—Cl2	89.19 (4)
Cd1—Cl2	2.6313 (6)	N1i—Cd1—Cl2^{i}	89.19 (4)
Cd1—Cl2^{i}	2.6313 (6)	N1—Cd1—Cl2^{i}	90.81 (4)
Cd1—Cl1	2.6508 (5)	Cl2—Cd1—Cl2^{i}	180.0
Cd1—Cl1^{i}	2.6508 (5)	N1i—Cd1—Cl1	88.11 (4)
Cd2—N3^{ii}	2.3168 (17)	N1—Cd1—Cl1	91.89 (4)
Cd2—Cl3	2.6365 (6)	Cl2—Cd1—Cl1	90.498 (17)
Cd2—Cl3^{ii}	2.6366 (6)	Cl2i—Cd1—Cl1	89.502 (18)
Cd2—Cl4^{ii}	2.6651 (6)	N1i—Cd1—Cl1^{i}	91.89 (4)
Cd2—Cl4	2.6651 (6)	N1—Cd1—Cl1^{i}	88.11 (4)
Cl2—Cd1—Cl1^{i}	89.502 (17)	N3—Cd2—Cl4^{ii}	91.45 (4)
Cl2i—Cd1—Cl1^{i}	90.498 (18)	N3ii—Cd2—Cl4^{ii}	88.55 (4)
Cl1—Cd1—Cl1^{i}	180.00 (2)	Cl3—Cd2—Cl4^{ii}	91.204 (17)
N3—Cd2—N3^{ii}	179.998 (1)	Cl3ii—Cd2—Cl4^{ii}	88.798 (17)
N3—Cd2—Cl3	88.38 (4)	N3—Cd2—Cl4	88.55 (4)
N3ii—Cd2—Cl3	91.62 (4)	N3ii—Cd2—Cl4	91.45 (4)
N3—Cd2—Cl3^{ii}	91.62 (4)	Cl3—Cd2—Cl4	88.797 (17)
N3ii—Cd2—Cl3^{ii}	88.38 (4)	Cl3ii—Cd2—Cl4	91.202 (17)
Cl3—Cd2—Cl3^{ii}	180.0	Cl4ii—Cd2—Cl4	180.00 (2)

Symmetry codes: (i) −x+2, −y+1, −z; (ii) −x+1, −y+2, −z+1.

Examination of the geometric features of the organic entity shows that the organic molecule exhibits a regular spatial configuration with C-C and C-N distances and C-C-C and C-C-N angles quite similar to those found in other compounds.[18]

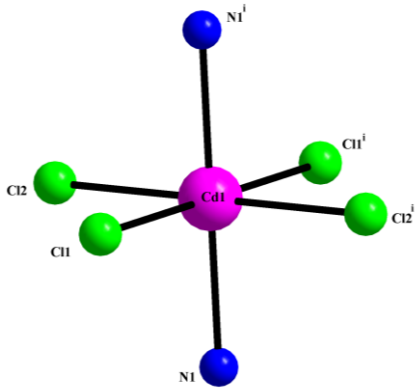

Figure 2. Geometry around the Cd(II) cation in [$(C_6H_9N_2)_2CdCl_4$]0.305H_2O. Symmetry code:(i) −x+2, −y+1, −z.

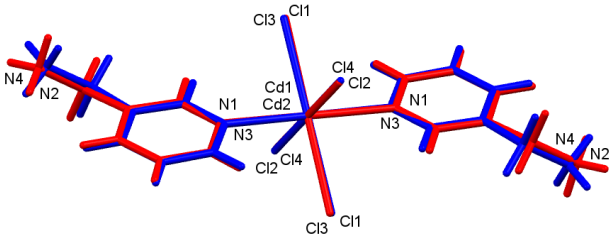

Figure 3. Least squares overlay of the two independent [$(C_6H_9N_2)_2CdCl_4$].0.305H_2O molecules, in red and blue, respectively.

Crystal packing is stabilized by intermolecular N-H...Cl hydrogen bonds that connect individual zwitter-ionic complexes into a three dimensional lattice (Fig. 4). Among these hydrogen bonds, one has a three centered interaction N4-H4C... (Cl1, Cl2) (Table 3, for symmetry operators, see table). The 3D-network is further stabilized through two π–π stacking interactions between aromatic rings of neighboring complexes, with centroid to centroid distances of 3.4406(14) and 3.7022(13)Å and interplanar separations of 3.299(1) and 3.302(1) Å (Fig 5). Interstitial space within the framework is partially filled with water molecules which are connected to the network through O-H...Cl and C-H...O hydrogen bonds (Table 3).

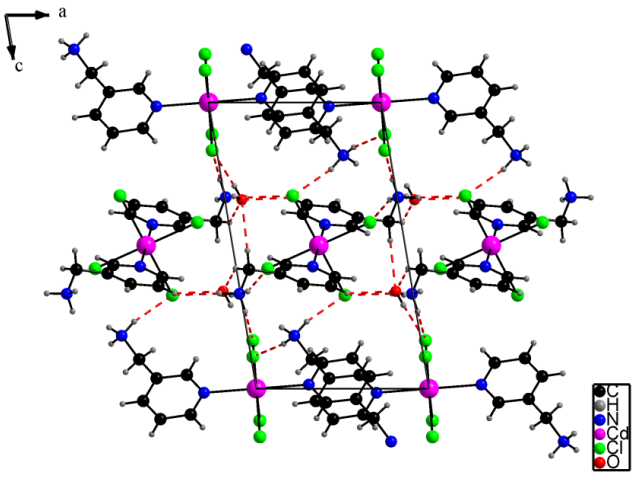

Figure 4. A projection of the structure of [$(C_6H_9N_2)_2CdCl_4$].0.305H_2O along the *b*-axis. The dotted lines indicate hydrogen bonds.

 DOI: 10.17628/ecb.2014.3.340-345

Table 3. Hydrogen-bond geometry (Å, º) for $(C_6H_9N_2)_2CdCl_4\times0.305(H_2O)$.

D—H···A	D—H	H···A	D···A	D—H···A
N2—H2*A*···Cl4^{i}	0.91	2.29	3.1866 (18)	167
N2—H2*B*···Cl2^{i}	0.91	2.51	3.2576 (18)	140
N2—H2*C*···Cl1^{ii}	0.91	2.26	3.1577 (18)	170
N4—H4*A*···Cl3^{iii}	0.91	2.29	3.1625 (18)	160
N4—H4*B*···Cl4^{iv}	0.91	2.32	3.1484 (19)	152
N4—H4*C*···Cl2	0.91	2.35	3.1632 (18)	148
N4—H4*C*···Cl 1	0.91	2.73	3.2413 (19)	117
C8—H8···O1	0.95	2.22	3.013 (6)	141
C12—H12*B*···O1^{v}	0.99	2.53	3.222 (7)	127
C12—H12*A*···O1^{vi}	0.99	2.57	3.428 (8)	145
O1—H1*B*···Cl3^{vii}	0.84 (2)	2.44 (9)	3.075 (6)	133 (11)
O1—H1*A*···Cl2^{vii}	0.84 (2)	2.27 (2)	3.109 (6)	176 (12)

Symmetry codes: (i) −*x*+1, −*y*+2, −*z*; (ii) −*x*+1, −*y*+1, −*z*; (iii) *x*, *y*−1, *z*; (iv) *x*+1, *y*−1, *z*; (v) −*x*+1, −*y*+1, −*z*+1; (vi) *x*+1, *y*, *z*; (vii) *x*−1, *y*, *z*.

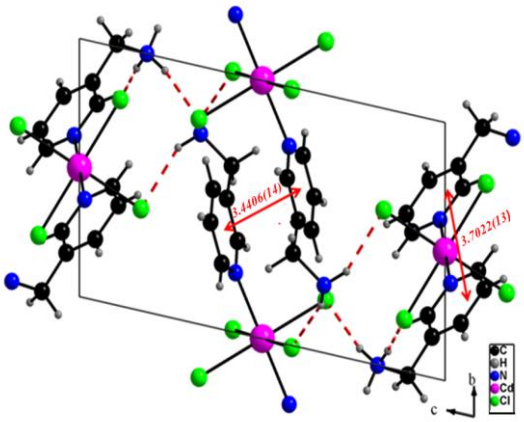

Figure 5. π- π stacking interaction in [$(C_6H_9N_2)_2CdCl_4$].0.305H_2O.

NMR spectroscopy

The ^{13}C CP-MAS NMR spectrum of the title compound is shown on Figure 6. In the aliphatic resonance domain, the spectrum displays two resonances at 41.1 ppm and 42.5 ppm, corresponding to two methylene C atoms. This result is consistent with the presence of two organic moieties in the asymmetric unit of the compound, in agreement with the X-ray diffraction data.

Density functional theory (DFT) calculations were undertaken in order to assign the NMR resonances to the different crystallographically unequivalent carbon atoms of the unit cell. These calculations were made at the B3LYP/6-31+G* level. The different atoms were labelled as depicted below:

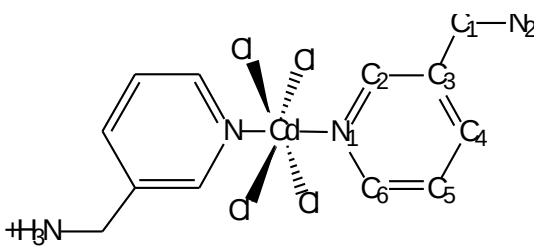

Three different calculations were made on the organic cation and in all cases the theoretical chemical shifts were subtracted from those of the reference (tetramethylsilane) calculated at the same level of theory:

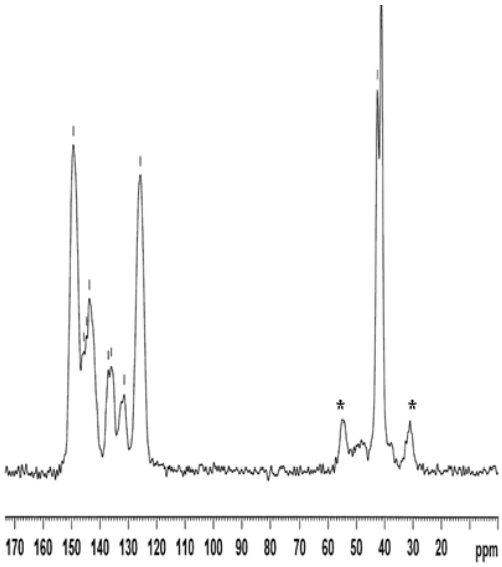

Figure 6. ^{13}C CP-MAS NMR spectrum of [$(C_6H_9N_2)_2CdCl_4$].0.305H_2O. * Spinning side bands of the aromatic peaks.

(1) Calculation of the NMR chemical shifts (with the GIAO method) by using the positions of atoms obtained by X-ray diffraction;

(2) Optimization of the positions of the protons in the above molecule and calculation of the NMR chemical shifts in this semi-optimized geometry. Indeed X-ray diffraction leads always to underestimated X-H bond lengths, due to the fact that it is sensitive to the electronic cloud and does not see the nuclei;

(3) Full optimization of all atoms and calculation of NMR chemical shifts. This calculation, compared to the above one will give indications on the steric hindrance around the organic cation and on the positions where it is the strongest.

 DOI: 10.17628/ecb.2014.3.340-345

The results are listed in Table 4. Clearly, there is a good agreement between the experimental and theoretical values calculated after optimization of the position of the protons, allowing unambiguously the attribution of the different NMR signals. A key point of the ^{13}C NMR spectrum is the presence of four resonances for the C3 carbon atom (Fig. 7, Table 4), while only two are expected from the X-ray data. These peaks are grouped in two doublets with an intensity ratio of ca. 4:6. This point is probably related to the fact that there is only 0.305 water molecule per unit cell resulting then in different environments of the aromatic rings. Even if the difference cannot be seen by crystallography it is observed by solid state NMR, which is more sensitive to the local order, The signals of the other carbon atoms are also probably formed of doublets but the linewidths prevent their observation.

The ^{15}N CP-MAS NMR spectrum of the title compound (Fig.8) two resonance peaks. The first one at 44.0 ppm is related to the two aliphatic nitrogen atoms, while the second one, at 281.3 ppm corresponds to the two aromatic nitrogen atoms (Table 4).

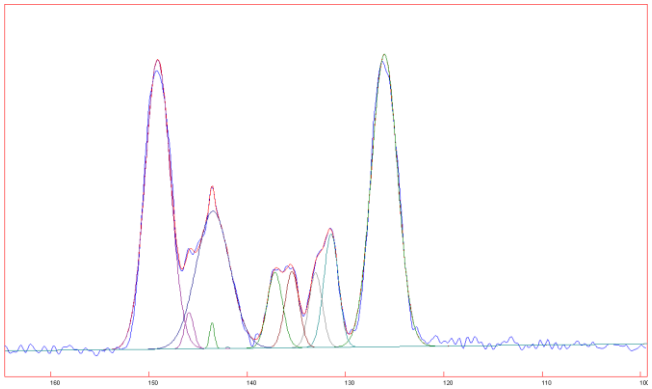

Figure 7. Aromatic region of the experimental and simulated ^{13}C CP-MAS NMR spectrum of [(C$_6$H$_9$N$_2$)$_2$CdCl$_4$].0.305H$_2$O.

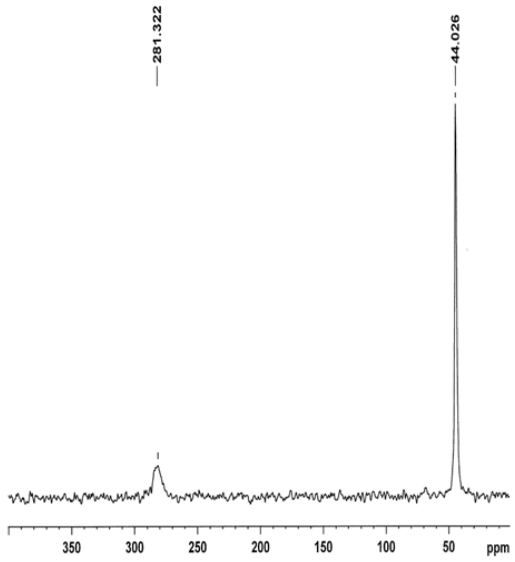

Figure 8. ^{15}N CP-MAS NMR spectrum of [(C$_6$H$_9$N$_2$)$_2$CdCl$_4$].0.305H$_2$O.

Table 4. Chemical shift values of the carbon atoms in (C$_6$H$_9$N$_2$)$_2$CdCl$_4$×0.305(H$_2$O).

Atom	X-rays	Full optimisation	Optimisation of hydrogens	Experiment
C1	33.7		47.5	42.5
	33.8	49.9	46.4	41.0
C2	153.1		158.0	149.1
	151.1	158.0	157.2	
C3				135.4
				137.2
	132.2		131.5	131.5
	132.8	133.1	130.8	133.5
C4	140.6		145.4	143.5
	132.8	146.6	137.0	
C5	125.7		129.6	126.05
	124.2	130.7	128.4	
C6	153.9		158.9	149.1
	151.4	158.6	156.8	
N1	327.0		328.7	282
	323.2	326.4	325.1	
N2	25.5		59.2	44
	18.5	62.1	51.6	

IR Spectroscopy at room temperature

The IR spectrum of crystalline [(C$_6$H$_9$N$_2$)$_2$CdCl$_4$].0.305H$_2$O is shown in Figure 9. The most representative and characteristic vibrational modes of this compound can be compared to those of similar complexes [19-21]. Some aspects of the performed assignments are briefly commented as follows:

In the high-frequency region, the broad bands between 3600 and 2500 cm^{-1} correspond to the valence vibrations of C-H, N-H and O-H groups [22].

The bands in the 1630-1100 cm^{-1} region can be attributed to the bending vibrations of N-H and O-H groups and to the stretching and bonding modes ν(C=C), ν(C-C), ν(C-N), δ(C-H) of the aromatic ring [23, 24].

The bands between 1000 and 600 cm^{-1} are assigned to the out of plane bending modes γ(C$_{ary}$-H), γ(C$_{ary}$-C) and γ(N-H).[25]

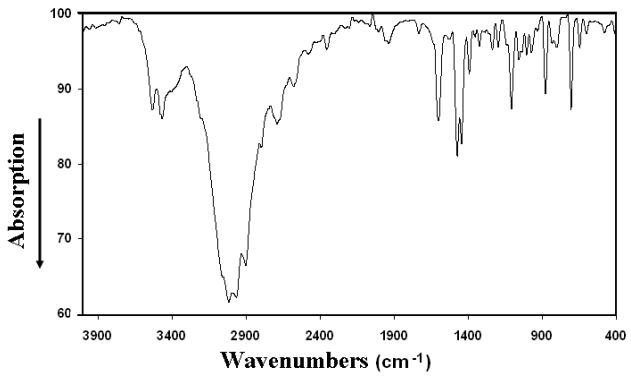

Figure 9. IR absorption spectrum of [(C$_6$H$_9$N$_2$)$_2$CdCl$_4$].0.305H$_2$O.

 DOI: 10.17628/ecb.2014.3.340-345

Conclusion

A new Cd(II) complex, $[(C_6H_9N_2)_2CdCl_4]0.305H_2O$, was synthesized in an aqueous medium and characterized by various physico-chemical methods. On the structural level, the metal centers have 6-coordinated octahedral geometry and both Cd atoms exhibit exact crystallographic inversion symmetry. Crystal packing is stabilized by intermolecular N-H...Cl hydrogen bonds that connect individual zwitter-ionic complexes into a three dimensional lattice, which is further stabilized through π–π stacking interactions between aromatic rings of neighboring complexes. Interstitial space is partially filled with water molecules which are connected to the network through O-H...Cl and C-H...O hydrogen bonds. The ^{13}C and ^{15}N CP-MAS NMR spectra are in agreement with the X-ray structure.

Supplementary data

Crystallographic data for the structural analysis have been deposited with the Cambridge Crystallographic Data Centre, CCDC No 961746. These data can be obtained free of charge via http://www.ccdc.cam.ac.uk/conts/retrieving.html, or from the CCDC, 12Union Road, Cambridge, CB2 1EZ, UK: fax: (+44) 01223-336-033; e-mail: deposit@ccdc.cam.ac.

Acknowledgments

We would like to thank the Tunisian Secretariat of State for Scientific Research and Technology for its financial support. The diffractometer was funded by NSF grant 0087210, by Ohio Board of Regents grant CAP-491, and by YSU.

References

[1]Tao, J., Yin, X., Jiang, L. F., Huang, R. B., Zheng, L. S., *Eur. J. Inorg. Chem.*, **2003**, 2678.

[2]Wang, X.-Li, Yang, S., Liu, G.-C., Zhang, J.-X, Lin, H.-Y., Tian, A.-X., *Inorg. Chim. Acta*, **2011**, *375*, 70.

[3]Subashini, A., Muthiah, P. T., Bocelli, G., Cantoni, A. *Acta Cryst.*, **2008**, *E64*, m250.

[4]Xiao, J.-M., *Acta Cryst.*, **2010**, *C66*, m348.

[5]Kaabi, K., El Glaoui, M., Silva, S. P., Silva, M. R., Ben Nasr, C., *Acta Cryst.*, **2010**, *E66*, m617.

[6]Filck, D. F., Kraybill, H. F., Dimitroff, J. M., *Environ. Res.*, **1971**, *4*, 71

[7]Caroll, P. E., *J. Am. Med. Assoc.*, **1966**, *198*, 267.

[8]Schroeder, H. S ., Balassa, J. J., *Am. J. Physiol.*, **1965**, *209*, 433.

[9]Dressing, S. A., Mass, R. P., Weiss, C. M., *Bull. Environ. Contam. Toxicol.*, **1982**, *28*, 172.

[10]Titus, J. A., Pfister, R. M., *Bull. Environ. Contam. Toxicol.*, **1982**, *28*, 703.

[11]Hung, Y.W., *Bull. Environ. Contam. Toxicol*., **1982**, *28*, 546.

[12]Apex2 v**2011**.2-0, Bruker Advanced X-ray Solutions, Bruker AXS Inc., Madison, Wisconsin, USA.

[13]Sheldrick, G. M., *Acta Cryst*., **2008**, *A64*, 112.

[14]Hübschle, C. B., Sheldrick, G. M., Dittrich, B., *J. Appl. Cryst.*, **2011**, *44*, 1281.

[15]Brandenburg, K., *Diamond Version 2.0 Impact GbR*, Bonn, Germany, **1998**.

[16]Macrae, F., Bruno, I. J., Chisholm, J. A., Edgington, P. R., McCabe, P., Pidcock, E., Rodriguez-Monge, L., Taylor, R., Van de Streek, J., Wood, P. A., *J. Appl. Cryst.*, **2008**, *41*, 466.

[17]Liang, W.-X., Qu, Z.-R., *Acta Cryst.*, **2008**, *E64*, m1254.

[18]Ha, K., *Acta Cryst.*, **2012**, *E68*, m176.

[19]Calve, N.L., Romain, F., Limage, M.H., Novak, A., *J. Mol. Struct*., **1989**, *200*, 131.

[20]Ratajczak, H. J., *J. Mol. Struct.*, **1969**, *3*, 27.

[21]Navak, A., *J. Mol. Struct.*, **1990**, *217*, 35.

[22]Smirani, W., Ben Nasr, C., Rzaigui, M., *Mat. Res. Bull.*, **2004**, *39*, 1103.

[23]Kaabi, K., Rayes, A., Ben Nasr, C., Rzaigui, M., Lefebvre, F., *Mat. Res. Bull.*, **2003**, *38*, 741.

[24]Oueslati, A., Ben Nasr, C., Durif, A., Lefebvre, F., *Mat. Res. Bull.*, **2005**, *40*, 970.

[25]Oueslati, A., Rayes, A., Ben Nasr, C., Lefebvre, F., *Mat. Res. Bull.*, **2005**, *40*, 1680.

Received: 25.02.2014
Accepted: 14.03.2014

EFFECT OF SURFACE ACTIVE AGENTS, CHELATING AGENTS AND ANTIBIOTICS ON L-METHIONINE FERMENTATION BY A MULTIPLE ANALOGUE RESISTANT MUTANT *CORYNEBACTERIUM GLUTAMICUM* X300

Subhadeep Ganguly[a] and Kunja Bihari Satapathy[a]*

Keywords: surface active agents; antibiotics; chelating agents; analogue resistant; mutant; *Corynebacterium glutamicum* X300; L-methionine; fermentation

In this present study, it was intended to examine the effects of different surface active agents (Tween 80, oleic acid, linoleic acid, palmatic acid, stearic acid , sodium laurylsulfate, laurylmethylgluceth-10-hydroxypropyldiammonium chloride, dimethyldicatadecylammonium chloride, tetramethyl ammonium hydroxide, Centimonium chloride and Bromidox), antibiotics(Penicillin G, Erythromycin, Chloramphenicol , Streptomycin, Tetracycline-HCl and Gentamycin) and chelating agents (EDTA, NTA, DTPA, Catechol, Protocatechuate and Citrate) on L-methionine fermentation by a multiple analogue resistant mutant *Corynebacterium glutamicum* X300. All these agents showed stimulatory effects on the fermentation process.

Corresponding Authors
E-Mail: res_biol@rediffmail.com
[a] Post-Graduate Department of Botany, Utkal University, Vani Vihar, Bhubaneswar-751004, Odisha

Introduction

L-methionine is an essential amino acid, required in human nutrition. Deficiency of L-methionine leads to developments such as rheumatic fever, muscular paralysis, hair loss, depression, toxemia, impaired growth etc.[1] Deficiency can be overcome by dietary supplementation. As per recommendation of Complementary Medicines Evaluation Committee (CMEC), L-methionine can be used therapeutically without any substance specific restriction. Because of inexpensive nature of fermentative production of other amino acids, efforts have been made to produce L-methionine by fermentation.[2-4]

Corynebacterium glutamicum is regarded as a model organism for L-amino acid production because of its simplified metabolic nature.[5,6] Thus, new strains can easily be produced from this parent strain by changing metabolic flux in order to produce L-methionine. The microbial production of L-methionine was performed in Japan in the 1970s.[7] In our previous study, we have already developed a high yielding multiple analogue resistant mutant of *Corynebacterium glutamicum* by protoplast fusion.[8] In this present investigation, we were intended to examine the effect of different surface active agents, antibiotics and chelating agents on L-methionine fermentation by the mutant *Corynebacterium glutamicum* X300.

Materials and methods

Selection of microorganism

A regulatory mutant *Corynebacterium glutamicum* X1 (accumulated only 0.6 mg mL^{-1} L-methionine) developed in our laboratory from its parent strain *Corynebacterium glutamicum* (basically a L-glutamic acid producing bacterium which does not accumulate L-methionine) which was isolated from North Bengal soil was subjected for mutational study.

Chemical and Physical mutagensis

To develop a high L-methionine yielding strain, the above mentioned regulatory strain was subjected to mutational treatments using ethyl methanesulfonate (EMS) and UV irradiations as chemical and physical mutagens, respectively, as follows:

Exposure to EMS

1 mL cell suspension (containing $3x10^8$ cells) was added to 9 mL EMS solution of different concentrations (221.8 mmol mL^{-1}, 186.3 mmol mL^{-1}, 76.9 mmol mL^{-1} respectively) and was incubated (10, 20, 30, 40 and 60 minutes respectively). From each sample, 1 ml cell suspension was then plated on CD agar medium and kept at 30 °C for 48 h.[8]

Treatment with UV irradiation

Strains (namely, *Corynebacterium glutamicum* X164 which is high L-methionine yielding and *Corynebacterium glutamicum* X124 which is a multiple analogue resistant strain) were selected for protoplast fusion. The cells were harvested in 100 mL growth medium composed of : glucose , 20 g L^{-1}; peptone, 10 g L^{-1}; yeast extract; 10 g L^{-1}; NaCl, 2.5 g; $MgSO_4.7H_2O$, 0.25 g.L^{-1}; $MnSO_4.4H_2O$, 0.1 g L^{-1}; K_2HPO_4, 1.0 g L^{-1}, KH_2PO_4, 1.0 g L^{-1} and biotin, 2 µg mL^{-1} in 250 ml Erlenmeyer conical flask at 30 °C: 2 ml cell suspension (containing $3x10^8$ cells mL^{-1}) was taken in a petridish (5 cm diameter) and expose it to UV irradiation, using Hanovia germicidal lamp (15 W) from a distance of 12 cm for different periods of time (1-9 min). The UV treated cells were plated in similar ways as mentioned above.[8]

Development of multiple L-methionine resistant strain

Multiple L-methionine analogue-resistant strain was develop by adding different L-methionine analogue (20-100 mg mL) to the growth medium (namely: α-methyl methionine , DL-methionine, D-methionine sulphate and DL-norleucine.[8]

Protoplast preparation, fusion and regeneration

Two superior for 24 hours. Then the cell suspensions were centrifuged separately at 10,000 rpm for 10 minutes. The pellets were collected and transferred aseptically to a protoplasting medium composed of: sucrose, 0.5 M, maleate buffer (pH 6.5), 0.02 M; $MgCl_2.H_2O$, 20 mM and lysozyme, 100 µg mL^{-1}. After protoplast fusion (observed under phase contrast microscope), protoplast were fused in a medium containing the same composition similar to the protoplasting medium along with polyethane glycol (30 %), dimethyl sulfide (15 %) and $CaCl_2$, 10 mM. The suspension was shaking at 50 rpm on a rotary shaker with incubator at 30 °C for 10 minutes and then it was diluted 10 fold with protoplast medium buffer (pH 6.5). The suspension was then centrifuged for 5 minutes at 25,000 rpm at 5 °C using a cold centrifuge apparatus (EPLX3761).

The pellet was collected and plated for colony formation for 48 h at 30 °C. The colonies were transferred to agar (2%) slants containing the same growth medium[8].

Viable counting of protoplast (Reversion of protoplast)

Protoplasts were diluted with 10 ml of dilution fluid and plated into Petri dish (diameter 5cm) containing agar medium allowed to grow at 30 °C for 48 h and subjected for subsequent fermentation trials.[8]

Composition of basal salt medium for L-methionine production

L-methionine production was carried out using the following basal salt medium (per litre): glucose, 60 g; $(NH_4)_2SO_4$, 1.5 g; K_2HPO_4, 1.4 g; $MgSO_4 \cdot 7H_2O$, 0.9 g; $FeSO_4 \cdot 7H_2O$, 0.01 g ;biotin, 60µg[8].

Optimum cultural conditions

Volume of medium, 25 ml; initial pH, 7.0; shaker's speed, 150 rpm; age of inoculum, 48 hours; optimum cell density, $4.0X10^8$ cells mL^{-1}; temperature 28 °C and period of incubation, 72 h.[9]

Composition of synthetic medium(per liter)

Glucose, 100 g; $(NH_4)_2SO_4$, 8.0 g (in terms of nitrogen); K_2HPO_4, 2.2 g; $MgSO_4.7\ H_2O$, 1.5 g; $FeSO_4.7H_2O$, 0.03 g; KH_2PO_4, 2.0 g; $ZnSO_4.7H_2O$, 1.6 mg; $CaCO_3$, 1.5 g; $Na_2MoO_4.2H_2O$, 5.0 mg; $MnSO_4.4H_2O$, 2.5 mg; biotin, 80 mg and thiamine-HCl, 70 µg.[10]

Addition of surface active agents

Varying concentrations of surface active agents (0.05-0.50 µl mL^{-1}) namely Tween 80, oleic acid, linoleic acid, palmitic acid, stearic acid, benzalkonium chloride, laurylmethylgluceth-10 hydroxypropyldiammonium chloride, dimethyl dicatadecyl ammonium chloride, tetramethyl-ammonium hydroxide, centrimonium chloride and bromidox were added separately to the synthetic medium in order to examine their effect on L-methionine fermentation by this mutant.[11]

Addition of antibiotics

Varying concentrations of antibiotics (5.0-20.0 µl mL^{-1}) of different antibiotics namely penicillin G, erythromycin, Chloramphenicol, Streptomycin Tetracycline-HCl and Gentamycin.[12]

Addition of chelating agents

Varying concentrations of chelating agents (10^{-3}-10^{-15} M) namely EDTA, NTA, DTPA, catechol, protocatechate and citrate.[13]

Analysis of L-methionine

Descending paper chromatography was employed for detection of L-methionine in culture broth and was run for 18 h on Whatman No.1 Chromatographic paper. Solvent system used include n-butanol: acetic acid: water (2:1:1). The spot was visualized by spraying with a solution of 0.2 % ninhydrin in acetone and quantitative estimation of L-methionine in the suspension was done using colorimetric method.[8] All the chemicals used in this study were analytical grade (AR) grade and obtained from E mark Borosil glass goods and triple distilled water used throughout the study.

Estimation of Dry Cell Weight (DCW)

The cell paste was obtained from the fermentation broth by centrifugation and dried in a dried at 100 °C until constant cell weight was obtained.[9]

Statistical analysis

All the data were expressed as mean±SEM.Data were analyzed using One Way ANOVA followed by Dunett's post hoc multiple comparison test using a soft-ware Prism 4.0.

Results

The effect of different surface active agents, antibiotics and chelating agents on L-methionine production by *Corynebacterium glutamicum* X300 has been presented in Table 1-3 as follows:

Table 1. Effect of surface active agents on L-methionine fermentation by *Corynebacterium glutamicum* X300

Surface active agents	Concentration, μg mL^{-1}	L-methionine, mg mL^{-1}	Dry Cell Weight, mg mL^{-1}
Tween80	0.0(control)	52.1±1.668	28.5±0.891
	0.05	52.8±1.202	*29.1±0.661
	0.10	*53.1±1.668	*29.3±0.983
	0.20	*53.6±0.913	**29.5±0.591
	0.50	*53.6±1.813	**29.5±0.993
Oleic acid	0.0(control)	52.1±1.831	28.5±0.662
	0.05	52.4±1.887	28.7±0.713
	0.10	*52.9±0.973	*29.0±0.683
	0.20	*52.9±1.854	*29.0±0.991
	0.50	*52.9±1.785	*29.0±0.772
Linoleic acid	0.0(control)	52.1±1.882	28.5±0.913
	0.05	52.4±1.683	28.7±0.683
	0.10	52.6±1.786	28.8±0.613
	0.20	52.6±1.991	28.8±0.551
	0.50	52.6±1.661	28.8±0.691
Palmatic acid	0.0(control)	52.1±1.661	28.5±0.771
	0.05	52.3±1.872	28.6±0.642
	0.10	52.7±1.601	28.8±0.773
	0.20	53.0±1.553	*29.0±0.613
	0.50	53.0±1.713	*29.0±0.661
Stearic acid	0.0(control)	52.1±1.662	28.5±0.672
	0.05	52.4±1.681	28.7±0.413
	0.10	52.7±1.881	28.9±0.662
	0.20	*53.1±1.682	*29.1±0.713
	0.50	*53.1±1.913	*29.1±0.463
Sodium Lauryl Sulfate	0.0(control)	52.1±1.992	28.5±0.441
	0.05	52.3±1.462	28.6±0.771
	0.10	52.6±1.562	28.8±0.683
	0.20	52.9±1.452	*29.0±0.421
	0.50	52.9±1.897	*29.0±0.613
Benzalkonium Chloride	0.0(control)	52.1±1.772	28.5±0.662
	0.05	52.3±1.813	28.6±0.591
	0.10	52.6±1.662	28.8±0.551
	0.20	52.6±1.811	28.8±0.613
	0.50	52.6±1.683	28.8±0.662
Laurylmethylgluceth-10 hydroxypropyldiammonium chloride	0.0(control)	52.1±1.662	28.5±0.491
	0.05	52.3±1.661	28.6±0.683
	0.10	52.5±1.261	28.8±0.613
	0.20	52.5±1.661	28.8±0.442
	0.50	52.5±1.713	28.8±0.681
Dimethyldicatadecyl-ammonium chloride	0.0(control)	52.1±1.662	28.5±0.436
	0.05	52.4±1.613	28.6±0.441
	0.10	52.7±1.661	*29.0±0.613
	0.20	52.7±1.662	*29.0±0.771
	0.50	52.7±1.715	*29.0±0.913
Tetramethylammonium hydroxide	0.0(control)	52.1±1.009	28.5±0.683
	0.05	52.3±1.613	28.6±-0.721
	0.10	52.7±1.662	28.8±0.991
	0.20	52.7±1.683	28.8±0.683
	0.50	52.7±1.653	28.8±0.772

Continuation of Table 1.

Centimonium chloride	0.0(control)	52.1±1.009	28.5±0.961
	0.05	52.3±0.986	28.6±0.777
	0.10	52.7±1.592	28.6±0.683
	0.20	53.1±1.821	28.9±0.661
	0.50	*53.1±1.452	28.9±0.513
Bromidox	0.0(control)	52.1±1.771	28.5±0.881
	0.05	52.3±1.562	28.6±0.771
	0.10	52.6±1.843	28.7±0.683
	0.20	53.0±1.661	*29.0±0.642
	0.50	53.0±1.832	*29.0±0.691

(Values were expressed as mean±SEM , where n=6, *p<0.05, **p<0.01 when compared to control)

Table 2. Effect of antibiotics on L- methionine fermentation by *Corynebacterium glutamicum* X300

Antibiotics	**Concentration, µg mL^{-1}**	**L-methionine, mg mL^{-1}**	**Dry Cell Weight, mg mL^{-1}**
Penicillin G	0.0(control)	52.1±1.683	28.5±0.991
	5.0	*53.2±1.771	28.1±0.891
	10.0	*53.9±1.913	*27.4±0.662
	15.0	**54.1±1.665	**27.0±0.814
	20.0	**54.1±1.567	**27.0±0.682
Erythromycin	0.0(control)	52.1±1.723	28.5±0.881
	5.0	52.6±1.835	*28.0±0.714
	10.0	53.0±1.623	**27.3±0.824
	15.0	*53.4±1.991	**27.0±0.591
	20.0	*53.4±1.613	**27.0±0.991
Chloramphenicol	0.0(control)	52.1±1.771	28.5±0.791
	5.0	52.4±1.825	*28.0±0.771
	10.0	52.9±1.992	**27.3±0.682
	15.0	*53.1±1.623	**27.1±0.814
	20.0	*53.1±1.719	**27.1±0.714
Streptomycin	0.0(control)	52.1±1.881	28.5±0.881
	5.0	52.4±1.913	28.1±0.692
	10.0	52.9±1.823	**27.3±0.661
	15.0	*53.1±1.913	**27.0±0.771
	20.0	*53.1±1.881	**27.0±0.651
Tetracycline-HCl	0.0(control)	52.1±1.852	28.5±0.881
	5.0	52.6±1.881	28.1±0.791
	10.0	52.8±1.826	**27.9±0.791
	15.0	52.8±1.001	**27.9±0.581
	20.0	52.8±1.825	**27.9±0.991
Gentamycin	0.0(control)	52.1±1.961	28.5±0.691
	5.0	52.3±1.991	28.3±0.661
	10.0	52.5±1.851	*28.0±0.813
	15.0	52.9±1.710	*27.8±0.792
	20.0	52.9±1.601	*27.8±0.681

(Values were expressed as mean±SEM , where n=6, *p<0.05, **p<0.01 when compared to control)

Table 3. Effect of chelating agents on L- methionine fermentation by *Corynebacterium glutamicum* X300

Chelating agent(s)	Concentration, µg mL^{-1}	L-methionine, mg mL^{-1}	Dry Cell Weight, mg mL^{-1}
EDTA	0.0(control)	52.1±1.915	28.5±0.661
	10^{-3}	52.6±1.993	28.7±0.913
	10^{-5}	53.0±1.682	*29.0±0.665
	10^{-10}	52.8±1.702	28.8±0.862
	10^{-15}	52.6±1.882	28.7±0.913
NTA	0.0(control)	52.1±1.602	28.5±0.771
	10^{-3}	52.4±1.883	28.6±0.684
	10^{-5}	52.3±1.991	28.6±0.661
	10^{-10}	52.0±1.003	28.4±0.813
	10^{-15}	51.7±1.875	28.1±0.813
DTPA	0.0(control)	52.1±1.992	28.5±0.661
	10^{-3}	52.6±1.915	28.8±0.613
	10^{-5}	52.9±1.683	28.9±0.882
	10^{-10}	*53.2±1.660	29.2±0.571
	10^{-15}	*53.2±1.503	29.2±0.882
Catechol	0.0(control)	52.1±1.991	28.5±0.613
	10^{-3}	52.4±1.962	28.6±0.661
	10^{-5}	52.9±1.889	28.8±0.711
	10^{-10}	52.6±1.993	28.6±0.945
	10^{-15}	52.3±1.691	28.4±0.661
Protocatechate	0.0(control)	52.1±1.713	28.5±0.683
	10^{-3}	52.6±1.002	28.8±0.702
	10^{-5}	*53.1±1.721	*29.1±0.817
	10^{-10}	52.8±1.005	28.9±0.864
	10^{-15}	52.6±1.691	28.8±0.883
Citrate	0.0(control)	52.1±1.188	28.5±0.613
	10^{-3}	52.4±1.682	28.6±0.771
	10^{-5}	52.7±1.773	28.8±0.956
	10^{-10}	*53.1±1.882	*29.1±0.887
	10^{-15}	*52.8±1.991	28.8±0.854

(Values were expressed as mean±SEM , where n=6, *p<0.05when compared to control)

Thus, maximum production of L-methionine can be obtained with Tween 80,0.10 µg mL^{-1}; oleic acid, 0.10 µg mL^{-1}; linoleic acid, 0.10 µg mL^{-1}; palmitic acid, 0.20 µg mL^{-1}; stearic acid, 0.20 µg mL^{-1}; gluceth-10-hydroxypropyl diammonium chloride, 0.10 µg mL^{-1}; dimethyl dicatadecyl-ammonium chloride, 0.10 µg mL^{-1}; tetramethylammonium hydroxide, 0.10 µg mL^{-1}; Centimonium chloride, 0.10 µg mL^{-1}; Bromidox,0.20 µg mL^{-1}; Penicillin G, 15.0 µg mL^{-1}; Erythromycin, 15.0 µg mL^{-1}; Chloramphenicol, 15.0 µg mL^{-1}; Streptomycin,15.0 µg mL^{-1}; Tetracycline-HCl, 10.0 µg mL^{-1}; Gentamycin, 15.0 µg mL^{-1}; EDTA,10^{-5} M; NTA, 10^{-4} M; DTPA, 10^{-10} M; catechol, 10^{-5} M; protocatechate, 10^{-5} M and citrate, 10^{-10} M.

Discussion

It has extensively been reported that small quantities of antibiotics can increase L-amino acid yield by different strains of bacteria[14-17]. Zaki *et al* . (1982) reported that erythromycin and tetracycline-HCl increase L-lysine accumulation by *Micrococcus glutamicus* when added to the fermentation broth[14]. Various surface active agents alter the permeability in microorganism and thereby can influence the accumulation of L-amino acids in fermentation broth [18-20]. Komicek *et al*. (1991) claimed that L-lysine accumulation by *Corynebacterium glutamicum* increased by Tween 80 due to alteration of cellular structure[20]. Takinami *et al*. (1963) reported the stimulatory effect of saturated fatty acids on L-glutamic acid fermentation[21]. Different chelating agents like EDTA, DTPA, NTA etc acting as 'metal buffer' under crucial condition and thus, may increase the secondary metabolite production by microorganisms[22].

Conclusion

From this present study it can tentatively be concluded that all these surface active agents, antibiotics and chelating agents examined showed positive impacts on L-methionine fermentation by this mutant. Thus, the production can be increased by using those agents in appropriate concentration.

References

[1]Rose, W. C., *Physiol. Rev*., **1938**, *18*, 109-136.

[2]Pham, C. B., Galvez, C. F. and Padolina, W. G., *ASEAN Food J*., **1992**, *7*, 34-37.

[3]Umerie, S. C., Ekwealor, I. A. and Nawabo, I. O., *Bioresour. Technol*., **2000**, *75*, 249-252.

[4]Odunfa, S. A., Adeniran, S. A., Teniola, O. D. and Nordstorm, J., *Int. J. Food Microbiol*., **2001**, *63*, 159-163.

[5]Lee, H.S. and Hwang, B.J., *Appl. Microbiol. Biotechnol*., **2003**, *62*, 459-467.

[6]Gomes, J. and Kumar, D., *Biotechnol. Adv*., **2005**, *23*, 41-61.

[7]Kase, H. and Nakayama, K., *Agric. Biol. Chem*., **1974**, *38*, 2021-2030.

[8]Ganguly, S., Satapathy, K. B. and Banik, A. K., *Res. J. Pharm. Dose Forms Technol.*, **2014**, *6*, 303-310.

[9]Ganguly, S., and Satapathy, K. B., *J. Bioprocess Technol.,* **2013**, Photon **98**, 303-307.

[10]Ganguly, S. and Satapathy, K. B., *Int. J. Multidiscip. Educ. Res.*, **2013**, *2*, 252-261.

[11]Ganguly,S. and Banik, A. K., *Int. J. Univers. Pharm. Life Sci*., **2011**, *1*, 94-97.

[12]Ganguly, S. and Banik, A.K., *J. Pure Appl. Microbiol*., **2012**, 6, 271-279.

[13]Ghosh, P., Ganguly, S. and Banik, A.K., *Int. J. Ind. Pharm. Biosci.,* **2012**, *1*, 1-7.

[14]Zaki, D., Galal, O., Hazino-Wahba, S. A., Morsi, K. I. and Wakell, E. A., *Nutr. Rep. Int*., **1982**, *26*, 537-546.

[15]Sen, S. K. and Chatterjee, S. P.,, *Folia Microbiol*., **1983**, *28*, 292-300.

[16]Sen, S. K. and Chatterjee, S. P., *Acta Biotechnol*., **1985**, *5*, 215-218.

[17]Israildes, C. J., Weir, A. N. and Bull, A. T., *Appl. Microbiol. Biotechnol*., **1989**, *32*, 134-136.

[18]Oshima, K., Tanaka, K. and Kinoshita, S., *J. Gen. Appl. Microbiol*., **1964**, *10*, 333-342.

[19]Smekal, F., Bulant, V., Kindlova, E ., *Kvasny Prum*, **1982**, *28*, 39-40.

[20]Komicek, J., Smekal, F. and Koniskova-Rodochora, M., *Folia Microbiol*., **1991**, *36*, 587-589.

[21]Takinami, K., Okada, H. and Tsunoda, T., *Agric. Biol. Chem*.,**1963**, *27*, 858-863.

[22]Chaudhury, A. Q. and Pirt, S. J., *J. Gen. Microbiol*.,**1966**, *43*, 71-81.

Received: 03.03.2014.
Accepted: 15.03.2014.

NOVEL ANTIOXIDANT ACTIVITY OF *CYATHULA PROSTRATA (L.) BLUME*)

Olawale H. Oladimeji,[a,]* Cyril O. Usifoh[b] and Emmanuel E. Attih[a]

Keywords: Free-radical; antioxidant; β-carotene; DPPH; *Cyathula prostrata*

Cyathula prostrata is a herbal recipe used in traditional medicine for the treatment of chest troubles, dysentery, diarrhea, craw-craw, scabies, sexual disease, rheumatism, tumours and inflammatory conditions amongst many others. There is not yet any claim on the use of the plant as an antioxidant agent, hence the need for this study. The crude extract, fractions and isolates tested positive for the characteristic rapid TLC free-radical scavenging activity with β-carotene and DPPH reagents. The ethyl acetate fraction gave marginally similar antioxidant activity (IC_{50}) as the crude extract at 0.76 µg mL^{-1} while the activity demonstrated by the butanol fraction was equally marginal at 0.77 µg mL^{-1}. However, HOO-1 and HOO-2 gave moderate activity at 0.53 µg mL^{-1} and 0.56 µg mL^{-1} respectively which were comparably better than the antioxidant activity obtained with vitamin E and A at 0.60 µg mL^{-1} and 1.11 µg mL^{-1} respectively. Furthermore, vitamin C recorded an IC_{50} of 0.49 µg mL^{-1} which was comparatively better than the activity given by either HOO-1 or HOO-2. The antioxidant activities given by the extract, fractions, HOO-1 and HOO-2 were instructive as the phytochemical screening of the *C. prostrata* indicated the presence of terpenes, flavonoids and tannins which have been reported in previous studies to exhibit antioxidant activities. The results of the antioxidant assays have revealed a novel potential for the use of *C. prostrata* as an antioxidant agent. Hence, it is proposed that the mechanism of action of the antioxidant activity obtained especially with HOO-2 could have proceeded in the same way (a 2H stabilized resonance) as that of the antiscurbitic activity of vitamin C in literature.

Corresponding Authors
Tel: +2347038916740
E-Mail: wale430@yahoo.co.uk, olawaleoladimeji@hotmail.com
[a] Department of Pharmaceutical and Medicinal Chemistry, Faculty of Pharmacy, University of Uyo, Uyo, Nigeria.
[b] Department of Pharmaceutical Chemistry, Faculty of Pharamceutical Sciences, University of Benin, Benin, Nigeria

INTRODUCTION

Free-radical oxygenated species (FROS) are believed to be responsible for inflammations. Also, free-radical damage and oxidative stress have become major health issues in recent years.

These chemical species have been implicated in many diseases and degenerative conditions such as Alzheimer's and Parkinson's diseases, heartdisease, stroke, cancer, pancreatitis, laryngitis, asthma, gastritis, dermatitis, hay fever, rheumatoid arthritis, wounds, atherosclerosis, emphysema, vitamin deficiencies, lung dysfunction, skin lesions, radiation injuries, premature aging and diabetes amongst many others.[1-12] *Cyathula prostrata* is employed in folklore medicine in the treatment and management of dyspepsia, scabies, craw-craw, diarrhea, dysentery, cholera, itch, ringworm, coughs, leprosy, sores,[13-18] articular arthritis, rheumatism,shingles, wounds, ulcers, inflammations[19-22] and sexually transmitted diseases.[23]

Though, its use in the treatment and management of inflammatory conditions is well known but there is yet any claims on its use as an antioxidant agent. Hence, the tests for free-radical scavenging (antioxidant) activity were considered relevant.

MATERIALS AND METHODS

The fresh aerial parts of *C. prostrata* (L.) Blume were collected in the month of July, 2011 on a farmland in Itak Ikot, Ikono Local Government Area, Akwa Ibom State, Nigeria. The authentication by comparison was done with herbarium samples of the Forestry Research Institute of Nigeria (FRIN) and the National Institute of Horticulture (NIHORT), both at Ibadan, in Oyo State, Nigeria. A voucher specimen of the plant (No H92) was deposited in the herbarium of the Faculty of Pharmacy, University of Uyo, Nigeria.

Extraction and processing

The plant was air-dried and powdered in an electric mill. The resultant coarse powder was then extracted with cold 96 % aqueous ethanol at room temperature (27± 2 ^{0}C) for 72 h. The filtrate was evaporated to dryness *in-vacuo* on a rotary evaporator (Buchi CH-920, Laboratorium Technic, Flawk/SG, Switzerland) and then stored in an amber bottle. Also, the aqueous extract of the plant was partitioned with organic solvents of increasing polarities namely, hexane, chloroform, ethyl acetate and butanol.The resultant mixtures were then bulked separately to obtain the hexane (3A), chloroform (3B), ethyl acetate (3C) and butanol (3D) fractions, respectively, which were then evaporated to dryness *in-vacuo* and then stored in a refrigerator at –4 ^{0}C prior to the antioxidant tests.

Chromatography

The ethyl acetate fraction (3C) was put through a combination of thin-layer, column and preparative chromatographies using silica-gel 254 (Sigma, USA) to obtain the isolates HOO-1 and HOO-2.

Initial rapid thin-layer chromatographic assays

β-Carotene assay

β-Carotene is a lipid soluble antioxidant which protects cell membranes from lipid peroxidation[24,25] hence, its selection in the screening of the plant for the initial free-radical scavenging activity.

This model involves the oxidation of linoleic acid (an unsaturated fatty acid) by Reactive Oxygen Species (ROS). The products formed will then initiate the carotene oxidation which leads to discolouration.[26,27]

2,2-Diphenyl-1-picryhydrazyl hydrate (DPPH) assay

This assay is based on the principle of reduction. The purple color of the methanolic solution of DPPH is bleached when it accepts hydrogen or electrons from extract/ fraction/ isolate/standard antioxidant drug.The crude ethanolic extract, fractions, HOO-1 and HOO-2 were tested. The tests were carried out by developing the samples in ethyl acetate:methanol (1:2) in duplicates. Ascorbic acid (Emzor, Nigeria) was spotted along to serve as positive control. One chromatogram was sprayed with 0.1% w/v methanolic solution of β-carotene (Sigma, USA) while the other was sprayed with 0.1% w/v methanolic solution of DPPH (Sigma, USA). The plates were irradiated with ultra-violet light at λ_m 366nm for 15 minutes. Spots which appeared white on a bleached background[7,28-30] or white against a purple background[29,31-33] were taken as evidence of positive tests indicating antioxidant activity.

Spectrophotometric determination of antioxidant activity using DPPH reagent

Substances capable of donating electrons or hydrogen atoms (free radical scavengers) are able to convert the purple-colored DPPH radical (2,2-diphenyl-1-picryl-hydrazyl hydrate) to its yellow-colored non-radical form (1, 1-diphenyl-2-picrylhydrazine).[33,34] This reaction can be monitored by spectrophotometry.

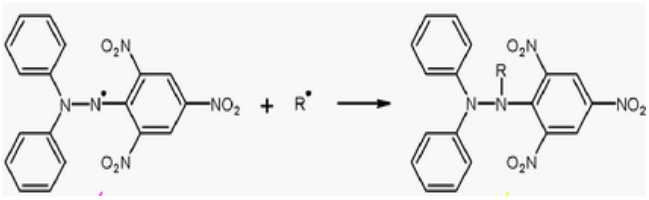

Scheme 1. DPPH + R^* (free-radical scavenger) = DPPH-R (Reduced DPPH)

This is the most widely reported method of screening for antioxidant activity in plants.[33-39] Hence, the antioxidant activity of *C. prostrata* was determined using the stable DPPH radical reagent.

Preparation of calibration curve for DPPH reagent

DPPH (4 mg) was weighed out and dissolved in methanol (100 mL) to produce a stock solution (0.004 % w/v). Serial dilutions were done to obtain the following concentrations; 0.0004, 0.0008, 0.0012, 0.0016, 0.0020, 0.0024, 0.0028, 0.0032 and 0.0036%w/v. The absorbance of each of the sample was obtained at λ_m 512nm[7,28-30] using ultra-violet spectrophotometer (Model No 3625, Unicam, England). A solution of methanol without DPPH was used as the blank for each of the determinations.Hence, the calibration curve for the DPPH reagent was prepared.

Determination of the antioxidant activity of crude extract, fractions, HOO-1 and HOO-2

2 mg of the crude ethanolic extract (2A), fractions (3A, 3B, 3C, 3D), HOO-1 and HOO-2 were separately dissolved in 50 ml of methanol. Serial dilutions were done to produce the following concentrations; 0.0008 mg mL^{-1}, 0.0016 mg mL^{-1} and 0.0024 mg mL^{-1} using methanol. 5 ml of each concentration was incubated with 5ml of 0.004 % w/v methanolic DPPH solution for optimal analytical accuracy.[28] After an incubation period of 30 minutes in the dark at room temperature (25 ± 2 ^{0}C), observation was made for a change in the color of mixture from purple to yellow.[33,34] The absorbance of each of the test samples was then taken at λ_m 512nm.[7,28-30,38] The Radical Scavenging Activity (RSA %) or Percentage Inhibition (PI %) of free radical DPPH was thus calculated: [34]

$$RSA(\%)(PI,\%) = 100\frac{A_{blank} - A_{sample}}{A_{blank}}$$

where

A_{blank} is the absorbance of the control reaction (DPPH solution without the test sample and

A_{sample} is the absorbance of DPPH incubated with the extract/ fraction/isolate/standard antioxidant drug.

Extract/fraction/isolate/standard antioxidant drug concentration providing 50 % inhibition (IC_{50}) was calculated using a graph of inhibition percentage against the concentration of the extract/fraction/isolate/standard antioxidant drug.[34,40,41]

DPPH assay of standard antioxidant drugs

Standard antioxidants namely, vitamin A (Fidson, Nigeria), vitamin C (Emzor, Nigeria) and vitamin E (Neimeth, Nigeria) were used. While vitamin C was in a tablet dosage form, vitamins A and E were formulated as gelatine capsules. The estimated weight of the formulations containing 2mg of the standard antioxidant drugs were determined by proportionality and then diluted. Methanol was used to dissolve vitamin C, while n-hexane was used to dissolve vitamins A and E. Thus, methanolic and n-hexane solutions of 0.004 % (w/v) DPPH were used for incubation of vitamin C, vitamin A and E respectively for 30 minutes. The absorbance values for the drugs were obtained at wavelength at λ_m 512nm and the IC_{50} determined.

RESULTS AND DISCUSSION

Collection, extraction and processing of plant

The plant was identified, authenticated and collected observing basic guidelines of plant collection. Also, the rules governing extraction and processing of extracts were kept, thus preventing any changes to the chemical composition of the crude extract.[42,43] Previous studies on the crude extracts revealed the presence of saponins, tannins, flavonoids, terpenes and cardiac glycosides while alkaloids, anthraquinones and cyanogenic glycosides were absent.[44-46]

Secondary metabolites such as saponins, cardiac glycosides, alkaloids, tannins and flavonoids have demonstrated in several previous studies[47-55] to be responsible for the cure or management of many ailments caused by microbes and different kinds of disease conditions in the ethno-medicine of plants.

Chromatography

The antimicrobial screening of the extract and fractions showed that the antimicrobial activity was most pronounced in the ethyl acetate fraction. Hence, the antimicrobial constituents of the crude extract resided largely in the ethyl acetate fraction, being the most active.

In addition, the ethyl acetate fraction extracted the largest amount of material. Consequently, silica-gel 254 chromatographic separation of the ethyl acetate fraction afforded HOO-1 and HOO-2.[45,46]

Rapid thin-layer chromatographic Analysis for antioxidant activity

The extract, fractions, HOO-1, HOO-2 and ascorbic acid gave white spots on bleached background when the chromatogram was sprayed with methanolic solution of β-carotene reagent.

The white spots (irrespective of initial spotted color) and the bleached background observed are pieces of evidence of carotene oxidation (discoloration). Also, the extract, fractions, HOO-1, HOO-2 and ascorbic acid showed white spots on a purple background when reacted with DPPH reagent.

The observed white spots (irrespective of initial spotted color) are evidence of the reduction of the DPPH reagent by the by free-radical scavenger in the samples.

Spectrophotometric determination of antioxidant activity

Preparation of calibration curve

A calibration curve was prepared for the DPPH radical reagent by measuring its absorbance at different concentrations. DPPH reagent obeys the Beer-Lambert law at concentrations of 50-100 μM.[31] The Beer-Lambert Law is the basis of absorption spectrophotometry.

Table 1. Preparation of calibration curve of methanolic solution of DPPH reagent

Concentration (%, w/v)	Absorbance, λ_{max} (512nm)
0.0004	0.065
0.0008	0.131
0.0012	0.191
0.0016	0.227
0.0020	0.264
0.0024	0.332
0.0028	0.373
0.0032	0.446
0.0036	0.518
0.0040	0.553

Therefore, a plot of absorbance against concentration for a cell of unit thickness (1cm) should give a straight line passing through the origin.[56,57] It was observed that a strict proportionality existed between the absorbance and concentration. Hence, a regression line which passed through the origin was obtained. The absorbance of the DPPH solution increased as the concentration increased as can be seen in **Table 1** and **Figure 1**.

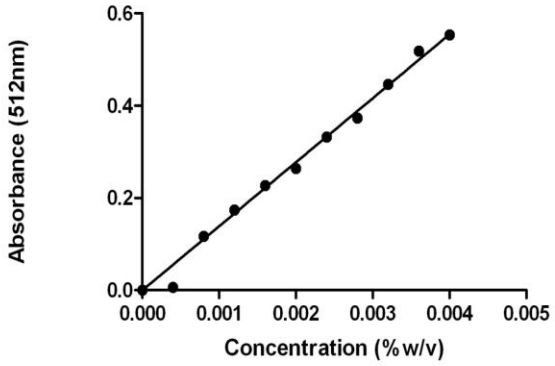

Figure 1. Calibration curve of methanolic solution of DPPH reagent.

Furthermore, the regression line buttresses this observation with a correlation factor of 0.99. Hence, the calibration curve obtained was used to correctly extrapolate subsequent concentrations of residual DPPH free radicals during the antioxidant test. Thus, the curve displayed in **Figure 1** confirms the purity, integrity and suitability of the DPPH reagent for the antioxidant assay.

Determination of the antioxidant activity of crude extract, fractions, HOO-1, HOO-2, vitamins A, C and E

The reduction of the DPPH radical was determined by measuring its absorption at a wavelength of λ_m 512 nm. It was observed that the absorbance of DPPH decreased as the concentration of added free radical scavenger (extract/fraction/isolate/standard antioxidant drug) increased which suggested that the DPPH reagent was being reduced. The results of the reduction are as presented in **Table 2**.

Table 2. Absorbance of test samples incubated with DPPH at different concentrations

Sample	Absorbance, λ_{max} (512 nm)		
	0.0008 mg mL^{-1}	**0.0016 mg mL^{-1}**	**0.0024 mg mL^{-1}**
2A	0.269	0.257	0.237
3A	0.299	0.299	0.304
3B	0.305	0.303	0.297
3C	0.268	0.259	0.244
3D	0.269	0.258	0.245
HOO-1	0.135	0.115	0.092
HOO-2	0.164	0.142	0.113
Vitamin A	0.292	0.257	0.243
Vitamin C	0.115	0.092	0.072
Vitamin E	0.154	0.154	0.154

Key: 2A=crude ethanolic extract of *Cyathula prostrata* 3A=hexane fraction; 3B=chloroform fraction; 3C=ethyl acetate fraction; 3D=butanol fraction; HOO-1=ethyl hexadecanoate (ethyl palmitate); HOO-2=7,9-di-tert-butyl-1-oxaspiro[4,5]deca-6,9-diene-2,8-dione.

The radical scavenging activity (RSA %) or percentage inhibition (PI, %) and the IC_{50} values of extract, fractions, isolates and standard antioxidant drugs were computed as **Table 3** shows. The RSA % is an indicator of the antioxidant activity of extract/fraction/isolate/ standard antioxidant drug.[33-38,58] The determined IC_{50} for the extract and ethyl acetate fraction were marginally similar at 0.76 µg mL^{-1}. Also, the antioxidant activity demonstrated by butanol fraction was equally marginal at 0.77 µg mL^{-1}. However, HOO-1 and HOO-2 gave moderate activity at 0.53 µg mL^{-1} and 0.56 µg mL^{-1}, respectively which were comparably better than the antioxidant activity obtained with vitamin A at 1.11 µg mL^{-1}. Vitamin C recorded an IC_{50} of 0.49 µg mL^{-1} which was comparatively better than the activity given by either HOO-1 or HOO-2 as can be seen in **Table 3.**

Table 3. Radical scavenging activity (percentage inhibition) of samples at different concentrations and IC_{50} of samples (blank absorbance of 0.004 w/v % methanolic DPPH reagent: 0.553)

Sample	RSA % (PI %)			IC_{50} mg mL^{-1}
	0.0008 mg mL^{-1}	**0.0016 mg mL^{-1}**	**0.0024 mg mL^{-1}**	
2A	51.28	53.53	57.22	0.76
3A	45.91	45.91	45.10	-
3B	44.92	45.26	46.38	-
3C	51.52	53.18	55.86	0.76
3D	51.28	53.42	55.75	0.77
HOO-1	75.53	79.29	83.30	0.53
HOO-2	70.29	74.31	79.53	0.56
Vitamin A	47.12	53.51	56.26	1.11
Vitamin C	79.21	83.34	86.92	0.49
Vitamin E	65.45	68.24	72.12	0.60

Key: Refer to Table 2; RSA % (PI %)=radical scavenging activity (percentage inhibition); IC_{50}=concentration at which 50 % of DPPH is scavenged or inhibited.

The antioxidant activities given by the extract, fractions, HOO-1 and HOO-2 were not surprising because the phytochemical screening of the *C.prostrata* indicated the presence of terpenes, flavonoids and tannins.[44-46] These classes of compounds have been reported in previous studies to exhibit antioxidant activities.[39,59-66] The results of the antioxidant assays have revealed a novel potential of *C. prostrata* as an antioxidant agent. A closer examination of the chemical structures of vitamin C and HOO-2 indicates some striking similarities between the two chemical entities as presented in **Figures 3** and **5**. There is a lactone ring common to both chemical substances. The mechanism of action of the antiscorbutic activity of vitamin C shows that there exists a 2H (2 hydrogen atom) stabilized resonance between the ascorbic acid and the dehydroascorbic acid isomers as reflected in **Figure 4.**[56,57]

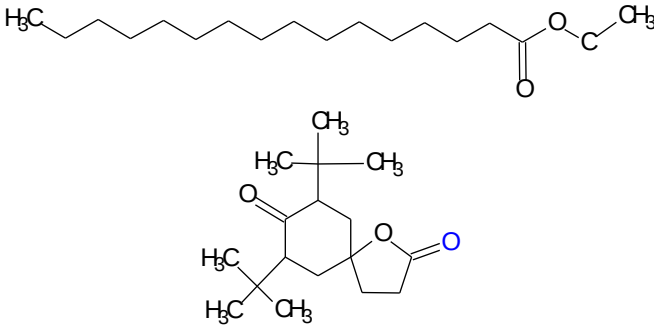

Figure 2. Chemical structures of HOO-1 (ethyl-hexadecanoate) and HOO-2 (7,9-di-tert-butyl-1-oxaspiro[4,5]deca-6,8-diene-2,8-dione

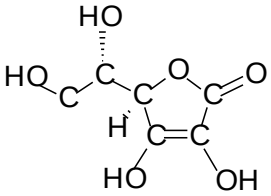

Figure 3. The Structure of Vitamin C

HOO-2 gave an antioxidant activity of 0.56 µg mL^{-1} which compare favourably with activity given by vitamin C at 0.49 µg mL^{-1}. Hence, it is proposed that the mechanism of action of the antioxidant activity obtained with HOO-2 might have proceeded in the same way (a 2H stabilized resonance) as that of vitamin C presented in **Figure 5**.

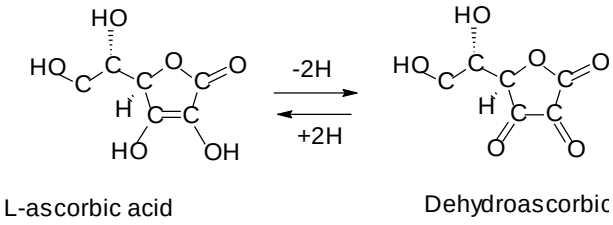

Figure 4. Mechanism of the antiscorbutic activity of Vitamin C

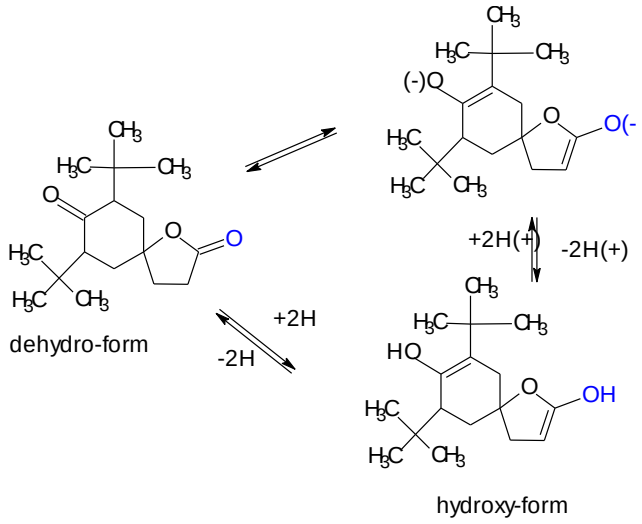

Figure 5. Proposed mechanism of the anti-oxidant activity of HOO-2 (7,9-di-tert-butyl-1-oxaspiro[4,5]deca-6,9-diene-2,8-dione).

Also, the importance of the radical scavenging ability of certain phytochemical compounds have found useful applications in the extension of shelf-life and control of deterioration of fatty foods, nutriceuticals and spices.[67-69]. Apart from the DPPH assay, other methods for determining the antioxidant activity of plants include the hydrogen peroxide, nitric oxide, conjugated diene, superoxide, phosphomolybdenum, peroxynitrile and xanthine oxidase assay methods amongst many others.[26,27]

ACKNOWLEDGEMENTS

The authors warmly acknowledge the material assistance of the Department of Pharmaceutical and Medicinal Chemistry, University of Uyo, Nigeria.

REFERENCES

[1]Takasu, N., Yamada, T., Shimizu, Y., *Biochem. Physiol. Res. Comm.*, **1987**, *148*, 1527-1532.

[2]Bryan, D., http://www.planthress.com/oxidative, **1996,** (2011-05-12).

[3]Thabrew, M. I.., Hughes, R. D., McFarlene, I. G., *Phytother. Res.*, **1998,** *12*(4), 288-290.

[4]Toda, S., Shirataki, Y., *Phytother. Res.*, **1998,** *12*(1), 59-61.

[5]Speroni, E., Guerra, M. C., Minghetti, A., Cerspi-Perellino, N., Pusini, P., Roda, A., *Phytother. Res.*, **1998,** *12*, 98-100.

[6]Ashcroft, G. S., *Natural Cell Biol.*, 1999, *1*(3), 260-266.

[7]Burits, M., Bucar, F., *Phytotheraphy Res.*, **2000**, *14*(5): 323-328.

[8]Baxter, J. D., Webb, P., Grover, G., Scanlan, T. S., *Trends Endocrinol. Metabol.*, **2004**, *15*, 154-155.

[9]Dufeng, H., Arthur, C., http://www.niaa.nih.com, **2004**, (2011-09-01).

[10]Guyton, M., Hall, B., *Textbook on Medical Physiology, 11th edition, Elsevier Publishers*, **2006**, 65-72.

[11]Piper, T., *Stedman's Medical Dictionary.* Lippincott Williams and Wilkins, 2006, 56-57.

[12]Nadier, http://www.beverlynadier.com/html/inflammation.html, **2007**, (2011-03-09).

[13]Dalziel, J. M., *Useful Plants of West Tropical Africa.* Crown Agents for Overseas Governments and Administrations, **1956**, 52.

[14]Burkill, H. M., *Useful Plants of West Tropical Africa. Vol.1 Fam A-D. Royal Botanical Gardens*, **1985**, 178.

[15]Etukudo, I., *Forests- Our Divine Treasure.* Dorand Publishers, **2000**, 164-165.

[16]Etukudo, I., *Ethnobotany.Conventional and Traditional Uses of Plants.* The Verdict Press, **2003**, 243.

[17]Kannappan, P., Sundaram, K. S., *J. Appl. Biosci.*, **2009**, *13*, 681-687.

[18]Trease, A., Evans, W. C., *Pharmacognosy.* 16th edition., W. B. Saunders Company, **2009**, 154-155 and 246-251.

[19]Keay, R. W., Hepper, F. N., *Flora of West Tropical Africa*, 2nd edition, Crown Office, **1953**.

[20]Breyer-Brandwijk, M. G., *Medicinal Poisonous Plants of Southern Eastern Africa*, E. and S. Livingstone Limited, **1962**, 1457.

[21]Iwu, M. M., *Handbook of African Medicinal Plants. C.R.C. Press*, **1993**, 12.

[22]Duke, J. A., *Borderline Herbs. C.R.C. Press*, **1984**, 21-24.

[23]Kayode, I., Kayode, G. M., *Ethnobotanical Leaflets*, **2008**, *12*, 44-45.

[24]Sies, H., *Am. J. Med.*, **1991,** *91*, 315-385.

[25]Sies, H., *Exp. Physiol.*, **1993,** *82*(2), 291-295.

[26]Bunta**,** G. W., Ingold, R. U., *Science*, **1984**, *224*, 569-573.

[27]Dapkevicius, A., Vanskulons, R., Van-Beek, T. A., Linssen, J. P., *J. Sci. Food Agric.*, **1998**, *77*(1), 140-146.

[28]Bondet, V., Brand-Williams, W., Berset, C., *Lebensmitt. Wissenshaft. Technol.*, **1997**, *30*, 609-615.

[29]Cuendet, M., Hostettmann, K., Potterat, O., *Helv. Chim. Acta*, **1997**, *80*(8), 1144- 1152.

[30]Kirby, A. J., Schmdt, R. J., *Int. J. Pharmacol.*, **1997**, *56*, 103-108.

[31]Blois, M. S., *Nature*, **1959**, *18*, 1199-1200.

32Brand-Williams, W., Cuvelier, M. E., Bersect, C., *Lebensmitt. Wissenshaft. Technol.*, **1995**, *28*, 75- 80.

[33]Nagalapur, S. K., Paramjyothi, S., *The Bioscan*, **2010**, *5*(1), 105-108.

[34]Guangrong, H., Jiaxin, J., Dehui, D., *Afr. J. Biotechn.***, 2008**, *7*(9), 1335-1338.

[35]Hu, C., Kitts, D. D., *J. Agr. Food Chem.*, **2000,** *48*, 1466-1472.

[36]Khaled, F. E., Ahmed, H. E, Amr, F., *Food Chem.*, **2002**, *78*(3), 331-336.

[37]Singh, R. P., Chidambara, M. K., Jayaprakash, G. K., *J. Agr. Food Chem.*, **2002,** *50*, 81-86.

[38]Nia, R., Paper, D. H., Essien, E. E., Oladimeji, O. H., Iyadi, K. C., Franz, G., *Nigerian J. Physiol. Sci.*, **2003,** *18*(1-2), 39-43.

[39]Oladimeji, H.O., Nia, R., Oforah, E., *J. Pharmacol.Toxicol.*, **2007**, *2*(6), 580-585.

[40]Lebeau, J., Furman, G., Bernier, J. L., Durietz, P., Teissier, E., Cotelle, N., *Free-Radicals Biol. Med.*, **2000,** *29*(9), 900-912.

[41]Leitao, G. G., Leitao, S. G., Vilegas, W., *Z. Naturforsch*, **2002**, *57C*, 1051-1055.

[42]Odebiyi, O. O., Sofowora, A., *Lloydia*, **1978,** *41*, 234.

[43]Odebiyi, O. O., Sofowora, A., *Phytochemical Screening of Nigerian Medicinal Plants-Part II. 2nd OAU/STRC Inter-Afr. Symp. Traditional Pharmacopoeia Afr. Medic. Plants. OAU/STRC Publishers No 115*, **1979,** 216.

[44]Oladimeji, O. H., Nia, R., Ajebesin, K., Igboasoiyi, A. C., Dalandi, B., *Global J. Appl. Med. Sci.*, **2005**, *4*(1-2), 9-12.

[45]Oladimeji, H. O., *Chemical and Bological Studies on Cyathula prostrata (L.) Blume.* Ph.D. Thesis, University of Uyo, **2012**, 189p.

[46]Oladimeji, H. O., Usifoh, C. O., *Int. J. Pharm. Sci. Res.*, **2013**, *4*(2), 628-633.

[47]Hillar, K., Bada, G., Schoopke, T., *Planta Medica*, **1990**, *56*, 644.

[48]Rios, J. L., Cholb, L., Huguet, I. A., Nora, A., Mariez, S., Paya, M., Alcarez, J. M., *Planta Medica*, **1990**, *56*, 644-645.

[49]Lamikanra, A., Ogundaini, A. O., Ogungbamila, F. O., *Phytother. Res*., **1990**, *4*(5), 198-200.

[50]Burapadaja, S., Bunchoo, A., *Planta Medica*, **1995**, *61*, 365-366.

[51]Harouna, H., Faure, R., Elias, R., Debrauwer R. L., Saadu L., Balansard M., Boudon, G., *Phytochemistry*, **1995**, *39*(6), 1483-1484.

[52]Aiyelaagbe, O., Adeniyi, B. A., Adesogan, K. E., Ekundayo, O., Gloer, J. B., *Conf. Natural Products Drug Develop.*,The Antimicrobial Plant Research Group, Faculty of Pharmacy, Obafemi Awolowo University,**1998**, 15.

[53]Adewunmi, R., Ibewuike J. C., Onawunmi, G. O., Ogundaini, O. A., *Conf. Natural Products Drug Development*, The Antimicrobial Plant Research Group, Faculty of Pharmacy, Obafemi Awolowo University, **1998**, 2.

[54]Ibewuike, J. C., Okeke, I. N., Mortimer, F., Houghton, P. J., Ogundaini, O. A., *Conf. Natural Products Drug Development.* The Anti-microbial Plant Research Group, Faculty of Pharmacy, Obafemi Awolowo University, **1998**, 4.

[55]Adesina, S. K., Idowu, O., Ogundaini, A. O., Oladimeji, H., Olugbade, T. A., Onawunmi, G. O., Pais, M., *Phytother. Res.*, **2000**, *14*, 371-374.

[56]Olaniyi, A. A., *Essential Medicinal Chemistry.* 1st edition, Shaneson C. I. Limited, **1989,** 137-154.

[57]Olaniyi, A. A., *Principles of Quality Assurance and Pharmaceutical Analysis.* Mosuro Publishers, **2000,** 151-158, 216-217, 264-269 and 443-457.

[58]Meir, S., Kanner, J., Akiri, B., *J. Agric. Food Chem.*, **1995,** *43*, 1813-1815.

[59]Tsimidou, M., Boskou, D., *Antioxidant Activity of Essential Oils from the Plants of Laminaceae Family. In: G. Charalampous Spices, Herbs and Edible Fungi.* Elsevier Publishers, **1994**, 273-284.

[60]Lagouri, V., Boskou, D., *Screening for Antioxidant Activity of Essential Oils Obtained from Spices. In: Charalampous G. Food Flavours. Generation, Analysis and Process Influence.* Elsevier Publishers, **1995,** 869-874.

[61]Yokosawa, T., Dong, E., Liu, Z. W., Shimizu, M., *In-vitro*, **1997,** *11*, 446-449.

[62]Daniel, R. S., Bifu, C. M., Devi, K. S., Augusti, K. T., *Indian J. Exp. Biol.*, **1998**, *36*, 902-906.

[63]Grassmann, J., Schneider, D., Weiser, D., Elsmer, E. F., *Arzneimittel- Forschung*, **2001**, *51*, 799-805.

[64]Alemika, T. E., Onawunmi, G. O., Olugbade**,** T. A., *J. Pharm. Bioresources*, **2004**, *1*(1), 7-11.

[65]Malaya, G., Upal, K. M., Ramanathan, S. K., Thangavel, S., Madgula, L., Mohan, V., *J. Pharmacol. Sci*., **2004**, *94*, 177-184.

[66]Svoboda, K., Brooker, J. D., Zrustova, J., *Acta. Horticul. (SHS)*, **2006**, *709*(1), 35-43.

[67]Thomas, P. G., Wade, A. M., *Official Gaz. US Trade Mark Office Patents*, **2001**, *1253*, 2.

[68]Braca, A., Polili, M., Sanogo, R., Sanou, H., Morelli, I., Pizza, C., De-Tommasi, N., *J. Agric. Food Chem.*, **2003**, *51*(23), 6689-6695.

[69]Liyana-Pathirana, C. M., Shahidi, F., *J. Sci. Food Agric.*, **2006**, *86*(3), 477-485.

Received: 12.01.2014.
Accepted: 17.01.2014.

BIOLOGICAL EVALUATION OF PYRAZINAMIDE DERIVATIVES AS AN ANTICANCER CLASS

Felipe A. R. Rodrigues,[a] Igor da S. Bomfim,[a] Bruno C. Cavalcanti,[a] Claudia Ó Pessoa,[a] Alessandra C. Pinheiro,[b] Camilo H. S. Lima,[b] Marcus V. N. de Souza[b]*

Keywords: antitumor activity, pyrazinamide, hydrazones, drugs

A series of fifty one pyrazinyl derivatives have been synthesized and evaluated for their activity against four cancer cell lines, exhibiting good citotoxicity (IC_{50} ranging from 1.1 to 5.6 μg mL^{-1}). The structure-activity relationship (SAR) analysis indicated that the hydroxyl group located in *ortho* position is critical for the biological activity of these compounds. The presence of hydroxyl groups on benzene ring plays an important role in the anticancer activity of this series, feature especially observed in disubstituted derivatives.

Corresponding Authors*
Tel.:+552139772404;
Fax: +552125602518
E-mail: marcos_souza@far.fiocruz.br
[a] Laboratório de Oncologia Experimental, Universidade Federal do Ceará, Fortaleza,CE, Brazil
[b] FioCruz-Fundação Oswaldo Cruz, Instituto de Tecnologia em Fármacos-Far-Manguinhos, Rua Sizenando Nabuco, 100, Manguinhos, 21041-250 Rio de Janeiro, RJ, Brazil

Introduction

The class of substances known as heteroaromatics is extremely important in drug discovery being present in many drugs used against different types of diseases. In this context could be mention the nucleus pyrazine, which possessed a wide range of biological activities being found in nature and in many drugs.[1]

For example, 2-isopropyl-3-methoxy pyrazine is an aroma compound found in coffee; pyrazinamide is a first line anti-tuberculosis drug;[2,3] oltipraz is a schistosomicide and also used for tumor prevention;[4,5] telaprevir is used to treat hepatite C;[6] bortezomib is used against multiple myeloma[7,8] and glipizide, an oral anti-diabete drug[9] (Figure **1**).

Due to the importance of pyrazine nucleus in drug discovery and our continuous search of new potent and safe anticancer agents the aim of this work is to present a series of fifty-one pyrazine hydrazone derivatives design by molecular hybridization (Scheme **1**), which were tested against four cancer cell lines with good results.

The reason to synthesized pyrazine hydrazone derivatives is because hydrazone functional group is also described with a wide range of pharmacological activities, such as anticancer agents.[10] It is important to mention that cancer disease is a leading cause of death worldwide and accounted for 7.6 million deaths (13 % of all deaths) in 2008[11] being urgently need new drugs and strategies to fight against this disease.

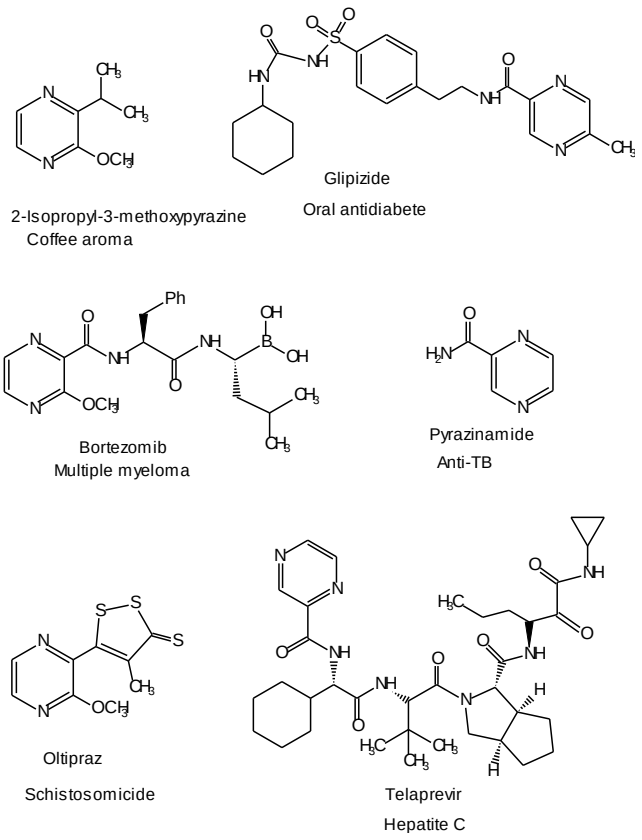

Figure 1. Biological activities of pyrazinyl derivatives

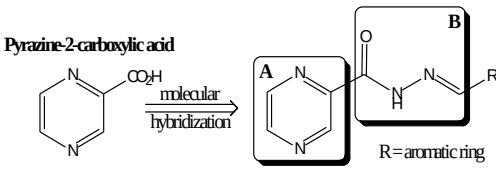

Scheme 1. Pyrazine hydrazone derivatives

 DOI: 10.17628/ecb.2014.3.358-361

Table 1. Growth Inhibition Percentage (*GI*, %) for three tumors cells line by the MTT Assay of compounds **1-51**.

Compound	R[b]	Growth Inhibition[a] (%)					
		SF-295	SD	HCT-116	SD	OVCAR-8	SD
1	H	49.40%	0.91%	50.06%	4.76%	66.30%	2.86%
2	2-NO_2	26.12%	3.83%	25.57%	2.81%	0.00%	0.00%
3	3-NO_2	16.,27%	1.32%	25.44%	0.91%	0.00%	0.00%
4	4-NO_2	24.66%	3.39%	28.37%	0.43%	5.83%	4.58%
5	2-F	35.49%	0.88%	11.21%	1.16%	0.00%	0.00%
6	3-F	41.03%	0.94%	16.26%	2.93%	11.43%	3.51%
7	4-F	17.43%	1.07%	17.12%	1.71%	0.00%	0.00%
8	2-Cl	32.20%	1.53%	13.37%	2.87%	0.00%	0.00%
9	3-Cl	36.02%	4.14%	13.80%	0.55%	11.97%	1.22%
10	4-Cl	47.60%	1.69%	9.23%	3.72%	8.41%	4.73%
11	3-Br	29.54%	1.55%	23.63%	3.11%	11.92%	4.35%
12	4-Br	16.81%	7.97%	22.85%	2.62%	10.79%	1.37%
13	2-CN	37.44%	2.26%	30.53%	1.04%	9.55%	6.03%
14	3-CN	26.34%	1.16%	22.25%	3.72%	0.00%	0.00%
15	4-CN	19.82%	1.69%	6.12%	3.23%	0.00%	0.00%
16	2-OH	42.32%	2.36%	53.17%	3.42%	52.37%	1.94%
17	3-OH	32.73%	1.63%	19.32%	2.87%	0.00%	0.00%
18	4-OH	41.43%	0.13%	12.25%	2.50%	2.80%	1.36%
19	3-OCH_3	9.62%	0.69%	23.33%	0.12%	8.31%	5.49%
20	4-OCH_3	31.54%	2.28%	13.45%	3.60%	0.00%	0.00%
21	3-OCH_2CH_3	32.65%	4.89%	30.27%	0.79%	15,16%	5.11%
22	4-OCH_2CH_3	0.70%	3.14%	23.11%	1.99%	2.7%	1.07%
23	2,3-diOH	90.41%	0.40%	53.21%	43.18%	51.78%	2.17%
24	2,4-diOH	74.24%	0.20%	74.37%	1.04%	94.48%	3.15%
25	2,5-diOH	64.07%	3.24%	49.70%	4.25%	74.24%	0.27%
26	3,4-diOH	47.61%	1.21%	27.44%	1.76%	34.61%	0.27%
27	2,3-diOCH_3	30.15%	1.46%	15.58%	7.77%	13.14%	0.41%
28	2,4-diOCH_3	49.69%	3.14%	22.39%	3.31%	6.17%	8.35%
29	2,6-diOCH_3	28.72%	4.25%	19.46%	1.24%	0.00%	0.00%
30	3,4-diOCH_3	38.59%	3.44%	23.12%	5.38%	7.53%	3.42%
31	3,5-diOCH_3	41.10%	3.74%	13.16%	1.24%	6.17%	0.96%
32	3,4,5-triOCH_3	31.45%	2.82%	17.38%	1.83%	6.96%	1.91%
33	2-OH; 3-OCH_3	90.84%	1.01%	89.75%	1.86%	91.58%	2.33%
34	2-OH; 4-OCH_3	87.33%	0.71%	92.46%	3.62%	93.03%	1.92%
35	3-OH; 4-OCH_3	39.24%	6.98%	10.53%	1.86%	4.24%	0.68%
36	3-OCH_3; 4-OH	53.55%	4.76%	25.17%	0.62%	13.44%	3.29%
37	2,3-Cl	48.83%	2.13%	25.83%	19.57%	12.08%	0.55%
38	2,4-Cl	29.50%	0.71%	10.23%	5.38%	0.00%	0.00%
39	2,6-Cl	30.36%	6.98%	2.76%	1.24%	4.04%	8.08%
40	3,4-Cl	46.68%	3.95%	18.14%	1.45%	0.00%	0.00%
41	2-OH; 5-NO_2	84.11%	1.01%	72.47%	1.18%	78.89%	1.86%
42	2,4-CH_3	57.99%	0.10%	15.80%	1.45%	4.04%	3.70%
43	2,4-F	39.67%	5.36%	10.89%	1.12%	0.00%	0.00%
44	4-N(OCH_2CH_3)$_2$	55.50%	3.58%	67.83%	2.32%	87.06%	2.29%
45	4-N(OCH_3)$_2$	41.83%	0.56%	19.02%	1.34%	21.04%	0.76%
46	2-furaldehyde	22.66%	1.60%	21.17%	2.68%	0.00%	0.00%
47	5-nitro-2-furaldehyde	41.48%	8.60%	85.68%	1.25%	88.57%	1.09%
48	5-amino-2-furaldehyde	23.28%	5.96%	24.19%	6.71%	1.35%	7.86%
49	5-nitro-2-thiophene-carboxaldehyde	30.12%	4.58%	68.26%	1.44%	26.81%	1.52%
50	2-pyridine carboxaldehyde	26.12%	1.60%	21.00%	2.56%	9.22%	1.64%
51	2-pyrrole carboxaldehyde	7.04%	0.94%	23.50%	0.37%	0.00%	0.00%

[a]Experiments were performed in triplicate. [b]In case of compounds **1-45**, R=substituents on a phenyl ring. SD – Standard Deviation.

 DOI: 10.17628/ecb.2014.3.358-361

Table 2. Cytotoxic activity of compounds **33**, **34** and **41** [IC_{50} (μg mL^{-1})] on tumor cell lines.

Compound	HCT-116	OVCAR-8	HL-60	SF-295
	IC_{50}, SD	IC_{50}, SD	IC_{50}, SD	IC_{50}, SD
33	4.099 3.213 to 5.228	1.564 0.8915 to 2.745	2.977 2.489 to 3.562	2.063 1.192 to 3.570
34	3.223 2.247 to 4.623	1.190 1.004 to 1.410	2.269 1.890 to 2.723	1.117 0.8968 to 1.390
41	4.595 4.121 to 5.122	5.606 4.436 to 7.086	3.828 3.184 to 4.603	1.550 1.024 to 2.345
Doxorubicin	0.125 (0.09 – 0.17)	0.265 (0.17 – 0.305)	0.02 0.01-0.02	0.23 0.19-0.25

* Data are presented as IC_{50} values and 95 % confidence intervals obtained by nonlinear regression for all cell lines colon (HCT-116), ovarium (OVCAR-8), (leukemia (HL-60), glioblastoma (SF-295), from three independent experiments. Doxorubicin (Dox) was used as positive control. Experiments were performed in triplicate. IC_{50} = concentrations that induce 50 % inhibition of cell growth in μg mL^{-1}.

Results and Discussion

Chemistry

These compounds have been previously synthesized, characterized and evaluated for their *in vitro* antibacterial activity against *Mycobacterium tuberculosis* H37Rv, displaying promising results also in this field.[12-14] Briefly, the synthesis of desired compounds involved the reaction of appropriate benzaldehydes and and 2-pyrazinecarbo-hydrazide, ethanol/water 1:1 ratio at room temperature for 4-24 hours. The compounds were obtained in 50-90 % yields.

Cytotoxicity Against Cancer Cell Lines

All compounds **1-51** were tested *in vitro* against three cancer cells: SF-295 (glioblastoma), HCT-116 (colon) and OVCAR-8 (human ovary) (National Cancer Institute, Bethesda, MD) at 5μg mL^{-1} by using MTT assay (Table **1**). Afterward, the compounds were classified by their growth inhibition (*GI*) percentage, at least in one cell line, as active (100 % *GI*), moderately active (75 % < *GI* < 100 %), or inactive (*GI* < 50 %).

Compounds **33**, **34** and **41** which displayed more than 84% of GI, were selected for *in vitro* anticancer activities evaluation against four human cancer cell lines: HCT-116 (colon), OVCAR-8 (human ovary), HL-60 (leukemia) and SF-295 (glioblastoma), using the MTT assay. A common feature of these active compounds is an *ortho*-hydroxy group in the phenyl ring, indicating the importance of this substituent in the biological activities. It is important to mention that the mono-substituted 2-hydroxy derivative, compound **16**, is only moderately active against these cell lines. This result suggests the importance of a second group into the ring, such as 3-methoxy (**33**), 4-methoxy (**34**) and 5-nitro (**41**) group, and that steric and/or electronic effects could play a critical role in anticancer activities.

The concentrations that induce 50 % inhibition of cell growth (*IC*50) in μg mL^{-1} are reported in Table **2**.

Conclusion

In this work we report a cytotoxicity activity of a series of fifth one pyrazinyl hydrazone derivatives, which have been evaluated for their activity against four human cancer cell lines. This study reveals the importance of hydroxyl substituent of aromatic ring located in ortho position, specially in dissubstituted compounds, indicating that the number, the positions and the type of substituents attached to aromatic ring can be critical for the biological activity and a good starting point to the discovery of new prototypes against cancer.

Acknowledgement

The authors are grateful to the Brazilian agencies Capes (Coordenadoria de Apoio à Pesquisa e Ensino Superior), CNPq (Conselho Nacional de Desenvolvimento Cientifico e Tecnológico), FUNCAP/CE (Fundação de Fundação Cearense de Pesquisa) and FAPERJ (Fundação de Amparo à Pesquisa do Estado do Rio de Janeiro) for fellowships and financial support.

References

[1]Miniyar, P. B., Murumkar, P. R., Patil, P. S., Barmade, M. A., Bothara, K. G., *Mini Rev. Med. Chem.*, **2013**, *13(11)*, 1607-1625. Doi: 10.2174/1389557511313110007

[2]Lima, C. H. S., Ferreira, M. L., De Souza, M. V. N., *Rev. Virtual Quim*., **2011**, *3*, 159-180.

[3]Pinheiro, A. C., De Souza, M. V. N., *Recent Patent Antiinfect. Drug. Discov*., **2013**, *8*, 130-138. Doi: 10.2174/1574891X113089990001

[4]Kang, S. G., Lee, W. H., Lee, Y. H., Lee, Y. S., Kim, S. G., *Carcinogenesis*, **2012**, *33(3)*, 661–669. Doi: 10.1093/carcin/bgr320

[5]Benson, A. B. III. *J. Cell Biochem.*, **1993,** *53(S17F)*, 278-291. Doi: 10.1002/jcb.240531041

[6]Akuta, N., Suzuki, F., Fukushima, T., Kawamura, Y., Sezaki, H., Suzuki, Y., Hosaka, T., Kobayashi, M., Hara, T., Kobayashi, M., Saitoh, S., Arase, Y., Ikeda, K., Kumada, H., *J. Clin. Microbiol.*, **2013**, *51(9)*, 2862-2868. Doi: 10.1128/JCM.01129-13

[7]Piperdi, B., Ling, Y., Liebes, L., Muggia, F., Perez-Soler, R., *Mol. Cancer Ther*., **2011**, *10*, 2029-2030. Doi: 10.1158/1535-7163.MCT-11-0745

[8]Paramore, A., Frantz, S., *Nat. Rev. Drug Discov*., **2003**, *2*, 611-612. Doi: 10.1038/nrd1159

[9]Hong, J., Zhang, Y., Lai, S., Lv, A., Su, Q., Dong, Y., Zhou, Z., Tang, W., Zhao, J., Cui, L., Zou, D., Wang, D., Li, H., Liu, C., Wu, G., Shen, J., Zhu, D., Wang, W., Shen, W., Ning, G., *Diabetes Care*, **2013**, *36(5)*, 1304-1311. Doi: 10.2337/dc12-0719

[10]Rollas, S., Küçükgüzel, Ş. G., *Molecules*, **2007**, *12*, 1910-1939. Doi: 10.3390/12081910

[11]World Health Organization, http://www.who.int/gho/ncd/mortality_morbidity/cancer/en/index.html (Accessed December, 2013)

[12]Vergara, F. M. F., Lima, C. H. S., Henriques, M. G. M. O., Candéa, A. L. P., Lourenço, M. C. S., Ferreira, M. L., Kaiser, C. R., De Souza, M. V. N., *Eur. J. Med. Chem*., **2009**, *44*, 4954–4959. Doi: 10.1016/j.ejmech.2009.08.009

[13]Ferreira, M. L., Candéa, A. L. P., Henriques, M. G. M. O., Kaiser, C. R., Lima, C. H. S., De Souza, M. V. N., *Lett. Drug Des. Discov.*, **2010**, *7(4)*, 275-280. Doi: 10.2174/1570180 10790945814

[14]Lima, C. H. S., Henriques, M. G. M. O., Candéa, A. C. S., Lourenço, M. C. S., Bezerra, F. A.F. M., Ferreira, M. L., Kaiser, C. R., De Souza, M. V. N., *Med. Chem*., **2011**, *7(3)*, 245-249. Doi: 10.2174/157340611795564303

Received: 10.03.2014.
Accepted: 18.03.2014.

PREPARATION OF NUCLEAR EXTRACTS FROM HeLa CELLS

Muhammad Tahman Shahid[a], Syeda Khair-ul-Bariyah[b]

Keywords: HeLa cells; nuclear extracts; immortal; cell lines; vaccines; polypeptide; RNA; DNA.

Stem cells are the powerful cells derived both from human and animal source. They have the ability to divide innumerably and differentiate into different cell types in the body. HeLa cells are the first immortal human cell lines grown in culture. These cell lines have proved beneficial in the development of polio vaccines and study of various viral cells. The present review aims to cover the studies done through nuclear extracts prepared from HeLa cells. Nuclear extracts from HeLa cells have been used to study the activation of ATM and ATR by double stranded DNA breaks, production of transcriptionally active extracts, analysis of RNA splicing in vitro using T7 RNA polymerase-derived splicing substrate RNAs and purification and characterization of proteins. By using these nuclear extracts, the mutational study of proteins still needs to be done to know exact reason of many unknown diseases. Wide variations of pH in extract preparation should be tested to get variations in extract obtained and methods should be modified for desired polypeptide length and to work with extracts at nano scale.

Corresponding Authors
E-Mail: skbariyah@gmail.com
[a] Center for Research in Molecular Medicine (CRIMM), The University of Lahore, Lahore, Pakistan.
[b] Department of Chemistry, Forman Christian College (A Chartered University), Lahore, Pakistan.

Introduction

Undifferentiated biological cells found in multicellular organisms are called stem cells. Through mitosis they differentiate into specialized cells and produce more stem cells. Stem cells have the property of self-renewal and the ability to differentiate into specialized cell types. In an adult organism, stem cells and progenitor cells make the repair system of the body and in a developing embryo differentiate into ectoderm, endoderm and mesoderm. According to potency, the stem cells may be totipotent, pluripotent, multipotent, oligopotent and unipotent.[1,2,3] Scheme 1 shows the hierarchy of stem cells.

Hierarchy of Stem Cells

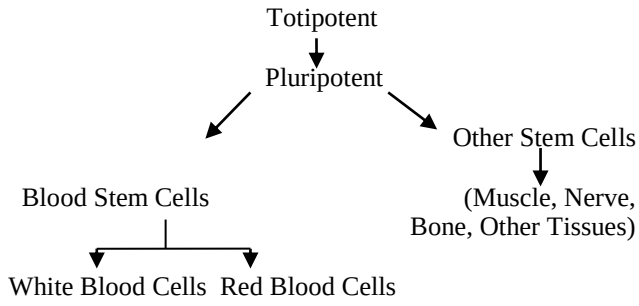

Scheme 1. Hierarchy of stem cells.

Two main types of stem cells are embryonic stem cells and adult stem cells. The embryonic stem cells are isolated from the inner cell mass of blastocysts whereas adult stem cells are found in various tissues and maintain and repair the tissue in which they are found. Three sources of adult stem cells are bone marrow, adipose tissue and blood. Embryonic stem cells are pluripotent and during development give rise to ectoderm, endoderm and mesoderm. The stem cells located in the organs of fetus are called fetal stem cells. They have two types: fetal proper stem cells and extraembryonic fetal stem cells. Fetal proper stem cells are multipotent as they come from fetus after abortion. They have a high level of division. Extraembryonic fetal stem cells cannot be distinguished from adult stem cells as they are obtained after birth. They are pluripotent and have a significant level of division.[4,5]

Stem cell treatment has proved to be promising in bone marrow transplants, Parkinson's disease, cancer, spinal cord injuries, Amyotrophic lateral sclerosis, muscle damage and multiple sclerosis. Many other diseases are still investigated where stem cells can prove to be potent and the risk of tumor formation due to multiple stem cells' division is also under study.[6,7,8] Scheme 2 shows the uses of stem cells.

Uses of Stem Cells

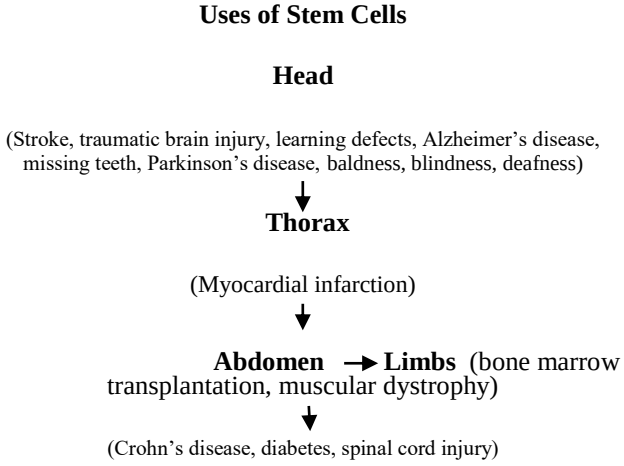

Scheme 2. Uses of stem cells.

The oldest and most commonly used cell line (stem cell) is HeLa cell, being an immortal cell line derived from cervical cancer cells of Henrietta Lacks, who died of cancer on February 8, 1951. The cells can divide innumerably as long as cell survival conditions are met, hence, they are called immortal. As these cells continue to mutate in cell culture, there are many strains of these. HeLa cells are the first successfully cloned human cells.[9,10,11] In 1950s, the first polio vaccine was tested by using HeLa cells.[12] Besides that, the effects of paro virus, oropouche virus and papillovirus were also studied by using these cell lines.[13,14] The ability of canine distemper virus to induce apoptosis in cancer cell lines is also revealed by HeLa cells.[15] The major research areas are cancer (apoptosis induction), gene mapping, effects of toxic substances and AIDS.[16] Figure 1 shows electron micrograph of apoptotic HeLa cells.

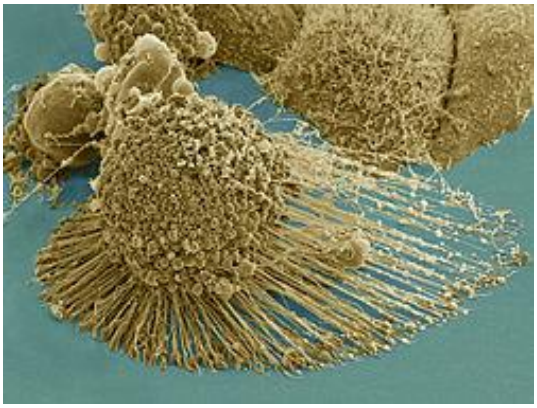

Figure 1. Electron Micrograph of HeLa Cells (http://en.wikipedia.org/wiki/File:HeLa-IV.jpg)

Nuclear extracts are prepared from HeLa cells since long to determine the mechanisms of splicing and polyadenylation. Characterization of these extracts has been done extensively.[17] The present review aims to cover the studies done so far on the nuclear extract preparation from HeLa cells and their uses.

Preparation of Nuclear Extracts

The general method for the preparation of nuclear extracts involves collecting cells from culture and microfuging them at 500 rpm for 10 minutes. The supernatant is discarded and the packed cell volume (pcv) is measured. The cell pellets are resuspended in a hypotonic buffer which is about 5 times in volume to pcv and centrifuged for 5 minutes at 5000 rpm. The supernatant is discarded and the packed cells are resuspended in a hypotonic buffer which is 3 times in volume to pcv. They are then allowed to swell for 10 minutes on ice. The cells are transferred to a glass Dounce homogenizer and homogenized by using 10 up and down strokes via type B pestle. The cells are again centrifuged for 15 minutes at 6500 rpm to collect nuclei. The packed nuclear volume (pnv) is measured and they are suspended in a low-salt buffer the volume of which is ½ pnv. In it high-salt buffer is added the volume of which is equal to ½ pnv. With continuous gentle mixing the nuclei are allowed to extract. By centrifuging the extracted nuclei for 30 minutes at 25000×g, the nuclei are pelleted. If the final volume is less than 100µL then it is made up to 100 µL by a solution containing equal volumes of high and low salt buffers. After dialyzing for 45 minutes, the dialysate is centrifuged for 20 minutes at 14500 rpm. The pellet is discarded and 5 µL of supernatant is removed for assay and the rest of it is cooled to –80 °C.

Preparation of Nuclear Extracts from HeLa Cells

The master regulators of DNA damage signalling pathway responding to a wide variety of DNA damage are Ataxia telangiectasia-mutated (ATM) and ATM-Rad3-related (ATR) kinases. An in vitro biochemical assay to study the activation of ATM and ATR by double stranded DNA breaks involves preparation of nuclear extracts from cultured HeLa cells followed by generation of DNA fragments using DNA oligonucleotides. Incubation of DNA fragments in extracts is then done along with analysis of the phosphorylation of ATM or ATR substrates.[18]

Many different DNA base lesions are corrected by base excision repair (BER) pathway. The BER activity of nuclear cell extracts from HeLa cells was investigated and the substrate used was a circular DNA molecule with either uracil or an AP-site in a defined position. From the same batch of cells, the BER activity of nuclear extracts varies inversely with the volume of nuclear extraction buffer relative to nuclei volume. Negative correlation was seen of the uracil-DNA glycosylase activity with the volume of extraction buffer. The method for the preparation of nuclear extracts was demonstrated to be an important factor along with conditions used in analysis.[19]

Many protocols for the preparation of splicing-competent extracts from whole cells, nuclei and cytoplasmic fractions and optimized production of transcriptionally active extracts from HeLa cells have also been reported.[20,21] A number of methods have been reported for the preparation of effective nuclear and cytoplasmic extracts from adenovirus-infected HeLa cells. Preparation of extracts from the infected cells along with analysis of RNA splicing in vitro using T7 RNA polymerase-derived splicing substrate RNAs has been investigated successfully.[22] For in vitro end joining using plasmid DNA as substrate, a protocol was reported which involved preparation of nuclear extracts from HeLa cells, plasmid substrate DNA preparation, in vitro DNA repair mechanisms and gel electrophoresis of the product. Overall the assay seemed powerful, but, it didn't consider the in vivo assembly of DNA into chromatin.[23]

In nuclear extracts of HeLa cells, 95-kDa CYP 450 2E1 promoter binding protein was found by bioaffinity mass spectrometry.[24] The protein was purified and characterized functionally from HeLa cells with the final preparation containing two polypeptides of 70 and 86 kDa mass, respectively. Interaction of both polypeptides was noted with a GC-stretch adjacent to the binding site of transcription termination factor 1. Electrophoretic mobility shift assay analysed specificity of binding to the barrier DNA. The biochemical properties of the protein resembled Ku antigen. In Ku depleted HeLa cell extracts, the recombinant Ku protein partially rescued the barrier activity, proving the synergic act of transcription termination factor 1 and Ku to prevent head-on-collision between the replication and transcription machinery.[25]

A high performance affinity purification technique was developed for cisplatin (CDDP)-damaged DNA binding proteins directly from HeLaS3 cell. Submicron beads made of styrene and glycidyl methacrylate (GMA) were used. Nonspecific protein adsorption was found to decrease. To prepare the beads for purification, immobilization of telomeric repeats (TTAGGG) (n) was done. Higher affinity to CDDP-DNA was shown by 9 proteins. These proteins were identified by amino acid sequence analysis including HMGB (high mobility group), hUBF (human upstream binding factor) and Ku autoantigen.[26] The electrophoretic mobility shift assay (EMSA) is for the study of the interaction of transcription factors to specific DNA sequences. The most important step in this assay is the preparation of high quality nuclear extracts. DNA-binding proteins were isolated from cultured cell lines and autopsy tissue samples from the human brain. Rapid method (RM) was used which followed low salt detergent lysis steps along with high salt extraction of nuclei. Three oligonucleotide probes (AP1, NF-κB and URE) were used to test the ability of nuclear extracts to form DNA-protein complex. The nuclear extracts taken by standard and RM methods showed similar capacity to form DNA-protein complex. Competition experiment was used to check the specificity of each nuclear extract forming the complex. Whether the nuclear extract was prepared by standard method or RM, unspecific bands were observed from both preparations. Hence, rapid method being simple allows preparation of nuclear extracts from several cell lines and tissue samples at the same time at much shorter time without affecting the DNA-binding activity. Cell type or tissue specificity can be determined efficiently and economically by using RM.[27] In mRNA decay, poly(A) tail removal is the rate limiting step, being responsible for translational silencing of maternal mRNA during oocyte maturation. Deadenylation in HeLa cell extracts and by PARN (purified mammalian poly (A)-specific exoribonuclease) was found to be stimulated by m(7)-guanosine cap on substrate RNAs. In the enzyme preparation, cap-binding proteins were not detectable and PARN was found to bind to m(7)GTP-Sepharose being eluted with the cap analogue m(7)GTP. During oocyte maturation, xenopus PARN catalyzed mRNA deadenylation. From oocyte extract, the enzyme was depleted with m(7)GTP-Sepharose. It could be linked to m(7)GpppG cap and could deadenylate m(7)GpppG-capped RNAs effectively than ApppG-capped RNAs. It proved PARN to be responsible for deadenylation during oocyte maturation.[28] For in vitro splicing, HeLa cell nuclear and cytosolic S100 extracts have also been prepared.[29] Chromatin degradation into oligonucleosomal and 30-50 Kb fragments is the basis of apoptosis. Both types of fragments can be recapitulated by crude nuclear extract from apoptotic rat thymocytes. The assay used HeLa cell nuclei as an exogenous substrate. By using size exclusion chromatography, a novel activity was identified producing 30-50 Kb DNA fragments and another 25 Kb activity that produced 30-50 Kb and oligonucleosomal fragments. DNA fragments with 3'-OH termini were produced by both activities. Inhibition of the activities was shown by serine protease inhibitors. By incubating the extracts with naked linear DNA, both activities turned insensitive to protease inhibitors. It indicated the presence of nuclease and protease activities in the preparation. Involvement of non-caspase proteases in apoptosis was proved and their function was supposed to be altering chromatin substructure and exposing it to nucleolytic attack.[30]

Modification of the preparation of crude nuclear extracts made it possible to establish an assay forming link between weak late and strong very late viral promoters. In case of both promoters, the virus-induced RNA polymerase initiates at a TAAG sequence motif. Investigation was done on the sequences responsible for functional TAAG motif and their role with respect to the strength of very late promoters. Hybrid promoters were constructed between the early pe38 and the very late polyhedrin promoters. The replacement of 7 nucleotides upstream of the non-functional TAAG sequences in the pe38 promoter with the corresponding sequences of the polyhedrin promoter was investigated to be sufficient for recognition by the virus-induced RNA polymerase. Replacement of the 5' untranslated sequences of the pe38 promoter by polyhedrin promoter and 7 nucleotides upstream of the TAAG motif established the strength of very late polyhedrin promoter.[31] A group of clones was isolated from a single cell line HeLa. They were methylated over the GPH alpha gene and showed a 400-fold range in its expression.[32] Various cellular components like mitochondrion, nuclear envelope, centromere etc are recognized by sera from patients with primary biliary cirrhosis. In these sera, a novel antibody reacts with a particular protein. By using rat liver cytoplasmic antigens, the antigen was identified by immunoprecipitation of [35S] methionine labelled HeLa cell extracts and by immunoblot using disrupted HeLa cell extracts.[33] Basic proteins which were normally lost by cathodic drift of carrier ampholyte focusing were separated from HeLa cells by 2D-electrophoresis using pH 12 with IPGs 8-12, 9-12 and 10-12. Due to IPG 9-12 the hectic procedure of nuclei preparation prior to histone extraction could be omitted.[34]Immunoaffinity purification on two types of affinity columns was used to prepare an antibody specific for human O6-methylguanine-DNA methyltransferase. The affinity columns had purified human and mouse methyltransferase proteins as ligands. The antibodies were used in Western blotting analysis of fractioned cell extracts and above 90% of the methyltransferase protein was recovered in the cytoplasmic fractions with MR-M cells and human HeLa S3 cells.[35]

Immunostaining confirmed the cytoplasmic localization of methyltransferase in HeLa S3 cells. The fractioned cell extracts from HeLa S3 cells treated with alkylating agents were analyzed by Western blotting analysis. Amount of the enzyme was found to decrease rapidly in the nuclear fraction than in the cytoplasmic fraction and slower recovery of the enzyme level was seen in the cytoplasmic fraction. It is therefore seen that after repair reaction methyltransferase protein is degraded in the nucleus and cytoplasmic enzyme is transported in it.[36] From nuclear extracts of HeLa cells, small nuclear ribonucleoproteins i.e snRNPs (U1, U2, U4, U6) were removed by antisense affinity depletion. Splicing activity was fully restored, after addition of a highly purified preparation of SR proteins, in reactions depleted of U1 snRNP. No reconstitution of splicing in reactions depleted of other snRNPs was noted. Reconstitution with SR proteins was seen of spliceosomes formed in the U1 snRNP-depleted reactions. The assembly of precursor messenger RNA (pre-mRNA) into a spliceosome is facilitated by high concentrations of SR proteins when there are no interactions with U1 snRNP.[37] The circular ribozyme has shown enhanced resistance to nuclear degradation as compared to linear form in nuclear and cytoplasmic extracts from HeLa cells.[38] Sterol regulatory element binding protein (SREBP)

was purified from nuclear extracts of human HeLa cells by ion exchange, gel filtration and DNA-affinity chromatography. A cluster of bands at 59-60 kDa were seen by sodium dodecyl sulfate gel electrophoresis of the purified preparation. As seen by cross-linking experiments, each band was bound to SRE-1 element. SREBP was found to work in coherrence with Sp1 nuclear factor to gain high level, sterol suppressible transcription of the gene for the LDL receptor.[39]

Characterization and differentiation of Su antigen has been carried out by Western immunoblotting and immunoprecipitation employing DNase CTNE and extracts of 35S-methionine labelled HeLa cells.[40] Nuclear extracts from various monkey and rat cell lines were yielded that could allow splicing of a model adenovirus pre-mRNA substrate.[41] A nuclear protein was identified from extracts of HeLa cells that could bind to the TAR element RNA in a sequence specific manner and moderated TAR activity in vivo.[42] By using antibodies raised against isolated rat liver nuclear matrix and cross-reactive with a 65-kDa HeLa cell nuclear matrix protein IGA-65, the role of nuclear matrix proteins in premessenger RNA splicing was investigated.[43]Incubation of SP6 generated mouse histone H4 mRNA precursors in nuclear extracts of HeLa cells yielded processed mRNA species ending on the 3' adenosine of the conserved terminal ACCA sequence.[44] By using HeLa nuclear extracts or ribonucleoproteins (RNPs) from rat liver nuclei as antigens, a monospecific anti-(U1)RNP serum was recognized in each preparation i.e. one polypeptide of 68 or 70 kD, respectively. HeLa nuclear extracts showed three additional antigenic polypeptides of 29, 28, and 16 kD with a serum of combined anti-Sm/(U1)RNP specificity, whereas, only two additional polypeptides of 27 and 16 kD were observed in rat liver RNPs.[45] By lysing mitotic HeLa cells in low-salt hypotonic buffer, cytoplasmic extracts were prepared and chromosomes were separated by centrifuging. The mitotic factors were extracted with high-salt (0.2 M-NaCl) buffer and both the protein fractions were evaluated for their maturation-promoting activity (MPA) in the Xenopus oocytes. The results showed that both the cytoplasmic and chromosomal fractions were identical in many respects, including their ability to induce GVBD, but the specific activity of the chromosomal fraction was at least 3-fold greater than that of the cytoplasmic fractions.[46] An enzyme was purified from uninfected HeLa cells that could cleave the 5'-terminal protein (VPg) from poliovirus RNA by rapid phenol extraction assay.[47]

Extracts were prepared from M cells which were as active in protein synthesis as S cell extracts. Binding of Met-tRNAf to 40S ribosomal subunits and binding of mRNA to ribosomes also exhibited similar activity in both extracts. In the preparation of cell-free systems, the difference in protein synthesizing activity was eliminated. The ribosomes of M cells had small molecular weight RNA, which inhibited protein synthesis in vitro and had possibly a nuclear origin causing reduction in the rate of protein synthesis in M cells.[48] A method for the covalent attachment of poly A and other nucleic acids to a methylene dianiline derivative of starch was described and its properties and use for the recovery of poly U sequences from both nuclear and cytoplasmic extracts of HeLa cells was also investigated.[49]

Conclusion

HeLa cells are the oldest stem cells, being the first human cell line to be isolated and cultured. The nuclear extracts from these cell lines have proved beneficial in the extraction of many proteins and enzymes. Moreover, RNA and DNA splicing and protein binding has been clarified. By culturing these cell lines in a variety of pH and temperature conditions (where the cells remain viable) and then taking extracts can uncover many unknown cellular and nuclear components. The area of genetic mutations should be focussed and methods still need to be modified to splice the DNA/RNA at the desired point and to get polypeptides of desired length. Moreover, by extracting nuclear extracts from HeLa cells of patients suffering from sarcoma of various types and diseases like HIV Aids, many unknown factors still unknown, can be explored and direction of studies can be shifted to success.

References

[1]Schöler, H. R., *Human Biotechnology as Social Challenge*, **2007**, 28.

[2]Mitalipov, S. and Wolf, D., *Adv. Biochem. Eng. Biotechnol.*, **2009**, *114*, 185-99.

[3]Ulloa-Montoya, F., Verfaillie, C. M. and Hu, W. S., *J. Biosci. Bioeng.*, **2005**, *100(1)*, 12-27.

[4]Ariff, B. and Eng, L. H., *Stem Cells: From Benchtop to Bedside*, **2005**, 5.

[5]Moore, K. L., Persaud, T. V. N. and Torchia, A. G., Philadelphia, PA: Saunders, Elsevier, **2013**.

[6]Lindvall, O., *Pharmacol. Res.*, **2003**, *47(4)*, 279-87.

[7]Goldman, S. and Windrem, M., *Phil. Trans. Roy. Soc. London B., Biol. Sci.*, **2006**, *361(1473)*, 1463-75.

[8]*Consumer Reports on Health*, **2005**, 8-9.

[9]Rahbari, R., Sheahan, T. and Badge, R.M., *BioTechniques*, **2009**, *46(4)*, 277-84.

[10]Scherer, W. F., Syverton, J. T. and Gey, G. O., *J. Exp. Med.*, **1953**, *97(5)*, 695-710.

[11]Puck, T. T. and Marcus, P. I., *Proc. Natl. Acad. Sci., USA*, **1955**, *41(7)*, 432-7.

[12]Scherer, W. F., Syverton, J. T. and Gey, G. O., *J. Exp. Med.*, **1953**, *97(5)*, 695-710.

[13]Acrani, G. O., Gomes, R. and Silva, M. L., V*irus Res.*, **2010**, *149(1)*, 56-63.

[14]Hou, S. Y., Wu, S. and Chiang, C., *J. Biol. Chem.*, **2002**, *277(47)*, 45619-29.

[15]Del Puerto, H. L., Martins, A. S. and Vasconcelos, A. C., *Virol. J.*, **2011**, *8*, 334.

[16]Smith and Van, *Baltimore City Paper*, **2002**.

[17]Nilsen, T. W., *Cold Spring Harb. Protoc.*, **2013**, *6*, 579-83.

[18]Shiotani, B. and Zou, L., *Methods Mol. Biol*., **2011**, *782*, 181-91.

[19]Akbari, M. and Krokan, H. E., *Mutat. Res*., **2011**, *736(1-2)*, 33-8.

[20]Kataoka, N. and Dreyfuss, G., *Methods Mol. Biol.*, **2008**, *488*, 357-65.

[21]Abmayr, S. M., Yao, T. and Parmely, T., *Curr. Protoc. Mol. Biol.*, **2006**.

[22]Mühlemann, O. and Akusjärvi, G., *Methods Mol. Med*., **2007**, *131*, 33-46.

[23]Iliakis, G., Rosidi, B. and Wang, M., *Methods Mol. Biol.*, **2006**, *314*, 123-31.

[24]Zhu, Y.I., Valdes, R.J. and Linder, M.W., *Clin. Chim. Acta*, **2006**, *371(1-2)*, 71-8.

[25]Wallisch, M., Kunkel, E. and Grummt, F., *Biol. Chem.*, **2002**, *83(5)*, 765-71.

[26]Tomohiro, T., Sawada, J. J. and Okuno, H., *Bioconjug. Chem*., **2002**, *13(2)*, 163-6.

[27]Lahiri, D. K. and Ge, Y., *Brain Res. Brain Res. Protoc*., **2000**, *5(3)*, 257-65.

[28]Dehlin, E. and Wahle, E., *EMBO J*, **2000**, *19(5)*, 1079-86.

[29]Mayeda, A. and Krainer, A. R., Methods Mol. Biol., **1999**, *118*, 309-14.

[30]Hughes, F. M. and Cidlowski, J. A., *Cell Death Differ*., **1998**, *5(12)*, 1017-27.

[31]Mans, R. M. and Knebel, D. M., *J. Virol.*, **1998**, *72(4*), 2991-8.

[32]Cox, G. S., Gutkin, D. W. and Cosgrove, D. E., *Biochim. Biophys. Acta*, **1998**, *1396(1)*, 67-87.

[33]Miyakawa, H., Kako, M. and Ueno, U., *Scand. J. Immunol*., **1998**, *47(1)*, 63-8.

[34]Görg, A., Obermaier, C. and Madjar, J. J., *Electrophoresis*, **1997**, *18(3-4)*, 328-37.

[35]Ishibashi, T., Nakabeppu, Y. and Sekiguchi, M., *Mutat. Res.*, **1994**, *315(3)*, 199-212.

[36]Ishibashi, T., Nakabeppu, Y. and Sekiguchi, M., *Mutat. Res.*, **1994**, *315(3)*, 199-212.

[37]Crispino, J. D., Blencowe, B. J. and Sharp, P. A., *Science*, **1994**, *265(5180)*, 1866-9.

[38]Puttaraju, M., Perrotta, A. T. and Been, M. D., *Nucleic Acids Res*., **1993**, *21(18)*, 4253-8.

[39]Wang, X., Briggs, M. R. and Brown, M. S., *J. Biol. Chem*., **1993**, *268(19)*, 14497-504.

[40]Treadwell, E. L., Müller, U. R. and Volkman, A., *J. Immunol. Methods*, **1991**, *142(2)*, 157-67.

[41]La Branche, H., Frappier, D. and Chabot, B., *Nucleic Acids Res.*, **1991**, *19(16)*, 4509-14.

[42]Marciniak. R. A., Gracia-Blanco, M. A. and Sharp, P. A., *Proc. Natl. Acad. Sci*., **1990**, *87(9)*, 3624-8.

[43]Smith, H. C., Harris, S. G. and Berget, S. M., *Exp. Cell Res.*, **1989**, *182(2)*, 521-33.

[44]Gick, O., Krämer, A. and Birnstiel, M. L., *EMBO*, **1986**, *5(6)*, 1319-26.

[45]Guldner, H. H., Lakomek, H. J. and Bautz, F. A., *J. Immunol. Methods*, **1983**, *64(1-2)*, 45-59.

[46]Adlakha, R. C., Sahasrabuddhe, C. G. and Rao, P. N., *J. Cell Sci.*, **1982**, *54*, 193-206.

[47]Ambros, V. and Baltimore, D., *J. Biol. Chem*., **1980**, *255(14)*, 6739-44.

[48]Tarnowka, M. A. and Baglioni, C., *J. Cell Physiol*., **1979**, *99(3)*, 359-67.

[49]Venkatesan, S., Nakazato, H. and Edmonds, M., *Nucleic Acids Res*., **1976**, *3(8)*, 1925-36.

Received: 12.03.2014.
Accepted: 19.03.2014.

SELF-ASSEMBLY OF SUPRAMOLECULAR COMPLEX OF Zn(II) AND 2,7-DITHIO-3,6-DIAZAOCTADIEN-3,5-DITHIOAMIDE-1,8 IN AN IMMOBILIZED $Zn_2[Fe(CN)_6]$-GELATIN MATRIX

Oleg V. Mikhailov[a]*and Denis V. Chachkov[b]

Keywords: template synthesis; gelatin-immobilized matrix; zinc(II) ethanedithioamide; DFT method; 2,7-dithio-3,6-diazaoctadien-3,5-dithioamide-1,8; self-assembly

A new complex formation process was occurred in the Zn(II)–ethanedithioamide–ethanedial three-components system when a *nano*-reactor consist of zinc(II) hexacyanoferrate(II)-gelatin immobilized matrix was contacted with an aq. alkaline (pH~12) solutions containing ethanedithioamide and ethanedial. It has been shown that self-assembly (template synthesis) of supramolecular (555)macrotricyclic Zn(II) coordination compound with chelating ligand 2,7-dithio-3,6-diazaoctadien-3,5-dithioamide-1,8 occurs under these conditions. Besides, ethanedithioamide and ethanedial act as ligand synthons in this process.

Corresponding Authors
E-Mail: olegmkhlv@gmail.com
[a] Department of Analytical Chemistry, Certification and Quality Managing, Kazan National Research Technological University, 420015 Kazan, Russia
[b] Kazan Branch of Joint Super-Computer Center of RAS, 420008 Kazan, Russia

Introduction

Complex formation processes proceeding in Co(II)–dithiooxamide– glyoxal, Ni(II)– dithiooxamide– glyoxal and Cu(II)– dithiooxamide– glyoxal systems under contact of corresponding metal(II) hexacyanoferrate(II)-gelatin-immobilized matrix (GIM) with aqueous-alkaline solutions containing dithiooxamide (ethanedithioamide) $H_2N–C(=S)–C(=S)–NH_2$ (EDTHA) and glyoxal (ethanedial) (EDA) HC(=O)–CH(=O), were described and analyzed.[1-4] The room-temperature self-assembly (template synthesis) of novel coordination compounds that was not formed in solution or the solid phase could be occurred in these specific conditions; besides, EDTHA and EDA were acted as ligand synthones in given process.

This paper is devoted to study similar self-assembly processes in the Zn(II)– EDTHA– EDA ternary system with using zinc(II) hexacyanoferrate(II)-gelatin-immobilized matrix ($Zn_2[Fe(CN)_6]$-GIM) at room temperature.

Experimentals

$Zn_2[Fe(CN)_6]$-GIM was prepared according to the original procedure.[5] Commercial X-ray film "Structurix D-10" was used as starting material. The samples were exposed with X-ray radiation with exposing doses of 0.01–1.0 Röntgen. Then, they were subjected to standard processing used in silver-halide photography[6] with treatment an aq. solution containing ($g·L^{-1}$) the following chemicals: methol 2.2, hydroquinone 8.8, Na_2SO_3 (96.0), Na_2CO_3 (48.0) and KBr (2.5) (this solution is known in silver-halide photography as developer D-19) for 6 min at 20 °C. After washing with running water for 5 min, the samples were treated with a 25 % aq. solution of $Na_2S_2O_3$ for 15 min at 20 °C and a running water washing was done for 15 min. The samples obtained as a result of given procedure (**Ag-GIM**) were treated with an aq. solution containing ($g·L^{-1}$): $K_3[Fe(CN)_6]$ (50.0), $K_4[Fe(CN)_6]$ (20.0), KOH or NaOH (10.0) and Na_2CO_3 (5.0) for 30 min at 20 °C. This treatment results formation of **$Ag_4[Fe(CN)_6]$-GIM** according to the reaction described by equation (1) (here and subsequently, substances immobilized into GIM, have been marked with bold type)

$$4Ag + 4[Fe(CN)_6]^{3-} \rightarrow \mathbf{Ag_4[Fe(CN)_6]} + 3[Fe(CN)_6]^{4-} \quad (1)$$

These matrixes were contacted with 0.1 M aq. solutions of zinc(II) chloride. The formation of zinc(II) hexacyanoferrate(II) and silver(I) chloride are occurred according to reaction (2):

$$\mathbf{Ag_4[Fe(CN)_6]} + 2ZnCl_2 \rightarrow \mathbf{Zn_2[Fe(CN)_6]} + 4AgCl \quad (2)$$

Finally, the samples obtained were contacted with a 25 % aq. solution of $Na_2S_2O_3$ at 20 °C for 5 min in order to remove AgCl from the matrix which results a zinc(II)hexacyanoferrate(II) containing GIM matrix according to the reaction (3)

$$4AgCl + 8Na_2S_2O_3 \rightarrow 4Na_3[Ag(S_2O_3)_2] + 4NaCl \quad (3)$$

The $Zn_2[Fe(CN)_6]$-GIM samples obtained in this way were washed with running water for 15 min. The resulting matrixes having 0.1-2.0 $mol·dm^{-3}$ zinc(II) hexacyanoferrate(II) concentration (C_F).

The samples were treated with an aqueous solutions containing the mixture (EDTHA + EDA). The concentration of EDTHA in the solutions (C_L^0) was ($1.0 \cdot 10^{-3}$ -$5.0 \cdot 10^{-1}$ mol·dm^{-3}). The molar EDTHA: EDA ratio was varied between 0.5 to 2.0, pH of the solutions were 12.0±0.1. The contact time of GIM with the EDTHA + EDA mixture solutions was 1-10 min at 20.0±0.5ºC. The gelatin layers containing the Zn(II) chelate complexes were washed with running H_2O for 15 min and then dried at room temperature. In order to determine the empirical formulas of coordination compounds formed in the GIM, these compounds were isolated from the corresponding matrixes by treating them with solutions of proteolytic enzyme (e.g. trypsine) as described in literature.[7] The Zn-complex containing GIM samples were placed in a 3 % aq. solution of trypsin or proteolytic enzyme of *Bacillus mesentericus*, then the solution was heated to 35-40 °C and hold at this temperature until the gelatinous layer of GIM was completely disappeared (typically it takes 15-20 min). The precipitate formed was filtered off from the mother liquor, washed with water and and dried at room temperature. The yield of Zn(II) chelate complex was in range 80-85 %. The precipitates isolated from GIM phase in the abovementioned way were subjected to chemical analysis. In order to determine the molecular masses of complexes obtained a Matrix-Assisted Laser Desorption/Ionization Time of Flight Mass spectroscopy (MALDI TOF) method was used with registration positively charged molecular ions (positive mode) signals. MALDI TOF mass spectra of substances isolated from GIM were obtained using a Dynamo (Finnigan) instrument in 4-nitroaniline matrix at 500 MHz frequency and 55.25 units of laser power.

Electron absorption spectra of the GIM substances were recorded using Specord UV-VIS (Karl Zeiss, Germany) and PU-8710 (Philips, The Netherlands) spectrophotometers in the 400-800 nm range. In order to record IR spectra in the 400-4000 cm^{-1} range, UR-20 and Specord M-80 spectrometers (Karl Zeiss, Germany) were used. The samples for IR measurements were suspended in vaseline oil. Thermal studies were made with using a Derivatograph 1000D (MOM, Hungary) instrument. Quantum-chemical calculations were carried out in the Kazan Branch of Joint Super-Computer Center of RAS (http://kbjscc.knc.ru).

Results and Discussion

A brownis-yellow colouring of the GIM phase was observed when the values of C_F and C_L^o were varied between 0.1 and 2.0 mol·dm^{-3}, or $5.0 \cdot 10^{-3}$ and $5.0 \cdot 10^{-1}$ mol·dm^{-3}, respectively, at 0.5-1.5 EDTHA:EDA molar ratio and t = 2-10 min reaction time. This colour does not change even upon treatment of the GIM phase formed with acids and alkalies. However, the coloured substance can be obtained only if $Zn_2[Fe(CN)_6]$-GIM phase is contacted with aqueous-alkaline solutions of both EDTHA and EDA, in the absence of EDA the formation of the brownish substance could not be occurred at all.

There is an intensive absorption band maximum in UV region of the electron absorption spectrum of this compound. It proves evidence that both EDTHA and EDA have to be participated in the formation of the brownish coloured compound.

The brownish-yellow color of GIM samples may be arisen from formation of a coordination compound can contain EDTHA and EDA ligands or a new ligand formed from EDA and EDTHA.

There are no data about existence Zn(II)-glyoxal (ethanedial) in the chemical literature. When $Zn_2[Fe(CN)_6]$-GIM was treated with an aqueous-alkaline solutions of EDA, no any changes in the spectral characteristics of gelatin mass could be detected. This fact unambiguously shows that Zn(II) does not form any complex with EDA either in the GIM or in aq. Phase, since EDA is a «hard» Pearson's base whereas Zn(II) is rather «soft» Pearson's acid.[8]

Supposing a mixed ligand complex formation of Zn(II) with EDTHA and EDA in the GIM-phase, it might be expected that the color of this mixed ligand-containing compound will differ from the color of homoligand Zn(II) complexes of EDTHA and EDA. Both $Zn_2[Fe(CN)_6$-GIM contains EDA and $Zn_2[Fe(CN)_6$-GIM contains EDTHA are yellow. The color changes of the GIM phase from slight yellow to brownish-yellow could only be observed, however, when EDTHA: EDA ratio is higher than 1:2.

Experiments with gelatin-immobilized **Zn(II)-EDTHA** chelate formed in the $Zn_2[Fe(CN)_6]$-GIM phase did not interact with aq. alkaline solutions of EDA at any pH and EDA concentration. Thus, the formation of a mixed ligand complex of Zn(II) with EDTHA and EDA seemed to be improbable based on the observed experimental data.

Since the absorption spectra of aqueous solutions containing only EDTHA and the aqueous solutions containing compositions of EDTHA + EDA at pH>9.0 were quite identical, if a new ligand was formed, then there was no doubt that the $Zn_2[Fe(CN)_6]$-GIM system had to play role in the formation of this new ligand.

Taking into consideration the all conditions and results, this possibility proved to be reality, namely, a new ligand formed in the Zn(II)– EDTHA–EDA system with self-assembling template synthesis o the new ligand in the $Zn_2[Fe(CN)]_6$-GIM "reactor".

When the polymeric GIM phase contains the Zn-complex (compound **1**) were destroyed according to the known method,[7] a brown substance having empirical formula $C_6H_4N_4S_4Zn$ (**1**) could be isolated [calcd. for this formula, %: C, 22.12; H, 1.24; N, 17.20; S, 39.37; Zn, 20.07; Found, %: C, 22.0; H, 1.3; N, 17.5; S, 40.0; Zn, 19.7]. The compound **1** proved to be practically insoluble in ethanol, acetone, chloroform, benzene and tetrachloromethane, and weakly soluble in coordinating solvents like DMFA, DMSO and HMPTA.

The band positions in the electron absorption spectra of the compound **1** measured in DMFA and DMSO solutions were completely coincided with bands observed in the UV spectrum of the reaction product of $Zn_2Fe(CN)_6$-GIM with EDTHA and EDA. This indicates that substance immobilized in the GIM is identical with the compound **1**.

The DTA data showed that this compound was extremely stable on heating and was not destroyed even at 400 ºC.

The mass-spectrum of compound **1** showed the peak of positive charged molecular ions having M/z^+= 326.0 ($C_6H_4N_4S_4Zn$, calculated value of M=325.7) and a fragment peak with M/z^+= 262 ($C_6H_6N_4S_4^+$, M=262.4, the free ligand arises from the destruction of complex).

There is a band at 3544 cm^{-1} in the IR spectrum of **1** which is characteristic for ν(NH) groups *coordinated* to metal ions, thus at least a part of NH groups in the compound **1** has to be connected to the zinc(II)-ion. Besides, IR spectrum of **1** exhibits intensive ν(C=N) and ν(C=S)bands at 1633 cm^{-1} and at 690 cm^{-1} as evidences the presence of C=S and C=N groups, respectively, in the complex **1**.[9] Bands belong to the C–S or N=C–S groups could not be detected at all, consequently C–S bond are not present the structure of complex **1**.

The ^{13}C NMR spectrum of compound **1** showed three signals. Based on the spectroscopic results, it can be concluded that the complex **1** is the (2,7-dithio-3,6-diazaoctadien-3,5-dithioamide-1,8)zinc(II) formed in the reaction (4).

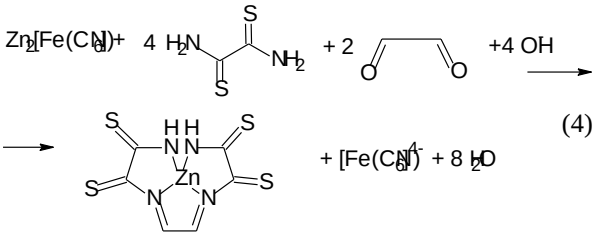

(4)

It should be noted that the reaction (4) cannot not been proceeded in the zinc(II)– **EDTHA**– **EDA** system at room temperature in aqueous solutions or in solid phase. Reacting $Zn_2[Fe(CN)_6]$ or other Zn(II) salt, e.g. $ZnCl_2$ with a mixture **EDTHA**+ **EDA** at pH 12.0, a brownish-yellow substance having empirical formula $C_4H_6N_4S_4Zn$ could be isolated from GIM (calcd. for this formula, %: C, 15.82; H, 1.99; N, 18.45; S, 42.22; Zn, 21.52; found, %: C, 16.1; H, 1.8; N, 18.3; S, 41.9; Zn, 21.7). The same product, $C_4H_6N_4S_4Zn$ was formed when $Zn_2[Fe(CN)_6]$ or $ZnCl_2$ reacted with aq. alkaline (pH 12.0) solution containing only **EDTHA**.

This substance was proved to be a Zn(II)-ethanedithioamide complex having metal ion: deprotonated **EDTHA** ratio was equal to 1:2 which formed according to a simple complex forming process (5)

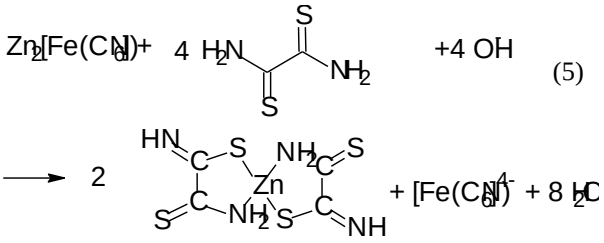

(5)

The coordination compound of Zn(II) with 2,7-dithio-3,6-diazaoctadien-3,5-dithioamide-1,8 (**1**) synthesized had not been known previously. Unfortunately, all of our attempts to isolate single crystal and doing X-ray diffraction analysis were failed, because the preparation method using $Zn_2[Fe(CN)_6]$-GIM always led to the amorphous form of the compound **1.** This amorphous form of compound **1** was unsuitable even for powder X-ray diffractometry as well. Due to this situation the exact spatial structure of the synthesized complex (1) is still open question which requires further studies.

The quantum-chemical calculations on the structural features of metal-macrocycle coordination mode in the compound **1** formed in the Zn(II)–EDTHA–EDA ternary system, however, obviously give some reliable structural information. One of the most suitable method for such kind of calculations was the hybrid method of the density functional theory, DFT B3LYP. In this work a DFT B3LYP level of theory with the 6-31G(d) basis set in Gaussian03 was used.[10-12] The preliminary results given by this method for various chelate complexes of 3*d*-elements showed that the method allows a good possibility to calculate the basic geometric parameters of these type of structures.

As it was expected from our experimental IR data, the ZnN_4-coordinated isomer proved to be more stable comparing that with the isomer with ZnS_2N_2 coordination mode. According to our calculations, the total energy of Zn(II) chelate complex formed in the template reaction (4) and contains ZnN_4 chelating group was less with 92.8 kJ mol^{-1} than the total energy of the ZnN_2S_2 chelate isomer complex.

Some quantum-chemical calculations were also carried out to determine the molecular structure as well fort eh compound formed according to the Eqn. (4) and contained ZnN_4 coordination mode. The molecular structure of "template" Zn(II) complex considered can be seen in Fig. 1, and the important parameters of the structure are given in the Table 1.

As it can be seen from the parameters given in Table 1, the complex **1** has distorted square-planar configuration of ZnN_4 (sum of valence angles ∠N4Zn1N1, ∠N3Zn1N2, ∠N2Zn1N1 and ∠N4N1N2 is 336.9°, which shows an important distortion from the ideal ZnN_4 square-planar configuration. However, the atom located in the three 5-membered metal chelate rings as well as the four (NNNN)-coordinating donor atoms are located in a plane.

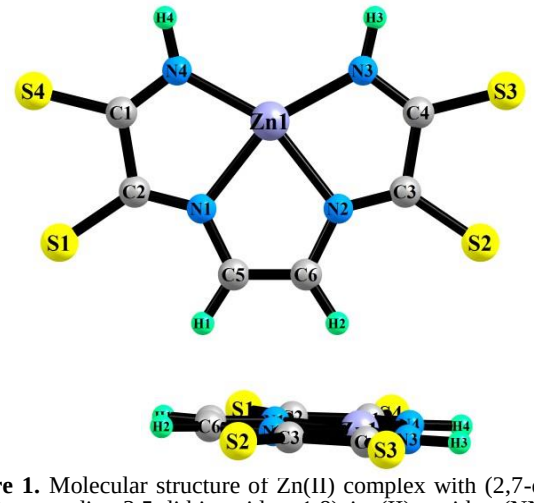

Figure 1. Molecular structure of Zn(II) complex with (2,7-dithio-3,6-diazaoctadien-3,5-dithioamidate-1,8)zinc(II) with (NNNN)-coordination: front view (*a*) and view from the side (*b*)

Table 1. Selected parameters of molecular structure of complex with (NNNN)-coordination of donor centers formed in the Zn(II)–ethanedithioamide– ethanedial ternary system.

Bond lengths, *pm*			
Zn1–N1	209.1	Zn1–N2	209.1
Zn1–N3	199.5	Zn1–N4	199.5
N1–C2	130.2	N2–C3	130.2
C1–C2	150.5	C3–C4	150.5
C1–N4	131.3	C4–N3	131.3
N1–C5	137.5	N2–C6	137.5
C2–S1	171.2	C3–S2	171.2
C1–S4	170.5	C4–S3	170.5
N3–H3	101.7	N4–H4	101.7
C5–C6	136.8		
Valence angles, °			
Valence angles in 5-membered cycle 1		**Valence angles in 5-membered cycle 2**	
∠Zn1N1C2	114.0	∠Zn1N2C3	114.0
∠N1C2C1	113.8	∠N2C3C4	113.8
∠C2C1N4	117.3	∠C3C4N3	117.3
∠C1N4Zn1	114.7	∠C4N3Zn1	114.7
∠N4Zn1N1	80.2	∠N3Zn1N2	80.2
Angles sum (VAS[51])	540.0	Angles sum (VAS[52])	540.0
Valence angles in 5-membered cycle 3		**Non-valence angles in NiN_2S_2 grouping**	
∠Zn1N1C5	115.6	∠N1N2N3	100.2
∠N1C5C6	116.2	∠N2N3N4	79.8
∠C5C6N2	116.2	∠N3N4N1	79.8
∠C6N2Zn1	115.6	∠N4N1N2	100.2
∠N2Zn1N1	76.3	Angles sum (NVAS)	360.0
Angles sum (VAS[53])	540.0		
Torsion angles, °			
∠N4Zn1N2C6	0.07	∠N1C2C1N4	0.06
∠N3Zn1N1C5	1.06	∠N2C3C4N3	0.06
∠Zn1N1C5C6	0.09	∠Zn1N1C2S1	180.0
∠Zn1N2C6C5	0.10	∠Zn1N2C3S2	180.0
∠N1C5C6N2	0.00	∠Zn1N4C1S4	180.0
∠N2C6C5N1	0.00	∠Zn1N3C4S3	180.0
∠Zn1N1C2C1	0.02	∠C2N1C5C6	180.0
∠Zn1N2C3C4	0.03	∠C3N2C6C5	180.0

The calculations performed on the structure of N2S2-coordinated Zn-complex of 2,7-dithio-3,6-diazaoctadien-3,5-dithioamide-1,8, the N2S2 coordination centers are not located in one plane , and the structure is extremely distorted (Fig. 2). This maiy be the main reason for its less stability comparing it with the ZnN4 coordinated isomer.

The calculated dipole moment of the complex is 1.75 Debye units, and ccording to our calculated parameters the ground state of the complex **1** is a spin singlet, thus it must be diamagnetic nature.

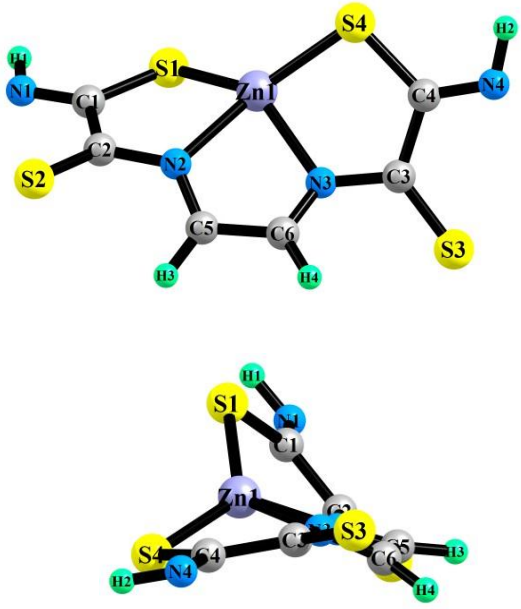

Figure 2. Molecular structure of Zn(II) complex with (2,7-dithio-3,6-diazaoctadien-3,5-dithioamidate-1,8)zinc(II) with (NSSN)-coordination: front view (*a*) and view from the side (*b*)

Conclusion

A reaction of ethanedithioamide and ethanedial with a $Zn_2[Fe(CN)_6]$-GIM (gelatin-immobiliozed matrix) system in the presence of aq. alkalies resulted specific conditions to form a "self-assembled" macrotricyclic distorted square-planar Zn(II) chelate complex with metal ion:ligand ratio of 1:1. This complex can be formed only in the GIM system but does not form either in solution or in solid phase, as it was observed in the reaction of of Cu(II), Co(II) and Ni(II) containing GIM phases with (N,S)-group abd carbonyl-group containing ligands.[13-15]

It should be noted that the Zn(II) complex has ZnN_4-coordination mode, which is different from the similar Cu(II), Ni(II) and Co(II) complexes of this ligand.

Acknowledgements

The financial support from Russian Foundation of Basic Researches (RFBR), grant N **09-03-97001** is acknowledged. Also, authors are grateful for Supercomputer Center of Kazan Scientific Center of Russian Academy of Sciences where all quantum-chemical calculations were carried out.

References

[1]Mikhailov, O. V. Khamitova, A. I., *Transit. Met. Chem.*, **2000**, *25*, 26.

[2]Mikhailov, O. V., Khamitova, A. I., Shigapova, L. S., Busygina, T. E., *Transit. Met. Chem.*, **1999**, *24*, 503.

[3]Mikhailov, O. V.,*Transit. Met .Chem.*, **2000**, *25*, 552.

[4]Mikhailov, O. V., Khamitova, A. I., Morozov, V. I., *Heterocyclic Commun.*, **2000**, *6*, 137.

[5]Mikhailov, O. V., *Russ. J. Gen. Chem*., **1998**, *68*, 827.

[6]James, T. H., *The Theory of Photographic Process*, New York, Macmillan Publishing Co., Inc.; London, Collier Macmillan Publishes, **1979**. Chapters 11, 15.

[7]Mikhailov, O.V., *Indian J. Chem.*, **1991**, *30A*, 252.

[8]Pearson, R. J., *J. Am. Chem. Soc.*, **1963**, *85*, 3533.

[9]Nakamoto, *K., Infrared and Raman spectra of inorganic and coordination compounds*, 4th Edit., Wiley, New York, **1991**.

[10]Becke, A. D., *J. Chem. Phys*., **1993**, *98*, 1372.

[11]Lee, C., Yang, W. Parr, R. Q., *Phys. Revs. B*, **1988**, *37*, 785.

[12]*Gaussian 03, Revision B.04,* Frisch, M. J. Trucks, G. W. Schlegel, H. B., Scuseria, G. E., Robb, M.A., Cheeseman, J. R., Montgomery, J. A., Vreven, T., Jr., Kudin, K. N., Burant, J. C., Millam, J. M., Iyengar, S. S., Tomasi, J., Barone, V., Mennucci, B., Cossi, M., Scalmani, G., Rega, N., Petersson, G. A., Nakatsuji, H., Hada, M., Ehara, M., Toyota, K., Fukuda, R., Hasegawa, J., Ishida, M., Nakajima, T., Honda, Y., Kitao, O., Nakai, H., Klene, M., Li, X., Knox, J. E., Hratchian, H. P., Cross, J. B., Adamo, C., Jaramillo, J., Gomperts, R., Stratmann, R. E., Yazyev, O., Austin, A. J., Cammi, R., Pomelli, C., Ochterski, J. W., Ayala P. Y., Morokuma, K., Voth, G. A., Salvador, P., Dannenberg, J. J., Zakrzewski, V. G., Dapprich, S., Daniels, A. D., Strain, M. C., Farkas, O., Malick, D. K., Rabuck, A. D., Raghavachari, K., Foresman, J. B., Ortiz, J. V., Cui, Q., Baboul, A. G., Clifford, S., Cioslowski, J., Stefanov, B. B., Liu, G., Liashenko, A., Piskorz, P., Komaromi, I., Martin, R. L., Fox, D. J., Keith, T., Al-Laham, M. A., Peng, C. Y., Nanayakkara, A., Challacombe, M., Gill, P. M. W., Johnson, B., Chen, W., Wong, M. W., Gonzalez, C. and Pople, J. A. //Gaussian, Inc., Pittsburgh PA, **2003**.

[13]Mikhailov, O. V., *J. Coord. Chem*., **2008**, *61*, 1333.

[14]Mikhailov, O. V., *Nanotechnol. Russia*, **2010**, *5*, 18.

[15]Mikhailov, O. V., *Inorg. Chim. Acta*, **2013,** *394*, 664.

Received: 12.03.2014.
Accepted: 20.03.2014.

CONVENIENT ROUTE FOR STUDYING REACTIVITY OF ISOTHIOCYANATES TOWARDS BARBITURYL ISOTHIOCARBAMIDE

Madhuri M. Sontakke,[a] Baliram N. Berad,[a] Chandrakant S. Bhaskar,[b] and Madhukar G. Dhonde[c]*

Keywords: Barbituryl isothiocarbamide; alkyl isothiocyanates; aryl isothiocyanates, barbituryl isodithiobiurets

The simple protocol for the synthesis of barbituryl isodithiobiurets without any catalyst has been developed. The reactivity of alkyl or aryl isothiocyanates towards barbituryl isothiocarbamide has been studied. The different reactivity, insolubility and high stability are output of our novel synthesized barbituryl isodithiobiurets. The mild reaction conditions, easy product workup and excellent yields, are the major advantages of present protocol.

Corresponding Authors
E-Mail: madhudash2001@yahoo.co.in
[a] Department of Chemistry, RTM, Nagpur University, Nagpur(MS), India – 440033.
[b] Department of Chemistry, Art's, Commerce & Science College, Koradi (MS), India – 441111.
[c] Department of Chemistry, Shri Mathuradas Mohota college of Science, Nagpur(MS), India – 440009. Fax-+91-712-2744992

INTRODUCTION

A large class of barbiturate drugs which are used as hypnotics, sedatives, anticonvulsants, anesthetics, as central nervous system depressants and also have industrial applications.[1-6] In 1903 Fischer and Von Mering synthesized the first therapeutically active derivative of barbiturates by replacing the C-5 hydrogens of the barbituric acid ring with ethyl substituents, upon administration of this new barbiturate derivative, human subjects fell into a state of hypnosis or deep sleep, this new diethyl barbiturate, commonly called Veronal (Fig. 1a).[7,8]

The barbiturate moiety show a wide spectrum of medicinal activities including treat anxiety, insomnia, seizure disorders, migraine headaches and use in surgery as general anesthetics (Fig 1b).[9] All of the barbiturate derivatives which have been reported to have pronounced hypnotic activity are disubstituted in 5-position. While the 5,5'-dialkyl barbituric acids are the hypnotics most commonly encountered, certain 1,5,5'-trialkyl derivatives (Fig. 1c) are active, producing narcosis of short duration. Some 1,3,5,5'-tetraalkyl derivatives (Fig. 1d) produce a hypnotic action of very transient character. The study of a series of 1,3,5-trialkyl barbituric acids (Fig. 1e), which was undertaken to determine whether such compounds have hypnotic activity comparable to their 1,5,5'-isomers or are inactive like the 5-monoalkyl and 1,5-dialkyl barbituric acids.[10] The synthetic protocol of mono C-alkylation and mono C-benzylation of barbiturate intermediates has been developed.[11]

A variety organic isothiocyanates are good building block moiety used as precursor in many organic transformations.[12-14] Highly electrophilic centre carbon atom of NCS group reacts rapidly, and under mild conditions with oxygen, sulfur or nitrogen centered nucleophiles to give rise to carbamates, thiocarbamides or thiourea derivatives respectively. Organic isothiocyanates have shown excellent and tremendous diverse biological, medicinal, pharmaceutical and other valuable properties such as goitrogenic, anti-bacterial, anti-fungal, anti-protozoal, anti-carcinogenic[15] inhibitory effects upon soil nitrification[16] and bio-conjugate activities.[17-18]

Literature review uncovered that there is no direct C-S coupled barbituric acids. But the β-position of side chain of barbituric acid has been substituted with sulphur using 5-n-amyl-5-(β–bromoethyl)-barbituric acid with potassium ethyl xanthate. The resulting products on pharmacological screening tests indicated that, such compounds are not suitable for anesthetia or hypnosis. [19] The same reaction protocol of the C-S bond formation products at β–position has been extended to include the potassium thiocyanate and isothiouronium salts but did not give products with anticonvulsant action by the electrical method. [20]

Owing to the simplicity of the desired starting material, barbituryl isothiocarbamide (**2**) was prepared by simple reaction of monobromobarbituric acid [21] and thiourea by employing a well-known literature method. [22] In continuation we are reporting first time the synthesis of barbituryl isodithiobiurets by involving the barbituryl isothiocarbamide and alkyl/aryl isothiocyanates, these may prove important intermediate if investigated thoroughly (Scheme 1).

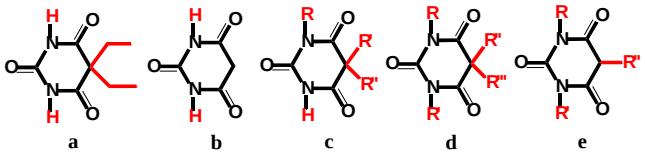

Figure 1. Barbiturates

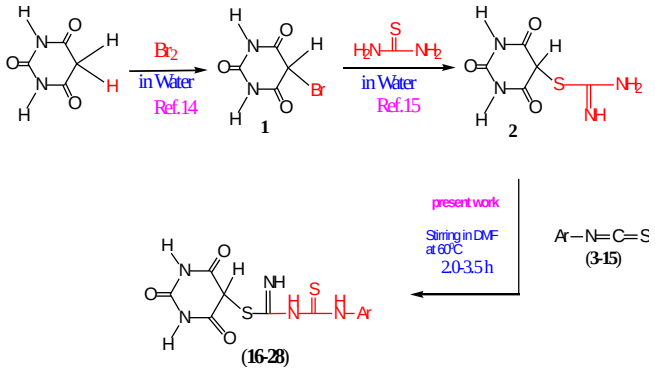

Scheme 1. Reactivity of alkyl/aryl isothiocyanates with barbituryl isothiocarbamide

EXPERIMENTAL

Synthesis of S-(2,4,6-trioxohexahydropyrimidin-5-yl)-1-(H)-5-aryl-2,4-isodithiobiurets (16-28)

A mixture of 2-(2,4,6-trioxo-hexahydropyrimidin-5-yl) isothiourea (**2**, 2.5 mmol), alkyl/aryl isothiocyanate (**3-15**, 2.5 mmol), was stirred in DMF (20 mL) at 60 ^{0}C for 2.5 h till the consumption of starting material took place to afford a solid products (**16-28**). The progress of reaction was monitored by TLC. After completion of the reaction, crude products were filtered and further purified by recrystallization. The products were desulphurised by alkaline plumbite solution showing positive test of C=S grouping (Table 1 and Graph 1). The newly synthesized compounds were characterized by IR, ^{1}H NMR, ^{13}C NMR and HRMS studies.

Table 1. Synthesis of barbituryl isodithiobiurets via unlike reactivity of isothiocyanates

2, mmol	3-15, mmol	Ar	Time, h	16-28	Yield,[a] %
2.5	3 (2.5)	C_6H_5	2.5	16	92
3.9	4 (3.9)	2-CH_3-C_6H_4	2.0	17	94
3.9	5 (3.9)	3-CH_3-C_6H_4	3.0	18	93
3.9	6 (3.9)	4-CH_3-C_6H_4	2.0	19	96
3.9	7 (3.9)	2-Cl-C_6H_4	2.0	20	94
3.9	8 (3.9)	3-Cl-C_6H_4	3.5	21	93
3.9	9 (3.9)	4-Cl-C_6H_4	2.5	22	97
3.9	10 (3.9)	2-$CH_3OC_6H_4$	2.5	23	93
3.9	11 (3.9)	3-$CH_3OC_6H_4$	3.0	24	91
3.9	12 (3.9)	4-$CH_3OC_6H_4$	2.5	25	96
3.9	13 (3.9)	$(CH_3)_3C$	3.5	26	90
4.9	14 (4.9)	CH_2-C_6H_5	3.0	27	92
4.9	15 (4.9)	CH_2=$CHCH_2$	3.5	28	93

[a] isolated yield

We have synthesized thirteen title compounds and characterized them on the basis of spectral analysis like, IR, ^{1}H, ^{13}C NMR and HRMS.

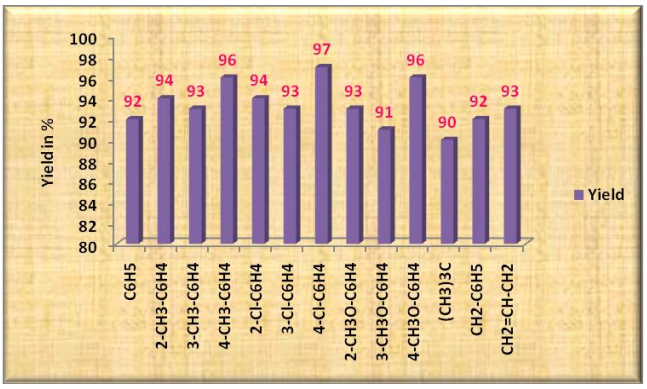

Graph 1. Isolated yields of the prepared compounds

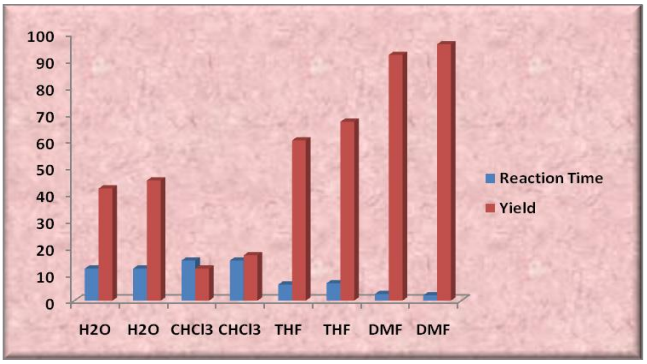

Graph 2. Yield of compound **16** and **19** as the function of reaction time in different solvents

Few of them were insoluble in most of the organic solvents. Title compounds **16**, **18**, **20**, **21** and **25** are soluble only in DMSO and rest of them including **17**, **19**, **22-24** and **26-28** are not soluble in suitable organic solvents, therefore we have provided the spectral data like IR, ^{1}H, ^{13}C NMR and HRMS of these title compounds but for rest of them only IR spectra have been given (Table 2).

RESULTS AND DISCUSION

The starting material barbituryl isothiocarbamide was prepared by the simple substitution reaction of monobromobarbituric acid with thiourea in water medium to produce C-S bond formation products. The nuclophilic addition reaction of barbituryl isothiocarbamide with aryl/alkyl isothiocyanates were carried out in DMF medium at 60 ^{0}C without any catalyst, not as much of required time for completion of reaction to accessible excellent yields.

During initial exploratory nucleophilic addition reaction of barbituryl isothiocarbamide (**2**) and aryl/alkyl isothiocyanates (**3-15**) were investigated to establish the feasibility of our strategy and to optimize the reaction conditions without any catalyst. It is further revealed that, when we have taken same proportion of reactant (**2**), and interacted with variable proportion of reactants (**3** and **6**) using four different solvents, but best result of C-N coupled products (**16** and **19**) were observed in DMF medium at 60 ^{0}C within very short period of time for completion of the reactions (Table 3 and Graph 2).

 DOI: 10.17628/ecb.2014.3.372-376

Table 2. Spectral data of synthesized compounds (**16-28**).

No.	Colour	Mp., °C[a]	IR, cm^{-1}	^{1}H NMR, DMSO-d_6, ppm	^{13}C NMR, DMSO-d_6 ppm	HRMS
16	White	297-300	3331.07, 3138.18, 3062.96 2837.19, 2357.57, 1714.72, 1651.07, 1633.71, 1556.55, 1253.73, 767.67, 694.71.	δ 9.749(s, 2H, NH), 7.483-7.095(s, 5H, Ar-H), 6.006(s, 1H, C-H), 2.020(s, 3H, NH).	δ 185.97, 171.07, 170.04, 152.47, 139.49, 128.45, 121.59, 118.06, 51.30.	Calcd. for $C_{12}H_{11}O_3N_5S_2$ 337.0337. Found: 337.0309.
17	Yellow	296	3332.09, 3074.53, 2951.09, 2357.01, 1712.79, 1693.50, 1681.93, 1556.55, 1263.37, 767.67, 717.52.	ISOS[b]	ISOS[b]	ISOS[b]
18	faint yellow	290	3323.91, 3074.53, 2970.38, 2337.72, 1712.79, 1693.50, 1666.50, 1556.55, 1253.73, 769.60, 731.02.	δ 9.537(s, 2H, NH), 7.340-6.900(s, 4H, Ar-H), 6.750(s, 1H, C-H), 2.075(s, 3H, CH_3), 2.041(s, 3H, NH).	δ 179.91, 173.29, 171.63, 167.36, 157.91, 137.80, 135.77, 136.85, 127.83, 125.70, 123.72, 53.44, 20.48.	Calcd. for $C_{13}H_{13}O_3N_5S_2$ 351.0460. Found: 351.0419.
19	yellow	310	3331.07, 3138.18, 3076.46, 2949.16, 2357.01, 1712.79, 1651.07, 1556.55, 1251.80, 812.03, 769.60.	ISOS[b]	ISOS[b]	ISOS[b]
20	faint yellow	265	3329.14, 3161.33, 3120.82, 3084.18, 2339.65, 1712.79, 1693.50, 1666.50, 1556.55, 1255.66, 765.74, 729.09.	δ 10.283(s, 2H, NH), 8.825-7.223(m, 4H, Ar-H), 6.605(s, 1H, C-H), 2.070(s, 3H, NH).	δ 181.12, 171.08, 170.18, 162.52, 152.78, 137.03, 136.16, 132.03, 128.18, 125.81, 122.15, 52.98.	Calcd. for $C_{12}H_{10}ClO_3N_5S_2$ 370.9914(Cl^{35}); 372.9884(Cl^{37}). Found: 370.9801(Cl^{35}); 372.9908(Cl^{37}).
21	cream	292	3331.07, 3159.40, 3045.60, 2339.65, 1714.72, 1693.50, 1681.93, 1556.55, 1253.73, 769.60, 729.09.	δ 10.282(s, 2H, NH), 8.247-7.252(m, 4H, Ar-H), 6.875(s, 1H, C-H), 1.225(s, 3H, NH).	δ 182.27, 170.74, 170.11, 166.27, 152.35, 140.89, 133.27, 130.08, 121.55, 117.74, 116.61, 51.11.	Calcd. for $C_{12}H_{10}ClO_3N_5S_2$ 370.9914(Cl^{35}); 372.9884(Cl^{37}). Found: 370.9901(Cl^{35}); 372.9808(Cl^{37}).
22	dirty cream	312	3323.35, 3147.83, 3047.53, 2339.65, 1714.72, 1693.50, 1681.93, 1556.55, 1255.66, 767.67.	ISOS[b]	ISOS[b]	ISOS[b]
23	dark yellow	275	3329.14, 3076.46, 2947.23, 2358.94, 1712.79, 1693.50, 1651.07, 1537.27, 1253.73, 767.50, 731.02.	ISOS[b]	ISOS[b]	ISOS[b]

Cont. of Table 2.

24	faint yellow	305	3329.14, 3076.46, 2947.23, 2358.94, 1712.79, 1693.50, 1651.07, 1556.55, 1253.73, 767.50, 731.02.	ISOS[b]	ISOS[b]	ISOS[b]
25	light cream	311	3331.07, 3138.18, 3074.53, 2949.16, 2337.72, 1712.79, 1693.50, 1666.50, 1556.55, 1251.80, 827.46, 769.60	δ 9.4094(s, 2H, NH), 7.2128-7.1945(d, 2H, J= 7.3Hz, Ar-H), 6.8265-6.8090(d, 2H, J= 7.0Hz, Ar-H), 6.5743(s, 1H, C-H), 3.7119(s, 3H, $ArOCH_3$), 2.080(s, 3H, NH).	δ 182.22, 170.92, 170.20, 166.28, 154.27, 149.74, 132.85, 127.35, 119.82, 113.78, 55.04, 49.49.	Calcd. for $C_{13}H_{13}O_4N_5S_2$ 367.0409. Found: 367.0397
26	pink	307	3331.07, 3074.53, 2951.09, 2358.94, 1714.72, 1693.50, 1651.07, 1556.55, 1255.66, 769.50.	ISOS[b]	ISOS[b]	ISOS[b]
27	dark yellow	269	3331.07, 3074.53, 2951.09, 2843.07, 2339.65, 1714.72, 1693.50, 1651.07, 1556.55, 1255.66, 767.67, 729.09.	ISOS[b]	ISOS[b]	ISOS[b]
28	dirty cream	302	3329.14, 3138.18, 2949.16, 2841.15, 2339.65, 1712.79, 1554.68, 1253.73, 910.60, 769.60.	ISOS[b]	ISOS[b]	ISOS[b]

[a]Compounds decomposed at particular temperature; [b] ^1H, ^{13}C NMR and HRMs data not given due to insolubility of compounds in organic solvents. (ISOS- Insolubility in Organic Solvents)

Table 3. Optimization of reaction conditions.

Entry	2 mmol	3 or 6 mmol	Products	Solvent	Reaction Time, h	Yield, %
1	39	3 (39)	16	H_2O	12	42[a]
2	39	6 (58)	19	H_2O	12	45[a]
3	39	3 (39)	16	$CHCl_3$	15	12[a]
4	39	6 (78)	19	$CHCl_3$	15	17[a]
5	39	3 (39)	16	THF	6	60[a]
6	39	6 (48)	19	THF	6.5	67[a]
7	39	3 (39)	16	DMF	2.5	92[b]
8	39	6 (39)	19	DMF	2.0	96[b]

[a] Reaction under reflux; [b]Reaction under stirring at 60 ^0C

For optimization, we have taken same fraction of reactant (2), and interacted with inconsistent quantity of reactants (**3** and **6**) using various solvents like chloroform, tetrahydrofuran and DMF to yield products respectively in 42-45 %, 12-17 %, 60-67 % and 92-96 % amounts. It was further clear that, the polarity of solvents was playing majorrole in reaction but polarity of solvent is not directly proportional to reactivity of reactants because though water

is more polar than THF, yields and requisite time for completion of reactions were unlike. Therefore it has been further cleared that, the polarity of solvent has no role to play for completion of reactions.

CONCLUSION

The synthesis of barbituryl isodithiobiurets presents real challenge for C-N bond formation due to the simple nucleophilic addition of alkyl/ aryl isothiocyanates, stirring in DMF at 60 ^{0}C. Therefore, we believe that present protocol for the synthesis of selective and structurally diverse C-N bond formation in DMF medium without any catalyst as a very efficient, simple, high yielding methodology to yield products with high melting points and high stability.

ACKNOWLEGEMENT

The authors are thankful to Shri Shivaji Science College, Akola, Indian Institute of Science, Bangalore and SAIF Chandigarh for recording the IR, NMR and Mass spectra. Thanks are due to Head, Department of Chemistry; RTM Nagpur University, Nagpur for providing necessary facilities.

REFERENCES

[1]Wolff, M. E., *Burger's Medicinal Chemistry and Drug Discovery*, Wiley, New York, **1997**.

[2]Oliva, A., Zimmermann, G., Krell, H. W., *International Patent* WO 98/58925.

[3]Gleason, M., Gosselin, R. Eds., *Clinical Toxicology of Commercial Products*, Williams & Wilkins Co, Baltimore, MA, **1963**, 26-27.

[4]Acheson, R. *Introduction to the Chemistry of Hetero-Cyclic Compounds*, Interscience Publishers, New York, **1967**, 339-42.

[5]Brown, D.; Evans, R.; Batterham, T. *The Pyrimidines Supplement* I, Wiley Interscience, New York, **1970**, 199-201.

[6]Zhou, W.; Kurth, M. J., *Polymer*, **2000**, *42*, 345.

[7]Neumann, D. *The design and synthesis of novel barbiturates of pharmaceutical interest*, University of New Orleans, Thesis and Dissertations, paper **2004**, 1040.

[8]Goth, A., *Medicinal Pharmacology principles and concept*, 4th ed., C.V. Mosby Co., St. Louis, MO. **1968**.

[9]Olin, B. R.; Ed.; *Central Nervous system Drugs, Sedatives and Hypnotics, Barbiturates. In Fact and Comparisons Drug Information*. St. Louis, MO: Facts and Comparisons, **1993**, 1398-1413.

[10]Cope, A. C.; Dorothea, H.; Dorothea, P.; Eide, C.; Arroyo, A., *J. Am. Chem. Soc*., **1941**, *63*, 356-58.

[11]Jursic, B. S., Stevens, E. D., *Tetrahedron Lett*. **2003**, *44*, 2203-10.

[12]Sakai, S., Fujinami, T., Aizawa T., *Bull. Chem. Soc. Japan*, **1975**, *48(10)*, 2981-82.

[13]Lewellyn, M. E., Wang, S. S., Strydom, P. J., *J. Org. Chem*. **1990**, *55*, 5230-31.

[14]Spirkova, K., Bucko, M., Stankovsky, S., *ARKIVOC*, **2005**, *v*, 96-102.

[15]Yuesheng, Z., Paul, T., *Cancer Res. Suppl.* **1994**, *54*, 1976s-1981s.

[16]Kinoshita, Y., Matsuda, N., Sakai, S., Oshima, Y., Harada, T.,Nishihara, T., *Agric. Biol. Chem*. **1966**, *30(5)*, 447-51.

[17]Patai, S. Ed.; *For a generally review on isothiocyanates and thioureas, see: the chemistry of cyanates and their thio derivatives*; Wiley: Chichester, **1977.**

[18]Fernandez, J. M. G., Mellet, C. O., Blanco, J. C. J., Moto, J. F., Gadelle, A., Coste S. A., Defaye, J., *Carbohydr. Res.* **1995**, *268*, 57-71.

[19]Glenn, S. S., John, B. B., *J. Am. Chem. Soc.***, 1950,** *72*, 1140-41.

[20]Glenn, S. S., William, H. W., *J. Am. Chem. Soc.*, **1952,** *74*, 498-99.

[21]Robert, B., Steven, J. C., Stephen, F., Doug, H., Gordo, S., David, T., *Synth. Commun*. **1996**, *26(22)*, 4195-209.

[22]Sontakke, M. M., Jichkar, A. A., Dhonde, M. G., Bhaskar, C. S., Berad, B. N., *Synth. Commun*., **2014**, *44*, 340-345.

Received: 02.03.2014.
Accepted: 21.03.2024.

APPLICATION OF CHLORANIL AND FLUORANIL π-ACCEPTORS FOR THE SPECTROPHOTOMETRIC DETERMINATION OF MESALAMINE IN PHARMACEUTICALS

Theia'a N. Al-Sabha,[a] Mohammed S. Al-Enizzi[b] and Omar A. Al-Taee[a]

Keywords: spectrophotometry, mesalamine, aqueous solution, *p*-chloranil, *p*-fluoranil

Two simple, sensitive and accurate spectrophotometric methods for the determination of mesalamine are described. The methods are based on charge-transfer complex formation reactions of the drug with two π-electron acceptors, *p*-chloranil and *p*-fluoranil, in aqueous medium. The coloured complexes having maximum absorbance at 346 nm and 347 nm by using *p*-chloranil and *p*-fluoranil reagents respectively. Under the optimized experimental conditions, the calibration curves showed a linear relationship over the concentration ranges of 1–35 and 1-30 μg ml^{-1} with molar absorptivity values 4.60×10^3 and 5.67×10^3 L mol^{-1} cm^{-1}. using above reagents respectively. The limits of detection and quantitation were found 0.376 and 1.25 μg ml^{-1} using *p*-chloranil, respectively, and 0.333 and 1.111 μg ml^{-1} using *p*-fluoranil, respectively. The complexes were found to be formed in ratio of 1:1 species in both methods, with stability constants of 6.9×10^4 and 5.1×10^5 L mol^{-1} for mesalamine complexes with *p*-chloranil and *p*-fluoranil respectively. The methods were applied successfully to the assay of mesalamine in pharmaceutical formulations and was agreed well with its certified value.

* Corresponding Authors
E-Mail: dr_theiaa@yahoo.co.uk
[a] Chemistry department, College of Education, Mosul University, Mosul, Iraq
[b] Chemistry department, Education College for Girls, Mosul University, Mosul, Iraq

Introduction

Mesalamine also known as mesalazine, chemically known as 5-aminosalicylic acid (Scheme1) is used for its local effects in the treatment of inflammatory bowel disease, including ulcerative colitis and Crohn's disease.[1,2] Mesalamine has been shown to be a potent scavenger of reactive oxygen species that play a significant role in the pathogenesis of inflammatory bowel disease, inhibition of natural killer cell activity, inhibition of antibody synthesis, inhibition of cyclo-oxygenase and lipoxygenase pathways and impairment of neutrophil function.[3,4]

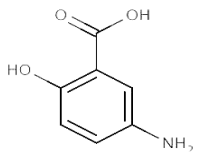

$C_7H_7NO_3$
M.wt=153.1

Scheme 1. Chemical structure of mesalamine

Different analytical methods have been described for determination of mesalamine such as potentiometry[5] HPLC,[6-8] differential pulse voltammetry[9] and fluorimetry.[10] These methods are often time-consuming, expensive, lack selectivity and cumbersome. Spectrophotometry continues to be very popular, because of its simplicity, versatility and low cost. Several spectrophotometric methods using different reagents have been reported for determination of mesalamine. Diazotization coupling method using resorcinol[11] and N-(1-naphthyl)ethylenediamine dihydrochloride[12] as coupling agents. Oxidative coupling reaction using orcinol, resorcinol and cresol in the presence of hydrogen peroxide and horseradish peroxidase[13] and 3-methyl-2-benzothiazolinone hydrazone in the presence of Fe III.[14] Schiff base formation reactions using vanillin,[15] p-dimethylaminobenzaldeyde and 1,2-naphthoquinone-4-sulphonate,[16] redox reactions using Folin Ciocalteu,[15] ferric chloride in the presence of 2,2'–bipyridyl or potassium ferricyanide[17] and ion-pairing spectrophotometric methods using bromocresol green and bromocresol purple.[18] However, the most of these methods involve complicated procedures, which require several manipulation steps,[11,12] low sensitivity,[14,15] using of organic medium,[16] indirect determination procedure[17] and an extraction step needed.[18] It is well known that *p*-benzoquinones such as 2,3,5,6-tetrachloro-1,4-benzoquinone (*p*-chloranil) and 2,3,5,6-tetrafluoro-1,4-benzoquinone (*p*-fluoranil) as π-electron acceptors often form highly colored charge transfer complexes with various donors which provides the possibility of determination of drugs by spectrophotometric methods. Previously, we reported charge transfer complex formation reactions for determination of mesalamine using *o*-chloranil,[19] tetracyanorthylene (TCNE) and 2,3-dichloro-5,6-dicyano-1,4-benzoquinone (DDQ) acceptors.[20] The aim of the present study is to extend the application of charge transfer complex formation reactions by using of other π-acceptors such as *p*-chloranil and *p*-fluoranil for the spectrophotometric determination of mesalamine in bulk and pharmaceutical formulations.

Experimentals

Apparatus

All absorption measurements were made on a Shimadzu UV-210A double - beam spectrophotometer supplied with a digital printer DP80Z and matched 1-cm optical silica cells. Heating of solutions was carried out on a water bath of frost instruments, LTD. The reading of pHs made on a PW 9420

pH meter supplied with an electrode type CE 10-12 pH. Weighing was carried out on a balance type of Mettler H 54 AR.

Materials and reagents

Mesalamine and its pharmaceutical formulations (tablet and capsule) were kindly provided by state company for Drug Industries and Medical Appliance-(SDI) Sammara-Iraq. *p*-Chloranil and *p*-fluoranil and other chemicals were obtained from Fluka and BDH companies. All solvents were analytical reagent grade and water was distilled.

Working standard solution of mesalamine: 250 μgml^{-1} mesalamine solution was prepared by dissolving of 0.025 g of its pure form in 5 ml ethanol and diluted to 100 ml with distilled water in a volumetric flask.

Reagent solution: 1×10^{-3} M *p*-chloranil (*p-CA*) and 2×10^{-3} M *p*-fluoranil (*p-FA*) solutions were prepared by dissolving 0.123 g and 0.018 g, respectively, in absolute ethanol and diluted to 50 ml in calibrated flasks with the same solvent.

Borate buffer solution (pH 9): 0.05 M sodium tetraborate was prepared in distilled water and adjusted to pH 9 by pH meter.

Analytical Procedure

Aliquots of the working solution of mesalamine were transferred into two series sets of 25 ml calibrated flasks. In the first set, 0.5 ml of pH9 and 2 ml of 1×10^{-3} M *p-CA* solutions were added, in the second set, 1ml of pH9 and 2 ml of 2×10^{-3} M *p-FA* solutions were added. The solutions were diluted to the mark with distilled water and left for 20 min at 40ºC and 50ºC using *p-CA* and *p-FA* respectively. The absorbance, for the first set, was measured at 346 nm and 347 nm for the second set against their respective reagent blank.

Analytical procedure for pharmaceutical formulations

Ten mesacol tablets or capsule contents (each tablet or capsule containing 400 mg mesalamine) were accurately weighed and pulverized. A portion of the fine and homogenized powder equivalent to 400 mg mesalamine was accurately weighed and dissolved in least amount of ethanol and diluted to 100 ml with distilled water, mixing well and filtered with Whatmann filter paper no.1. The filtrate was diluted to the 100 with distilled water in a volumetric flask obtaining 4000 μg mL^{-1}. a suitable volume was diluted, and the above procedure was followed.

Results and discussion

The interaction of mesalamine, as n-donor, with *p*-chloranil and p-fluoranil, as π-acceptors, in the presence of borate buffer solution of pH9 yielded intense purple coloured species in aqueous medium having new bands with maximum absorption at 346 nm and 347 nm respectively where the corresponding blank gave low absorbance at these wavelengths (Fig. 1). These new bands may be attributed to the formation of radical cation for mesalamine and radical anions for both acceptors of charge transfer complexes.

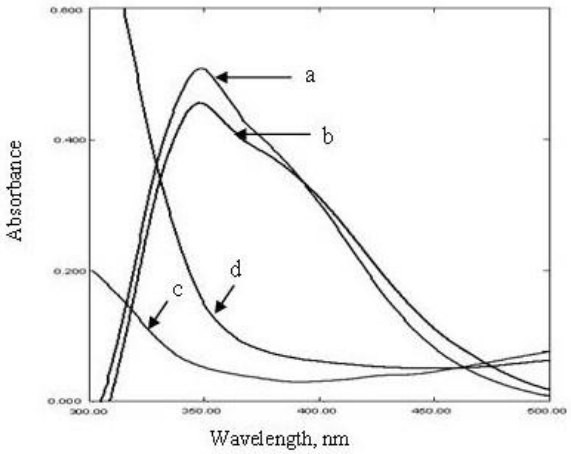

Figure 1. Absorption spectra of 10 μg mL^{-1} mesalamine with *p-FA* (a) and *p-CA* (b) against their reagent blank (c) and (d) respectively.

Optimization of reaction conditions

The influence of different parameters on the color development was studied to determine optimum conditions for the assay procedures.

Effect of pH and buffer solution

The effect of pH on the absorbance of complex solutions containing mesalamine (10μg mL^{-1}) and *p-CA* (1×10^{-3} M) or *p-FA* (2×10^{-3} M) were studied. It was found that complexes are formed in basic medium in the presence of NaOH with maximum absorbance at pH 9.0, (Fig.2). The effect of buffer solutions such as, borate, carbonate and phosphate buffers with pH 9.0 were examined.

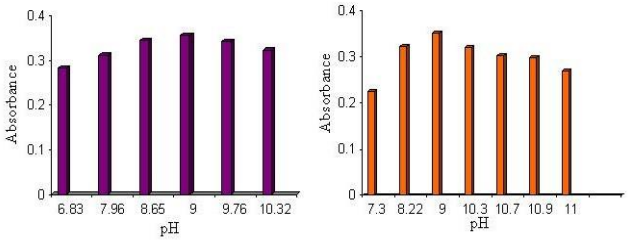

Figure 2. Effect of pH on the absorption intensity of 10 μg mL^{-1} mesalamine complexes with *p-CA* (purple) and *p-FA* (red).

It was found that borate buffer solution increased the sensitivity of the complexes. However; the optimum amount of borate buffer solution of pH 9.0 has been studied and Figure 3 shows that 0.5 and 0.75 ml are the optimum amounts using *p-CA* and *p-FA* respectively which are recommended in the subsequent experiments.

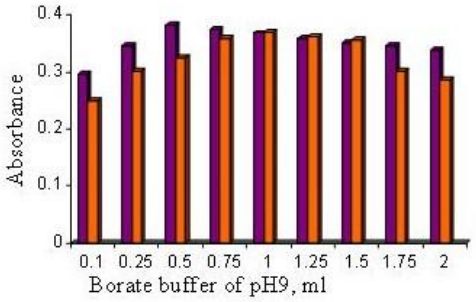

Figure 3. Effect of borate buffer solution (pH 9) amount on the intensity of 10 µg mL^{-1} mesalamine complexes with *p-CA* (purple) and *p-FA* (red)

Effect of reagents concentration

The effect of changing the *p-CA* and *p-FA* concentrations on the absorbance of solution containing a fixed amount of mesalamine (10µg mL^{-1}) were studied. It was observed that the absorbance increases with increasing the reagent concentrations and reached maximum on using 2.0 ml of 1×10^{-3} M *p-CA* and 2×10^{-3} M *p-FA* (i.e. 0.8×10^{-4} M and 1.6×10^{-4} M in final solution respectively), (Figure 4). Therefore, these volumes of these concentrations were used in the subsequent work.

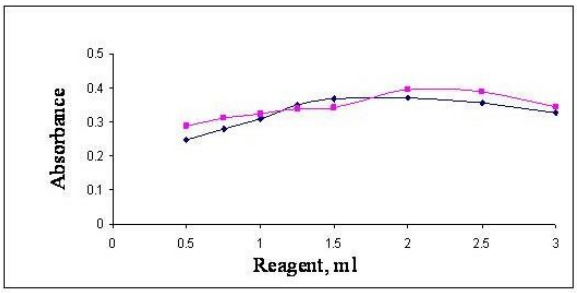

Figure 4. Effect of *p-CA* (1×10^{-3}M) (▪) *and p-FA* (2×10^{-3}M) (♦) volumes on the absorption of 10 µg mL^{-1} mesalamine

Effect of surfactant

Effect of various surfactants including sodium dodecyl sulphate (SDS), cetylperydinum chloride (CPC), cetyltrimethylammonium bromide (CTAB), Tween-80 and Triton x-100 were tested. It was found that these surfactants decreased the absorbance of solutions.

Effect of order of addition

The order of addition of reactants on the color development was examined. Maximum sensitivity was achieved when mesalamine and pH9 were added before adding the *p-CA* or *p-FA* reagents (Fig. 5). Hence, the method was performed in the order: Mesalamine + pH 9 + *p-CA:* or Mesalamine + pH 9 + *p-FA*

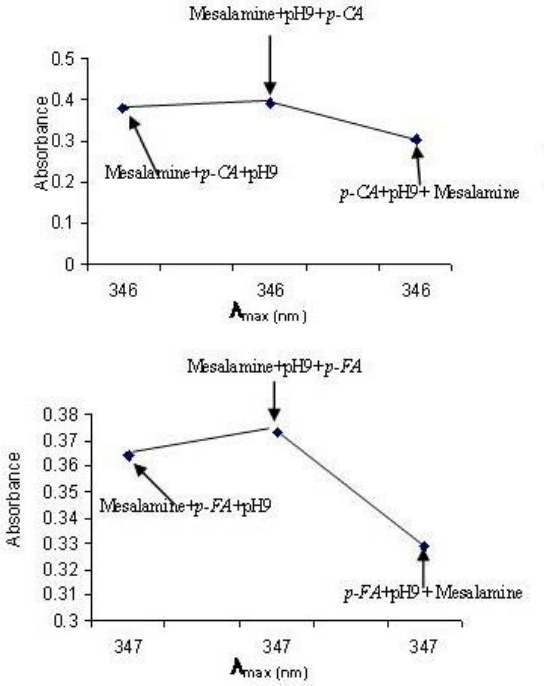

Figure 5. Effect of order of reactants on the absorption of 10 µg mL^{-1} mesalamine

Effect of temperature and reaction time

The reaction time was determined by following the color development at room temperature and in thermostatically controlled water-bath at different temperatures up to 60°C. The absorbance was measured at 5 and 10 minutes intervals against reagent blank treated similarly. It was observed that the complexes were formed at room temperature after addition of *p-CA* or *p-FA* immediately and the absorbance were increased with increasing the temperature and reached at maximum after 20 min and remain constant for 50 min at 40ºC and 50ºC for both complexes using *p-CA* and *p-FA* reagents respectively, (Fig. 6). However; after these temperatures and time stability the absorbance was decreased indicating the dissociation of the complexes. Therefore; 20 min developing time at 40ºC and 50ºC as optimum temperatures were selected using *p-CA* and *p-FA* reagents respectively in the subsequent experiments.

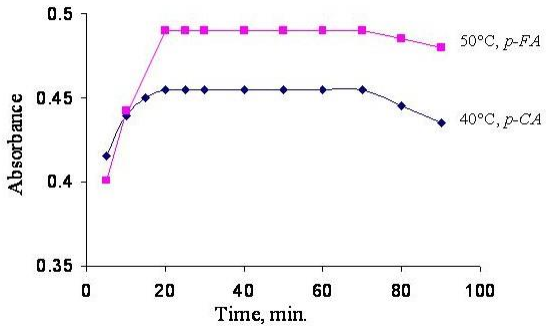

Figure 6. Effect of temperature and reaction time on the absorbance of 10 µg mL^{-1}mesalamine in the presence of *p-CA* and *p-FA* reagents.

 DOI: 10.17628/ecb.2014.3.377-383

Method validation

In order to investigate the range in which the colored complex adhere to Beer's law, the absorbance of the complexes were measured at 346 nm and 347 nm using *p-CA* and *p-FA* reagents respectively, after developing the color by following the recommended procedure for a series of solutions containing increasing amounts of mesalamine. The Beer's law limits and molar absorptivity values were evaluated and given in Table 1, which are indicated that the method is sensitive. The linearity was represented by the regression equations and the corresponding correlation coefficients for the studied determined drug by the proposed method represents excellent linearity. The relative standard deviation (RSD) and accuracy (average recovery %) for the analysis of five replicates of each three different concentrations for pure mesalamine indicated that the method is precise and accurate. Limit of detection (LOD) and limit of quantitation (LOQ) are determined by taking the ratio of standard deviation of the blank with respect to water and the slope of calibration curve by applying the following equations:

$$LOD=\frac{3.3\sigma B}{S} \qquad LOQ=\frac{10\sigma B}{S}$$

whereas:

σB= Standard deviation for six determinations of blank

S= slope of calibration graph for each isomer

LOQ is approximately 3.3 times LOD. Naturally, the LOQ slightly crosses the lower limit of Beer's law range

Table 1. Summary of optical characteristics and statistical data for the proposed method

Parameter	*p-CA*	*p-FA*
Beer's law limits, µg mL^{-1}	1-35	1-30
Molar absorptivity, L mol^{-1} cm^{-1}	4.60×10^3	5.67×10^3
LOD, µg mL^{-1}	0.376	0.333
LOQ, µg ml^{-1}	1.250	1.111
Average recovery, %*	99.16	98.80
Correlation coefficient	0.996	0.997
Regression equation, Y**		
Slope, *a*	0.0301	0.0371
Intercept, *b*	0.1058	0.0993
RSD [a]	≤ 1.53	≤ 2.07

*Average of five determinations.**$Y=aX+b$, where X is the concentration of drug in µg mL^{-1}.

Interference

The extent of interference by some excipients which often accompany pharmaceutical preparations were studied by measuring the absorbance of solutions containing fixed amount of mesalamine and various amounts of diverse species, which is present the pharmaceutical formulations of mesalamine, in a final volume of 25 ml. It was found that the studied excipients up to 25 fold excess did not interfere seriously (Table 2). However; an error of 5.0 % in the absorbance readings was considered tolerable.

Analytical applications

The proposed method was successfully applied to determine mesalamine in pharmaceutical tablets and capsules preparations. The obtained results were compared statistically by a Student's *t*-test for accuracy at the 95 % confidence level with three degrees of freedom. As cited in Table 3, the results showed that the experimental *t*-test was less than the theoretical values (t=4.303), indicating that the method is accurate.

Comparison of the proposed method with other spectrophotometric methods

The proposed spectrophotometric method for determination of mesalamine have been compared favorably with other spectrophotometric methods depending on charge transfer complex formation reactions using different π-acceptor reagents such as *o*-chloranil, tetracynoethylene (TCNE) and 2,3-dicloro-5,6-dicyno-p-benzoquinone (DDQ). As seen in Table 4, *p*-chloranil reagent is more sensitive than *o*-chloranil reagent but less than TCNE and DDQ reagents, where as the linearity range of *p*-fluoranil method is more than other methods. However; other parameters seem to be the same with some different in λ_{max}, pH and temperature.

Stoichiometry and stability constant

The molar ratio of the n-π charge transfer complex formed between the mesalamine with *p-CA* and *p-FA* reagents were investigated by applying the continuous variation (Job's) method.[21] Experiments were performed by mixing different volumes of equimolar solutions of drug and reagents [1.63×10^{-3}M] and keeping total volume at 6 ml at final dilution of 25 ml. Under the optimum conditions described above, the plot of absorbance *vs* molar ratio between drug and reagents were prepared, and results indicated that complexes were formed in the ratio of 1:1 (Figures 7). This finding supports that the n-π CT complexes are formed through amino group present in mesalamine. The stability constant (K_{st}) of the complexes were calculated using the following equation:

$$K_{st}=\frac{1-\alpha}{\alpha^2 C}$$

$$\alpha=\frac{A_m-A_s}{A_m}$$

where

K_{st} is the stability constant, L mol^{-1},

α the dissociation degree,

C the concentration of the product which is equal to the concentration of mesalamine,

Am the absorbance of the complexes at optimum amount of *p-CA* or *p-FA* reagent and

As the absorbance of the complexes at stoichiometric amounts of *p-CA* or *p-FA* reagent according to the 1:1 ratios under the optimum conditions reaction.

It was found 6.9×10^4 and 5.1×10^5 L.mol^{-1} using *p-CA* and *p-FA* reagents respectively, indicating good stability.

 DOI: 10.17628/ecb.2014.3.377-383

Table 2. Effect of excipients for assay of mesalamine

Excipient	Recovery % of 10 μg mL^{-1} of mesalamine per μg mL^{-1} foreign added							
	p-CA				*p-FA*			
	20	50	100	250	20	50	100	250
Lactose	102.00	104.28	104.94	103.71	96.19	95.16	98.42	100.47
Sodium chloride	95.98	96.40	98.20	98.53	96.74	95.95	100.19	98.98
Arabic Gum	98.53	96.87	101.72	101.85	100.47	101.77	100.47	102.51
Starch	103.38	101.39	98.07	96.07	98.98	96.16	98.23	101.95
Sucrose	105.61	105.00	103.85	103.28	97.95	96.74	99.72	95.23
Glucose	95.64	95.50	95.65	97.00	97.21	99.44	99.81	102.73

Table 3. Assay of mesalamine in pharmaceutical preparations using the proposed method and comparison with the official method

Procedure applied	Pharmaceutical preparation	Drug amount present, μg mL^{-1}	Recovery, %±SD[a]	Average recovery, %	Labeled amount, mg
p-CA method	Mesacol tablet	5.0 10.0 20.0	103.00 ± 0.77 97.80 ± 0.58 101.15 ±0.62	100.65 (1.73)[b]	400
	Mesacol capsule	5.0 10.0 20.0	97.40 ± 0.79 101.70 ±0.68 100.20 ±0.51	99.76 (0.63)	400
p-FA method	Mesacol tablet	5.0 10.0 20.0	97.20 ± 0.83 101.80 ± .66 99.55 ± 0.42	99.51 (1.35)	400
	Mesacol capsule	5.0 10.0 20.0	98.60 ± 0.56 99.20 ± 0.48 100.60 ±0.48	397.88 (1.84)	400

[a]Average of three determinations. [b]Figures in parenthesis are the calculated values for *t*.

Table 4. Comparison of spectrophotometric methods for mesalamine determination

Analytical parameters	Present method		Literature method		
	p-Chloranil	*p*-Fluoranil	*o*-Chloranil [18]	TCNE[19]	DDQ[19]
λ_{max}, nm	346	347	571.5	346	420
pH	9	9	9.8	3	9
Temp., °C	40	50	25	R.T	40
Development time, min	20	20	5	10	50
Stability period, min	50	50	45	30	>60
Beer's law, μg mL^{-1}	1-30	1-35	1.25-30	0.8-12	0.4-10
Molar absorptivity, L mol^{-1}cm^{-1}	4.60×10^3	5.67×10^3	3.4×10^3	2.9785×10^4	5.9586×10^4
LOD, μg mL^{-1}	0.333	0.376	0.143	1.018	0.893
LOQ, μg mL^{-1}	1.111	1.250	0.4773	3.393	2.976
Recovery, %	98.80	99.16	100.44	100.40	100.51
RSD, %	≤ 2.07	≤ 1.53	1.67	≤0.80	≤2.15
Applications	Tablet, Capsule	Tablet, Capsule	Tablet, Capsule	Capsule	Capsule

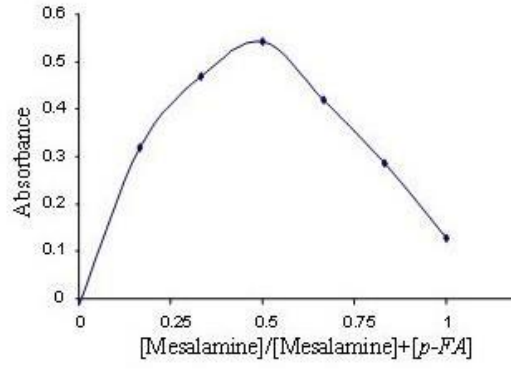

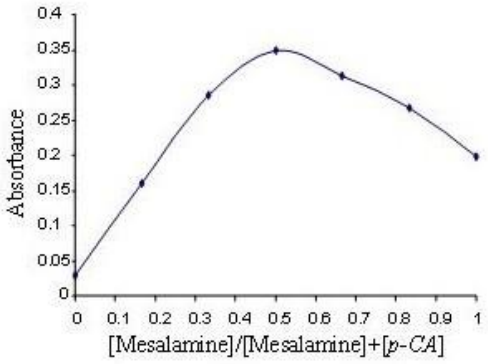

Figure 7. Continuous variations plots for complexes of mesalamine (1.63×10^{-3}M) with 1.63×10^{-3}M of each *p-CA* and *p-FA* under the optimum reaction conditions.

Proposed chemical reactions

The charge transfer complex forming reactions occur when π-acceptors react with the basic nitrogenous compounds which act as n-donors. Charge-transfer complex formation is characterized by electronic transition(s) to an excited state in which there is a partial transfer of electronic charge from the donor to the acceptor moiety, followed by the formation of a radical anion. Complete electron transfer from the donor to the acceptor moiety took place with the formation of intensely colored radical ions.[22]

Therefore, aliphatic and aromatic amines, nitrogenous base acting as n-donor, is made to react with *p-CA* and *p-FA* as π-acceptors to produce a colored charge transfer complexes in aqueous medium according to the scheme 2.

Conclusion

Determination of mesalamine is based on n-π charge transfer complex formation reactions using *p-CA* and *p-FA* acceptors. The proposed method is found to be simple. It has the advantage of being accurate, does not require the removal of excipients, temperature control and solvent extraction step. The statistical parameters and recovery study data clearly indicate the reproducibility and accuracy of the method. It was applied successfully to pharmaceutical preparations.

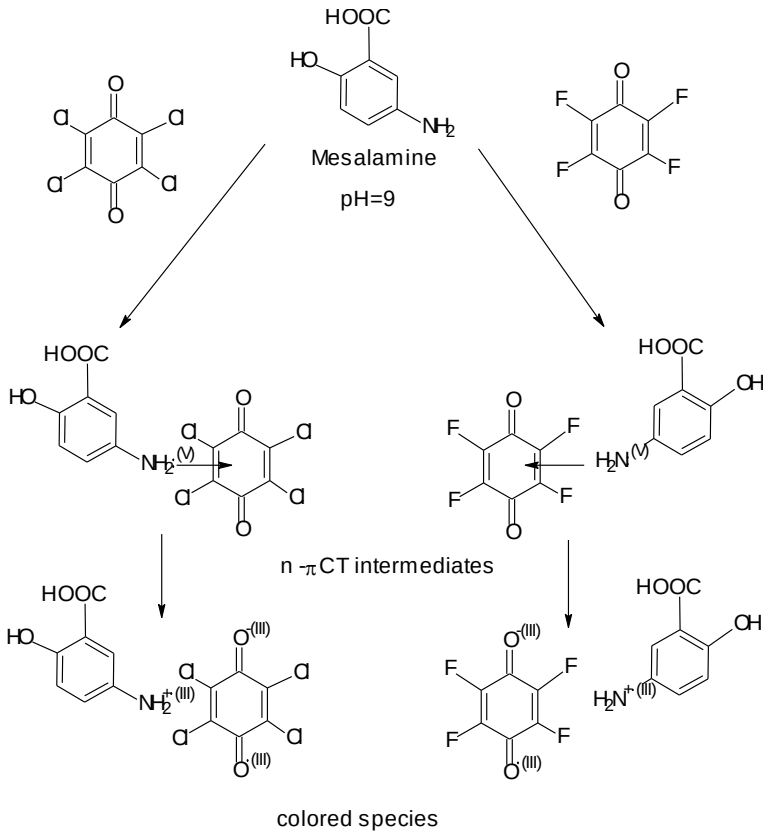

Scheme 2. Proposed mechanism of charge transfer complex formation reactions for determination of mesalamine by *p-CA* and *p-FA*.

 DOI: 10.17628/ecb.2014.3.377-383

References

[1]Cai, Q. X., Zhu, K. J., Chen, D. and Gao, L. P., *Eur. J. Pharm. Biopharm.*, **2003**, *55*, 203.

[2]Gotti, R., Pomponio, R., Bertucci, C. and Cavrini, V., *J. Chromatogr. A*, **2001**, *916*, 175.

[3]Geier, D. L. and Miner, P. B., *Am. J. Med.*, **1992**, *93*, 208.

[4]Palumbo, G., Carlucci, G. and Mazzeo, P., *J. Pharm. Biomed. Anal. Oxford*, **1995**, *14*, 175.

[5]British Pharmacopoeia Commission, *British Pharmacopeia*, London, Stationery Office, **2003**, *2*, 1257, [CD-ROOM].

[6]*United States Pharmacopeia 24*. Ed. Rockville, United States Pharmacopeial Convention, **2000**, [CD-ROOM].

[7]Pastorini, E., Locatelli, M., Simoni, P., Roda, G., Roda, E. and Roda, A., *J. Chromatogr. B Anal. Technol. Biomed. Life Sci.*, **2008**, *872*, 99.

[8]Nigović, B. and Simunić, B., *J. Pharm. Biomed. Anal.*, **2003**, *31*, 169.

[9]Darak, V., Karadi, A. B., Appal, R. S., Arshad, M. D. and Ganure A. L. , *Pharma Sci. Monitor*, **2012**, *3*, 74.

[10]Zadeh, H. A. and Kohansal, S., *J. Braz. Chem. Soc.*, **2012**, *23*, 473.

[11]Reddy, M. P., Prabhavahi, K., Reddy, N. R. and Reddy, P. R., *Global J. Pharmacol.*, **2011**, *5*, 101.

[12]Patel, K. M., Patel, C. N., Panigrahi, B., Parikh, A. S. andn Patzel, H. N., *J. Young Pharm.*, **2010**, *2*, 284.

[13]Shakeela, S., Ram, B. S. and Sekaran, C. B., *Chiang Mai J. Sci.*, **2011**, *38*, 551.

[14]Narala, S. R. and Saraswathi, K., *Int. J. Pharm. Sci. Res.*, **2011**, *2*, 366.

[15]Chandra, B. S., Bhogela, S. S., Shaik, M., Vadlamudi, C. S., Chappa, M. and Maddirala, N. S., *Quim. Nova*, **2011**, *34*, 1068.

[16]Sama, N. S., Gurupadayya, B. M. and Kumar, A., *J. Pharm. Res.*, **2011**, *4*, 39.

[17]Narala, S. and Saraswathi, K., *Int. J. Res. Pharm. Biomed. Sci.*, **2010**, *1*, 10.

[18]Darak,V., Karadi, A. B., Arshad, M. D. and Raju, S., *Appl. Res. J. Pharm. Techn.*, **2011**, *4*, 962,.

[19]Al-Enizzi, S. M., Al-Sabha, T. N. and Al-Ghabsha, T. S., *Jordan. J. Chem.*, **2012**, *7*, 87.

[20]Al-Sabha, T. N. and Al-Taee, A. O., *J. Educ. Sci*., **2008**, *21*, 49.

[21]Hargis, L. G., *Analytical Chemistry, Principles and Techniques*, Prentice- Hall Inc., Jersey, **1988**, 424.

[22]Alzoman, N. Z., Sultan, M. A., Maher, H. M., Alshehri, M. M., Wani, T. A. and Darwish, I. A., *Molecules*, **2013**, *18*, 7711.

Received: 22.02.2014.
Accepted: 22.03.2014.

TEMPLATE SYNTHESIS, CHARACTERIZATION AND ANTIMICROBIAL STUDY OF NEW METAL COMPLEXES FROM 2,6-DIAMINOPYRIDINE AND 1,4-DIHYDROQUINOXALIN-2,3-DIONE

Mahmoud Najim Abid Al-Jibouri

Keywords: template synthesis; 2,6-diaminopyridne; 1,4-dihydroquinoxaline-2,3-dione; zinc(II); cadmium(II); mercury(II) and zirconyl complexes; Schiff base, quinoxalines, benzopyrazine, antimicrobial activity, N_2O_2 metal complexes

A new series of tetradentate N_2O_2 acyclic complexes of type $[MLCl_2]$ (M: Zn(II), Cd(II), Hg(II); L: tetradentate acyclic ligand) and $[ZrOL]Cl_2$ have been prepared on the basis of condensation of 2,6-diaminopyridine and 1,4-dihydroquinoxalin-2,3-dione by template method. The ligand coordinates through the two imine nitrogen atoms formed up on condensation of $-NH_2$ of 2,6-diaminopyridine with -C=O group in 2-position of quinoxalin-2,3-dione, as well as the lactam form of metal complexes confirm the participation of oxygen atoms in coordination with the metal ions. However, the pyridine nitrogen atoms do not take part in coordination with the metal ions. These complexes have been characterized with the help of various spectral techniques ^1H and ^{13}C NMR, FT-IR, electronic spectra, elemental analyses, and measurements of molar conductance in DMF solutions. Furthermore the determination of chloride content in the metal complexes assists in the investigation the concluded structures. The octahedral geometry was proposed for Zn(II), Cd(II) and Hg(II) while, Zr(IV) complex structure was proposed to be square pyramidal. The new metal complexes were investigated for antibacterial and antifungal properties of gram-positive bacteria (*Staphylococcus auerus*), gram-negative bacteria (*Escherichia. Coli*) and fungi *Aspergillus fumigates* and *Candida* were used in this study to assess their antimicrobial properties. The results showed that this skeletal framework exhibit marked potency as antimicrobial agents.

Corresponding Author
Tel: +964007713460946
E-Mail: mahmoudnajim71@yahoo.com
[a] Chemistry Department, College of Science, Al-Mustansiriya University, Baghdad, +964, Iraq

Introduction

The chemistry of macrocyclic complexes has attracted the interest of both inorganic and bioinorganic chemists in recent years.[1] The field of coordination chemistry of macrocyclic complexes has undergone remarkable growth during the past few decades and undergone remarkable growth during the past few decades and become a growing class of research. This enormous growth is due to synthesis of great number and variety of synthetic macro cycles which behave as coordinating agents for metal ions.[2] Template reactions lie at the heart of macro cyclic chemistry and are the best aids for the preparation of macro cyclic complexes.[3,4] Generally transition metal ions have been used as templates.[5] The importance of macro cyclic complexes in coordination chemistry is because of its various applications in biological processes such as photosynthesis and dioxide transport catalytic properties, potential applications as metal extract ants and radio therapeutic agents.[6] The importance of macrocyclic complexes is due to their resemblance with *in-situ* one pot template synthesis is the most widely adopted method for preparation of macrocyclic complexes.[7] A number of nitrogen donor and oxygen macrocyclic and acyclic derivatives have been used for a long time in analytical, industrial and medical applications.[8,9] The macrocyclic complexes have attracted attention because bacterial and fungal growth.[10] Some macrocyclic complexes have been reported to have anti-inflammatory approach.[11] Several macrocyclic complexes with tetra aza macrocyclic ligands, such as cyclam, or bicyclam have been reported to exhibit antitumor activity.[12] Macrocyclic metal complexes are of great importance due to their resemblances with many natural systems such as porphyrins and cobalamines.[11]

Satish and co-workers have investigated the binuclear Co(II), Ni(II), Cu(II) and Zn(II) complexes with tetradentate Shiff bases derived from 2,6-diformyl-4-methylphenol with 2-hydroxy-3-hydrazinoquinoxalin.[12] In recently published papers some Mn(II), Cr(III), Fe(III), V(IV) and Zn(II) complexes with tetradentate N_2O_2 type quinoxaline organic moieties were isolated involving template synthesis and investigated them with using GC-MS, ^1H NMR and other analytical techniques.[13,14] The template metal(II) complexes involving quinoxalin-2-one have been found to exhibit potential antibacterial activities and abnormal electronic characterizations.[15] The continuous interesting with coordination chemistry of quinoxaline derivatives, in the present paper, synthesis and characterization of Zn(II), Cd(II), Hg(II) and Zr(IV) complexes derived from 2,6-diaminopyridine and 1,4-dihydroquinoxalin-2,3-dione have been prepared, characterized and biologically tested against some selected bacteria and fungi.

Experimental

The anhydrous metal chlorides $ZnCl_2$, $CdCl_2$, $HgCl_2$ and $ZrOCl_2.8H_2O$ were purchased from Sigma-Aldrich company and used without purification. The oxalic acid, 2,6-diaminopyridine, 1,2-phenylenediamine and solvents were supplied from Fluka company in 99% purity. All other chemicals used were of Analar grade.

Synthesis of 2,3-quinoxaline-dione

The 2,3-quinoxaline-dione was prepared according to the method published in literature,[14] Scheme 1.

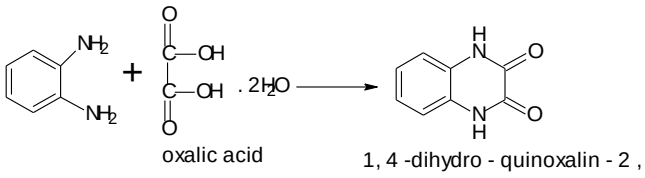

Scheme 1. Preparation of 1,4-dihydroquinoxalin-2,3-dione

Isolation of complexes

Our several attempts to isolate the free macrocyclic or acyclic ligand were unsuccessful. Hence, all the complexes were obtained by template synthesis. To a stirring methanol solution (~60 mL) of 2,6-diaminopyridine (10 mmol) was added divalent $ZnCl_2$, $CdCl_2$, $HgCl_2$ and zirconyl acetate (that obtained from direct reaction of $ZrOCl_2.8H_2O$ with sodium acetate) (5 mmol) dissolved in minimum quantity of methanol (20 mL). The resulting solution was refluxed for 18-20 h, and after overnight cooling a dark colored precipitate formed which was filtered, washed with methanol, acetone, diethyl ether and dried in desiccators. The complexes were found soluble in DMF and DMSO, acetonitrile but were insoluble in water and other organic solvents like ethanol, methanol and chloroform. They were thermally stable up to ~350 °C and then decomposed. The template synthesis of the complexes may be represented by Scheme 2.

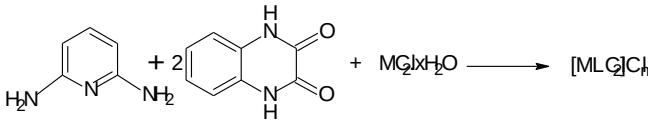

Scheme 2. Synthesis of Zn, Cd and Hg(II) complexes, *n*=2 for M=ZrO, *n*=0 for M(II)=Zn, Cd and Hg

Instrumentation

The elemental analyses of the new solid complexes were determined using Carlo-Erba 1106 Elemental analyzer. Electronic spectra were recorded for solutions of quinoxalin-2,3-dione and its metal template complexes using Shimadzu spectrometer in the range 200-800 nm in DMF solvent. The ^1H and ^{13}C NMR spectra were carried at Al-Bait University, Amman, Jordan on Bruker 300 MHz spectrometer in DMSO-d_6 solvent. The Fourier transform infrared spectra of the prepared complexes were recorded in KBr and CsI discs on Shimadzu model FT-IR-8400 spectrometer. The molar conductance measurements were made on an ELICO conductivity bridge type CM-82 with a cell having a cell constant of 0.51 cm^{-1} in DMF solutions. The percents of metal contents of the complexes were determined by flame atomic absorption on Shimadzu AA-670 spectrometer at instrumental analyses. Finally the estimation of ionic chloride content in the prepared complexes was done by conductometric titrations with standard solution of silver nitrate.[15]

Antibacterial activity

Primary screening

The antibacterial activities of the newly synthesized complexes were evaluated by the Agar Well Diffusion Assay Technique against two gram-positive and negative bacteria, *Staphylococcus aureas* and, *Escherichia coli*, two gram-negative and positive fungi, *Aspergillus fumigates* and *Candida albicans*. The bacterial cultures were maintained on the nutrient agar media by sub-culturing them on fresh slants after every 4-6 weeks and incubating them at the appropriate temperature for 24 h. All stock cultures were stored at 5 °C. For the evaluation of antimicrobial activity of the synthesized complexes, a suspension of each test microorganism was prepared. The turbidity of each suspension was adjusted to 0.5 McFarland units by suspending the cultures in sterile distilled water. The size of final inoculums was adjusted to 6×120 CFU mL^{-1}. Volume of 20 mL of agar media was poured into each Petri plate and the plates were swabbed with broth cultures of the respective micro-organisms and kept for 15 min for adsorption to occur. Using a punch, ≈8 mm diameter wells were bored in the seeded agar plates and a 100 µL volume of each test compound reconstituted in DMSO was added into the wells. DMSO was used as the control for all the test complexes. After holding the plates at room temperature for 2 h to allow diffusion of the compounds into the agar, the plates were incubated at 37 °C for 24 h.[16] The antibacterial activity was determined by measuring the diameter of the inhibition zone. The entire tests were performed in triplicate and the mean of the diameter of inhibition was calculated. The antimicrobial activities of the complexes were compared against standard drugs.

Minimum inhibitory concentration (MIC)

Nutrient broth was adjusted to pH=7.0 for the determination of the *MIC* of synthesized Zn(II), Cd(II), Hg(II), and ZrO(IV) complexes. The minimum inhibitory concentration (*MIC*) is the lowest concentration of an antimicrobial agent that prevents the development of visible growth of microorganism after overnight incubation. The inoculum of the test micro organisms were prepared using 20 h-old cultures adjusted by reference to the 0.8 McFarland standards (11 cells mL^{-1}). These cultures were further diluted up to 5-fold with nutrient broth to obtain an inoculum size of 1.5×10^6 CFU mL^{-1}. A positive control (containing inoculum but no complex) and a negative control (containing complex but no inoculums) were also prepared. A stock solution of 5 mg mL^{-1}. of each compound was prepared in DMSO and further appropriately diluted to obtain final concentrations ranging from 100 to 3.0 µg mL^{-1}. The requisite quantity of antifungal drug (cyclohexamide) was added to the broth to obtain its desirable final concentration of 250 µg mL^{-1}. Separate flasks were taken for each test dilution. To each flask was added 100 µL of inoculum. Then the appropriately diluted test sample was added to each flask having broth and microbial inoculum. The contents of the flask were mixed and incubated for 36 h at 37 °C. The test bacterial cultures were spotted in a predefined pattern by aseptically transferring 10 µL of each bacterial culture onto the surface of solidified agar-agar plates and incubated at 37 °C for 24 h for determining the *M.I.C.* value.

Table 1. The physical properties and elemental analysis of the prepared metal complexes.

Compound	Color	M.p. °C*	Molecular Formula	C, % Cald. (found)	H, % Cald. (found)	N, % Cald. (found)	Cl, % Calcd. (found)	M, % Cald. (found)
$[ZrOL]Cl_2$	Pale yellow	370	572.52 $C_{21}H_{15}Cl_2N_7O_3Zr$	53.14 (54.07)	2.65 (2.99)	15.77 (16.22)	12.32 (11.98)	13.9 (13.88)
$[ZnLCl_2]$	Red	329^D	533.68 $C_{21}H_{15}Cl_2N_7O_2Zn$	47.62 (46.99)	2.67 (2.21)	18.37 (17.55)	13.29 (12.77)	12.25 (12.16)
$[HgLCl_2]$	Brown	356^D	668.89 $C_{21}H_{15}Cl_2N_7O_2Hg$	37.71 (36.92)	2.26 (2.22)	14.66 (15.09)	10.60 (9.76)	29.29 (28.80)
$[CdLCl_2]$	Pale yellow	360^D	581.70 $C_{21}H_{15}Cl_2N_7O_2Cd$	43.83 (42.50)	2. 63 (2.10)	17.04 (17.99)	12.21 (11.44)	15.15 (14.97)

*D=decomposed.

Antifungal study

Potato dextrose medium (PDA) was prepared in a flask and sterilized. To check the growth of bacterial culture in the medium, the requisite quantity of the standard antibiotic (ampicillin) was added to obtain the desired final concentration of 100 μg mL^{-1} of the medium. Test samples were prepared in different concentrations (10, 50 and 100 μg mL^{-1}) in dimethyl sulphoxide and 200 μL of each sample was spread on the PDA media contained in sterilized Petri plates.

Mycelial discs taken from the standard cultures of fungi (*Aspergillus fumigatus* and *Candida albicans*) were grown on the PDA medium for 5-7 days. These cultures were used for the aseptic inoculation in the sterilized Petri dish. Standard cultures inoculated at 28±1 °C were also used as the control.

The efficacy of each sample was determined by measuring the radial mycelial growth. The radial growth of the colony was measured in two directions at right angle to each other and the average of two replicates was recorded in each case. The data are expressed as percent inhibition over the control obtained from the size of colonies. The percent inhibition (φ) was calculated using the formula:

$$\varphi = 100\frac{C-T}{C} \qquad (1)$$

where

C is the diameter of fungus colony in the control plate after incubation for 96 h and

T is the diameter of the fungus colony in the tested plate after the same incubation period. [16]

Results and discussion

The analytical and physical data of template metal complexes are listed in Table 1. The percent's of C, H, N and M content obtained from elemental and analyse are in good agreement with the general molecular formula proposed for the complexes $[MLCl_2]$ (M: Cd(II), Zn(II) and Hg(II)) and $[ZrOL]Cl_2$, where L = acyclic N_2O_2 organic segment formed by template route between 2,6-diaminopyridine and 1,4-dihydroquinoxalin-2,3-dione, as shown in Figure 3.

IR spectra

The IR spectra of acyclic metal template complexes has shown the absence of uncondensed functional groups $–NH_2$ and C=O of 2,6-diaminopyridine and quinoxalin-2,3-dione (i.e., stretching modes of starting materials) which confirm the formation of the proposed acycle organic moiety involving imine –C=N- and –C=O groups[13,14] (Table 2.) The appearance of strong absorption band in the region 1600-1630 cm^{-1} corresponds to υC=N stretching frequency. A medium absorption recorded in the regions 3300-3250 cm^{-1} may be ascribed to υN-H in 1 and 4 positions of pyrazine ring, thus confirms the lactam form corresponding to quinoxaline moiety.[14,15] Furthermore, no strong absorption band was observed near 1675-1660 cm^{-1} indicating the absence of >C=O of quinoxalin-2,3-dione at 2-position, this confirms the condensation of carbonyl group of quinoxaline and amino groups of 2,6-diaminopyridine.[12-14] These results provide strong evidence for the formation of acyclic frame.[13] A strong absorption band in the region ~1585-1613 cm^{-1} may be attributed to the C=N group.[14-15] The lower values in the wave numbers of ν(C=N) may be explained on the basis of drift of lone pair density of imine nitrogen towards metal atoms.[15-17] The bands present at ~3050-2966 cm^{-1} may be assigned due to ν(C-H) vibrations of quinoxaline and pyridine moieties. The bands present in the range ~1150-1130 cm^{-1} are assigned due to ν(C-N) vibration. The IR spectra of the complexes do not show any change in the pyridine ring vibrations and interestingly enough, it appears that in these complexes pyridine nitrogen does not take part in coordination.[17-18] Thus, in the presence of metal salts, a quadridentate acyclic system is formed which coordinates through imine nitrogen and two oxygen atoms of –C=O posit ionized in 3 position of lactam quinoxaline of while pyridine nitrogen does not take part in coordination. Moreover, the coordination through pyridine nitrogen does not take place, as it will result in the formation of unstable four member rings.[14,15]

The far IR spectra show bands in the region ~550-490 and 433-460 cm^{-1} corresponding to νM-N and νM-O vibrations, respectively.[18] As well as the tautomer's of in position 2 of quinoxaline ring between C=O and C=N- supports the coordination of organic moiety with appearance of strong bands at 1680-1640 cm^{-1}. Thus, the acyclic tetradentate ligand behaves as N_2O_2 system. Furthermore, the strong band at 880 cm^{-1} in the spectrum of zirconium(IV) complex may be assigned to Zr=O vibration.[19] The Zn(II), Cd(II) and Hg(II) displayed weak absorptions in the regions 260-380 cm^{-1} which confirms the M-Cl bond.[19]

Table 2. FT-IR absorptions of the quinoxalin-2,3-dione and its template metal complexes in cm^{-1}.

Complex	νNH, νC=N-	νC= O	νAr-CH,	νC-N	νM-N	νM-O	Other bands
Quinoxalin-2,3-dione	3250,1590(s)	1680(s)	3050[b], 2962(m)	1150(s)			790-895 [b]
$[ZrOL]Cl_2$	3180 (m),1533(m)	1657(s)	3060 (w) 2870(m)	1130(m)	450(w)	506(w)	880(Zr=O)
$[ZnLCl_2]$	3180(m), 1580(s)	1677(s)	3080-2970(w)[b]	1140(m)	433-460(w)	550	265-370[a](w),766(m)
$[HgLCl_2]$	3235 , 1610(s)	1666(s)	3100(w),[b] 2980	1148(s)	421(m),	469(w)	260-380(w)[a] 2997[b](w)
$[CdLCl_2]$	3169, 1530(s)	1640(s)	3050 (w) 2968[b]	1145(s)	490 (w)	544(m)	270,378(w),780-890(w)[b]

s=strong,m=medium,br.=broad,w=weak,a =far I.R spectrum of M-Cl and b=vibrational modes of Ar-H.

NMR spectra

The ^1H NMR spectrum of mercury(II) complex shows a multiple signals observed at δ 6.6-8.5 ppm that may be attributed to Ar-H and quinoxaline protons (Fig. 1.) The multiple absorption in the region 9.1-12.5 ppm may be assigned to the spin resonance of the deshielded lactam-NH protons the are effected strongly by the electronic withdrawing of Hg(II) ion (Figure 2). The chemical shifts in the region 4.5-5.3 ppm confirms the tautomerism of –C=N- imine group with C=N- of pyrazine ring, thus support the expected structure of the Hg(II) complex.[13,14] Moreover, the ^{13}C NMR spectrum of Hg(II) complex displays resonances at 40, 110, 130, 150 and 170-200 ppm that are attributed to CH_3(DMSO), C=C-(Ar-), C=N, and C=O groups, respectively.[14]

The data obtained from ^1H and ^{13}C NMR spectra for Hg(II) complex in DMSO-d_6 solvent were shown as below: ^{13}C NMR (300 MHz, DMSO-d_6, δ, ppm): 38-40(S, *J* = 7.2 Hz, DMSO), 155.0 (2C, C=O), 131.0 (1C, Ar-*C*), 128.1 (2C, N=*C*), 126.3 (2C, N-*C*), 128-126 (4C, Ar-C),110-123(4C,C-N-Pyridine) 62.3 (1C, *Py-C*), 63.2 (1C, C=*C*H pyridine).

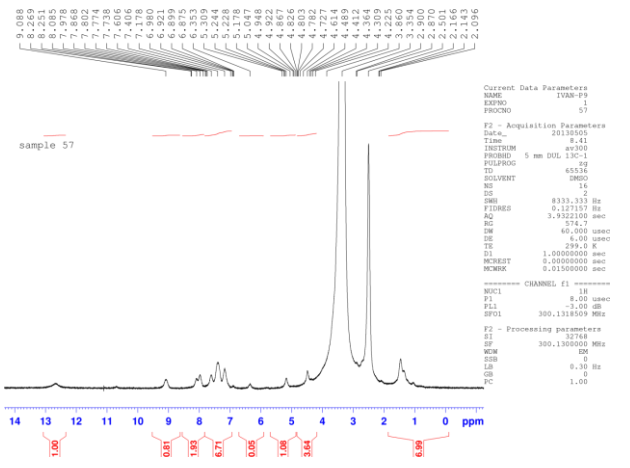

Figure. 1. ^1H NMR of $[HgLCl_2]$ complex in DMSO-d_6 solution**.**

Electronic spectra and molar conductivity

The quinoxalin-2,3-dione solution in ethanol shows high intensity peaks at 31446 and 36100 cm^{-1} that related to electronic transitions of C=N-, C=O and C=C- groups of the types ($\pi\rightarrow\pi^*$ and $n\rightarrow\pi^*$).[13,15,19] The electronic spectra of the complexes were recorded in DMF solutions. The pale yellow solution of Zn(II) complex in DMF exhibits two distinct peak in the region 34448 and 27777 cm^{-1} that are consistent with ligand field and ligand to metal charge transfer transitions, respectively. The UV-visible spectra of Zn(II), Cd(II) and Hg(II) complexes show high intensity peaks at 22880-34448 due to M→L charge transfer transitions, respectively.[22] The electronic spectrum of the zirconium(IV) complex exhibits bands at 20660 and 30288 cm^{-1} which are assignable to charge transfer of Zr=O moiety and ligand field transitions, respectively.[20,21] The geometry of the zirconium(IV) complex was proved to be square pyramidal based on the charge transfer bands of Zr=O in the UV region besides the 1:2 electrolyte behaviour.

The molar conductance of Zn(II), Cd(II) and Hg(II) complexes in DMF were recorded in the range 10-22 ohm^{-1} cm^2 mol^{-1} indicating that these complexes were neutral and agree well with the other spectral and elemental analyses. [23] However, the zirconium(IV) complex solution in DMF shows electrolytic behavior in 1:2 ratio of molar conductance 175 ohm^{-1} cm^2 mol^{-1} due to the presence of two chloride ions in the outer sphere of the complex, Table 3.

Table 3. The electronic spectra λ (cm^{-1}) and molar conductance, Λ_m, (S mol^{-1} cm^2) of the prepared complexes

Complex	UV-Visible λ, nm	Λ_m, S mol^{-1} cm^2	Geometry
Quinoxaline-2,3-dione	277, 318	10	
$[ZnLCl_2]$	290, 360	18	Octahedral
$[HgLCl_2]$	311, 357	12	Octahedral
$[ZrOL]Cl_2$	330, 485	175	Square pyramidal
$[CdLCl_2]$	325, 396	22	Octahedral

Λ_m = molar conductances were measured in DMF solutions.

 DOI: 10.17628/ecb.2014.3.384-389

Table 4. Antimicrobial activity of the prepared metal complexes

Compound	Inhibition			
	E. coli	*S. aurea*	*Fungi*	
	G^+	G^-	*Asp.*	*Cand.*
$[ZnLCl_2]$	70	66	50	22
$[CdLCl_2]$	49.2	21	18	19
$[HgLCl_2]$	29	17	23	11
$[ZrOL]Cl_2$	22	33	20	44
Control DMSO	10	13	12	9
Streptomycine	25	30	38	33

Antimicrobial studies

In this study, all the chemically synthesized complexes were evaluated against gram-positive and gram-negative bacteria. The MIC values of the synthetic complexes were determined by the method given by Andrews.[23,24] Standard antibiotic, namely streptomycin was used for comparison with the antibacterial activities exhibited by these complexes. All the complexes of the tested series possessed some antibacterial activity against gram-positive bacteria as well as Gram-negative bacteria, Table 4. In the whole series, complexes Zn(II) was found to be most effective against all the tested bacterial strains, showing zone of growth inhibition at 70 mm. The complexes of Cd(II) and Hg(II) exhibited good activity against all the tested bacterial strains with a zone of inhibition in the range from 33.2-49.44 mm and 23.03-29.96 mm, respectively. The ZrO(IV) complex showed activity in the region (22-33 mm) against *E. coli* and *S. aurea*, while it inhibition toward *Candida fungus* was 44 mm. The complexes of Zn(II) and Cd(II)showed the highest zone of inhibition 60-70 and 21-49.2 mm, respectively 36.70 mm against *Staphylloccus aurea* and *Esherichia coli* (Table 4). This would suggest that the chelation could facilitate the ability of a complex to cross a cell membrane and can be explained by Tweedy's chelation theory.[16,25-23] The chelating will enhance the lipophilic character of the central metal atom, which subsequently favors its permeation through the lipid layers of the cell membrane and blocking the metal binding sites on enzymes of microorganisms.[26-29]

Conclusion

According to the results obtained from elemental analyses, FT-IR, UV-Visible spectra, magnetic and molar conductivity measurements, the octahedral geometry was proposed for Zn(II), Cd(II) and Hg(II) complexes with formula $[MLCl_2]$, while the zirconyl complex was suggested as square-pyramidal geometry of the formula $[ZrOL]Cl_2$. The data obtained from infrared spectra revealed that nitrogen atoms of imine groups and two oxygen atoms of carbonyl participate in coordinating with the central metal ions. As well as, this study is a preliminary evaluation of antibacterial activity of acyclic metal complexes against two types of bacteria and fungi. The quinoxaline system is very active biologically. It indicates that the complexes have the potential to generate new antimicrobial metabolites. The acyclic metal complexes demonstrating antibacterial activity could result in the discovery of new chemical classes of antibiotics that could serve as selective agent for the maintenance of animal or human health and provide biochemical tools for the study of infectious diseases.

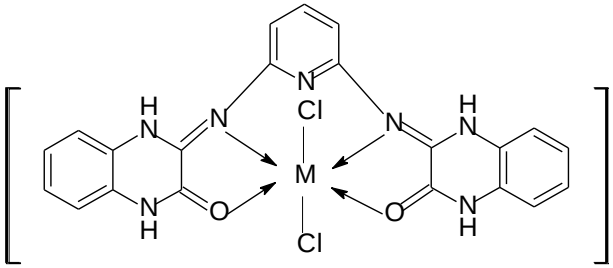

M= Zn(II), Cd(II) and Hg(II)

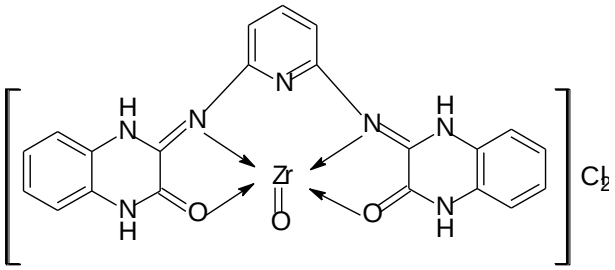

Figure 3.Stereochemical structures of metal complexes.

References

[1]Vigato, P. A., Tamburim, S., *Coord. Chem. Rev.* **2004**, *248*, 1717-2118.

[2]Di Bella, S., Fragala, I., Ledoux, I., Marks, T. J., *J. Am. Chem. Soc.* **1995**, *117*, 9481-9485.

[3]Singh, D. P., Bhantnagar, J. M., *Talanta* **2010,** *57*, 775-780.

[4]Patole, J., Singhnapurkar, D., Padhye, S., Ratledge, C., *Bioinorg. Med. Chem. Lett.*, 2006, *16*, 1514-1517.

[5]Khan, A., Sarkar, S. S. D., Int. *J. Antimicrob. Agents* 2008, *32*, 40-45.

[6]Daniel, V. P., Murukan, B., Kumari, B. S., Mohanau, K., *Spectrochim. Acta A.* **2008**, *70*, 403-410.

[7]Srinivas, Kumar, C. N. S. S. P., Rao, V. J. and Palaniappan, S., *J. Mol. Catal.* **2007**, *265*, 227-230.

[8]Tarallo, M. B., Costa-Filho, A. J., Vieira, E. D., Monge, A., Leite, C. Q., Pavan, F. R., Borthagaray, G., Gambino D. and Torre, M. H. *J. Arg. Chem. Soc*., **2009**, *97*, 80-89.

[9]Wang, X. L., Lin, H. Y., Liu, G. C:, Zhao, H-Y., Chen, B. K., *J. Organomet. Chem*., **2008**, *69*, 2767.

[10]Hu, J., Xie, Z-F., Hui, Y-H., Mo X-X., Sun, N. X., Liu, F.-M., *Chin. J. Org. Chem*., **2007**, *279*, 1162-1166.

[11]Zhu, W., Sintic, M., Ou, Z., Sintic, P. J., McDonald, J. A., Brotherhood, P. R., Crossley, M. J., Kadish, K. M., *Inorg. Chem*., **2010**, 49, 1027-1031.

[12]Mohamed, G. G., El-Gamel, N. E. A., *Spectrochim. Acta A.* **2004**, *60*, 3141-3151.

[13]Al-Jibouri, M. N., *J. Appl. Chem.*, **2014**, *6(6)*, 64-73.

[14]Al-Jibouri, M. N., Emad, A., *Al-Mustansiriyah J. Sci.* **2013**, *24(2)*, 49-64.

[15]Satish, M. A., Sathisha, M. P. and Revankar, V. K., *Trans. Met. Chem*., **2007**, *32*, 81-87.

[16]Atlas, R. M., Brown, A. E., and Parks, L. C., "*Laboratory Manual Experimental Microbiology*", Mosby-Year Book Inc. **1995**.

[17]Nakamoto, K., *Infrared and Raman spectra of Inorganic and Coordination Compounds* ", **1986**, Wiley, New York.

[18]Siddappa, K., Reddy, T., Mallikarjun, M. and Reddy, C. V., *Eur. J. Chem*., **2008**, *5(1)*, 155-162.

[19]Silverstein, R. M., Bassler, G. C. and Morrill, T. C., *Spectrometric Identification of Organic Compounds*, 4th ed., Wiley, New York, **1981**.

[20]Sutton, D., *Electronic Spectra of Transition Metal Complexes*, McGraw-Hill: London, **1968**, 388.

[21]Cotton, F. A., Wilkinson, G., Murillo, C. A., Bochmann, M., *Adv. Inorg. Chem.,* 6th edition, John Wiley & Sons, **1999**.

[22]Singh, D. P., Malik, V., Kumar, R., Kumar, K., *Rasayan J. Chem.*, **2009**, *2(1)*, 133-138.

[23]Geary, W. J., *Coord. Chem. Rev*., **1971, *7,*** 81-122.

[24]Sanmartin, J., Bermejo, M. R., Deibe, A. M. G., Maneiro, M., Lage, C., Filho, A. J. C., *Polyhedron*, **2000**, *19*, 185-192.

[25]Rani, D. S., *Synthesis and structural studies of transition metal compounds derived from multidentate disubstituted quinoxalines*, Ph.D. Thesis, Osmania University, **1995.**

[26]Raman, N., Raja, J. D., Sakthivel, A., *J. Chilean Chem. Soc*., **2008**, *53*, 3-9.

[27]Singh, D. P., Kumar, K., Dhiman, S., Sharma, J., *J. Enzyme Inhib. Med. Chem.,* **2009**, *24(3)*, 795-803.

[28]Singh, D. P., *Eur. J. Med. Chem.*, 2009, *44(1)*, 63-69.

[29]Singh, D. P., Kumar, R., Singh, J., *Eur. J. Med. Chem.*, **2009**, *44(4)*, 1731-1736.

Received: 09.03.2014.
Accepted: 23.03.2014.

A NEW MODEL OF METALLIC STRUCTURE AND BONDING

Peter F. Lang[a]* and Barry C. Smith[a]

Keywords: metallic structure, metallic bonding, metallic radii, free electrons in metals, enthalpy of formation, work function.

This paper briefly describes the current physical model of metallic structure and bonding. An alternative model is introduced. It shows that the new model, which calculated internuclear distances of Group 1 and Group 2 crystalline binary salts to a remarkable degree of accuracy, can be applied to calculate metallic radii (equal to half the internuclear distances) of Group 1 and Group 2 metals precisely. A simple expression previously used to calculate lattice energies using the soft-sphere radii concept is applied to calculate enthalpies of formation of Group 1 and Group 2 metal ions and results compare well with observed values. A few of the limitations of the current models are described and properties of metals which can be accounted for by the soft-sphere model are discussed. The work functions of Group 1 and Group 2 metals are shown to be inverse functions of the soft sphere ionic radii.

* Corresponding Author
E-Mail: p.f.lang@gmail.com
[a] Birkbeck College (University of London), Malet Street, London, UK WC1E 7HX.

Introduction

Living organisms that made up much of nature are composed of molecules consisting of both metallic and non-metallic elements. An understanding of how atoms bond together is therefore very important in the study of natural science. However, even though over 70% of elements are metals, metallic bonding and structure are still not well understood. It is well known that most metals have hexagonal, cubic close packed or body centred cubic structures.[1] Paul Drude,[2] in 1900, was the first to propose the "free electron" model for electricity conduction in metals and metallic bonding. He suggested that in crystalline metals, positive ions were surrounded by an "electron gas". Estimates of the number of "free" electrons in a metal have also been described since the early twentieth century.[3] Other common accounts on electrical conductivity in metals include band theory,[4] which postulates the existence of energy bands in solids that influence the behaviour of electrons. In his book, *The Nature of the Chemical Bond*,[5] Pauling provided extensive details on the closest packing of spheres, metallic orbitals, metallic valencies, bond lengths, and bond numbers in metals. However, some other common properties of metals (see below) were not discussed in his book nor were they accounted for in the models of metallic structure and bonding.

In recent years, the theory of metallic bonding and structure has shown little advance on the "free electron" model. It is still very common to describe metallic structures and metallic bonding as "bonding which involves the delocalisation of electrons throughout the metal solid"[6] or as "metal cations in a sea of electrons".[7] It has been demonstrated[8] that the standard model used to describe metallic structure and properties is inadequate. The electrical conductivity of copper is higher than most metals. It has been reported that graphene, which is covalently bonded carbon, is a much better conductor of electricity than copper.[9] Surely, this must mean that electrons in a metallic bond are not "free" and better a model for describing metallic structure and bonding is needed.

Theory

We propose here an alternative "soft-sphere" model which considers that in a metallic crystal, the outermost electron(s) in each atom is/are not exactly "free" nor completely delocalised. The outermost electron(s) is/are separated/detached from the atom which forms a positive ion with one or more of the "detached" electron(s) behaving like negative ions. The detached outermost electron(s) can occupy certain equivalent positions that are at the midpoints between the nearest neighbours of the positive ions (similar to ionic crystals, where positive ions occupy positions between negative ions) but can move within these midpoint positions in a unit cell. For the remainder of this paper, these midpoint positions will be called "midpoint sites". Depending on the Group and metallic structure (hcp, fcp or bcc) the most likely number of outermost electrons detached from each individual metal atom range from 1 to a maximum of 5. The soft-sphere ionic radii of Group 1 and Group 2 metals (excluding beryllium) have already been determined very accurately[10] and in this work we use members of these 2 Groups to demonstrate the soft-sphere model of metallic structure and bonding.

Consider any crystal with a hexagonal (hcp) or cubic closed pack (fcp) structure of identical atoms, each atom has 12 co-ordination or 12 closest neighbours and in a body centred cubic (bcc) each atom has 8 closest neighbours. There are 2 atoms in each unit cell in a body centred cubic, 6 atoms in each unit in a hexagonal closed pack and 4 atoms per unit cell in a face centred cubic[11] crystal.

At room temperature, all Group 1 metals have a bcc structure and each atom has 1 outermost electron. In the soft-sphere model of metallic structure/bonding, each atom has a single outermost electron which it loses to form a unipositive (1^+) ion. Each positive ion has 8 nearest identical neighbours of positive ions. Hence there are 8 equivalent sites that are midpoint between the internuclear distance of a positive ion and its 8 neighbouring positive ions. The outermost electron which is detached from the atom can occupy and move around any one of these 8 midpoint sites in a unit cell at any *one* time. Since there are 2 positive ions in each unit cell, there are only 2 detached electrons in each cell and, therefore, at any *one* time only 2 of the 8 (or a

Table 1. Soft-sphere ionic radii and atomic/metallic radii of Group 1 and Group 2 metals

Element	Soft-sphere radii Å	Cell constants		Internuclear separation Å	Atomic radii Å
		a	c		
(A)	(B)	(C)	(D)	(E)	(F)
Li	1.094	3.509		3.039	1.520
Na	1.497	4.291		3.716	1.858
K	1.971	5.321		4.608	2.304
Rb	2.160	5.700		4.937	2.469
Cs	2.368	6.176		5.348	2.674
Be	0.750	2.286	3.584	2.256	1.128
Mg	1.282	3.209	5.211	3.203	1.602
Ca	1.657	5.580		3.946	1.973
Sr	1.861	6.086		4.303	2.152
Ba	2.084	5.023		4.350	2.175

quarter of) midpoint sites are occupied and the rest are vacant and under certain conditions can be occupied by other detached electrons moving in from other unit cells.

Group 2 metals present a slightly more complicated problem in that beryllium and magnesium have hcp structures at room temperature whereas calcium and strontium possess a ccp structure and barium has a bcc structure respectively.[12] In any Group 2 metal crystal, each metal atom loses its 2 outermost electrons to form a dipositive (2^+) ion. In a barium crystal (with a bcc structure), each dipositive ion has 8 identical nearest neighbours of positive ions. Since there are 2 positive ions in each unit cell, there are 4 detached electrons in a cell. Hence, at any *one* time there are 4 electrons occupying the 8 equivalent midpoint sites between the positive ions, which mean that only half of the 8 sites are occupied. In calcium and strontium (with fcp structures), there are 4 positive ions and 8 detached electrons (with each atom losing 2 electrons) occupying 24 equivalent midpoint sites per unit cell. Thus, at any *one* time, only a third of the sites are occupied. Similarly for beryllium and magnesium (hcp), with 6 positive ions and 12 detached electrons per cell, at any *one* time only a third of the 36 sites are occupied.

The atomic/metallic radius of a metal atom (which is half the internuclear distance between the nearest neighbours) or distance between the centres of the positive ion and the detached outermost electron, just as in the case of an ionic crystal, can be calculated from the relationship:[10]

$$S(\text{calc})^k = [M]^k + [e]^k$$

where S is the radius of the metal atom, $[M]$ is the ionic radius of the positive ion, $[e]$ is the "radius" of the midpoint site containing the detached electron and the exponent k is defined in previous work.[10]

Column B of Table 1 shows the soft-sphere ionic radii determined by previous work,[10] the observed unit cell constants[13] quoted to appropriate number of decimal places (after taking account of the size of experimental uncertainties) are shown in columns C and D. Internuclear separations (between nearest neighbours) calculated from unit cell constants of Group 1and Group 2 metals are listed in Column E. The distances between the centres of the positive ions and space occupied by the detached electron (or the metallic radii of the atoms) are given in Column F of the table. All figures are given in Angstrom (Å) units, where 1 Å equals 10^{-10} m. Since the soft-sphere radius of beryllium has not been determined previously, for this work we have extrapolated from the known soft-sphere radii of Group 2 metals to obtain an estimate of 0.75±0.02 Å.

We have made an empirical assumption that (a) *e*, the "radius" of the midpoint sites containing the separated/detached electron(s) and (b) the exponent *k*, are different for Group 1 and Group 2 metals because of the difference in charge on the positive ion, the value of *k* may also be influenced by the number of nearest neighbours. However, in order to limit the number of values of *k* in the calculations we have used *k* equals 1.5 for Group 1 and *k* equals 1.3 for Group 2. All Group 1 metals have 1 outermost electron and all have bcc structure, therefore we assume that the value of *e* is the same for all 5 elements is the same. By trial and error, an estimated value of 0.8 is obtained to give the best results. For Group 2 metals, beryllium, magnesium, calcium and strontium have 12 co-ordination and we assume that *e* is the same for all 4 elements and has the value of 0.565. Barium has 8 co-ordination and the value of *e* is 0.22.

Results and Discussion

The observed metallic radii (or half the internuclear distance) of Group 1 and Group 2 metals are shown in Column B and the calculated radii in Column C of Table 2, respectively. As shown in Column D of the table, differences between the observed and calculated are in all cases less than 0.01 Å. This is very good agreement since the experimental uncertainties of the appropriate cell constants can be as great as 0.01 Å (as in the case of calcium). The root mean square (r.m.s.) deviation δ is given at the top of Table 2.

The lattice energy of a compound is the energy change when 1 mole of the compound at one atmospheric pressure is converted into gaseous positive and negative ions which are separated from each other at infinity. Lattice energies

can be calculated using the Born-Haber cycle or from equations such as the Born-Lande/Born-Mayer equations or the improved Kapustinskii equation. The enthalpy of formation of a positive univalent Group 1 or divalent Group 2 metal ion is the energy change when 1 mole of the crystalline metal is converted into one mole of the gaseous positive metal ion separated from 1 (in the case of Group 1) and or 2 (in the case of Group 2) moles of electrons. In the case of a metal solid, the detached electron is treated as be equivalent to the "negative ion" bonded to positive ion. Under this assumption, the energy change when a crystalline metal is converted into 1 mole of the gaseous positive ion and the respective number of moles of "electrons" can then be regarded as equivalent to the lattice energy of an ionic crystal. The enthalpies of formation of gaseous metal atoms for Group 1 and Group 2 metals are shown in Column B of Table 3. The first and (for Group 2 only) second ionisation energies of the metals are listed in Columns C and D respectively. Ionisation energies are converted from eV (electron volts) to kJ mol^{-1} by the relationship of 1 eV = 96.49 kJ mol^{-1}. The enthalpies of formation of the appropriate gaseous ions are shown in Column E of the Table. All ionisation energies, enthalpies of formation, work functions, bond dissociation energies and enthalpies of formation that are utilised in this work are quoted from the *CRC Handbook of Chemistry and Physics*.[14]

Table 2. Comparison of observed and soft-sphere atomic/metallic radii of Groups 1 Group 2 metals

Element	Observed Å	Soft-sphere calculated, Å	Obs – Calc Å
(A)	(B)	(C)	(D)
Li	1.520	1.512	0.008
Na	1.858	1.865	–0.007
K	2.304	2.298	0.006
Rb	2.469	2.474	–0.005
Cs	2.674	2.669	0.005
Be	1.128	1.124	0.004
Mg	1.602	1.610	–0.008
Ca	1.973	1.964	0.009
Sr	2.152	2.158	–0.006
Ba	2.175	2.175	0.000

[a]The root mean square (r.m.s.) deviation is δ=0.00629.

We have previously developed a simple expression to calculate lattice energies of Group 1 and Group 2 salts.[10] The results produced agreed well with lattice energies calculated from the Born-Haber cycle. We reproduce the expression here as follows:

$$E_L = \frac{R\frac{H_0}{M}M^{k-1}}{\left(X^{k-1.3333}\right)\left(0.5^{0.33333}\right)\left(\sum Q^2\right)}$$

where

E_L is the lattice energy,

R is the Rydberg constant for infinite mass converted to kJ mol^{-1},

H_o is the classical Bohr radius,

M is the size of the cation,

X is the size of the anion and

Q_i is the charge on the ions.

Hence, for sodium chloride $\Sigma Q_i^2 = 1 + 1 = 2$ and for calcium chloride it is 4 + 1 + 1 = 6 etc. ΣQ_i^2 is the sum of all the squares of the charges on the ions, since the higher the charge on the ions the more electrons need to be removed from the overlap region and the more energy is required to separate them. R is the amount of energy needed to remove an electron from a species the size of a hydrogen atom, (H_o/M) provides a ratio of the distance of the electron from the nucleus, since the greater the size the less is the energy needed to remove the electron**.** $(M^{k-1})/(X^{k-1.3333})$ gives an approximation of the overlap, this is multiplied by a factor which is approximated to (½ $^{0.33333}$) because the electron is not removed to infinity away from both ions (but rather removed from the overlap region).

We have applied the same expression given above with only two very minor differences to calculate the enthalpies of formation of Group 1 and Group 2 metal ions. X, rather than being the size of an anion, is the "radius" of the space occupied by the electrons detached from the metal atom. In the above expression, ΣQ_i^2 is the sum of the squares of the charges on the positive ions and the detached outermost electron(s). For Group 1 metals, Q_i^2 of the positive ion is 1 since each ion has a +1 charge. However, Q_i^2 of the outermost electron is only 0.25 since at any *one* time only a quarter of the available midpoint sites is occupied. Hence, ΣQ_i^2 is equal to 1 + 0.25 (1.25) for all the Group 1 metals. For elements of Group 2, Q_i^2 for the positive ions in all cases is 4 (since they are all dipositive). However, there are 2 different values of ΣQ_i^2. For the first 4 elements, only a third of the sites are occupied by electrons. Hence, Q_i^2 for the electrons is $(1^2 + 1^2)\cdot 0.3333$ and ΣQ_i^2 is approximately 4.7. As for barium, since half of the available midpoint sites are occupied at any *one* time, Q_i^2 for the electrons is $(1^2 + 1^2)\cdot 0.5$. Hence ΣQ_i^2 has a value of 4 plus 1 which equals 5. The soft-sphere calculated values are shown in Column B of Table 4. The conventionally produced results are shown in Column C and the absolute percentage differences are shown in Column D of the Table. Differences between observed and soft-sphere calculated are less than 10% for all cases.

Metals are malleable and ductile because not all available midpoint sites are occupied by electrons. When a metal is twisted or bent, electrons can move from 1 site to another within a unit cell, allowing the shape of the metal to change without any bonds being broken. It has been shown that when sodium is under very high pressure the resistance of the metal increases drastically and acts more like an insulator[15] than a conductor of electricity.

This behaviour cannot be easily explained by the standard model. However, this can be accounted for by the soft-sphere model. When a metal is under high pressure, the shape and size of the unit cell changes. This reduces the volume of the site(s) occupied by the detached electron(s) and if the volume is reduced sufficiently it can no longer be occupied. When the shape of the unit cell changes, the distance between some of the midpoint sites may increase to such an extent, the detached electrons occupying those sites may no longer be able to move from one site to another.

Table 3. Enthalpies of formation of Group 1 and Group 2 metal ions

Element	Enthalpies of formation of M(g) kJ mol^{-1}	Ionisation energies		Enthalpies of formation M^+(Group 1)/M^{2+}(Group 2) kJ mol^{-1}
		1st eV (kJ mol^{-1})	2nd, eV (kJ mol^{-1})	
(A)	(B)	(C)	(D)	(E)
Li	159.3	5.392 (520.25)		679.55
Na	107.5	5.139 (495.87)		603.37
K	89.0	4.341 (418.83)		507.83
Rb	80.9	4.177 (403.05)		483.95
Cs	76.5	3.894 (375.72)		452.22
Be	324.0	9.323 (899.55)	18.211 (1757.19)	2980.74
Mg	147.1	7.646 (737.78)	15.035 (1450.75)	2335.64
Ca	177.8	6.113 (589.86)	11.872 (1145.50)	1913.16
Sr	164.4	5.695 (549.50)	11.030 (1064.29)	1778.19
Ba	180.0	5.212 (502.87)	10.004 (965.27)	1648.14

Table 4. Comparison of observed and calculated enthalpies of formation of M^+(Group 1)/M^{2+}(Group 2)

Element	Observed kJ mol^{-1}	Soft-sphere calcd., kJ mol^{-1}	Abs. difference, %
(A)	(B)	(C)	(D)
Li	679.55	683.56	0.6
Na	603.37	584.35	3.2
K	507.83	509.26	0.3
Rb	483.95	486.47	0.5
Cs	452.22	464.61	2.7
Be	2980.74	3108.22	4.3
Mg	2335.64	2135.67	8.5
Ca	1913.16	1784.55	6.7
Sr	1778.19	1645.25	7.5
Ba	1648.14	1569.24	4.8

Hence, if there are no vacant sites which can facilitate electron movement or if the electrons cannot move between sites in neighbouring unit cells the metal becomes a virtual insulator. Assuming that in a metal the positive ions are truly surrounded by "a sea of electrons", then it may be reasonable to assume that the work function of any metal is not a significant value since electrons from the "electron sea" can move freely to the surface of the metal. However, the work functions of some metals are much higher than some bond dissociation energies and ionisation energies. For example, the work function of beryllium is 480.5 kJ mol^{-1} and the bond dissociation energy of C-H is 338.4 kJ mol^{-1}, that of Cl-Cl is just 242.4 kJ mol^{-1} and that of Ca-Ca is only 16.5 kJ mol^{-1}. The first ionisation energy of caesium is 3.8939 eV (or 375.6 kJ mol^{-1}).

In the soft-sphere model, the separated/detached outermost electrons can only occupy midpoint sites between 2 positive ions inside a unit cell, which means that there is almost no outermost electron on the surface of the metal. Hence, energy has to be expended to draw those electrons onto the surface of the metal. The work function is an inverse function of the soft-sphere radius since the further the outermost electron(s) is/are from the nucleus of the positive metal ion the less energy is required to draw it/them to the surface. The work functions of the Group 1 and Group 2 metals can be approximated by the following simple expression:

$$W = \frac{C}{R^{0.5}}$$

where

W is the work function,

R is the soft-sphere ionic radius and

the constant *C* is 3.08 for Group 1 and 3.85 for Group 2 metals.

Column B of Table 5 lists the soft-sphere radii, Column C shows the work functions (in eV) calculated by the above formula, Column D shows the observed work functions in eV. The absolute percentage differences are shown in Column E of Table 5. With the exception of beryllium, all values agree to better than 90%.

The detached electrons can move around different mid-point sites inside a unit cell. As discussed above, only some of those sites are occupied at any *one* time. Since all unit cells in a metal are identical and there are vacant sites which facilitate electron movement, a very small potential difference between the ends of a metal strip or wire can generate an electron flow along the wire (i.e. an electric current). When a metal wire with an electric current flowing through it is placed in a transverse magnetic field, a potential difference is developed across the wire at right angles to both the field and the length of the wire.[16] This is known as the Hall effect.[17] It happens because the magnetic field at right angles to the length of the wire creates a force acting on each electron and since, within every unit cell, there are many vacant sites between the positive ions for the electrons to occupy, detached electrons can move across at right angles to the length of the wire and congregate into more sites on one side of the wire than the other, thus developing a potential difference across the cross section of the wire and at right angles to the field and length of the wire.

Enthalpies of fusion of most halides, oxides and other binary compounds can be many times higher than that of the metals. For example, Column B of Table 6 lists the enthalpies of fusion of Group 1 and Group 2 metals, Columns C and D show the enthalpies of the chlorides and oxides of those metals respectively.

Table 5. Observed and Soft-sphere calculated work functions of Group 1 and Group 2 metals

Element	**Soft-sphere radii** Å	**Soft-sphere** calculated, eV	**Observed** work functions, eV	**Abs. difference** %
(A)	(B)	(C)	(D)	(E)
Li	1.094	2.94	2.93	0.5
Na	1.497	2.52	2.36	6.7
K	1.971	2.19	2.29	4.2
Rb	2.160	2.10	2.26	7.3
Cs	2.368	2.00	1.95	2.6
Be	0.750	4.45	4.98	10.7
Mg	1.282	3.40	3.66	7.1
Ca	1.657	2.99	2.87	4.2
Sr	1.861	2.82	2.59	8.9
Ba	2.084	2.67	2.52	5.8

Table 6. Enthalpies of fusion of Group 1 and Group 2 metals and some halides

Element	**Metal** kJ mol^{-1}	**Chloride** kJ mol^{-1}	**Oxide** kJ mol^{-1}	**Nr of times difference between** chloride/metal	oxide/metal
(A)	(B)	(C)	(D)	(E)	(F)
Li	3.00	19.80	35.60	6.6	11.9
Na	2.60	28.16	47.70	10.8	18.3
K	2.34	26.28	27.00	11.2	11.5
Rb	2.19	24.40	20.00	11.1	9.1
Cs	2.09	20.40	20.00	9.8	9.6
Be	7.90	8.66	86.00	1.1	10.9
Mg	8.48	43.10	77.00	5.1	9.1
Ca	8.54	28.05	80.00	3.3	9.4
Sr	7.43	16.22	81.00	2.2	10.9
Ba	7.12	15.85	46.00	2.2	6.5

The number of times that the enthalpies of the chlorides and oxides are greater than that of the metals (enthalpy of chloride/oxide divided by enthalpy of respective metal) are listed in Columns E and F respectively. These figures clearly show that, with the exception of beryllium, the enthalpies of fusion of the chlorides and oxides are at least twice or up to 18 times the enthalpy of the respective metal.

This cannot be easily accounted for by the standard model even if it is assumed that the bond formed between the metal and chlorine/oxygen is much stronger than the bonding in the metal itself. However, as we have already shown above, in every unit cell in a metal crystal, each positive ion is surrounded by only 2 (in Group 1) or 4 (in Group 2) detached electrons in the midpoint sites between the positive ions. Whereas, in the halide or oxide crystals, every positive ion/negative ion (depending on the structure of the crystal) is always surrounded by more than twice number of oppositely charged ions. So for example, in sodium chloride each sodium ion is surrounded by 6 chloride ions and vice versa. This means that, for every mole of metal, fewer bonds are made when a metal solidifies, but many more bonds are made when a metal halide or oxide solidifies. Beryllium chloride is an exception because its structure is different from other chlorides and oxides (beryllium chloride possesses a chain structure[18] whereas most other halides and oxides of Groups 1 and 2 metals have typical crystal structures such as the NaCl, wurtzite, rutile or fluorite structures).

It has been suggested by some authors that the number of free (or loosely attached) electrons in a metal lies in the range of 1 to 3.5 per atom.[19] Calculations have also shown that only a very small percentage of electrons in a metal are "free".[20] This can easily be accounted for by the soft-sphere model. There are only a limited number of sites that the "free" electrons can occupy. For example, in a body centred cubic, there are only 8 available midpoint sites for the detached electrons and since there are 2 atoms per unit cell the maximum number of electrons that can be detached from each atom is 4. Hence, it is not surprising that the number of "free" electrons per atom is limited to a very low number.

Conclusion

In contrast to the standard "electron sea" model, we are able to show that, for Group 1 and Group 2 metals, the atomic/metallic radii and enthalpy of formation of the positive ions calculated with the soft-sphere model and soft-sphere radii give very good agreement with experimental values. We also showed that the work functions of Group 1 and Group 2 metals are inverse functions of the soft-sphere radii. Additionally, the soft-sphere model can (in a qualitatively manner) account for the differences between the enthalpies of fusion of metals and their halides and oxides. The changes in resistance of a metal under pressure can also be interpreted by the soft-sphere model.

There is strong evidence that the soft-sphere model is a more realistic representation of the structure and bonding of metals than the "electron sea" model.

References

[1]Wells, A. F., *Structural Inorganic Chemistry*, 5th edn., Oxford University Press, 1984.

[2]Drude, P., *Ann. Phys.*, **1900**, *306*, 566.

[3]Hall, E. H., *Proc. Natl. Acca. Sci. USA*, **1925**, *11*, 36.

[4]Coulson, C. A., *Valence*, 2nd edn., Oxford University Press, 1961.

[5]Pauling, L., *The Nature of the Chemical Bond*, 3rd edn., Cornell University Press, 1960.

[6]For example see Cox, P. A., *Instant Notes in Inorganic Chemistry*, 2nd edn., BIOS Scientific, 2004.

[7]For example see Zumdahl, S. S., Zumdahl, S. A., *Chemistry*, 8th edn., Cengage Learning, 2010.

[8]Matsuoka, T., Shimizu, K., *Nature*, **2009**, *458*, 182.

[9]Evans, J., *Chem. World*, **2014**, *11*, 44.

[10]Lang, P. F., Smith, B. C., *Dalton Trans*., **2010**, *39*, 7786.

[11]Bunn, C. W., *Chemical Crystallography*, Oxford University Press, 1961.

[12]Mingos, D. M. P., *Essentials of Inogranic Chemistry 1*, Oxford University Press, 1995.

[13]Donohue, J.,*The Structures of the Elements*, John Wiley & Sons, 1974.

[14]Lide, D.R., ed.*CRC Handbook of Chemistry and Physics*, 89th edn., Chemical Rubber Company, 2008-2009.

[15]Ma, Y., Eremets, M., Oganov, A. R., Xie, Y., Trojan, I., Medvedev, S. Lyakhov, A. O., Valle, M., Prakapenka, V., *Nature*, **2009**, *458*, 182.

[16]Hall, E.H., *Proc. Natl. Acad. Sci. USA*, **1925**, *11*, 416.

[17]Sears, F. W., Zemansky, M. W., Young, H. D., *University Physics*, 5th edn., Addison-Wesley, 1980.

[18]Greenwood, N. N., Earnshaw, A., *Chemistry of the Elements*, Pergamon, 1984.

[19]Fishbane, P. M., Gasiorowicz, S., Thornton, S.T., *Physics for Scientists and Engineers*, 2nd edn., Prentice Hall, 1996.

[20]Girifalco, L. A., *Statistical Mechanics of Solids*, Oxford University Press, 2000.

Received:.17.03.2014.
Accepted:.23.03.2014.

AN EFFICIENT AND ECO-FRIENDLY SYNTHESIS OF 2-ARYL-BENZIMIDAZOLES USING SILICA GEL AS CATALYST

Swati Samanta,[a] Chayan Guha[a] and Asok K. Mallik[a]*

Keywords: Eco-friendly synthesis; 2-arylbenzimidazoles; silica gel catalyst; solvent-free synthesis

An efficient and eco-friendly method for synthesis of 2-arylbenzimidazoles has been developed simply by grinding intimate mixtures of *ortho*-phenylenediamine, aromatic aldehyde and TLC grade silica gel at room temperature for 30-50 minutes. This one pot synthesis involves aerial oxidation of an intermediate 2-arylbenzimidazoline formed by condensation of the reactants followed by cyclization.

*Corresponding Authors
Fax: +91 033 2414 6484
E-Mail: mallikak52@yahoo.co.in
[a] Department of Chemistry, Jadavpur University, Kolkata-700 032, India

Introduction

Benzimidazoles represent a class of medicinally important nitrogen heterocycles which have wide variety of biological and pharmacological activities such as analgesic,[1] antiamoebic,[2] antimicrobial,[3] antihypertensive,[4] antiparasitic,[5] anti-inflammatory[6] and antitumor[7] activities. *N*-Ribosyl-dimethylbenzimidazole serves as an axial ligand for cobalt in vitamin B_{12}. Benzimidazole derivatives exhibit significant activity against several viruses such as HIV,[8] human cytomegalovirus (HCMV),[9] influenza,[10] etc. A good number of methods have been reported in the literature for the synthesis of 2-substituted benzimidazoles using *o*-phenylenediamines and aldehydes as precursors. Many of the reported methods require long reaction time, use of expensive catalysts and organic solvents.[11-19] The current literature shows that there has been a growing trend towards green synthesis of these compounds.[20-22] The recent trend towards development of solvent-free reaction conditions for organic synthesis[23-27] encouraged us to study the same reaction at room temperature without use of any solvent. Thus, we have been successful in achieving an efficient and eco-friendly synthesis of 2-arylbenzimidazoles simply by grinding an intimate mixture of *ortho*-phenylenediamine and aromatic aldehyde over TLC grade silica gel in open air, which is presented herein.

Results and Discussion

When an intimate mixture of *ortho*-phenylenediamine (**1**) and an aromatic aldehyde (**2**) (1:1 mole ratio) was ground over TLC grade silica gel (silica gel G) in open air, it was found to be converted smoothly to corresponding 2-arylbenzimidazole (**3**) within 30-50 minutes. In some combinations 1-benzyl-2-arylbenzimidazoles (**4**) were also resulted as minor product (Scheme 1, Table 1).

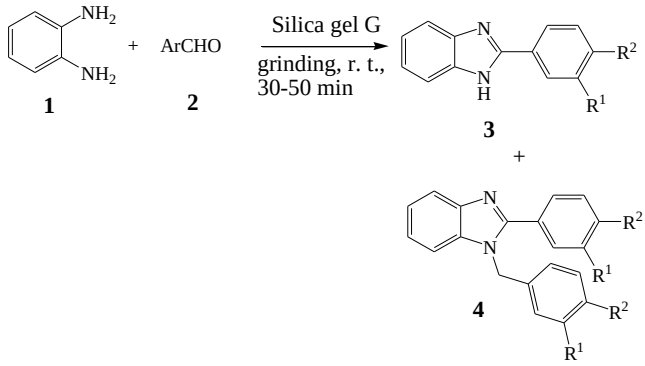

3a Ar=C_6H_5, **3b** Ar=4-BrC_6H_4, **3c** Ar=2-ClC_6H_4, **3d** Ar=4-ClC_6H_4, **3e** Ar=4-MeC_6H_4, **3f** Ar=4-MeOC_6H_4, **3g** Ar=3,4-OCH_2O-C_6H_3, **3h** Ar=2-$NO_2C_6H_4$, **3i** Ar=4-$NO_2C_6H_4$, **3j** Ar=4-$Me_2NC_6H_4$, **3k** Ar=2-pyridyl, **3l** Ar=2-thienyl, **4a** Ar=C_6H_5; **4e** Ar=4-MeC_6H_4, **4f** Ar=4-MeOC_6H_4

Scheme 1. Synthesis of benzimidazoles from of *o*-phenylene-diamine and aromatic aldehydes.

The scope of recyclability of the silica gel G catalyst was then investigated. It has been observed that the catalyst can be recovered after completion of the reaction and it can be used further with no significant loss of activity (Table 2).

The mechanisms for formation of 2-arylbenzimida-zoles (**3**) and 1-arylmethyl-2-arylbenzimidazoles (**4**) from **1** and **2** have been discussed in a number of recent papers[14,16,28]. From the mechanisms suggested therein (Scheme 2), it is observed that the formation of **3** requires an oxidation (aerial or catalytic) of an intermediate 2-arylbenzimidazoline (**6**). For the formation of **4**, 2 molar proportion of aldehyde is required and here the conversion of the intermediate diimine **7** to the product takes place by cyclization followed by intramolecular hydride transfer. In the method being reported, it is observed that in cases of use of aromatic aldehydes containing electron withdrawing groups, 2-arylbenzimidazoles (**3**) are formed as the only product even if 2 molar proportion of the aldehyde is used. This result suggests that for reactions involving such aldehydes cyclization of 2-benzalaminoanilines (**5**) (Step 1a) is significantly faster than their reaction with another molecule of aldehyde (Step 2).

Table 1. Synthesis of benzimidazoles under solvent-free conditions

Entry	Ar in ArCHO	Time, min	Mole ratio of the reactants 2 and 1			
			1:2		1:1	
			Yield of 3, %[a]	Yield of 4, %[a]	Yield of 3, %[a]	Yield of 4, %[a]
1.	C_6H_5	40	49	17	45	15
2.	4-BrC_6H_4	30	89	0	91	0
3.	2-ClC_6H_4	30	94	0	96	0
4.	4-ClC_6H_4	30	89	0	92	0
5.	4-MeC_6H_4	45	47	14	43	10
6.	4 -$MeOC_6H_4$	45	46	17	45	10
7.	3,4(OCH_2O)C_6H_3	45	67	5	62	6
8.	2- $O_2NC_6H_4$	30	86	0	84	0
9.	4- $O_2NC_6H_4$	45	74	0	71	0
10.	4-$Me_2NC_6H_4$	45	63	0	60	0
11.	2-pyridyl	30	76	0	74	0
12.	2-thienyl	30	79	0	78	0

[a] Isolated yield with respect to the amount of **1.**

Table 2. Recyclability of the catalyst[a]

No. of cycles	Reaction time, min	Yield,%[b] of 3c (using 1 and 2-ClC_6H_4CHO)	Yield, %[b] of 3d (using 1 and 4-ClC_6H_4CHO)
Fresh	30	96	92
Run 1	30	94	89
Run 2	35	92	88
Run 3	35	91	86

[a] In each time the reaction was carried out by grinding an intimate mixture of **1 (**1 mmol), **2** (aldehyde, 1 mmol) and silica gel G (4 g) in open air at room temperature. [b]Isolated yield with respect to the amount of **1.**

For use of aromatic aldehydes without having any electron withdrawing group, the said cyclization is relatively slower and that ultimately widens the possibility of formation of **4** as a minor product.

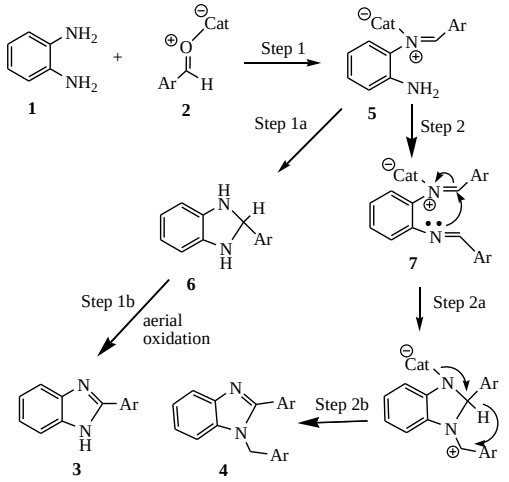

Scheme 2. Suggested mechanisms for formation of benzimidazoles from of *o*-phenylenediamine and aromatic aldehydes.

In the present method it is a common observation that the reactions are very clean, and the crude products obtained in the entries 2-4 and 8-12 were pure enough. Their crystallization from ethyl acetate-petroleum ether was sufficient to provide analytically pure samples of **3**.

The crude product obtained in each of the other entries could be resolved into two pure products (**3** and **4**) by a single column chromatography over silica gel.

Experimental

General.

Melting points were recorded on a Köfler block. IR spectra were recorded on a Perkin Elmer FT-IR spectrophotometer (Spectrum BX II) in KBr pellets. ^1H and ^{13}C NMR spectra were recorded in $CDCl_3$ and in DMSO-d_6 on a Bruker AV-300 (300 MHz) spectrometer. Analytical samples were routinely dried *in vacuo* at room temperature. Microanalytical data were recorded on two Perkin-Elmer 2400 Series II C, H, N analyzers. HRMS were measured with a Waters HRMS instrument [Xevo G2QTof] spectrometer. Column chromatography was performed with silica gel (100-200 mesh) and TLC with silica gel G made of SRL Pvt. Ltd. Petroleum ether had the boiling range 60-80 °C.

General method for synthesis of benzimidazole derivatives (3 and 4).

An intimate mixture of *o*-phenylenediamine (**1,** 1 mmol), an aromatic aldehyde (**2,** 1 mmol) and silica gel G (4g, quality mentioned above) was taken in a mortar and it was ground in open air at room temperature for the time period mentioned in Table 1. The progress of the reaction was monitored by TLC over silica gel. When the reaction was found to be complete, the reaction mixture was washed thoroughly with ethyl acetate. The crude material obtained by concentration of this ethyl acetate extract on crystallization from ethyl acetate-petroleum ether gave pure 2-arylbenzimidazoles (**3**) in the entries 2-4 and 8-12 (Table 1). The similar material obtained in each of the other entries was subjected to column chromatography over silica gel which resulted in separation of the products **3** and **4**. These two products were finally crystallized from ethyl acetate-petroleum ether.

 DOI: 10.17628/ecb.2014.3.396-399

All the products **3a-l** were known compounds and they were characterised by comparison of their physical and spectral data with those reported in literature.

Compound 3a.

Colourless needles, m.p. 287-288 °C (lit.[14] 288-289 °C). ^{1}H NMR (300 MHz, DMSO-d_6) δ: 7.22 (br. s, 2H), 7.50-7.56 (m, 4H), 7.67 (1H, br. d, J = 7.1 Hz), 8.18 (d, 2H, J = 7.2 Hz), 12.93 (br. s, 1H).

Compound 3b.

Colourless needles, m.p. 297-298 °C (lit.[30] 299-300 °C). ^{1}H NMR (300 MHz, DMSO-d_6) δ: 7.24 (br. s, 2H), 7.52-7.72 (m, 2H), 7.76 (d, 2H, J = 8.4Hz), 8.12 (d, 2H, J = 8.4 Hz), 13.02 (br. s, 1H).

Compound 3c.

Colourless needles, m.p. 225-227 °C (lit.[14] 227-229 °C). ^{1}H NMR (300 MHz, DMSO-d_6) δ: 7.18-7.26 (m, 2H), 7.47-7.56 (m, 3H), 7.62 -7.69 (m, 2H), 7.87-7.90 (m, 1H), 12.70 (s, 1H). ^{13}C NMR (75 MHz, DMSO-d_6) δ: 111.8, 119.4, 123.3, 128.6, 129.4, 129.5, 135.0, 135.5, 144.2, 150.6.

Compound 3d.

Colourless needles, m.p. 281-282 °C (lit.[14] 281-283 °C).; IR (KBr): ν_{max} = 3338, 2923, 1624, 1448, 1487 cm^{-1}; ^{1}H NMR (300 MHz, DMSO-d_6) δ: 7.17-7.26 (m, 2H), 7.54 (br. d, 1H, J = 7.5 Hz), 7.62-7.69 (m, 3H), 8.18 (d, 2H J = 8.7 Hz), 12.99 (br. s, 1H).

Compound 3e.

Colourless needles, m.p. 292-293 °C (lit.[14] 293-294 °C).; IR (KBr): ν_{max} = 3340, 3016, 2854, 1625, 1439, 1288 cm^{-1}; ^{1}H NMR (300 MHz, DMSO-d_6) δ: 2.39 (s, 3H), 7.20 (br. s, 2H), 7.37 (d, 2H, J = 7.5 Hz), 7.59 (br. s, 2H), 8.07 (d, 2H, J = 7.8 Hz), 12.83 (br. s, 1H). HRMS $(M+H)^+$ Calcd. for $C_{14}H_{12}N_2$: 209.26; Found: 209.13. Anal. Calcd. for $C_{14}H_{12}N_2$ (208.26): C, 80.74; H, 5.81; N, 13.45. Found: C, 80.56; H, 5.61; N, 13.21%.

Compound 3f.

Colourless needles, m.p. 230-231°C (lit.[14] 231°C). ^{1}H NMR (300 MHz, DMSO-d_6) δ: 3.82 (s, 3H), 7.10 (d, 2H, J = 8.7 Hz), 7.14-7.16 (m, 2H), 7.47 (d, 2H, J = 6.2 Hz), 7.59 (d, 1H, J = 6.6 Hz), 8.09 (d, 2H, J =8.7 Hz), 12.72 (br. s, 1H),

Compound 3g.

Colourless needles, m.p. 251-252°C (lit.[29] 252 °C). ^{1}H NMR (300 MHz, DMSO-d_6) δ: 6.10 (s, 2H), 7.07 (d, 1H, J = 8.1 Hz), 7.17 (br. s, 2H), 7.48 (br. d, 1H, J = 6.5 Hz), 7.60 (br. d, J = 6.6 Hz, 1H), 7.66-7.71 (m, 2H), 12.73 (br. s, 1H).

Compound 3h.

Colourless needles, m.p. 211°C (lit.[29] 210 °C). ^{1}H NMR (300 MHz, DMSO-d_6) δ: 7.24 (br. s, 2H), 7.62 (br. s, 2H), 7.74 (t, 1H, J = 7.5 Hz), 7.85 (t, 1H, J = 7.5 Hz), 7.96 (d, 1H, J = 7.5 Hz), 8.01 (d, 1H, J = 7.8 Hz), 13.04 (br. s, 1H),

Compound 3i.

Colourless needles, m.p. 316 °C (lit.[29] 316 °C). ^{1}H NMR (300 MHz, DMSO-d_6) δ: 7.26 (br. s, 2H), 7.59 (br. s, 1H), 7.71 (br. s, 1H), 8.39 (s, 4H), 13.30 (br. s, 1H).

Compound 3j.

Colourless needles, m.p. 291-292 °C (lit.[14] 292-294 °C). ^{1}H NMR (300 MHz, $CDCl_3$) δ: 3.04 (s, 6H), 6.77 (d, 2H, J = 8.7 Hz), 7.20-7.23 (m, 2H), 7.60 (br. s, 2H), 7.92 (d, 2H, J = 8.7 Hz).

Compound 3k.

Colourless needles, m.p. 218-219°C (lit.[29] 218 °C). ^{1}H NMR (300 MHz, $CDCl_3$) δ: 7.28-7.31 (m, 2H), 7.37 (t, 1H, J = 6.6 Hz), 7.48 (br. s, 1H), 7.84-7.90 (m, 2H), 8.45 (d, 1H, J = 7.8 Hz), 8.63 (d, 1H, J = 4.5 Hz), 10.88 (br. s, 1H).

Compound 3l.

Colourless needles, m.p. 331-332 °C (lit.[30] 332 °C). ^{1}H NMR (300 MHz, $CDCl_3$) δ: 7.16 (t, 1H, J = 4.2 Hz), 7.24-7.29 (m, 3H), 7.47 (d, 1H, J = 5.1 Hz), 7.62 (d, 2H, J = 3.3 Hz).

Compound 4a.

Colourless needles, m.p. 135-136°C (lit.[28] 135-136 °C). ^{1}H NMR (300 MHz, $CDCl_3$) δ: 5.46 (s, 2H), 7.11 (br. d, 2H, J = 7.8 Hz), 7.19-7.26 (m, 2H), 7.28-7.36 (m, 4H), 7.45-7.50 (m, 3H), 7.69 (dd, 2H, J = 7.5 Hz and 2.4 Hz), 7.87 (d, 1H, J = 8.1Hz).

Compound 4e.

Colourless needles, m.p. 131-132 °C (lit.[28] 132-133 °C). ^{1}H NMR (300 MHz, $CDCl_3$) δ: 2.36 (s, 3H), 2.43 (s, 3H), 5.43 (s, 2H), 7.02 (d, 2H, J = 7.8 Hz), 7.16 (d, 2H, J = 7.8 Hz), 7.21-7.35 (m, 5H), 7.61 (d, 2H, J = 8.0 Hz), 7.88 (d, 1H, J = 7.8 Hz). HRMS $(M+H)^+$ Calcd for $C_{22}H_{20}N_2$: 313.16; Found: 313.19. Anal. Calcd. for $C_{22}H_{20}N_2$ (312.16): C, 84.58; H, 6.45; N, 8.97. Found: C, 84.31; H, 6.33; N, 8.78%.

Compound 4f.

Colourless needles, m.p. 130-131°C (lit.[28] 131-132 °C). ^{1}H NMR (300 MHz, $CDCl_3$) δ: 3.78 (s, 3H), 3.85 (s, 3H), 5.38 (s, 2H), 6.84 (d, 2H, J = 8.7 Hz), 6.97 (d, 2H, J = 8.7 Hz), 7.03 (d, 2H, J = 8.5 Hz), 7.21-7.32 (m, 3H), 7.64 (d, 2H, J = 8.7 Hz), 7.84 (d, 1H, J = 8.7 Hz).

Recovery of the catalyst.

The catalyst separated from the reaction mixture was washed thoroughly with ethyl acetate till the washings became almost colourless. It was then dried in a hot air oven at 100 °C for 1h. The dried catalyst was cooled to room temperature and then used further.

Conclusion

We report here a very simple, efficient and eco-friendly method for synthesis of 2-arylbenzimidazoles (**3**) avoiding the use of any solvent. The sets yielding **3** as the only product did not require any chromatographic purification.

Acknowledgements

Financial assistance from the UGC-CAS and DST-PURSE programs, Department of Chemistry is gratefully acknowledged. The authors also acknowledge the DST-FIST program to the Department of Chemistry, Jadavpur University for providing the NMR spectral data. SS is thankful to the CSIR and CG to the UGC, New Delhi for their research fellowships.

References

[1]Mohammed, B. G., Abdel-Alim, A. M., Hussein, M. A., *Acta Pharm*., **2006**, *56*, 31-48. (http://public.carnet.hr/acphee/3106.pdf)

[2]Bharti, N., Shailendra, M. T., Garza, G., Cruz-Vega, D. E., Catro-Garza, J., Saleem, K., Naqvi, F., Maurya, M. R., Azam, A., *Bioorg. Med. Chem. Lett.*, **2002**, *12*, 869-871. (http://ac.els-cdn.com/S0960894X02000343/1-s2.0-S0960894X02000343-main.pdf?_tid=cc52ecbe-a36b-11e3-9ca000000aab0f6b&acdnat=1393917093_9c01305bb4bf64f4eeeaa5b28e726cdc)

[3]Singh, N., Pandurangan, A., Rana, K., Anand, P., Ahmad, A., Tiwari, A. K., *Int. Curr. Pharm. J.*, **2012,** *1*, 119-127. (http://www.icpjonline.com/documents/Vol1Issue5/05.pdf)

[4]Sharma, M. C., Kohli, D., Sharma, S., Sharma, A. D., *Adv. Appl. Sci. Res.*, **2010**, *1*, 101-112. (www.pelagiaresearchlibrary.com)

[5]Valdez, J., Cedillo, R., Hernandez-Campos, A., Yepez, L., Hernandez-Luis, F., Navarrete-Vazquez, G.,Tapia, A., Cortes, R., Hernandez, M., Castillo, R., *Bioorg. Med. Chem. Lett.*, **2002,** *12*, 2221-2224. (http://www.google.co.in/url?sa=t&rct=j&q=&esrc=s&source=web&cd=1&ved=0CCUQFjAA&url=http%3A%2F%2Fwww.researchgate.net%2Fpublication%2F11251267_Synthesis_and_antiparasitic_activity_of_1Hbenzimidazole_derivatives%2Ffile%2Fd912f50881866d37e6.pdf&ei=YoUVU8qmA8XqrAfH8oCwCA&usg=AFQjCNFT6nEum2nWcVaXMEX0XSF-c3hp-w)

[6]Achar, K. C., Hosamani, K. M., Seetharamareddy, H. R., *Eur. J. Med. Chem.*, **2010**, *45*, 2048-2054. (http://europepmc.org/abstract/MED/20133024/reload=0;jsessionid=rw72cJv1BlXA7PasQvXs.10).

[7]Mann, J., Baron, A., Opoku-Boahen, Y., Johansoon, E., Parkmson, G., Kell, L. R., Neidle, S., *J. Med. Chem.*, **2001**, *44*, 138-144. (http://pubs.acs.org/doi/pdf/10.1021/jm000297b).

[8]Morningstar, M. L., Roth, T., Farnsworth, D. W., Smith, M. K., Watson, K., Buckheit Jr., R. W., Das, K., Zhang, W., Arnold, E., Julias, J. G., Hughes, S. H., Michejda, C. J., *J. Med. Chem.*, **2007,** *50*, 4003-4015. (*http://pubs.acs.org/doi/pdf/10.1021/jm060103d)*

[9]Porcari, A. R., Devivar, R. V., Kucera, L. S., Drach, J. C., Townsend, L. B., *J. Med. Chem.*, **1998,** *41*, 1252-1262. (http://pubs.acs.org/doi/pdf/10.1021/jm970559i).

[10]Tamm, I. Sehgal, P. B., *Adv. Virus Res.*, **1978**, *22*, 187-258.

[11] Qu, Y., Pan, L., Wu, Z., Zhou, X., *Tetrahedron*, **2013**, *69*, 1717-1719. (http://dx.doi.org/10.1016/j.tet.2012.12.039)

[12]Abdollahi-Alibeik, M., Moosavifard, M., Poorirani, S., *Synth. React. Inorg., Met.-Org., Nano-Met. Chem.*, **2013**, *43*, 1365-1371. **(http://www.tandfonline.com/doi/pdf/10.1080/15533174.2012.761233)**

[13]Barbero, M., Cadamuro, S., Dughera, S., *Arkivoc*, **2012,** *2012*, 262-279. (http://www.arkat-usa.org/get-file/46325/)

[14]Eshghi, H., Rahimizadeh, M., Shiri, A., Sedaghat, P., *Bull. Korean Chem. Soc.*, **2012**, *33*, 515-518. (http://dx.doi.org/10.5012/bkcs.2012.33.2.515)

[15]Tran, N. T., Cho, C. S., *Bull. Korean Chem. Soc.*, **2012**, *33*, 4188-4190. (http://dx.doi.org/10.5012/bkcs.2012.33.12.4188).

[16] Shaikh, K. A., Patil, V. A., *Org. Commun.*, **2012**, *5*, 12-17. (http://www.acgpubs.org/OC/2012/Volume%205/Issue%201/2-OC-1112-234.pdf)

[17]Kim, Y., Kumar, M. R., Park, N., Heo, Y., Lee, S., *J. Org. Chem.*, **2011**, *76*, 9577-9583. (dx.doi.org/10.1021/jo2019416)

[18]Shingalapur, R. V., Hosamani, K. M., *Catal. Lett.*, **2010** *137*, 63-68. (DOI 10.1007/s10562-010-0340-1).

[19] Mukhopadhyay, C., Datta, A., Butcher, R. J., Paul, B. K., Guchhait, N., Singha, R., *Arkivoc*, **2009**, *2009*, 1-22. (http://www.arkat-usa.org/get-file/31204/)

[20] Thakuria, H., Das, G., *Arkivoc*, **2008**, *2008*, 321-328. (http://www.arkat-usa.org/get-file/26706/)

[21]Kathirvelan, D., Yuvaraj, P., Babu, K., Nagarajan, A. S., Reddy, B. S. R., *Indian J. Chem. B*, **2013**, *52*, 1152-1156. (http://nopr.niscair.res.in/bitstream/123456789/20511/1/IJCB%2052B%288%29%201152-1156.pdf)

[22]Mamada, M., Perez-Bolivar, C., Anzenbacher Jr., P., *Org. Lett.*, **2011**, *13*, 4882-4885. (http://pubs.acs.org/doi/pdf/10.1021/ol201973w)

[23]Samanta, S., Sarkar, S., Pal, R., Mallik, A. K., *Org. Chem. Int.*, **2013**, *2013*, Article ID 512074, 5 pages (http://dx.doi.org/10.1155/2013/512074).

[24] Strukil, V., Igrc, M. D., Fabian, L., Eckert-Maksic, M., Childs, S. L., Reid, D.G., Halasz, I., Mottillo, C., Friscic, T., *Green Chem.*, **2012**, *14*, 2462-2473 .(**DOI:** 10.1039/C2GC35799B)

[25] Das Gupta, A., Samanta, S., Mondal, R., Mallik, A. K., *Chem. Sci. Trans.*, **2013**, *2*, 524-528. (DOI:10.7598/cst2013.388)

[26] Tanaka, K., Toda, F., *Chem. Rev.*, **2000**, *100*, 1025-1074. (http://pubs.acs.org/doi/pdf/10.1021/cr940089p)

[27]Varma, R. S., *Clean Products and Processes*, **1999**, *1*, 43-55. (http://www.google.co.in/url?sa=t&rct=j&q=&esrc=s&source=web&cd=1&ved=0CCUQFjAA&url=http%3A%2F%2Fwww.researchgate.net%2Fpublication%2F228607695_Solventfree_accelerated_organic_syntheses_using_microwaves%2Ffile%2F79e4150b52f0f81818.pdf&ei=GKAVU7SjHcn9rAe23IGAAQ&usg=AFQjCNGCH1XXjCm71YI7QDWtziAFyd-i2Q&bvm=bv.62286460,d.bmk)

[28]Zhang, L.-J., Xia, J., Zhou, Y.-Q., Wang, H., Wang, S.-W., *Synth. Commun.*, **2012**, *42*, 328-336. (http://dx.doi.org/10.1080/00397911.2010.524337)

[29]Alloum, A. B., Bougrin, K., Soufiaoui, M., *Tetrahedron Lett.*, **2003**, *44*, 5935-5937. (doi:10.1016/S0040-4039(03)01387-X)

[30] Saha, D., Saha, A., Ranu, B. C., *Green Chem.*, **2009**, *11*, 733-737. (http://pubs.rsc.org/en/content/articlepdf/2009/gc/b823543k)

Received: 05.03.2014.
Accepted: 26.03.2014.

SUGARCANE BAGASSE AND MODIFIED RICE HUSK FOR THE REMOVAL OF MALACHITE GREEN FROM AQUEOUS WASTES

Hamid Dezhampanah[a]* Amineh Mousazadeh[a] and Issa Mousazadeh[b]

Keywords: malachite green; isotherm; kinetics; rice husk; sugarcane bagasse.

Adsorption of malachite green (MG) using sugarcane bagasse (SB) and rice husk (RH) were studied by batch method. Factors influencing dye adsorption such as the initial dye concentration, sorbent dosage, exposure time, temperature effect and pH, were investigated. The Langmuir, Freundich-Temkin and Dubinin–Radushkevich (D-R) isotherms were used to fit the equilibrium data, and the results showed that the Freundlich and Langmuir model provided the best correlation of the experimental data for SB and RH, respectively. Adsorption kinetic data were tasted using pseudo-first-order, pseudo-second-order and intra particle diffusion models. It was observed that the pseudo-second-order kinetic equation could explain the biosorption kinetics of dye on both adsorbents and intra particle diffusion showed that dye adsorption was controlled by multi-adsorption stages with bagasse surface area. The results showed that both of them can be an economical sorbent for removal of dye from aqueous systems.

* Corresponding Authors: Hamid Dezhampanah
Fax: + 98-131-3233262
E-Mail: h.dpanah@guilan.ac.ir
[a] Laboratory of physical Chemistry, Department of Chemistry, Faculty of Science, University of Guilan P.O. Box 1914, Rasht 0098, Iran.
[b] Shahid Rajaei Technical and Vocational University, Tarbiat moallem Ave. lahijan, Guilan, Iran. Postal code: 4416777158, Po. Box: 1478

Introduction

Disposal of dyeing industry wastewater pose one of the major problems, because such effluents contain a number of contaminants including acid or base, dissolved solids, toxic compounds, and color. Out of these, color is the first contaminant to be recognized because it is visible to the human eye. Removal of many dyes by conventional waste treatment methods is difficult since these are stable to light and oxidizing agents and are resistant to aerobic digestion.

Adsorption techniques have proved to be an effective and attractive process for removal of on biodegradable pollutants (including dyes) from wastewater.[1,2] The most widely used adsorbent for the removal of dyes is activated carbon, which is expensive and has a high regeneration cost.[3,4] Therefore, interest is growing to find alternatives to carbon adsorbents. Recently, attention has been focused on the development of low-cost adsorbents for applications concerning the treatment of wastewater.[2,5] Agricultural by-products such as peanut husk,[6] apple pomace and wheat straw,[7] wheat shell,[8] cereal chaff,[9] fruit peel,[10] bark,[7] and leaves[11] have been widely studied for dye removal from wastewater. Generally, the sorption capacities of crude agricultural byproduct are low. For improving the sorption capacity of crude agricultural byproduct, chemical modification was used.[12-15]

Food and pharmaceutical industries worldwide use synthetic dyes as additives in their products. In the food industry, dyes are used to make products more attractive to consumers. However, dyes have no nutritional value and may have toxic effects, causing from a simple allergy to intolerance to cancer. Dyes that have N=N bonds and sulfonic groups in their structures are considered acid and belong to the azo-dye class.[3,4] Dyes are extensively used in food industries to improve the sensorial aspects of its products.[1,5] Due to losses in the process, a considerable amount of these food dyes are present in the industrial effluents.[2,5]

Malachite Green (MG) is a popular dye and widely used for the dyeing of leather, wool and silk, distilleries, jute, paper, as a food coloring agent, food additive, in medical disinfectant and fish industries.[6,7] Discharge of MG into the hydrosphere can cause environmental degradation as it gives undesirable color to water and reduces sunlight penetration. The consumption of MG has many adverse effects due to its carcinogenic, genotoxic, mutagenic and teratogenic properties of MG are due to presence of the nitrogen.

Since the removal of dyes from wastewater is considered an environmental challenge and government legislation requires textile wastewater to be treated, therefore there is a constant need to have an effective process that can efficiently remove these dyes.[9,10]

The removal of contaminants from industrial wastewaters is currently of great importance in recent years. Precipitation, ion exchange, solvent extraction, biosorption, filtration, electrochemical treatment and adsorption on oxides are the conventional methods for the removal of contaminants from aqueous solutions.[11-13]

In this work, the removal of Malachite Green from aqueous solutions was investigated using sugarcane bagasse and rice husk adsorbent from aqueous solutions under different experimental conditions. Batch adsorption studies were performed under various parameters such as the pH, initial concentration and contact time, agitation rate, temperature, and sorbent dosage. The equilibrium sorption behavior of the adsorbents has been studied using the

adsorption isotherm technique. Experimental data have been fitted to various isotherm equations to determine the best isotherm to correlate the experimental data.

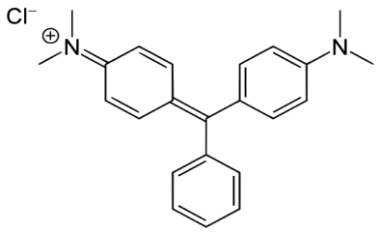

Figure 1. Chemical structure of Malachite Green

Experimental

Adsorbent

The milled rice husk and sugarcane bagasse were obtained from farms in the north of Iran, Guilan. Then, it was used as an adsorbent. The SB and RH sieved through the sieves, 50-80 mesh size particles. Then adsorbents in above particle size rinsed with distilled water to remove dust and soluble impurities. For better purification, sugarcane bagasse mixed by 5 wt. % HCl at room temperature and after that it was soaked into distilled water for 48 h then washed with distilled water. Finally the adsorbents were dried in an oven at 70 °C overnight and stored and labeled as sugarcane bagasse (SB) and rice husk (RH).

Dye solution

Malachite Green acetate was product of Sigma-Aldrich and was used as received without further purification (Fig. 1). A stock solution of dye was prepared by dissolving 0.025 g of it in 50 mL of double distilled water. Working solutions of different concentrations (10–50 mg L^{-1}) were prepared by further dilutions. The concentration of the dye MG was determined using a UV-vis spectrophotometer (WTW 6100) at a wavelength corresponding to the maximum absorbance of the dye. Calibration curve was plotted based on the absorbance versus concentration of the dye solution at the maximum wavelength of the dye (617 nm) using Beer's law. A Metrohm pH meter (model 827) with a combined double junction glass electrode was used for showing pH values. pH adjustments were carried out using dilute NaOH and HCl solutions.

An accurate weighed quantity of dye was dissolved in 250 mL double distilled water to prepared stock solution. Experimental solution of the desired concentration was obtained by successively dilutions. The characteristics and some properties of MG are listed in Table1.

Sorption experiments

The adsorption of MG on SB and RH in liquid–solid system has been studied using a standard batch technique. The adsorption experiments have been carried out in 100 mL beaker by mixing a pre-weighed amount of desired adsorbent and 50 mL of aqueous dye solution of fixed concentration. The beakers were shaked for the required time period in a mechanical shaker. The agitation rate is same for all experiments. The parameters such as initial dye concentration, pH of the medium, time of contact, and adsorbent dosage are varied during different sets of batch experiments. After adsorption, the samples are filtered out using the Whatman filter paper number-42. The left out concentration in the supernatant solution after adsorption process has been analysed using UV–VIS spectrophotometer (WTW 6100) by recording the absorbance changes at a wavelength of maximum absorbance (617 nm for MG).

The amount adsorbed of MG onto SB and MRH at equilibrium was calculated from the mass balance equation as follows:

$$q_e = \frac{(C_0 - C_e)V}{W} \quad (1)$$

where

C_0 and C_e are the initial and the equilibrium concentrations (mg L^{-1}) of malachite green solution, respectively;

V is the volume (L), and

W is the weight (g) of the adsorbent.

Results and discussions

Scanning electron microscopic study

Scanning electron microscopy (SEM) is a technique to characterize the surface structure and morphology of the biosorbent material. It is used to determine the particle shape and porous structure of biomass. Micrographs (Fig. 2) show that SB and RH particles have fibrous character. These images (Fig. 2 (A)) exhibit that SB samples have compacted layer that related to cellulosic material and they have lap joint structure. As the image shows the small layer pores may also take part in the adsorption process and also rice husk (Fig. 1 (B)), possesses smooth, flat and cloudy surface due to the presence of lignin, hemi-cellulose and wax. The small pores at rice husk surface probably participate in the adsorption process.

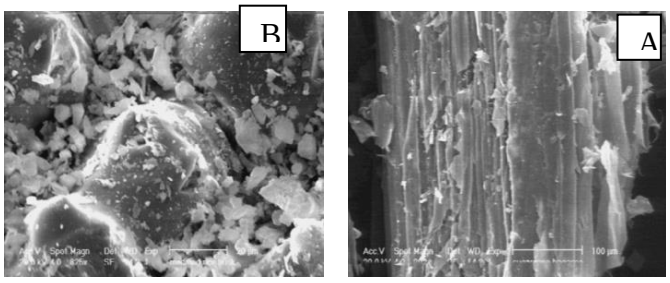

Figure 2. SEM images of adsorbents; A: SB; B: RH

 DOI: 10.17628/ecb.2014.3.400-406

Effect of pH

The effects of pH on the adsorption of MG on the SB and RH were studied in the pH ranging from 3–9 respectively. The results obtained are presented in Fig. 3, which describes maximum adsorption of around 81 and 98 % for SB and RH, respectively, at pH 8. Hence, all the succeeding investigations were performed at pH 8 for both adsorbents.

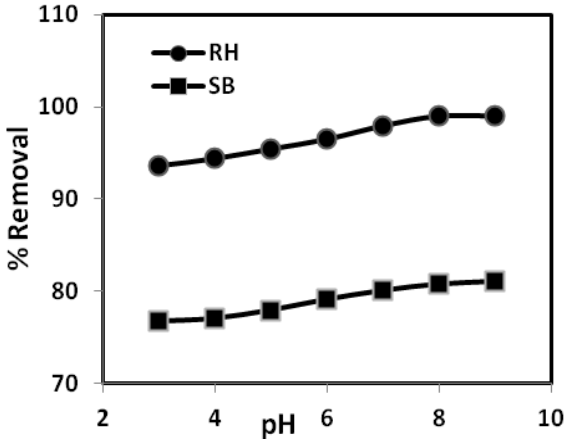

Figure 3. Effects of pH on MG dye removal at various concentrations (SB: absorbent dosage: 0.50 g; contact time: 40 min; temperature: 25 ºC) (RH: absorbent dosage: 0.50 g; contact time: 40 min; temperature: 25 ºC).

Effect of adsorbent dose

Fig. 4 shows the effect of adsorbent dose (SB and RH) on the removal of MG at C_0=30 mg L^{-1} and 25 °C. It can be seen that the MG removal increases with increase SB and RH up to 0.60 g, thereafter remained fairly constant despite an increase in the amount of the both adsorbents to 0.6 g. At the equilibrium time, the % removal increased from 95.25 to 99.92 % for an increase in rice husk dose from 0.2 to 1.0 g and also for SB solution the % removal increase from 96.71 % to 98.91 % for an increase in SB dose from 0.2 to 1.0 g. So as the Fig. 4 shows the optimum dosage for both adsorbents were selected 0.60 g.

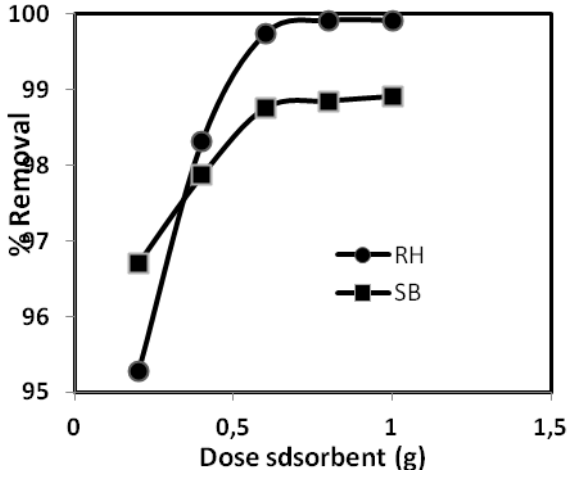

Figure 4. Influence of adsorbents dosage on dye removal (SB: contact time: 30 min; pH: 7.0; temperature: 25 ºC). (RH: contact time: 30 min; pH: 7.0; temperature: 25 ºC)

Effect of contact time on dye removal

Adsorption of MG was measured at given contact times for the different initial MG concentrations from 5 to 20 mg L^{-1}. From Fig. 5, the plot reveals that the percent MG removal is higher at the beginning; this is probably due to a larger surface area of the RH and SB being available at the beginning for the adsorption of MG. As the surface adsorption sites become exhausted, the uptake rate is controlled by the rate at which the adsorbate is transported from the exterior to the interior sites of the adsorbent particles. Most of the maximum percent MG removal was attained after about 30 min of shaking time for both adsorbents at different concentrations. The increasing contact time increased the MG adsorption and it remained constant after equilibrium was reached in 30 min for different initial concentrations.

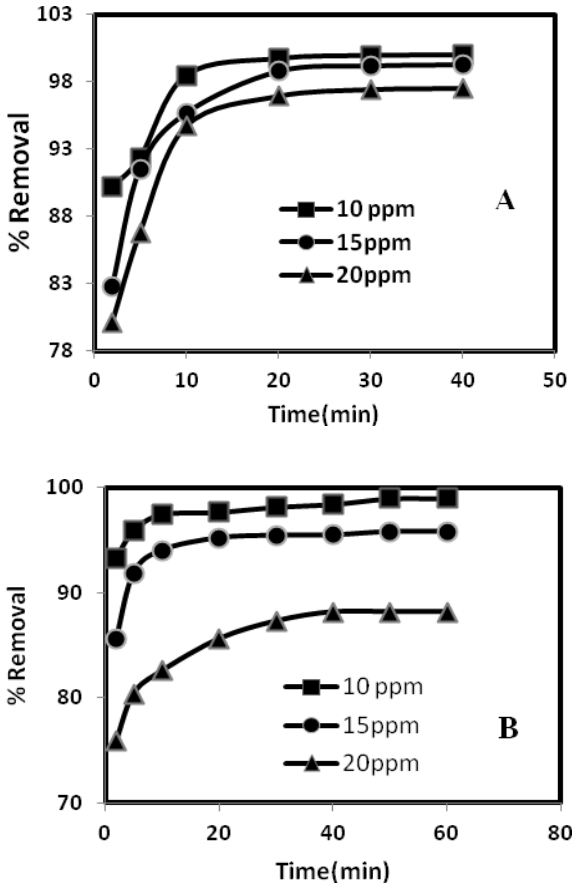

Figure 5. Effects of contact time of the dye removal at various concentrations. (**A**: RH; adsorbent dosage: 0.6 g; pH: 7.0; temperature: 25 ºC) (**B**: SB; adsorbent dosage: 0.4 g; pH: 7.0; temperature: 25 ºC).

Effect of initial dye concentration

It has been observed that for both the adsorbents, adsorption of the dye increases with increasing concentration at 25 ºC. Fig. 6 presents typical dye concentration versus amount adsorbed for RH and SB adsorption at 25 ºC. It is observed that with increasing concentration of the dye from 10 to 50 mg L^{-1}, the percentage removal decreases from 98.5 to 94.5 % for RH and 97.5 to 84.6 % for SB.

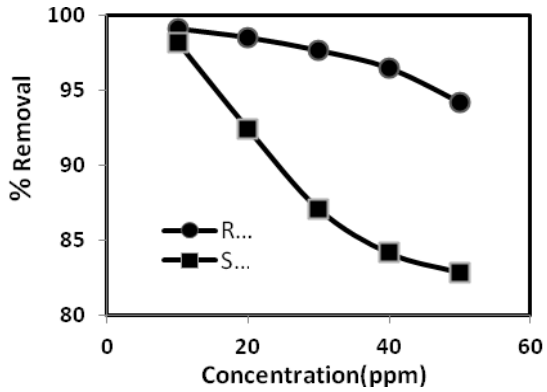

Figure 6. Effect of initial dyes concentration on its sorption onto SB (RH: absorbent dosage: 0.40 g; contact time: 45 min; temperature: 25 ºC)

Adsorption isotherms

The adsorption isotherm indicates how the adsorbed molecules distribute between the liquid phase and the solid phase when the adsorption process reaches an equilibrium state. the experimental data points were fitted to the Langmuir, Freundlich, Temkin and Doubinin–Radushevich (D–R) isotherm equations[14,15] and the constant parameters of the isotherm equations were calculated (Table 2).

The Langmuir isotherm

The Langmuir isotherm model suggests that the biosorption onto the adsorbent surface is homogeneous in nature with negligible interaction between adsorbed molecules. The linear form of the Langmuir model is given by:

$$\frac{C_e}{q_e} = \frac{1}{q_m b} + \frac{C_e}{q_m} \qquad (2)$$

where

q_m shows the monolayer adsorption capacity (mg g^{-1}),

b is Langmuir constant (L mg^{-1}),

C_e is equilibrium dye concentration in the solution (mg L^{-1}) and

q_e exhibit amount of dye adsorbed on biosorbent at equilibrium (mg g^{-1}).

The significant aspect of the Langmuir isotherm model can be defined by the dimensionless constant separation factor R_L which is expressed by the following equation:

$$R_L = \frac{1}{1+bC_0} \qquad (3)$$

where

C_0 is the initial concentration of dye (mg L^{-1}) and

b is the Langmuir constant (L mg^{-1}),

R_L shows the nature of biosorption mechanism.

R_L value	Nature of biosorption mechanism
$R_L>1$	Unfavorable
$R_L=1$	Linear
$0< R_L<1$	Favorable
$R_L<0$	Irreversible

In this study, the value of R_L was obtained to be in the range of 0-1, telling that the biosorption process is favorable for the both dyes.

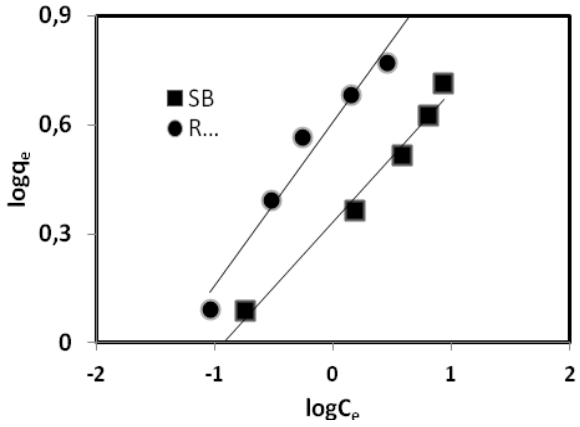

Figure 7. Langmuir adsorption isotherm.

Freundlich isotherm

The Freundlich isotherm is derived by assuming a heterogeneous surface with a non-uniform distribution of heat of sorption over the surface. It can be expressed in the linear form as follows:

$$\log q_e = \log K_f + \frac{1}{n}\log C_e \qquad (4)$$

where

K_F (L mg^{-1}) and n are isotherm constants indicate the capacity and intensity of the adsorption, respectively.

As the value of n is lower than 10 so the biosorption process is favorable. On the other hand the heterogeneity factor of $n^{-1}<<1$ indicates heterogeneous adsorbents, while values close to or even 1.0 indicate materials with relatively homogenous binding sites. According to the analysis in Table 2, the calculated n^{-1} was lower than 1, which indicated that SB and RH were heterogeneous adsorbent.

Temkin isotherm

The Temkin isotherm model suggests an equal distribution of binding energies over the number of the exchanging sites on the surface. This model considered the effects of some indirect adsorbate/adsorbate interactions on adsorption isotherms and suggested that because of these interactions

the heat of adsorption of all the molecules in the layer would decrease linearly with coverage It can be expressed in the linear form as follows:

$$q_e = B\ln A + B\ln C_e \quad (5)$$

where

A is the equilibrium binding constant corresponding to the maximum binding energy and B is corresponding to the heat of sorption.

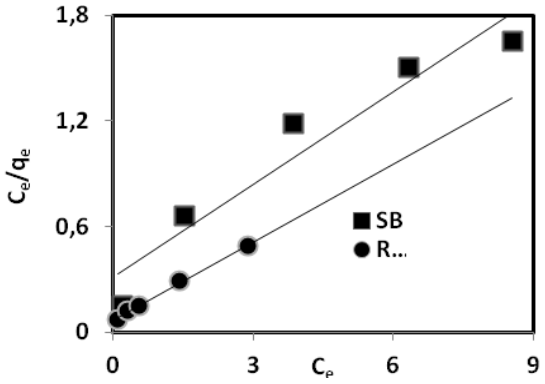

Figure 8. Freundlich adsorption isotherm.

Dubinin-Radushkevich isotherm

Doubinin–Radushkevich model is a more generalized model as compared to the Langmuir isotherm. This model is based on the fact that there is no homogeneous surface or constant adsorption potential. The linear form of (D–R) isotherm model can be seen below:

$$\ln q_e = \ln q_o - B\varepsilon^2 \quad (6)$$

where

q_0 is the maximum sorption capacity,

B is the activity coefficient related to the mean sorption energy and

ε is the Polanyi potential, given by

$$\varepsilon = RT\ln\left(1+\frac{1}{C_e}\right) \quad (7)$$

The sorption energy can be determined using the following equation:

$$E = \frac{1}{(2B)^{1/2}} \quad (8)$$

The mean adsorption energy (E) gives information about chemical and physical nature of adsorption. If the energy of activation is < 8 kJ mol^{-1}, the adsorption is physical and if the energy of activation is 8-16 kJ mol^{-1}, the adsorption is chemical in nature. The calculated values of D-R parameters for the adsorption of MG are also given in Table 1. The values of (E) that are shown in Table 2 indicate that the physico-sorption mechanism played an important role in the biosorption of cationic dye on the sugarcane bagasse and rice husk.

Adsorption kinetic

Kinetic studies are necessary to optimize different operating conditions for the biosorption. Various kinetic models have been suggested for explaining the order of reaction. To examine the controlling mechanism of adsorption processes, such as mass transfer and chemical reaction, the pseudo-first-order adsorption and the pseudo-second-order adsorption models were used to test the adsorption of dye onto sugarcane bagasse and rice husk. The best-fit model was selected based on the linear regression correlation coefficient (R^2). The two kinetic models' equations are given as follows:

Table 1. Isotherm models constants and correlation coefficients for the adsorption of Malachite green onto sugarcane bagasse and rice husk.

Isotherm models	Rice husk 10 mg L^{-1}; 0.5 g	Sugarcane bagasse 10 mg L^{-1}; 0.4 g
Langmuir		
q_m (mg g^{-1})	6.8	5.71
b (L mg^{-1})	0.487	0.559
R_L	0.17	0.15
R^2	0.997	0.926
Freundlich		
K_F	4.07	2.15
n	2.21	2.77
R^2	0.965	0.981
Temkin		
A(L g^{-1})	3.19	14.01
B	1.37	0.938
R^2	0.992	0.882
Doubinin - Radushkevich		
E (kJ mol^{-1})	2.921	2.935
R^2	0.930	0.873

Pseudo-first order model

The pseudo first-order kinetic model was proposed by Lagergren. A linear form of pseudo-first order model:

$$\ln(q_e - q_t) = \ln(q_e) - k_1 t \quad (9)$$

where

q_e is the amount of dye adsorbed at equilibrium (mg g^{-1})

q_t is the amount of dye adsorbed at time t (mg g^{-1})

k_1 is the equilibrium rate constant of pseudo-first order kinetics (min^{-1}).

The values of rate constant k_1, q_e calculated, q_e experimental and R^2 of MG and PR are presented in Table 3. The none similarity of calculated values (q_e, cal) and the experimental values (q_e, exp) and also non linearity of the plots (R^2) showing that the biosorption of MG is not likely to follow the pseudo-first-order kinetic model.

Pseudo-second order model

Linear form of pseudo-second order model was illustrated as:

$$\frac{t}{q_t} = \frac{1}{k_2 q_e^2} + \frac{t}{q_e} \quad (10)$$

where

q_e is the amount of dye adsorbed at equilibrium (mg g^{-1})

q_t is the amount of dye adsorbed at time t (mg g^{-1})

k_1 is the equilibrium rate constant of pseudo-second order kinetics (min^{-1}).

The second order parameters k_2, q_e calculated, q_e experimental and R^2 of MG and PR are shown in Table 2. The values of q_e calculated and q_e experimental for both dyes are quite same. The coefficients of determination for both dyes are also very high which showed that the pseudo-second-order kinetic model well fitted to kinetic data. The results showed that the pseudo-second-order kinetic model is more appropriate and effective than pseudo-first order kinetic model.

Table 2. The kinetic parameters for the adsorption of Malachite green onto sugarcane bagasse and rice husk.

Kinetic models	Rice husk, mg L^{-1}		Sugarcane bagasse, mg L^{-1}	
	10	20	10	20
Pseudo-first order				
K_1, min^{-1}	0.215	0.192	0.054	0.039
q_e (exp) mg g^{-1}	0.031	0.046	0.052	0.192
R^2	0.981	0.987	0.887	0.964
Pseudo-second order				
K_2, g mg^{-1} min^{-1}	18.6	11.3	3.84	1.52
q_e (exp), mg g^{-1}	0.834	1.66	1.24	1.11
R^2	1	1	1	0.999
q_e, cal mg g^{-1}	0.832	1.66	1.24	1.14
Intra particle diffusion				
K_{id}	0.0089	0.016	0.029	0.027
C_i	0.8	1.61	1.13	0.946
R^2	0.945	0.999	0.968	0.998

Conclusions

This study demonstrated the effectiveness of sugarcane bagasse and rice husk biomass to remove the dye from aqueous solution. The results reveal the removal of malachite green increase with decreasing initial dye concentration, increasing adsorbent dosages and contact time up to equilibrium. The solution pH played a significant role in influencing the capacity of adsorbent towards two dyes. The experiments show that the optimum pH for removing dye is 7. The high correlation coefficients for adsorption by SB reflect that the experimental data agree well with the Freundlich adsorption isotherm model and on the other hand the correlation coefficients for adsorption by RH shows that data agree with Langmuir isotherm. The kinetics study of dye on both adsorbents was performed based on pseudo-first order, pseudo-second order and intra particle diffusion equations.

The data indicate the adsorption kinetics follow the pseudo-second order rate with intra particle diffusion as one of the rate determing steps. Based on its excellent adsorption performance, it is concluded that sugarcane bagasse and rice husk could be used as a low-cost and efficient adsorbent for removal of anionic and cationic dye from wastewater and has good potential for further application in effluent treatment.

Acknowledgements

We gratefully acknowledge the Research Council of University of Guilan for supporting this work.

References

[1]Sharma, Y. C., Singh, B. and Uma, *The Open Environ. Pollut. Toxicol. J.*, **2009**, *1*, 74.

[2]Dotto, G. L., Moura, J. M., Cadaval, T. R. S., Pinto, L. A. A., *Chem. Eng. J.*, **2013**, *214*, 8.

[3]Robinson, T., McMullan, G., Marchant, R., Nigam, P., *Bioresour. Technol.*, **2001**, *77*, 247.

[4]Aksu, Z., *Process. Biochem.*, **2005**, *40*, 997.

[5]Wang, X. S., Zhou, Y., Jiang, Y., *Adsorpt. Sci. Technol*. **2009**, *27*, 537.

[6]Ansari, R. and Dezhampanah, H., *Eur. Chem. Bull.*, **2013**, *2(4)*, 220.

[7]Dezhampanah, H., Mohammad-Khah, A., Naghi Aghajani, N., *Eur. Chem. Bull.*, **2013**, *2(10)*, 709-714.

[8]Han, R. P., Han, P., Cai, Z. H., Zhao, Z. H., Tang, M. S., *J. Environ. Sci.* **2008**, *20*, 1035–1041.

[9]Saliba, R., Gauthier, H., Gauthier, R., Petit-Ramel, M. *Adsorpt. Sci. Technol.*, **2002**, *20*, 119–129.

[10]Bulut, Y., Aydin, H., *Desalination*, **2006**, *194*, 259–267.

[11]Han, R. P., Wang, Y. F., Han, P., Shi, J., Yang, J., Lu, Y. S., *J. Hazard. Mater.*, **2006**, *137*, 550–557.

[12]Sivaraj, R., Namasivayam, C., Kadirvelu, K., *Waste Manag.* **2001**, *21*, 105–110.

[13]Han, R. P., Wang, Y., Zhao, X., Wang, Y. F., Xie, F. L., Cheng, J. M., Tang, M. S., *Desalination*, **2009**, *245*, 284–297.

[14]Gong, R. M., Zhong, K. D., Hu, Y., Chen, J., Zhu, G. P., *J. Environ. Manag.*, **2008**, *88*, 875–880.

[15]Gurgel, L. V. A., Freitas, R. P., Gil, L. F., *Carbohyd. Polym.*, **2008**, *74*, 922.

[16]Ong, S. T., Lee, C. K., Zainal, Z., *Bioresour. Technol*., **2007**, *98*, 2792.

[17]Sciban, M., Klasnja, M., Skrbic, B., *Desalination*, **2008**, *229*, 170.

Received: 12.03.2014.
Accepted: 30.03.2014.

INHIBITION OF CORROSION OF ALUMINIUM IN ALKALINE MEDIUM BY POLY(VINYL ALCOHOL) (PVA)

R. Kalaivani[a]*, P. Thillai Arasu [b] and S. Rajendran[c]

Keywords: polyvinylalcohol; aluminium; weight-loss method; synergistic effect; protective film

The inhibition efficiency of polyvinylalcohol (PVA) in controlling corrosion of aluminium in well water in the absence and presence of Zn^{2+} has been evaluated by weight loss method. The formulation consisting of 250 ppm of PVA and 25 ppm of Zn^{2+} offers 85 % inhibition efficiency. It is found that the inhibition efficiency of PVA increases by addition of Zn^{2+} ion. A synergistic effect exists between PVA and Zn^{2+}. The mechanistic aspects of corrosion inhibition have been studied using polarization study. Also FTIR spectra reveal that the protective film consists of PVA - Zn^{2+} complex and $Zn(OH)_2$. The scanning electron microscopy confirms the protection of aluminium surface by strong adsorption of PVA. A suitable mechanism for corrosion inhibition is proposed based on the results from the above studies.

* Corresponding Authors
*E-Mail: vaniraj21@yahoo.com
[a] Department of Chemistry, Research Scholar, Manonmanium SundaranarUniversity,Thirunelveli 627132,Tamilnadu, India.
[b] Deparment of Chemistry,Kalasalingam, University,Srivilliputhur 626126, Tamilnadu, India.
[c] RVS School of Engineering & Technology, Dindigul - 624 005,Tamilnadu, India.

Introduction

Water is the most commonly used cooling fluid to remove unwanted heat from heat transfer surfaces. In recent years, the need to conserve water in order to meet the demand of industry. Presently, due to environmental Concerns, non-polluting inhibitors are used. Among various inhibitors polyvinyl alcohol is chosen as corrosion inhibitors because polyvinyl alcohol has excellent film forming,[1-3] emulsifying, and adhesive properties. It is also resistant to oil, grease and solvent. It is odorless and non toxic. It have functional groups such as –OH linkage, this group interact with metal surface through active centers of polymer.[4-6] It acts as protective film and prevents corrosion. The study of corrosion inhibition of aluminium in H_2SO_4 in presence of polyvinylalcohol (PVA) and polyethylene glycol(PEG) as inhibitors at 30-60 $^{\circ}$C by using gravimetric, gasometric and thermometric techniques,[7] found that corrosion inhibition efficiency increases with increase in concentration of PVA and PEG. Rajendran et al[8] investigated the corrosion behaviour of carbon steel using polyvinyl alcohol(PVA) in neutral aqueous solution containing 60 ppm of Cl^- in the absence and presence of ions using weight loss method. It offered 81% inhibition efficiency, the corrosion and inhibition behaviour of aluminium[9] in HCl in the presence of polyvinyl pyrrolidone (PVP) and polyacrylamide (PAL) their blends in the temperature range of using weight loss and hydrogen evolution techniques has been reported that polyvinylalcohol, used in eye drops and hard contact lens solution as a lubricant, PVA fiber, as reinforcement in concrete, as a surfactant for the formation of polymer encapsulated nanobeads. Much work has not been done on aluminium metal by polyvinyl alcohol.

Molecular structure of polyvinylalcohol is shown in scheme 1. Space filling model of is shown in scheme 2.

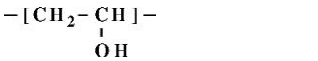

Scheme 1. Polyvinylalcohol (ethene-1-ol)

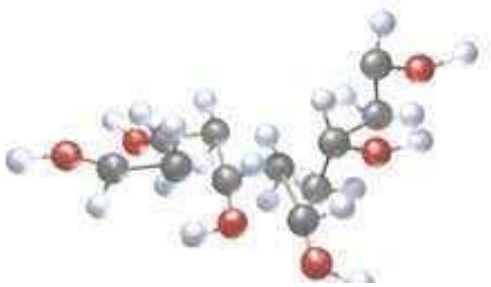

Scheme 2. Space filling model of polyvinyl alcohol

The present work deals

i) To evaluate the inhibition efficiency of polyvinylalcohol(PVA) in controlling corrosion of aluminium at *pH* 11 in the absence and presence of Zn^{2+}

ii) To study the synergistic effect exist between PVA - Zn^{2+} system.

iii) To analyse the protective film by FT-IR spectra and SEM techniques.

iv) To study the AC impedance spectra to know the mechanistic aspects of corrosion inhibition.

v) To propose a suitable mechanism of corrosion inhibition based on the results from the above studies.

Materials and methods

Preparation of the specimens

The commercial aluminium specimens (95 % of purity) of the dimentions 1.0 x 4.0 x 0.2 cm were polished to a mirror finish and degreased with trichloroethylene and used for the weight-loss method and surface examination studies were made.

Weight – loss method

Aluminium specimens were immersed in various concentrations of the inhibitor solution in the presence and absence of Zn^{2+} for a period of 24 h.The weight of the specimens before and after were determined using Shimadzu balance, model AY62. The corrosion products were cleansed with Clarke's solution. The inhibition efficiency (%) was then calculated using the equation

$$E = 100\left[1 - \frac{W_2}{W_1}\right] \quad (1)$$

where

W_1 = corrosion rate in the absence of the inhibitor and
W_2 = corrosion rate in the presence of the inhibitor.

AC impedance measurements

The AC impedance spectra were recorded in the same instrument which was used for polarization study. The cell set up was the same as that used for polarization measurements. The real part (Z') and imaginary part (Z'') of the cell impedance were measured in ohms at various frequencies. The values of charge transfer resistance R_t, and the double layer capacitance C_{dl} were calculated.

$$R_t = (R_s + R_t) - R_s \quad (2)$$

where

R_s = solution resistance

$$C_{dl} = 1 / 2\pi R_t f_{max} \quad (3)$$

where

f_{max} = maximum frequency

Surface examination study

The aluminium specimens were immersed in various test solutions for a period of 24 hours and then taken out and dried. The nature of the film formed on the surface of the metal specimens was analysed for surface analysis technique by FTIR spectra and fluorescence spectra.

FT-IR Spectra

The film formed on the metal surface was carefully removed and mixed thoroughly with KBr. The FTIR spectra were recorded in a Jasco 460+ spectrophotometer.

RESULTS AND DISCUSSION

Analysis of the results of weight loss method

The *IE* values of PVA at different concentrations in the absence and presence of Zn^{2+} in well water for a period of one day obtained from the weight loss method are given in Table 1.

The inhibition efficiency of PVA increases as its concentration increases. From the table it is clear that Zn^{2+} in the absence of inhibitor also has some *IE*. As the concentration of Zn^{2+} increases, inhibition efficiency also increases. A synergistic effect exist between PVA and Zn^{2+}. It is observed from the Table 1, 250 ppm of PVA only has 50 % *IE* and 25 ppm of Zn^{2+} alone has 22 % *IE*. However, their combination consisting of 250 ppm of PVA and 25 ppm of Zn^{2+} has 85% inhibition efficiency. The observed improvement in the protection efficiency is attributed to the synergistic effect,[10-13] which results from the combination of two inhibitors PVA and Zn^{2+} which results in the formation of complex between Zn^{2+}-PVA, hence the inhibitor molecules are readily transported from the bulk to the metal surface. A thin film was observed on the surface of the inhibited metal during the weight-loss measurements.

The corrosion rates of aluminium with various concentrations of PVA and Zn^{2+} systems immersed in well water for the same period are given in Table 1. From the Table 1, it is clear that in the presence of Zn^{2+} corrosion rate (*CR*) decreases as the concentration of PVA increases. This behaviour is due to the increase in the adsorption amount of the inhibitor on aluminium metal surface.[14-15]

Table 1. *IE* and *CR* of aluminium in solution containing various concentration of PVA in presence and absence of Zn^{2+} at *p*H 11

PVA ppm	Zn^{2+}, ppm					
	0		25		50	
	IE, %	*CR*, mdd	*IE*, %	*CR*, mdd	*IE*, %	*CR*, mdd
0	----	----	22	14.2	11	16.1
50	50	9.1	68	5.8	65	6.4
100	56	8.0	75	4.5	70	5.4
150	60	7.3	80	3.6	72	5.1
200	63	6.7	85	2.7	75	4.5
250	65	6.4	85	2.7	80	3.6

Synergism parameter (S_I)

The synergism parameter (S_I) is calculated using the relation

$$S_I = \frac{1-\theta_{1+2}}{1-\theta'_{1+2}}$$

where

$\theta_{1+2} = (\theta_1 + \theta_2) - ((\theta_1 . \theta_2)$
θ_1 = surface coverage of inhibitor (PVA)

 DOI: 10.17628/ecb.2014.3.407-411

θ_2 = surface coverage of co-inhibitor (Zn^{2+})

θ'_{1+2} =combined surface coverage of inhibitors (PVA) and (Zn^{2+})

Surface coverage = *IE*/100

S_I approaches 1 when no interaction between the inhibitors. $S_I > 1$, synergistic effect exist between the two inhibitors. In the case of . $S_I < 1$, negative interaction takes place between system are shown in Figs. 1-3. It is clear from the plots that the impedance response of aluminium was significantly changed after addition of the two inhibitors, (i.e *CR* increases). The calculated synergism parameter values for PVA and Zn^{2+} system are given in Table 2a and in 2b respectively. In the case of PVA - Zn^{2+} system , the S_I value is found to be greater than one for 25 ppm of Zn^{2+} with various concentrations of PVA, indicating the synergistic effect exist between Zn^{2+} of concentrations of 25 ppm with various concentrations of PVA. S_I value is found to be less than unity for 50 ppm Zn^{2+} with various concentrations of PVA which indicates a lack of synergism between 50 ppm of Zn^{2+} with various concentrations of PVA.[16-18]

Table 2a. Synergism parameters for PVA - Zn^{2+} (25 ppm) system when aluminium immersed in well water

PVA, ppm	θ_1	θ_2	θ'_{1+2}	S_I
50	0.50	0.37	0.66	0.96
100	0.56	0.37	0.72	0.93
150	0.60	0.37	0.75	0.90
200	0.63	0.37	0.77	0.92
250	0.65	0.37	0.78	1.1

Table 2b. Synergism parameters for PVA-Zn^{2+} (50 ppm) system when aluminium immersed in well water

PVA, ppm	θ_1	θ_2	θ'_{1+2}	S_I
50	0.50	0.15	0.58	1.33
100	0.56	0.15	0.63	1.45
150	0.60	0.15	0.66	1.7
200	0.63	0.15	0.68	2.1
250	0.65	0.15	0.75	1.99

Analysis of the results of AC impedance spectra

AC impedance spectra have been used to detect the formation of film on the metal surface. Nyquist plot and Bode plot representations of aluminium in well water in the absence and presence of the inhibitors. The impedance diagrams obtained almost have a semicircular appearance. This indicates that the corrosion of aluminium in alkaline solution is mainly controlled by a charge transfer process. The impedance parameters namely charge transfer resistance (R_t) and double layer capacitance (C_{dl}) are given in Table 4.

When aluminium is immersed in solution containing 250 ppm of PVA and 25 ppm of Zn^{2+} at *p*H 11 in the presence and absence of inhibitors are shown in Fig 1.

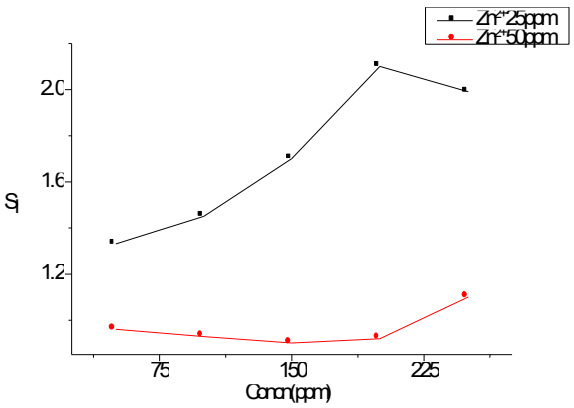

Figure 1. Graph of synergism effect exist in PVA- Zn^{2+} system in the corrosion of aluminium immersed in well water (Immersion period-one day)

It is found that when aluminium in well water at pH11, the R_t value is 396.4 Ω cm^2 and C_{dl} value is 1.2865×10^{-8} μF cm^{-2}. When 250 ppm of PVA and 25 ppm Zn^{2+} are added the R_t value tremendously increased to 2086 ohm cm^2 and the C_{dl} value is decreased to 2.44×10^{-9} μF cm^{-2}.[19-24] This indicates the protective film is formed on the metal surface in the presence PVA .The bode plots are shown in Fig 4. It is observed that in the absence of the inhibitors the real impedance value [(log(*Z ohm*$^{-1}$)] is 2.69. In the presence of inhibitors this value increases to 3.38.

Table 3. The impedance parameters of aluminium immersed in well water at *p*H 11 in presence and absence of inhibitor obtained by AC impedance method

System	R_t Ohm cm^2	C_{dl} F cm^{-2}	Impedance (log *Z* ohm^{-1})
Well water	396.4	1.2865×10^{-8}	2.69
Test solution PMMA=250 ppm+Zn^{2+}=25ppm	2086	2.44×10^{-9}	3.38

Analysis of the FT-IR spectra

FTIR spectra have been used to analyze the protective film formed on metal surface. FTIR spectrum (KBr) of pure PVA is given in Fig.4a. The aliphatic C-H stretching frequency peaks appears at 2928.5 cm^{-1}. The secondary alcoholic C-O stretching absorption peak takes place at 1062 cm^{-1}. The bands at 1383 cm^{-1} and 765.88 cm^{-1} are due to bending C-H of methyl groups. The FT-IR spectrum of the film formed on the aluminium surface after immersion in the well water for one day containing 250 ppm of PVA and 25 ppm of Zn^{2+} is shown in Fig 4b. The OH stretching frequency decreased from 3459 cm^{-1} to 3417 cm^{-1}. The C-O stretching frequency decreased from 1062 $cm^{-1}$to 1116 cm^{-1}. This suggest that the oxygen atom of PVA was coordinated with Al^{3+} on the anodic sites of the aluminium metal surface, resulting in the formation of Al^{3+} - PVA complex. The peak at 620 cm^{-1} which may be due to Zn-O bending mode of vibration. The band at 3459 cm^{-1} is due to OH stretching frequency of $Zn(OH)_2$ the formed at cathodic sites metal surface.[25]

 DOI: 10.17628/ecb.2014.3.407-411

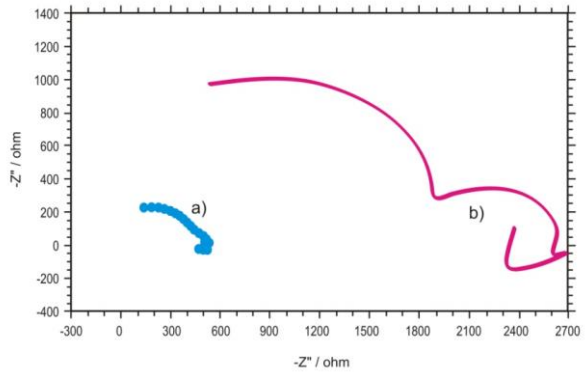

Figure 2. AC impedance spectra of aluminium immersed in various test solutions a) well water b) well water containing 250 ppm of PVA and 25 ppm of Zn^{2+}

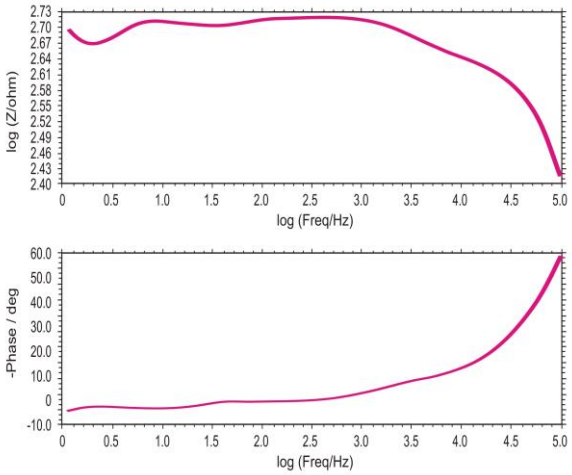

Figure 3a. Bode plots of aluminium immersed in well water

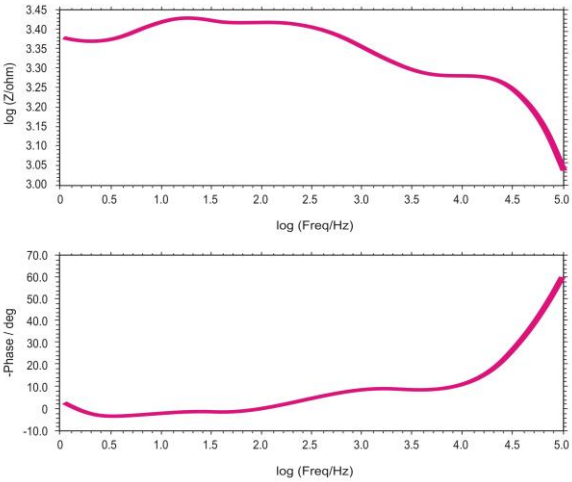

Figure 3b. Aluminium immersed in well water + 250 ppm of PVA and 25 ppm of Zn^{2+}

Analysis of surface metal by SEM

SEM technique provides a pictorial representation of the surface.To understand the nature of the surface film in the presence and absence of inhibitors and the extent of corrosion products of aluminium, the SEM micrographs of the surface are examined.[26-28]

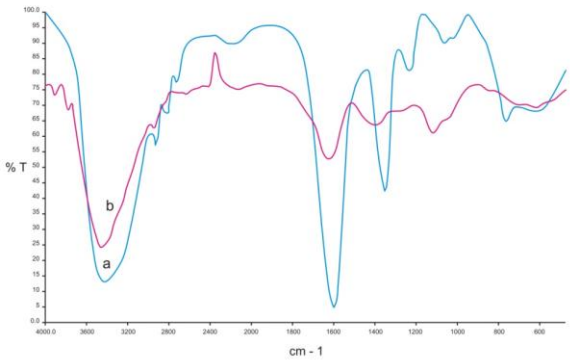

Figure 4. FTIR Spectra a) pure PVA b) film formed on metal surface after immersion in well water containing 250 ppm of PVA and 25 ppm of Zn^{2+}

The SEM images of different magnifications (X1000) of aluminium specimen and aluminium immersed in well water for one day in the presence and absence of inhibitors system are shown in Figure 5 as images (a, b and c) respectively.

The SEM micrographs of the surface of the polished aluminium metal (control) in Fig 5 images (a) illustrate the very smooth surface of the metal. These show the absence of any corrosion products formed on the metal surface.

The images (b) denote the SEM micrographs of aluminium surface immersed in well water. They show the type of rough surface of the uniform corrosion of the aluminium surface in well water, indicating in an inhibitor free solution, the surface is highly corroded.

Images (c) confirm that in the presence of 250 ppm of PVA and 25 ppm of Zn^{2+} at *p*H 11in well water, the rate of corrosion is suppressed , as it seen from the decrease in corroded areas. This is a result of the formation of insoluble complex on metal surface (PVA - Al^{3+}) and the surface is covered by a thin layer of inhibitors which effectively controls the dissolution of aluminium metal from corrosion process. The above results are line with the interpretation made by.[29,30]

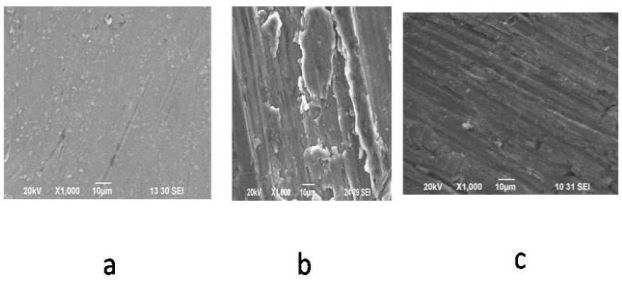

Figure 5. SEM micrographs of (magnification the surface of the polished aluminium (x1000) of a) polished aluminium metal b) aluminium immersed in well water c) aluminium immersed in well water + 250 ppm of PVA and 25 ppm of Zn^{2+}

Mechanism of corrosion inhibition

The weight – loss reveals that the formation of aluminium immersed in solution containing 250 ppm of PVA and 25 ppm of Zn^{2+} offers 95 % IE at *p*H 11. A synergistic effect exist between PVA and Zn^{2+}. AC impedance spectra reveal

that a protective film formed on the metal surface also it confirmed by FTIR spectra. SEM showed the surface morphology of metal surface.

The mechanism of corrosion inhibition was proposed by the following ways:

When the formulation consisting of 250 ppm of PVA and 25 ppm of Zn^{2+} at *p*H 11 was prepared, there is formation of PVA - Zn^{2+}complex in solution.

When aluminium is immersed in the solution, the PVA - Zn^{2+} complex diffuses from the bulk of the solution towards the metal surface.

On the surface of metal PVA - Zn^{2+} complex is converted to PVA - Al^{3+} complex and Zn^{2+} is released.

$$[PVA - Zn^{2+}] + Al^{3+} \rightarrow [PVA - Al^{3+}] + Zn^{2+}$$

$$Zn^{2+} + 2OH^{-} \rightarrow Zn(OH)_2$$

Conclusion

The formulation consisting of 250 ppm of PVA and 25 ppm of Zn^{2+} offers 85 % inhibition efficiency to aluminium immersed in solution at *p*H 11 by the weight-loss method. A synergistic effect exists between PVA and Zn^{2+}. AC impedence study showed that a protective film formed on metal surface. FTIR spectra analysed the film formed on the metal surface.

References

[1]Lorenz, W. J., Mansfeld, F., *Corros.Sci*., **1981**, *121*, 647.

[2]Al-Kharafi, F. M., Badawy, W. A., *Corros*., **1998,** *54*, 377.

[3]Macdonald,, D. D., Real, S., Smedley, S. I., Urquidi-Macdonald, J., *J. Electrochem. Soc*., **1988**, *135*, 1631.

[4]Mercier, D., Herinx, M., Barthes- Labrousse, M. G., *Corros. Sci*., **2010**, *52*, 3405.

[5]Mu, G., Li, X., *J. Colloid Interfac. Sci*., **2005**, *289*, 184.

[6]Lebrini, M., *Bull. Electrochem*., **2003**, *19*, 209.

[7]Umoren, S. A., Ogbobe, O., Ebenso, E. E., Okafor, P. C., *J. Appl Polym. Sci*., **2007**, *105*, 3363.

[8]Rajendran, S., Sridevi, S. P., Anthony, N., John Amalraj, A. and Sundaravadivelu, M., *Anticorros. Methods Mater.*, **2012**, *52*, 102.

[9]Umeron, S. A., Ebenso, E. E., *Ind. J.Chem. Techn*, **2008**, *15(4)*, 355.

[10]Manivannan, M., Rajendran, S., *Res. J. Chem. Sci.*, **2011**, *1(8)*, 42.

[11]Rajendran, S., John Amalraj, A., Jasmine Joice, M., Anthony, N., Trivedi, D. C. and Sundaravadivelu, M., *Corros. Rev*., **2004**, *22(3)*, 2337.

[12]Rajendran, S., Apparao, B. V., Palaniswamy, J., *J. Electrochem. Soc*., **1998**, *47(1)*, 43.

[13]Rajendran, S., Maria Joany, B. R., Apparao, B. V. and Palaniswamy, N., *Trans. SABST*, **2000**, *35(3-4)*, 113.

[14]Umoren, S. A., *Surf. Rev. Lett*., **2009**, *6(6)*, 831.

[15]Tallman, D. E., Pae, Y-G., Chen, G.-L., Bierwagenz, G. P., Reems, B., Gelling, V. J., *Cond. Polym. Plast.*, **1999**, 201.

[16]Rajendran, S., Apparao, V. B., Palaniswany, N., *Bull. Electrochem.*, **2001**, *17 (4)*, 171.

[17]Rajendran, S., Raji, A., Arockia Selvi, J., Rosaly, A. and Thangaswamy, S., *J. Mater.*, **2007**, *29*, 245.

[18]Rajendran, S., Raji, A., Arockia Selvi, J., Rosaly, A. and Thangaswamy, S., *Edutracks*., **2007,** *6*, 30.

[19]Benita Sherine, H., Jamal Abdul Nassar, A. and Rajendran, S., *Indian J. Eng. Sci. Technol*., **2010**, *24*, 341.

[20]Mary Anbarasi, C., Rajendran, S., *J. Electrochem. Sci. Eng*., **2012**, *2(1)*, 1.

[21]Ruba Helen Florence, G., Noreen Anthony, A., Wilson Sahayaraj, J. and Rajendran, S., *Indian J. Chem. Technol*., **2005**, *12*, 472.

[22]Rajendran, S., Apparao, B. V. and Palaniswamy, N., *Electrochim. Acta*., **1998**, *44*, 533.

[23]Rajendran, S., Apparao, B. V. and Palaniswamy, N, *Anticorros. Methods Mater*., **1999**, *46*, 111.

[24]Gomal, V., Sribharathy, V., Rajendran, S., *J. Electrochem. Sci. Eng*., **2012**, *2*, 121.

[25]Li, W-H., Hu, L.-C., Zhang, S-T. and Hou, B-R., *Corros. Sci*., **2011**, *53 (2)*, 735.

[26]Manivannan, M. and Rajendran, S., *Res. J. Chem. Sci*., **2011**, *1(8)*, 1.

[27]Manivannan, M. and Rajendran, S., *J. Chem. Biol. Phys. Sci*., **2011**, *1 (2)*, 241.

[28]Benita Sherine, H and Rajendran, S., *Arab. J. Sci. Eng*., **2011**, *36* , 517.

[29]VasconcelosTorres, V., Salgado Amado, R., Faia de, C. and Lopez Ferandez, T., *Corros. Sci*., **2011**, *53*, 2385.

[30]Delimi, A., Galopin, E., Coffinier, Y., Pisareketal, M., *Surf. Coat. Technol*., **2011**, *205*, 4011.

Received: 03.03.2014.
Accepted: 01.04.2014.